# The Manufacture and Commercial Applications of Metastannic Acid and of Tin Dioxide - Based Semiconducting Materials

A Thesis Submitted for the Degree
of Doctor of Philosophy in the Faculty
of Science at The City University

By

Stephen A. Lawrence

The Department of Chemistry,
The City University,
Northampton Square,
London,
EC1V 0HB.

September 1984

To

My Parents

and Beverley

## Acknowledgements

My thanks are extended to Prof. J. D. Donaldson for his invaluable supervision of my research project and also to Dr. K. C. Bass for his helpful counselling.

Finally, I would like to take this opportunity to thank Mr. D. K. German and Mr. H. A. Morriss of Keeling and Walker Ltd. whose comments and encouragements upon my work have been most appreciated.

## Abstract

The financing of the research project by Keeling and Walker Ltd. resulted from a need for a greater knowledge of the properties of metastannic acid and also for an understanding of the reaction parameters controlling the manufacture of the material. Once these criteria had been defined it was hoped that it would be poss--ible to design a full sized manufacturing plant for the production of metastannic acid of a fine particle size. Several series of investigative experiments into metastannic acid production were carried out at The City University and at Keeling and Walker's factory in Stoke-on-Trent and material analysis was carried out at The City University and at The British Ceramic Research Association in Stoke-on-Trent. The interpretation of results obtained from these experiments enabled a new metastannic acid production plant to be designed together with a proposed operating cycle as part of this work.

As well as manufacturing metastannic acid Keeling and Walker Ltd. also produce a range of tin dioxide based semiconductors for ind--ustrial applications. Work was carried out in this project to try to find a suitable synthetic route for the large scale manu--facture of low resistivity indium tin oxide. Extensive experi--mental trials resulted in the consistent production of a low resistivity material prepared from the thermal decomposition of indium tin benzoate.

Other areas of research covered in this project were, the prepar--ation of tin (IV) oxide by new synthetic routes, mössbauer spectro--scopic studies of tin oxides and an investigation into the hydrous metal oxide chemistry of tin, titanium, zirconium and hafnium.

Contents

# Chapter One - An Introduction to Metastannic Acid and to the Analytical Instumentation used in this Investigation

## Section 1.1 - The Preparation and Properties of Metastannic Acid

1.1.1 - Introduction to Metastannic Acid

1.1.2 - Analysis of Metastannic Acid by Thermal Gravimetry

1.1.3 - Differential Thermal Analysis of Metastannic Acid

1.1.4 - Analysis of Metastannic Acid by Infra-Red Spectroscopy

1.1.5 - Analysis of Metastannic Acid by Mössbauer Spectroscopy

1.1.6 - Analysis of Metastannic Acid by Mercury Porosimetry

## Section 1.2 - Analytical Methods and Instrumentation

1.2.1 - Introduction

1.2.2 - Particle Size Analysis

(a) Sedigraph

(b) Coulter Counter

1.2.3 - Determination of Surface Area

(a) B.E.T.

(b) Mercury Porosimetry

1.2.4 - Mössbauer Spectroscopy

1.2.5 - Powder X-Ray Diffraction

1.2.6 - Thermal Analysis

(a) Thermal Gravimetric

(b) Differential Thermal

# Chapter One - An Introduction to Metastannic Acid and to the Analytical Instrumentation used in this Investigation

## 1.1 The Preparation and Properties of Metastannic Acid

### 1.1.1 Introduction to Metastannic Acid

The literature contains reports on three hydrous tin (IV) oxide gels which are said to be distinct and which have been called ortho, meta and para - stannic acids. All three stannic acids may be prepared by precipitation from solutions of tin (IV) salts, the ortho and para forms are most commonly prepared by alkali controlled precipitation from aqueous solutions of stannic halides, the meta form however can only be prepared from the direct hydrolysis of tin nitrate produced in situ from the action of nitric acid upon tin metal. Metastannic acid is precipitated from this reaction as a finely divided white powder with a density of about $5 \cdot 2 g/cm^3$. Metastannic acid is desc--ribed as a hydrous form of tin (IV) oxide, the prefix hydrous implies that water is present in the material bound both chemically and phys--ically onto the surface of the oxide in non-stoichiometric proportions. Thus metastannic acid is best represented by the chemical formula $SnO_2 \cdot nH_2O$ where n may vary approximately between values of 0·1 and 4·0 depending upon how the material is prepared. When the hydrous oxide is dehydrated by heating at about $600^oC$ it is converted into tin (IV) oxide.

From a survey of the chemical literature it is obvious that in the past a great deal of confusion and controversy existed as to the exact chemical nature of metastannic acid. Fremy[1] gave ortho and metastannic acid the formulae $(H_2SnO_3)_n \cdot xH_2O$ and $(H_2Sn_yO_{2y+1}) \cdot zH_2O$ respectively and was of the opinion that metastannic acid was a condensed polymer comprised of orthostannic acid monomer units.

Kleinschmidt[2], however was able to show that metastannic acid could not be a condensation polymer of orthostannic acid because samples of the two species could be prepared with identical compositions. Kleinschmidt[2] proposed a cyclic pentameric structure, $(H_2SnO_3)_5$ for metastannic acid, shown in figure one, consisting of five orthostannic acid monomers.

Figure One - Kleinschmidt's Proposed Metastannic Acid Structure.[2]

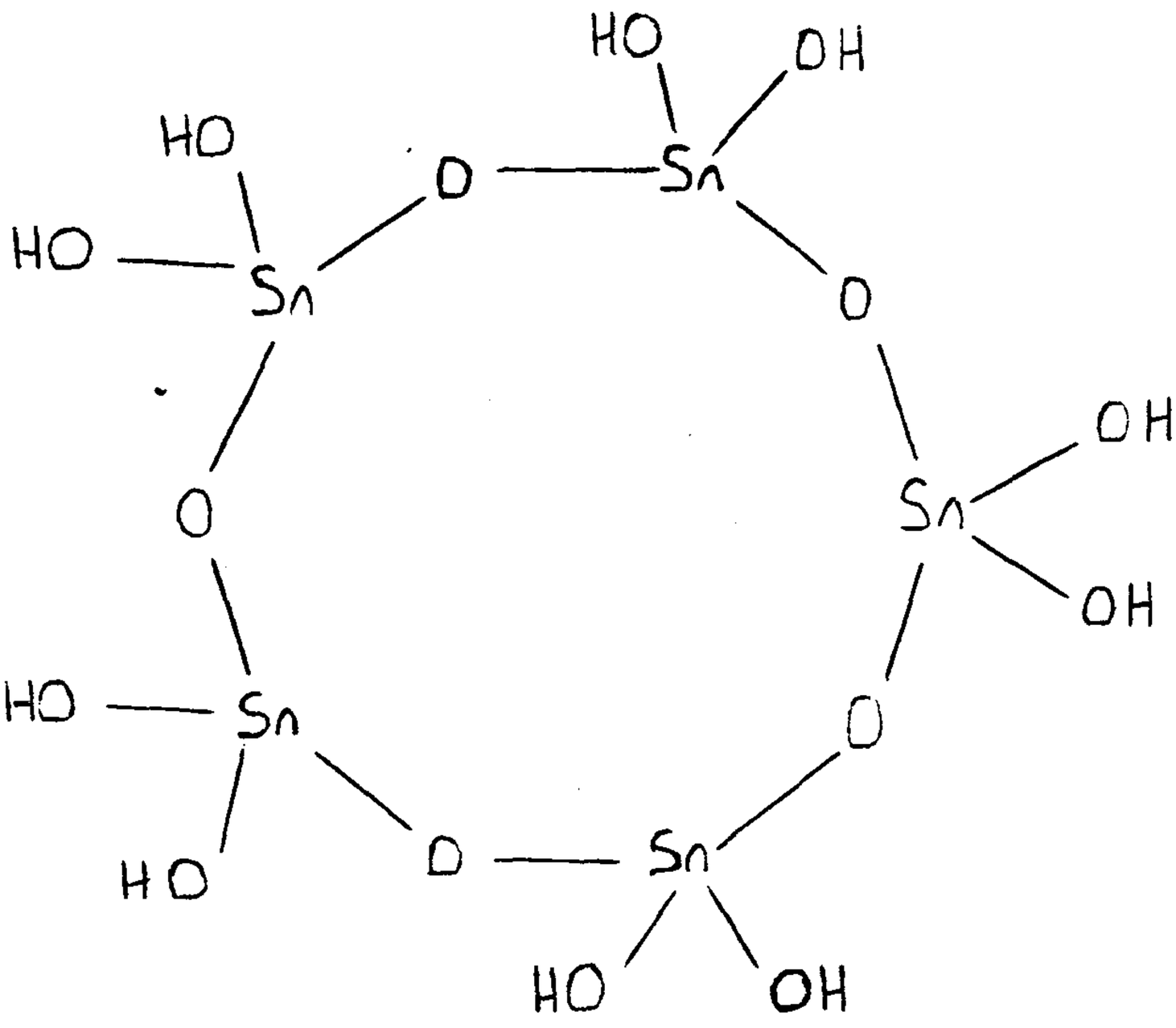


Other hypotheses on the stucture of metastannic acid have been for--warded in the past by Van Bemmellen[3], Lorenz[4] and Meckelberg[5-8]. These workers all concluded that metastannic acid was best represented as being a microcrystalline agglomeration of tin(IV) oxide primary particles containing water held by adsorbtion. The differences in chemical and physical behaviour between the ortho and metastannic acids were attributed to differences in the primary particle sizes of the two materials, with the primary particles of the ortho form being smaller than those of the meta form.

The differences in particle sizes were confirmed by Menon[9] who used Rayleigh light scattering techniques to determine the relative primary particle sizes of the two materials.

The nature of the stannic acids has also been discussed more recently by Babeshkin, Fabrichny and Nesmeianov[10], Donaldson and Fuller[11], Fuller, Walton and Warwick[12] and Goodman and Grieg[13]. Babeshkin _etal_[10] analysed ortho and metastannic acid using $^{1}H$ N.M.R. which revealed the presence of two different types of water in the material, which they termed mobile and immobile water. As the $^{1}H$ N.M.R. spectrum of a sample of 'wet' tin (IV) oxide showed only one line corresponding to mobile water, they concluded that the ortho and metastannic acids were chemically distinct species from wet tin (IV) oxide. Attempts by Babeshkin _etal_[10] to determine the size of the primary components of ortho and metastannic acid were unsuccessful as the two materials were found to be essentially amorphous and consequently no broadening of x-ray lines by interference could be detected. Donaldson and Fuller[12] found that the mössbauer spectra of metastannic acid and tin (IV) oxide were identical and so concluded that the tin to oxygen bonding in metastannic acid was unaffected by the presence of surface water. This was confirmed by the observation that the mössbauer spectra of metastannic acid samples which were saturated on the surface with $M^{2+}$ ions were also identical with the mössbauer spectrum of tin (IV) oxide. Electron microscopy and pore size distribution studies on ortho and metastannic acids conducted by Fuller, Warwick and Walton[12] showed that the freshly precipitated stannic acids age through ordered condensation of polynuclear hydroxy--lated species, and that this ageing process was found to occur at a faster rate upon heating. The process of ageing was found to occur very rapidly for metastannic acid, a fact which was attributed to the exothermic nature of the preparation of the material by the oxidation of tin in nitric acid.

The effect of this rapid ageing is manifested in the low degree of cross linkage found between the primary particles making up the mat--erial. Orthostannic acid was found to age much more slowly than metastannic acid and consequently to have a higher degree of cross--linkage between its primary particles. Goodman and Grieg[13] helped confirm this work by finding an empirical relationship between the extent of the ageing process in ortho and metastannic acid and their pore size distributions.

The chemical literature relating to metastannic acid is discussed at greater length in a review of material compiled at The City University commissioned by Keeling and Walker Ltd[14].

In contrast to ortho and para stannic acids, which may be prepared by precipitation from aqueous solutions of any tin (IV) salt, metastannic acid can only be prepared from the hydrolysis of tin containing nitrate solutions produced in situ from the reaction between tin metal and nitric acid. The earliest literature reference to the reaction between tin metal and nitric acid is that of Knuckel[15] in 1716 who reported that the reaction resulted in the precipitation of a white tin calx. Berzelius[16] in 1813 was the first to show that the hydrous oxide of tin prepared from the reaction of tin with nitric acid was different to the hydrous oxide prepared from the alkaline hydrolysis of tin (IV) chloride.

The mechanism of the reaction between tin and nitric acid was invest--igated independently by Engel[17,18] and Kleinschmidt[2] who both conc--luded that tin metal was first taken into solution as tin (II) nitrate which then reacted with nitric acid to give tin (IV) nitrate

and that it was the aqueous solution of tin (IV) nitrate which hydrolised on heating to precipitate out metastannic acid. The reaction was therefore written as a three stage process.

$$\text{(I)}\quad Sn \xrightarrow{HNO_3} Sn(NO_3)_2$$

$$\text{(II)}\quad Sn(NO_3)_2 \xrightarrow{HNO_3} Sn(NO_3)_4$$

$$\text{(III)}\quad Sn(NO_3)_4 \xrightarrow[\Delta H]{H_2O} SnO_2.nH_2O$$

If the reaction between tin and nitric acid is carried out using cold concentrated acid the reaction sequence can be stopped at stage (II) to give a stable green solution of tin (IV) nitrate. However attempts to precipitate out tin (IV) nitrate from this solution usually only result in its explosive decomposition to tin (IV) oxide. Experimentally it was found in this investigation that tin metal will only produce metastannic acid when reacting with nitric acid of concen--trations between 32% and 80%. When nitric acid of concentration lower than 32% is used the reaction stops at the tin (II) nitrate stage and when nitric acid of concentration greater than 80% is used a surface layer of oxide causes the tin to be passivated to further attack.

The preparation of metastannic acid by synthetic routes other than from tin and nitric acid have been reported in the literature. Scheurer-Kestner[19] reported that metastannic acid can be precipitated from a boiling solution of tin (II) chloride in nitric acid and Neuman[20] mentions vanadium (V) oxide as being a useful catalyst for this reaction. Gay Lusaac[21] reported that metastannic acid was the reaction product obtained on boiling a solution of nitric acid and tin (IV) chloride. However attempts at repeating these experiments in this investigation resulted in parastannic acid being precipitated out as the reaction product.

In view of the lack of information on the physical and chemical properties of metastannic acid in the literature a thorough investigation into the material was carried out as part of the investigation decribed in this thesis. Analyses of metastannic acid by thermal gravimetric and differential thermal methods, mercury porosimetry and infra-red and mössbauer spectroscopy were carried out in the course of this work and the methods are described in subsequent sections of this chapter under the appropriate headings.

### 1.1.2. Analysis of Metastannic Acid by Thermal Gravimetry

Thermal gravimetric analysis is an analytical technique which involves measurement of the weight of a sample either as a function of time at constant temperature or as a function of some parametric temperature as the system temperature changes. The sample analysis is usually plotted out in the form of an integral curve with absolute weight as the ordinate and time or temperature as the abcissa. Thermal gravi--metric analysis (T.G.) was carried out upon many samples of meta--stannic acid to determine the material's water content, and a typical thermograph of metastannic acid is shown in figure one, section 2.1. The thermal analysis curve of metastannic acid in figure one was recorded using a Stanton Redcroft Model Number STA-780 Simultaneous Thermal Analyser and using the conditions shown. The thermograph shows a two stage weight loss from the analyte. The first peak which extends from $50^{o}C$ to $150^{o}C$ corresponds to the loss of physisorbed water i.e. physically bonded to the surface of the oxide through hydrogen bonding. The second peak corresponds to the loss of chemi--sorbed water i.e. chemically bonded to the surface of the oxide as hydroxyl groups. The presence of chemisorbed water as hydroxyl groups on metastannic acid's surface can be demonstrated by infra-red spec--troscopy and is discussed later in this section.

Kittaka, Kanemoto and Morimoto[22] suggest a ratio of 1:3 for the relative proportions of physisorbed to chemisorbed water on the metastannic acid surface, they propose that two out of every three hydroxyl groups are actively involved in physisorbtion for every one non-participating hydroxyl group which is sterically blocked, viz figure two.

Figure Two - Kittaka etals' proposed mechanism for physisorbtion occurring on Tin (IV) Oxide surfaces[22].

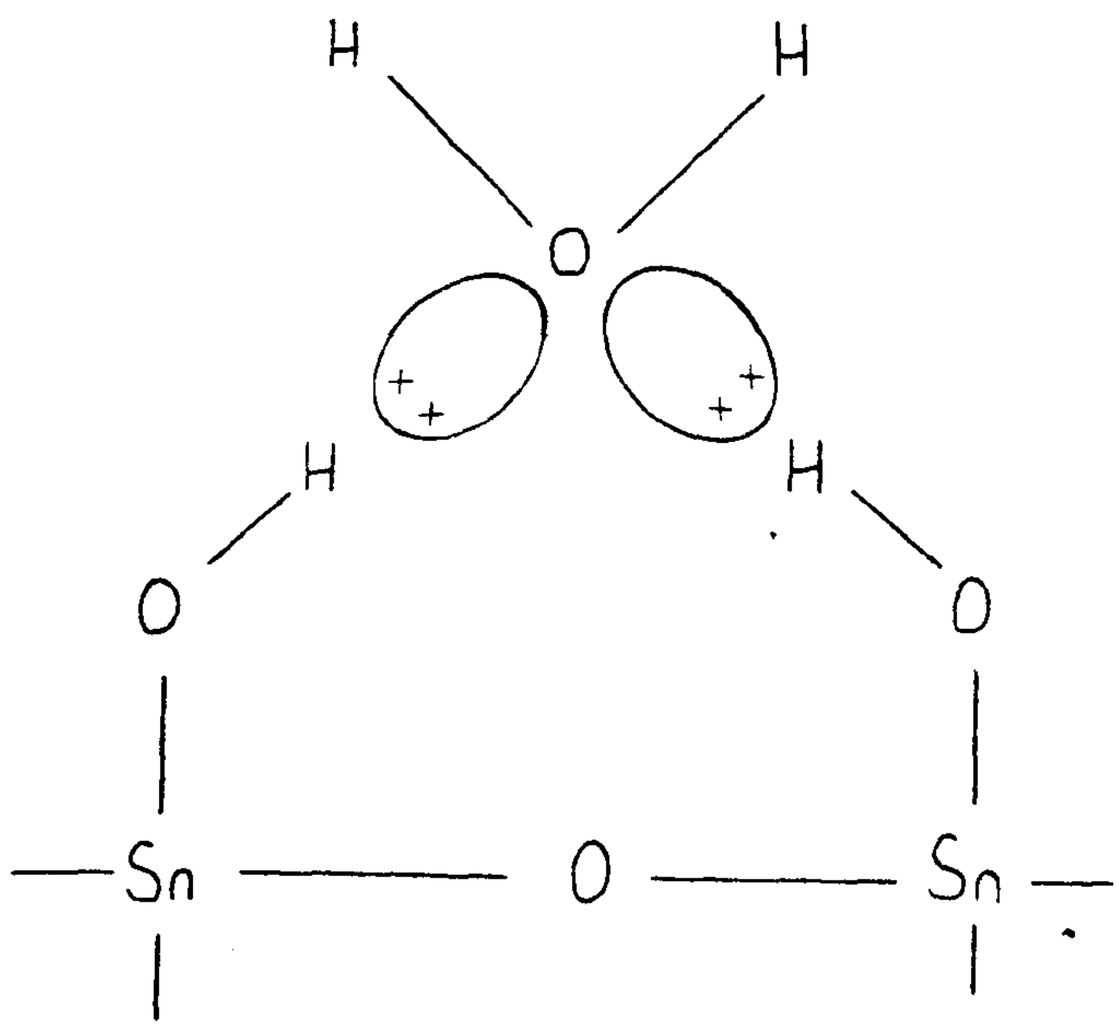


Tests carried out on a wide range of metastannic acid samples showed that the average composition of the material was $SnO_2.nH_2O$, with $n=0{\cdot}94$ (for samples with mean particle diameter 3-5 microns and oven dried at $110^{o}C$). This gives a ratio of physisorbed to chemisorbed water of 1:3·3 (or 3:10) which is in good agreement with Kittaka, Kanemoto and Morimotos' results.

### 1.1.3 Differential Thermal Analysis of Metastannic Acid

Differential thermal analysis (D.T.A.) is an analytical technique which involves heating a sample and a reference material in close proximity at some linear heating rate in a furnace and recording any differences in temperature which occur between the analyte and the reference samples. A differential thermograph thus consists of a record of the measured difference plotted as a function of time, sample temperature, reference temperature or furnace temperature. A differential thermogram of metastannic acid is shown in figure one, section 2.1 and the data are recorded below in table one, together with peak assignments.

Table One - The Differential Thermal Gravimetric Analysis of Metastannic Acid

| Peak Onset /$^{o}$C | Peak Max /$^{o}$C | Peak Ends /$^{o}$C | Peak Type | Assignment |
|---|---|---|---|---|
| 50 | 105 | 155 | Endotherm | Loss of Physisorbed Water |
| 155 | 200 | 600 | Endotherm | Loss of Chemisorbed Water |
| 300 | >1000 | >1000 | Exotherm | Crystallisation of Stannic Oxide |

The D.T.A. curve of metastannic acid consists only of two endothermic peaks corresponding to the loss of physisorbed and chemisorbed water from the hydrous material. At around 300$^{o}$C a major portion of meta--stannic acid in the sample has become converted into stannic oxide, thus superimposed upon the second endothermic peak there can be seen a broad exothermic peak which corresponds to the slow growth of a tetragonal form of tin (IV) oxide. This crystallisation process continues above 1000$^{o}$C and so cannot be followed any further using this instrumentation, though Goodman and Gregg[13] quote 1100$^{o}$C as being the peak temperature for the process.

## 1.1.4. Analysis of Metastannic Acid by Infra-Red Spectroscopy

The infra-red spectra of metastannic acid and tin (IV) oxide were recorded as part of this investigation using a Perkin Elmer 599 Infra-Red Spectrophotometer, and are shown in figure three and table two.

When infra-red radiation is incident on a molecule with frequencies corresponding to the characteristic molecular frequencies of the species, energy can be exchanged from one system to the other provided a linkage or coupling is available. This coupling is usually the change in the molecular dipole moment. The oscillating electric field of the radiation thus tends to alternate the molecular charge distribution causing changes in the dipole moment. In doing so the molecule is caused to vibrate, energy is exchanged from the radiation to the molecule and radiation is so absorbed. The infra-red spectrum of a material therefore represents an analysis of the molecular vib--rations in a species.

For chemically similar species like tin (IV) oxide and metastannic acid it might be predicted, bearing in mind that samples of tin (IV) oxide will invariably contain some moisture, that their infra-red spectra would be very similar, which was shown to be the case. The spectrum of metastannic acid exhibits two absorbtion bands attributed to the presence of physisorbed water (at 3600 to 2600cm$^{-1}$ and 1650 to 1450cm$^{-1}$) which match well with the infra-red absorbtion bands found for free water ($\nu_1$= 3652cm$^{-1}$, $\nu_2$= 3756cm$^{-1}$ and $\nu_3$= 1595cm$^{-1}$). Tin (IV) oxide exhibits only one of these bands, which occurs at 1650 to 1450cm$^{-1}$ and can be attributed to the presence of moisture in the sample.

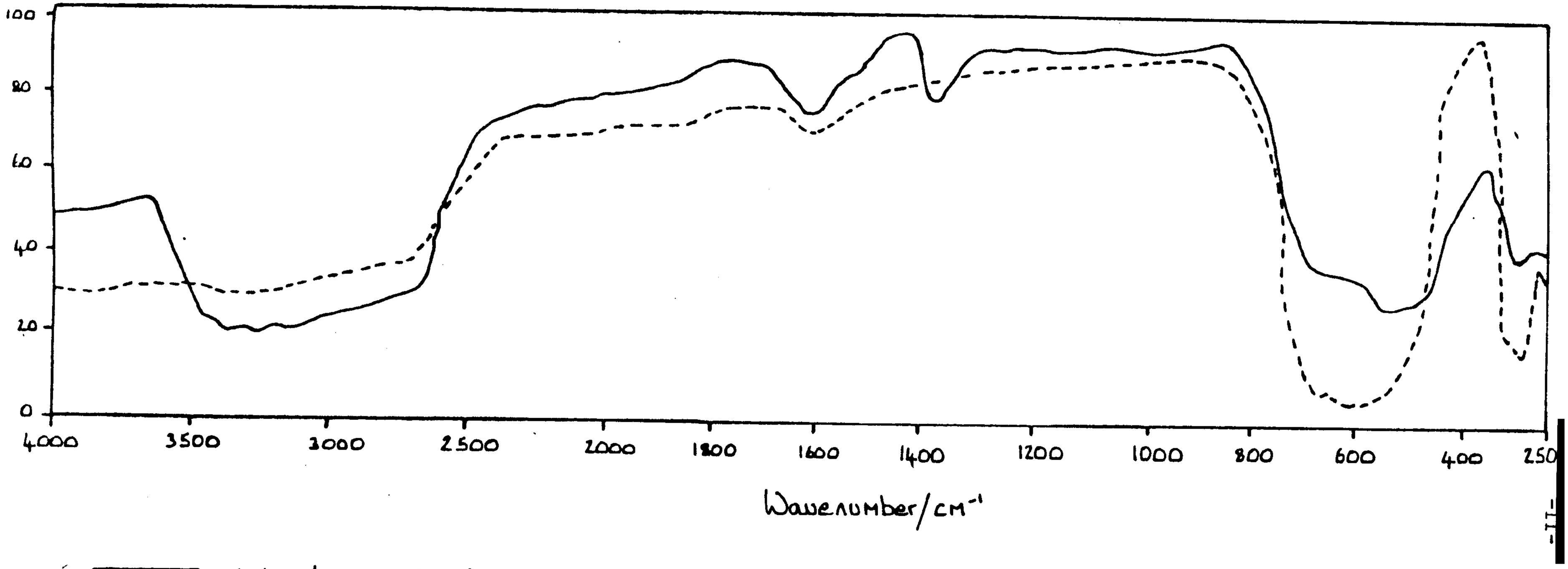


——— Metastannic Acid

------ Stannic Oxide

Figure Three - The Infra-Red Spectra of Metastannic Acid and Tin (IV) Oxide

Table Two - The Infra-Red Spectra of Metastannic Acid and Tin (IV) Oxide

| Species | Absorbtion Band Position /$cm^{-1}$ | Band Width + Intensity f.s.d.=100 | | Assignment |
|---|---|---|---|---|
| Metastannic Acid | 3600 - 2600 | Broad | 75 | -OH, Sn-OH and H-OH |
| | 1650 - 1450 | Medium | 22 | -OH, Moisture |
| | 1380 - 1350 | Medium | 20 | -OH, Surface Hydroxyl |
| | 650 - 600 | Broad | 60 | $\nu$ Sn(IV)-O |
| | 600 - 500 | Broad | 68 | $\nu$ Sn(IV)-O |
| Tin (IV) Oxide | 1650 - 1450 | Medium | 18 | -OH, Moisture |
| | 700 - 500 | Broad | 84 | $\nu$ Sn(IV)-O |

An interesting feature of the metastannic acid spectrum is the absorbtion band which occurs at $1380cm^{-1}$ and which is attributed to the out of plane bending of the hydroxyl group. This peak occurs at similar wave-lengths in the infra-red spectra of other hydrous metal oxide systems such as those of silicon, aluminium, titanium and zirconium and is indicative of surface chemisorbed water. This is in agreement with the results of the thermal analysis work with regard to chemisorbed water being present in the material and in addition infra-red spectro-scopy is able to further show that hydroxyl groups are present on the metastannic acid surface bonded directly to tin atoms.

## 1.1.5. Analysis of Metastannic Acid by Mössbauer Spectroscopy

An investigation into the effects of calcination upon the structure of metastannic acid was carried out as part of this investigation, using mössbauer spectroscopy. This area of metastannic acid chem-istry was thought worthy of investigation as samples of the material were found to take on a strong yellow colouration upon heating. This discolouration was also found to persist in the material on subsequent cooling to room temperature. The mössbauer spectra of two samples of metastannic acid, one calcined for two hours at 750°C, and the other untreated, were obtained at 80K in order to investigate this phenomenon. The data obtained for these two samples are in table three.

Table Three - The Mössbauer Spectra of Metastannic Acid Samples

| Sample | No. of Peaks in Spectrum | Nature | Chemical Shift $\delta$ in mmsec rel to $SnO_2$ | Full Width at ½ height in mmsec |
|---|---|---|---|---|
| Metastannic Acid | One | Singlet | 0·012±0·005 | 1·58 |
| Calcined Metastannic Acid | One | Singlet | 0·225±0·03 | 3·42 |

Mössbauer spectroscopy provides a useful analytical tool for the determination of the formal oxidation state of a nucleus in the solid state as well as providing information relating on the way in which tin uses its valence electrons in bonding. This is discussed in greater detail in section 1.2.4. of this chapter.

The mössbauer spectrum recorded for metastannic acid exhibits virtually no chemical shift from stannic oxide's resonance line. Therefore the results of mössbauer analysis indicate that metastannic acid possesses a structure with a tin enviroment similar to that of tin (IV) oxide.

The thermally treated metastannic acid shows a chemical shift of 0·225 $mmsec^{-1}$ from the position of the stannic oxide resonance line and this shift can be explained as being due to the sample being oxygen deficient after calcination. Oxygen loss during calcination is a common feature of metal oxide chemistry, the best known example being that of zinc oxide, which upon heating undergoes a colour change from white to yellow. The high temperature colouration of these materials is attributed to colour centres arising from lattice defects at vacant oxygen sites. Upon cooling oxygen is able to re-enter the lattice and the original colour is restored. The zinc oxide 'wurtzite' structure is more open than the stannic oxide rutile structure and so oxygen is more able to move freely in and out of the lattice upon heating and cooling. For stannic oxide the situation is different and oxygen experiences difficulty in entering the rutile structure at room temperature and the yellow colour persists. The recorded mössbauer spectrum thus represents this oxygen deficient species which has a slightly greater 's' electron density at the nucleus than stannic oxide.

### 1.1.6. Analysis of Metastannic Acid by Mercury Porosimetry

From a review of chemical literature to date it became apparent that all porosity and surface area analyses performed on metastannic acid had been done using the B.E.T. technique, with no mention of mercury porosimetry. An investigation on metastannic acid using B.E.T. has been reported by Fuller, Warwick and Walton[12] who found that it had a microporous structure with a specific surface area of around $100m^2/g$. One problem associated with the B.E.T. technique, however, is that prior to analysis all samples have to be degassed. For most samples this involves prolonged heating at elevated temperatures and under vacuum.

Metastannic acid loses virtually its entire water content and is con--verted into tin (IV) oxide by the degassing proc e dure. With mercury porosimetry however the need for extensive vacuum degassing is elim--inated and a five minute vacuum degassing at room temperature is sufficient for most samples.

Mercury porosimetry differs from B.E.T. in that the later technique determines the specific area of solids by gas adsorbtion and determination of the monlayer capacity of the analyte. These techniques are described in greater detail in section 1.2.3. of this chapter. Mercury porosim--etry is based upon the fact that, because mercury has a high surface tension, an applied pressure is required to force the liquid through orifices, such as those which exist in the structure of porous materials. Thus by measuring the mercury uptake of a porous material against applied pressure the surface area and porosity of materials may be determined.

Mercury porosimetric analysis was carried out on two samples of meta--stannic acid of different particle sizes which are listed together, with the results of analysis in table four. All experimental work was carried out at Brunel University using a Carlo Erba Strumentazione Porosimeter Model M.O.D.. These results are also shown graphically in figure four. From figure four it can be seen that the two samples analysed give very similar pore volume/applied pressure plots, this type of curve is usually taken to be indicative of non-porous powders. The initial uptake of mercury by the sample (region one) can be assumed as being due to mercury filling the interparticular voids in the mat--erial, once all of the interparticular voids have become filled the intrusion volume can be calculated which can be used to give an indic--ation of the sample's particle size as well as the surface area for non-porous materials.

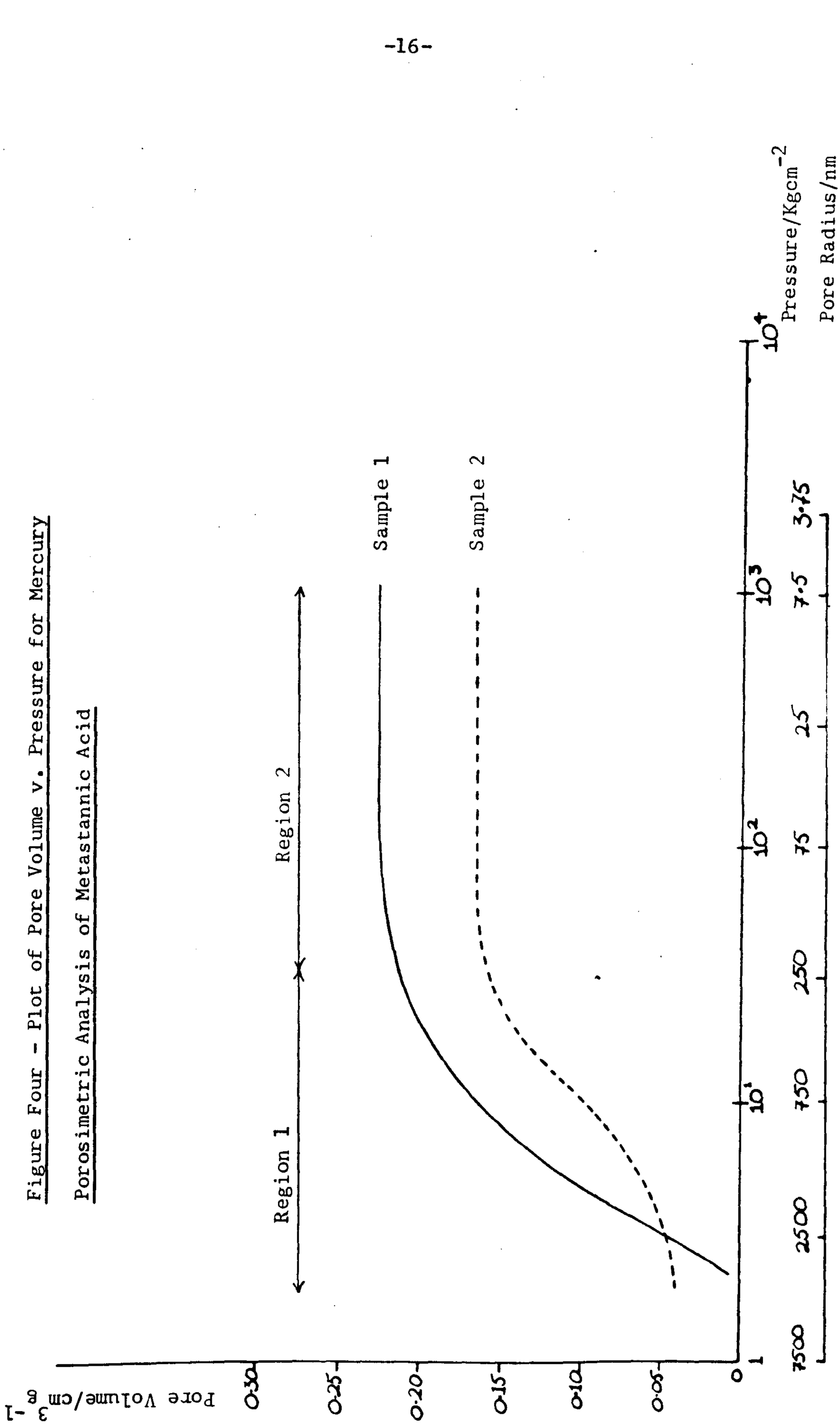


Figure Four - Plot of Pore Volume v. Pressure for Mercury Porosimetric Analysis of Metastannic Acid

Fuller, Walton and Warwick's[12] figure of around $100m^2g^{-1}$ therefore represents the internal surface area of the dehydrated porous material.

Lastly mention should be made of the intrusion volumes for the two samples which imply that the particle size of sample two is larger than that of sample one. This is in agreement with the results of Coulter Counter particle size analyses of the two samples.

## 1.2 Analytical Methods and Instrumentation

### 1.2.1. Introduction

In the course of this investigation a range of physical and chemical analytical techniques were used to characterise novel materials synth--esised in the course of the work. This chapter contains a brief introduction to the background of the analytical techniques and instru--mentation used in this investigation.

### 1.2.2. Particle Size Analysis

Particle size analysis is defined as the quantative determination of the size, shape and polydispersity of particles in the disperse system under study. The term particle is applied to those parts of a disperse phase which are separated from their environment by a continuous surface. In this respect, primary particles must be distinguished from agglom--erates, formed by the association of several primary particles: Agglomerates are called secondary particles. In the course of this investigation particle size analysis was carried out using two different types of instrument, the sedigraph and the coulter counter. Both forms of instrumentation are described in detail in sections (a) and (b) below.

(a) The Sedigraph

The principle of the sedimentation method involves determining the size of particles from their sedimentation rate in a gravitational field.

The force acting upon a spherical particle of diameter d and density $\rho$ in a medium of density $\rho_o$ under the influence of gravitational acceleration g is expressed by the equation.

$$F_1 = \frac{4}{3}\tau\frac{d^3}{8}(\rho - \rho_o)\, g$$

A spherical particle of diameter d travelling at a velocity v in a medium of viscosity $\eta$ similarly experiences a Stokes frictional force given by

$$F_2 = -3v\pi d\eta$$

Therefore when the particle reaches its terminal velocity

$$F_1 + F_2 = 0$$

Rearranging gives

$$d = \left[\frac{18\eta v}{(\rho - \rho_o)g}\right]^{\frac{1}{2}}$$

Now the rate of sedimentation is defined as

$$v = \frac{l}{t}$$

where l = sedimentation distance

and t = time

Thus, for monodisperse particles

$$l = kp$$

where p = weight percentage of sedimented particles

and k = conversion constant

so

$$v = \frac{l}{t} = \frac{kp}{t}$$

Therefore the particle size is thus defined by the slope, s, of a graph of p against t, according to the equations

$$p = st$$

and

$$d = \left[\frac{18\eta ks}{(\rho - \rho_o)g}\right]^{\frac{1}{2}}$$

This second equation is the Stokes Equation.

Modern sedimentometers (photosedimentometers) combine gravitational settling together with photoelectric measurement. The principle of the technique is that a narrow horizontal beam of parallel light is projected through a suspension at a known depth onto a photocell.

Assuming an initially homogeneous solution, the concentration of part--icles in the light beam will be the same as the concentration in the suspension. If the particles are allowed to settle, the number of particles leaving the light beam will be balanced by the number entering it from above. However, after the largest particle present in the suspension has fallen from the surface to the measurement zone, the emergent light flux will begin to increase since there will be no more particles of this size entering the measurement zone from above. Hence the concentration of particles in the light beam at any time will be the concentration of particles smaller than $d_s$, where $d_s$ is given by the Stokes equation.

It can be shown that the attenuation of the beam of light is related to the projected surface area of the particles in the beam and from this relationship the particle size may be determined.

A natural extension to the use of white light is to use x-rays. In this case the x-ray density is proportional to the weight of powder in the beam.

$$I = I_o \exp(-BC)$$

where B = calibration constant

and C = concentration of powder in the beam

The x-ray density, D, is defined by

$$D = \log_{10}(I/I_o)$$

Oden[23] developed a graphical method, called the method of tangential intercepts, which permits the sedimentation function to be converted into a cumulative function. This graphical method is nowadays carried out automatically on a sedimentation analyser which will plot out the results directly in the form of a graph of weight percentage against diameter.

Figure Five - Schematic Diagram of the Sedimentometer and Block Diagram of the Electrical Circuit

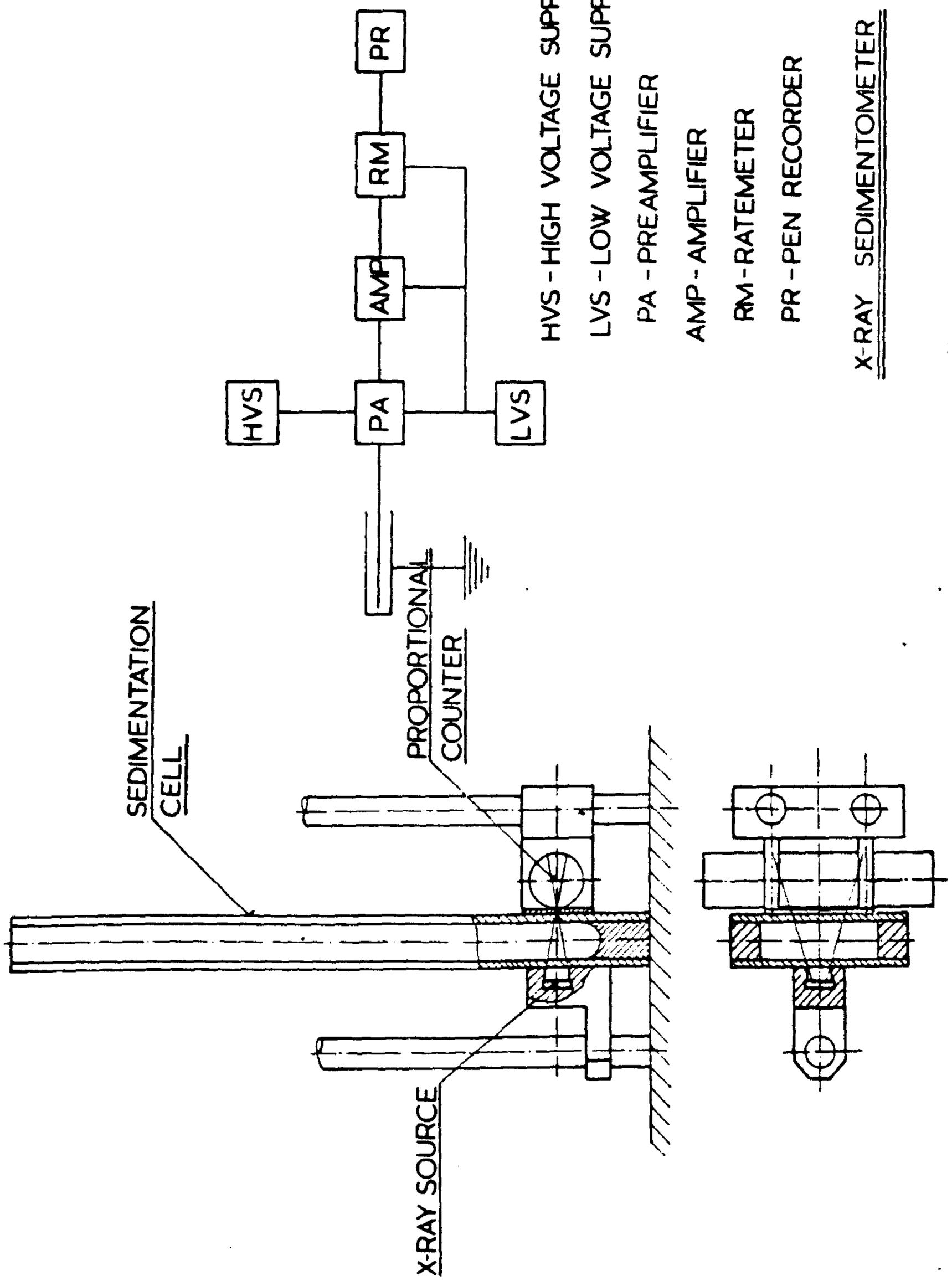

Figure Five - Schematic Diagram of the Sedimentometer and Block Diagram of the Electrical Circuit

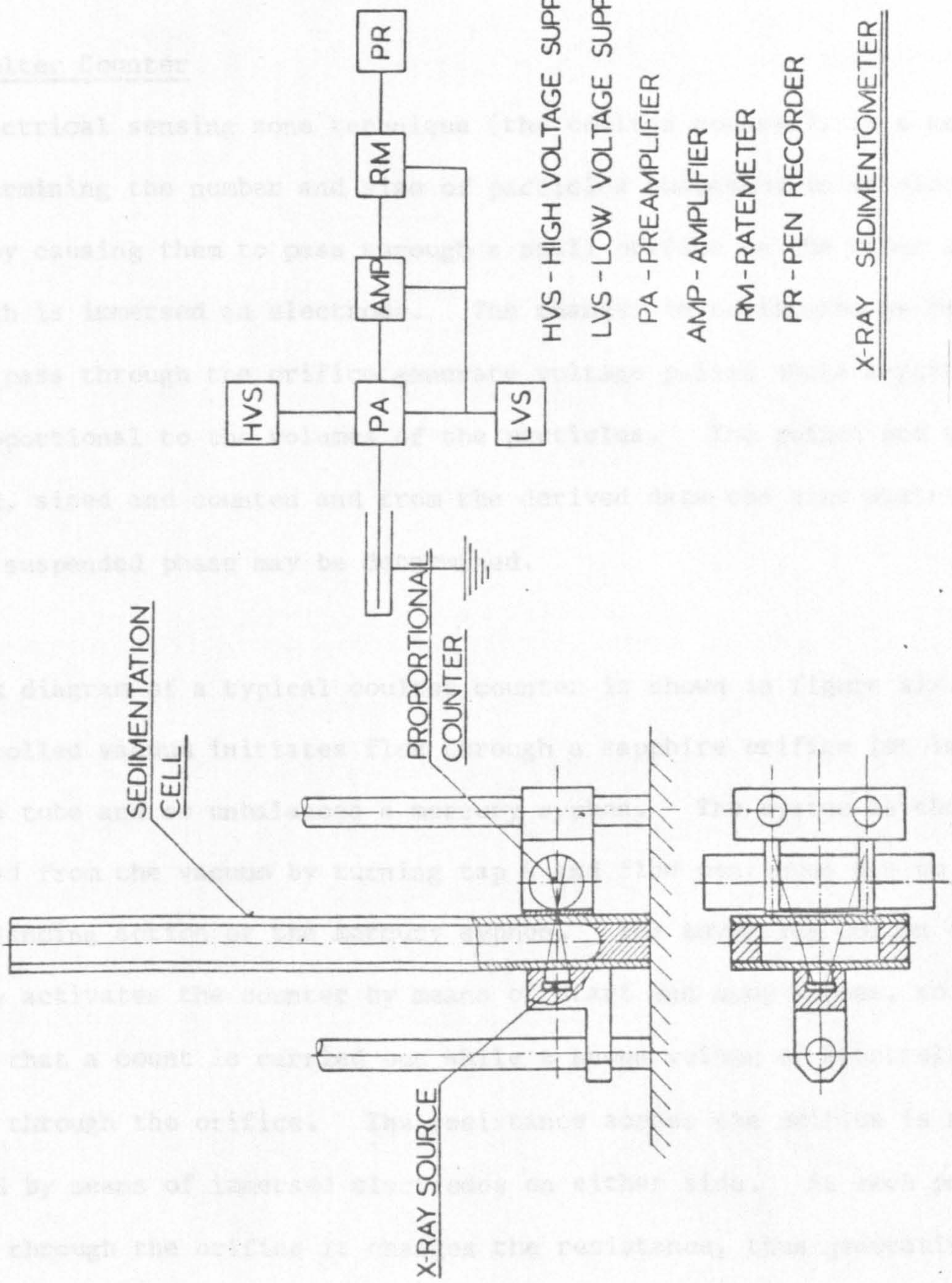

A schematic diagram of a modern x-ray sedimentometer is shown in figure five. The sedimentometer used in this investigation was a Sedigraph X-Ray Analyser, and all analyses were performed by B.C.R.A. at Stoke- -on-Trent.

(b) The Coulter Counter

The electrical sensing zone technique (the coulter counter), is a method of determining the number and size of particles suspended in an electro- -lyte by causing them to pass through a small orifice on the other side of which is immersed an electrode. The changes in resistance as part- -icles pass through the orifice generate voltage pulses whose amplitudes are proportional to the volumes of the particles. The pulses are amp- -lified, sized and counted and from the derived data the size distribution of the suspended phase may be determined.

A block diagram of a typical coulter counter is shown in figure six. A controlled vacuum initiates flow through a sapphire orifice let into a glass tube and so unbalances a mercury syphon. The system is then isolated from the vacuum by turning tap A and flow continues due to the balancing action of the mercury syphon. The advancing column of mercury activates the counter by means of start and stop probes, so placed that a count is carried out while a known volume of electrolyte passes through the orifice. The resistance across the orifice is mon- -itored by means of immersed electrodes on either side. As each particle passes through the orifice it changes the resistance, thus generating a voltage pulse which is amplified, sized and counted. The amplified voltage pulses are fed to a threshold circuit having an adjustable threshold level. All pulses above the threshold level are counted and this count represents the number of particles larger than some determin- -able volume proportional to the appropriate threshold setting.

Figure Six - The Coulter Counter

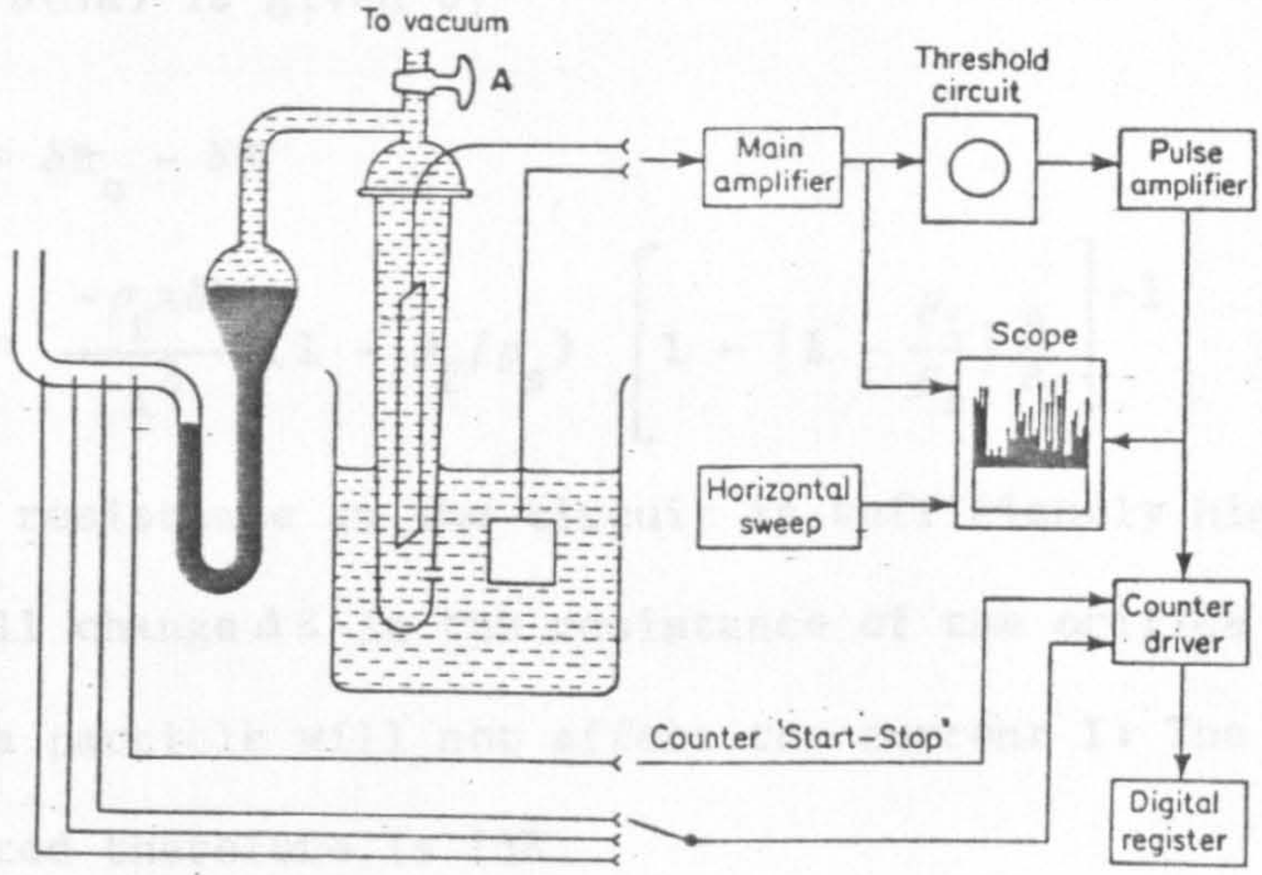


By taking a series of counts at various amplifications and threshold settings data are directly obtained for determining numerical frequency against volume.

The theory underlying the operation of the coulter counter is that the response, i.e. the voltage generated when a particle passes through the orifice, is directly proportional to particle volume. The relationship between response and particle size may be determined in the following manner based on dimensions defined in figures seven and eight.

Figure seven shows a particle passing through the orifice and figure eight an element of the particle and orifice.

Resistance of element without a particle, $\delta R_o$, is given by

$$\delta R_o = (\rho_f \delta l)/A$$

Resistance of element with a particle included is that of two resistors in parallel.

$$\delta R = \left[ \frac{A - a}{\rho_f \delta l} + \frac{a}{\rho_s \delta l} \right]^{-1}$$

$\rho_f$ and $\rho_s$ are the resistivities of the particle and fluid repectively

Thus the change in resistance of the element due to the presence of the particle $\delta(\Delta R)$ is given by

$$\delta(\Delta R) = \delta R_o - \delta R$$

$$= \frac{-\rho_f a \delta l}{A^2} (1 - \rho_f/\rho_s) \left[1 - [1 - \frac{\rho_f}{\rho_s}] \frac{a}{A}\right]^{-1}$$

The external resistance in the circuit is sufficiently high to ensure that the small change $\Delta R$ in the resistance of the orifice due to the presence of a particle will not affect the current I: The voltage pulse generated therefore is $I\Delta R$.

In practice it is found that the response is independant of the resist-ivity of the particle. Berg[24] suggested that this may be due to the ionic inertia of a helmholtz double layer and associated solvent molecules present on the surface of the particle, thus the resistivity of the part-icle would become practically infinite. One consequence of this would be that terms involving $(\rho_f/\rho_s)$ in the equation defining $\delta(\Delta R)$ may be neglected and the equation becomes.

$$\delta(\Delta R) = \left[\frac{-\rho_f a \delta l}{A}\right] \Big/ \left(1 - \frac{a}{A}\right)$$

The response therefore is not proportional to the volume of particle but is modified due to the term (a/A).

For a spherical particle of radius b, the change in resistance due to an element of thickness $\delta l$ at a distance l from the center of the sphere may be determined and this can be integrated to give the resistance change due to the particle.

$$\Delta R = \frac{-2\rho_f \pi^2}{A} \int_0^b \frac{b^2 - l^2}{\left[1 - \frac{\pi(b^2 - l^2)}{A}\right]} \, dl$$

Figure Seven - The Passage of a Particle Through the Orifice of a Coulter Counter

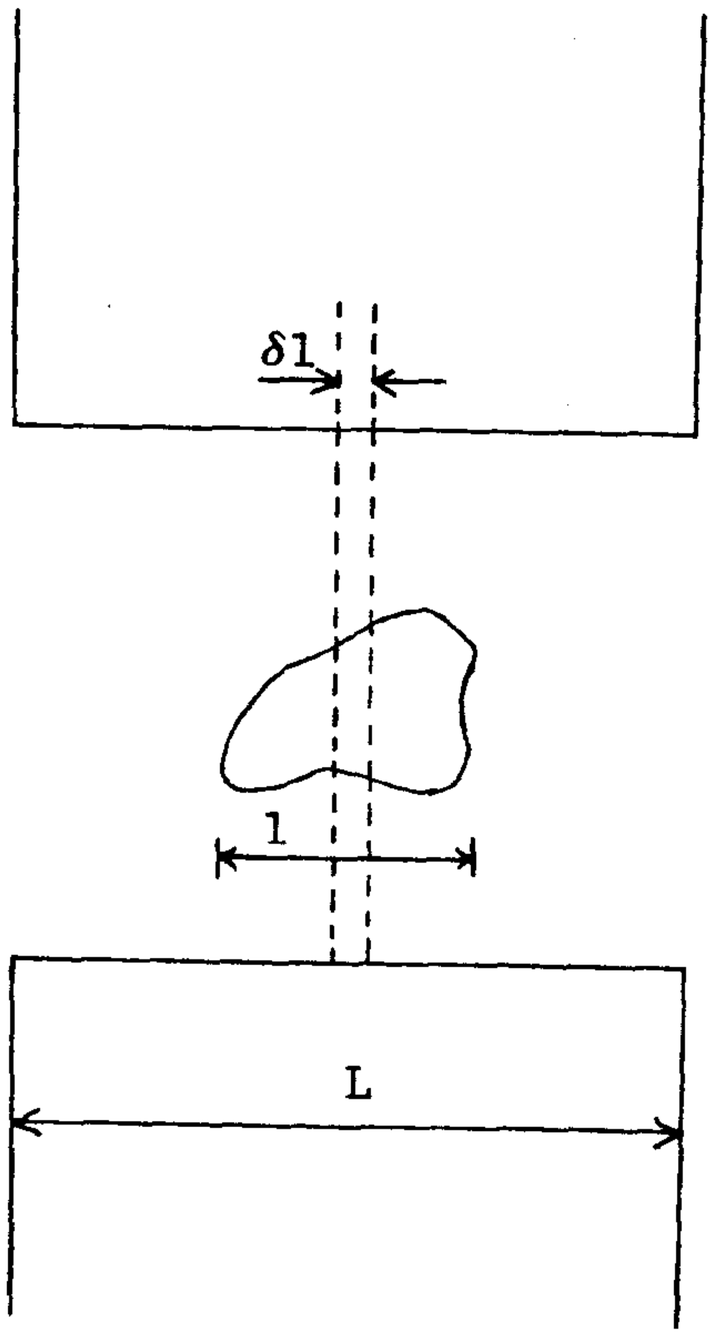


Figure Eight - An Element of the Particle and Orifice

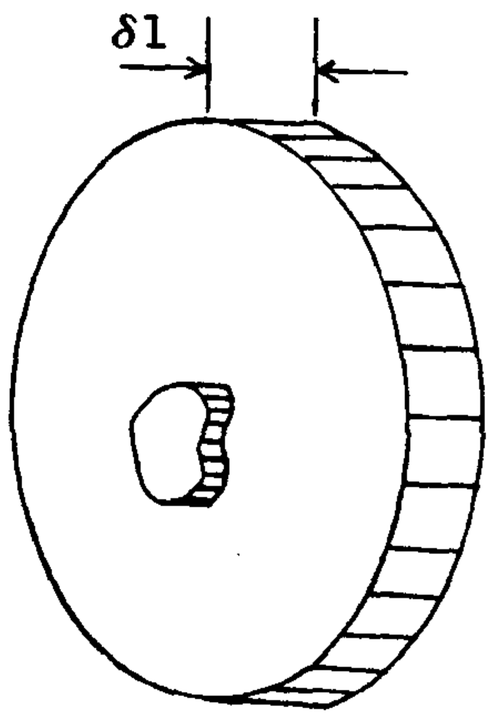


Cross Sectional Area of Orifice A = $\pi d^2/4$

Cross Sectional Area of Particle = a

$$\Delta R = \rho_f \frac{v}{A^2} F$$

where v = volume of suspension measured for each count

and F = shape parameter

The coulter counter used in this investigation was a Model (D) Indust-rial Counter fitted with a 200 $\mu$m diameter orifice tube.

### 1.2.3. Determination of Surface Area

Although particulates can (and do) assume all regular geometric shapes most particle size measurements are based on the so called equivalent spherical diameter. This is defined as the diameter of a sphere which would behave in the same manner as the test particle being measured in the same instrument. Attempts at measuring surface area using analytical instrumentation based upon the equivalent spherical diameter concept will always yield results significantly less than the true value, in some cases by factors up to $10^4$ depending upon the surface shape, porosity and other deviations from ideal sphericity of the particles. For this reason it is necessary to use special types of instrumentation for surface area determination, such as the B.E.T. analyser and the mercury porosimeter which were both used in this investigation.

(a) The B.E.T. Method

The B.E.T. method provides a very usefull analytical tool for giving detailed information about the specific surface area and pore structure of powders. The B.E.T. method (named after its discoverer's Brunauer, Emmett and Teller[25]) is based on the priciple that by enveloping each particle of a powder sample in an inert film of an inert gas it is possible to probe surface irregularities and pore interiors in a sample right down to the atomic level.

During the process of physical adsorbtion (physisorbtion) at very low relative pressure, the first sites to be covered are the more energetic ones. Accordingly as the adsorbate pressure is allowed to increase the surface will become progressively coated. However prior to complete surface coverage the surface will become progressively clogged and the probability will increase that a gas molecule will strike and become adsorbed onto a previously bound molecule. Thus the commencement of second and third adsorbed layers will begin prior to complete surface coverage. The effectiveness of the B.E.T. method lies in the fact that it enables an experimental determination of the number of molecules required to form a monolayer to be carried out despite the fact that exactly one monolayer is never actually formed. The B.E.T. theory assumes that the uppermost layers in the adsorbed stacks are in dynamic equilibrium with the vapour. Since the equilibrium is dynamic the actual location of the surface sites covered by one, two or more layers may vary, but the number of molecules in each layer will remain constant. B.E.T. theory uses the Langmuir equation (1) as a starting point.

$$(1) \qquad N_m \theta_1 v_1 e^{-E_1/RT} = kP\theta_o A_1$$

Where $N_m$ = No. of adsorbate molecules in a completed monolayer of area $1cm^2$

$\theta_1$ = Fraction of the surface covered by adsorbate molecules

$v_1$ = Adsorbates vibrational frequency normal to the surface when adsorbed

$E_1$ = Energy of adsorbtion

$P$ = Adsorbate pressure

$A_1$ = Condensation coeffient

B.E.T. theory assumes that for all layers formed above the first monolayer the terms v, E and A remain constant, thus the Langmuir equation becomes (2).

(2) $$N_m \theta_n v e^{-L/RT} = kP\theta_{n-1}A$$

Where L = Heat of liquefaction.

The B.E.T. equation is derived from this modified Langmuir equation and in its full form is given below (3)

(3) $$\frac{1}{W((P_o/P)-1)} = \frac{1}{W_m C} + \frac{C-1}{W_m C}\left(\frac{P}{P_o}\right)$$

Where W = Weight of adsorbate adsorbed

$W_m$ = Monolayer weight

C = B.E.T. constant

P = Adsorbate pressure

$P_o$ = Saturated vapour pressure

Therefore a plot of $W((P_o/P)-1)^{-1}$ against $P/P_o$ will give a straight line of slope s and intercept i, where

$$W_m = \frac{1}{s+i} \qquad \text{and} \qquad C = \frac{s}{i} + 1$$

A typical B.E.T. plot is shown in figure nine.

Figure Nine - A Typical B.E.T. Plot

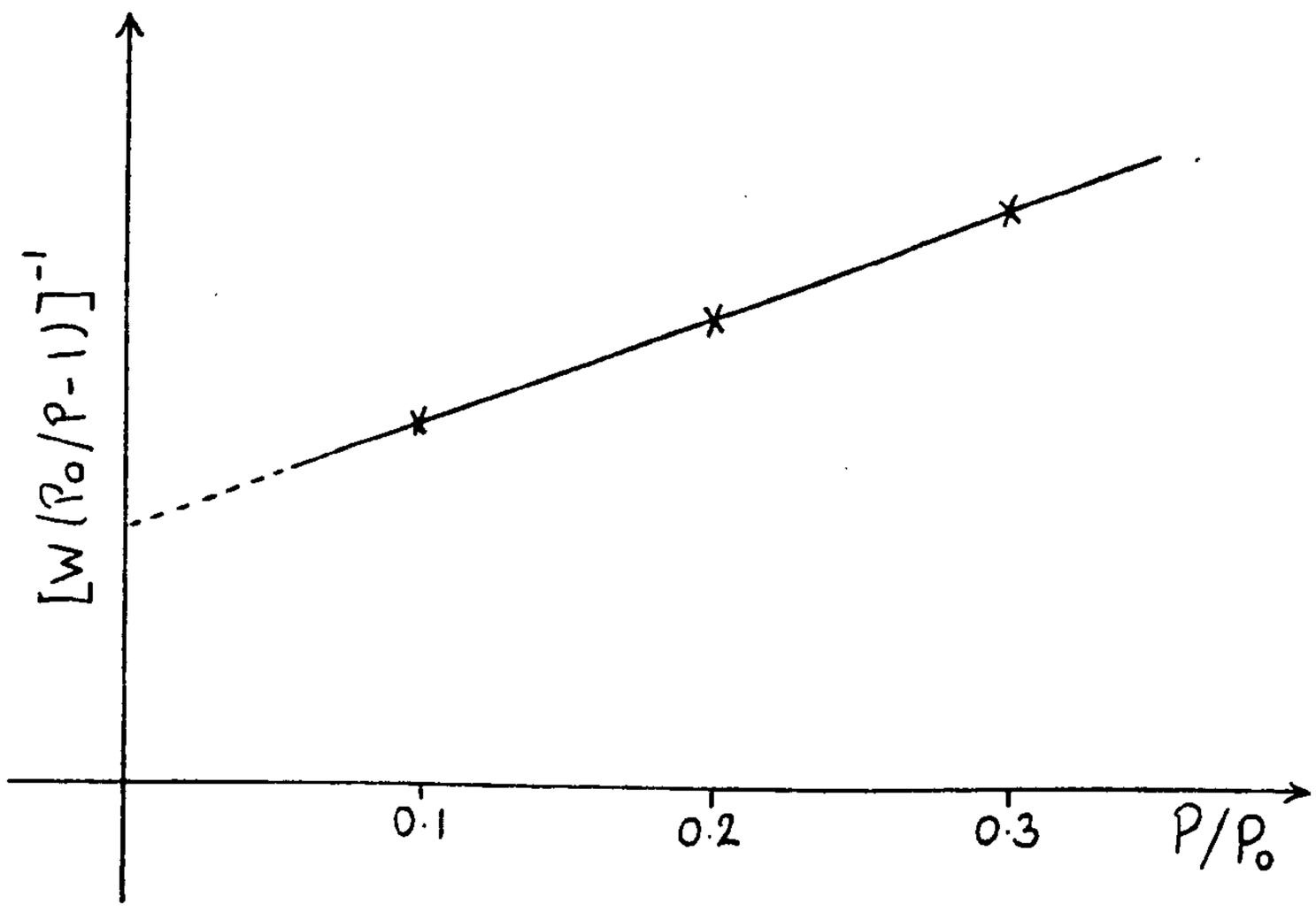

The total surface area can then be calculated from equation (4).

(4) $$S_t = \frac{W\,\bar{N}A}{M}$$

Where $\bar{N}$ = Avogadro's number

and A = Cross sectional area of the adsorbate

The specific surface area can then be determined by dividing $S_t$ by the sample weight.

As B.E.T. plots are always straight lines with finite intercepts, s, for reasonably high values of C, the intercept s is very small and may be neglected. Therefore by reducing experimental measurement to one point and drawing the B.E.T. plot as a straight line through the one measured point and the origin little accuracy is lost and a great deal of time is saved. This method is known as the B.E.T. single point technique and when using it the B.E.T. equation becomes.

$$\frac{1}{W((P_o/P) - 1)} = \frac{C - 1}{W_m C}\left(\frac{P}{P_o}\right)$$

Now $(W_m C)^{-1} = 0$

Therefore $$W_m = W\left[1 - \frac{P}{P_o}\right]$$

So that $$S_t = W\left[1 - \frac{P}{P_o}\right]\frac{\bar{N}}{M}\,A$$

The level of error involved when using this approximation is usually less than 5%, depending upon the value of C.

Modern B.E.T. instrumentation provides an internal computer fitted within the analyser to enable direct calculation of the sample's surface area which may then be conveniently read off a dial. In this invest--igation the instrument used was a 'Micrometric' Surface Area Analyser which took three measurement points in its sample analysis procedure.

The surface area of the sample was given directly by the instrument and was then divided by the sample weight to give the specific surface area. A diagram of a typical B.E.T. analyser similar to the one used in this investigation is shown in figure ten.

Figure Ten - B.E.T. Apparatus for Surface Area Determination by Gas Adsorbtion

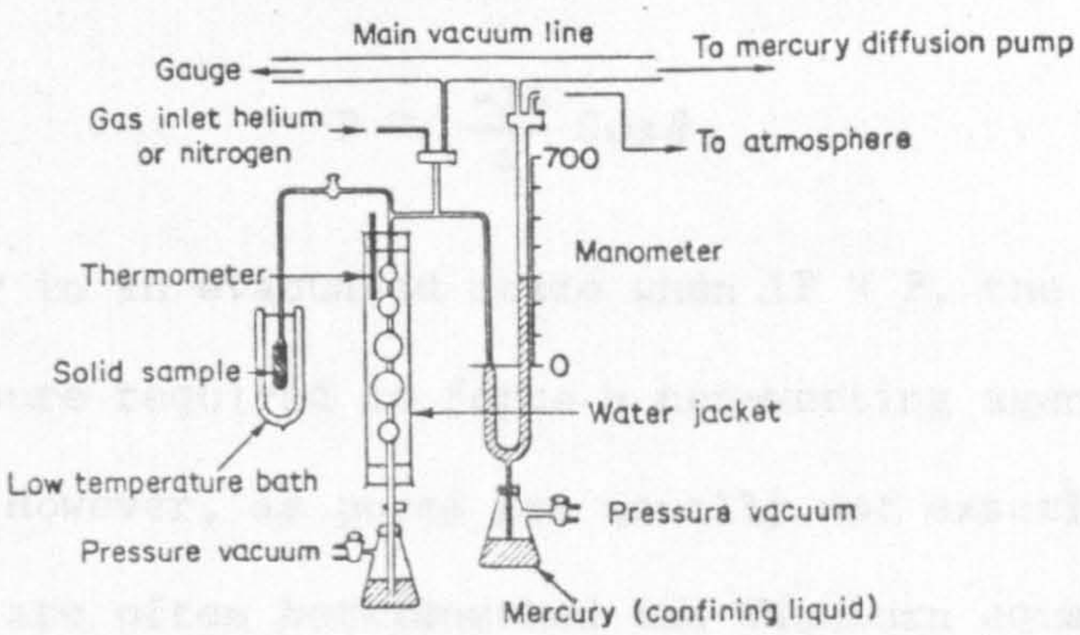


(b) Mercury Porosimetry

Mercury porosimetry is a technique widely used for the determination of the pore size distribution and the specific surface area of porous materials. The technique itself is based on an experimental observ--ation of the capillary rise phenomenon whereby an applied pressure is required to force a non-wetting liquid to climb up a narrow capillary. The pressure difference across a capillary interface is given by the Young and Laplace equation (1).

(1) $$P = \gamma\left[\frac{1}{r_1} + \frac{1}{r_2}\right] \cos\theta$$

Where $\gamma$ = Surface tension of the liquid

$r_n$ = Mutually perpendicular radii

$\theta$ = Angle of contact

If the capillary is circular in cross section and not too large in radius the meniscus will be approximately hemispherical. The two radii of curvature are thus equal to each other and to the radius of the capillary. The Young and Laplace equation then reduces to the Washburn equation (2), where r = radius of the capillary.

(2) $$P = \frac{-2\gamma}{r} \cos\theta$$

For a powder in an evacuated state when $\Delta P = P$, the absolute pressure is the pressure required to force a non-wetting agent into a pore of radius r. However, as pores are usually not exactly circular in cross section and are often bottlenecked the Washburn equation is at best only an approximation to a real system but in spite of this it has found widespread application in the field of mercury porosimetry.

A schematic diagram of a typical mercury porosimeter, similar to the one used in this investigation is shown in figure eleven. The sample cell which is usually constructed of glass consists of two parts shown in figure twelve, (a) is the portion which contains the sample and (b) is the cap with a precision bore tubing which constitutes the penetrato-meter. A weighted sample of powder is placed in the sample space, part (b) is then fitted onto part (a) and the sample holder is inserted into the pressure chamber. The sample is then subjected to a vacuum degassing, which for throughly dried materials need only consist of a few minutes outgassing at a pressure of 20mmHg. When the degassing is complete, mercury is introduced into the sample chamber until it completely covers the sample, and the container is full of mercury.

Figure Eleven - Continuous Recording Mercury Porosimeter

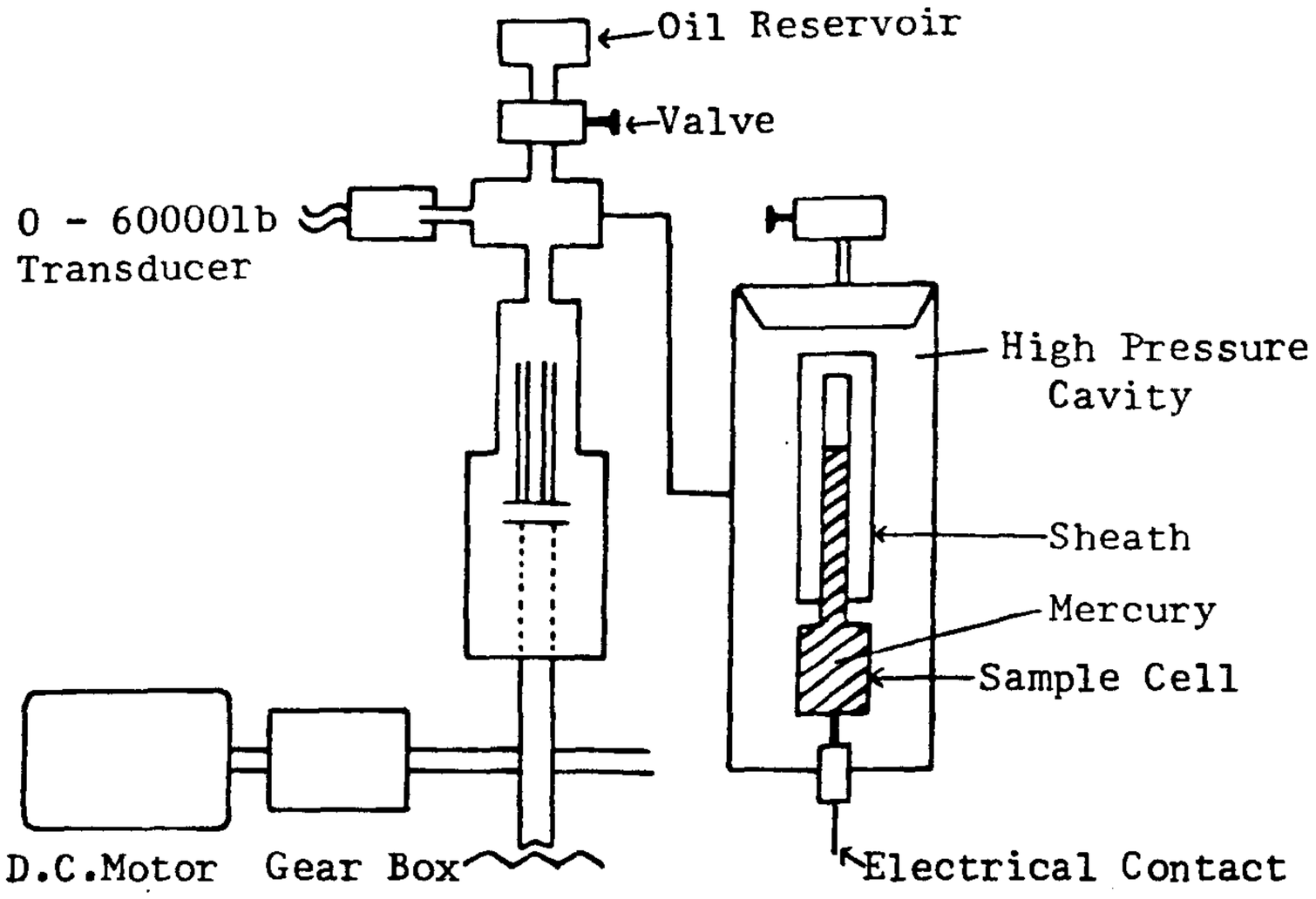


Figure Twelve - The Mercury Porosimeter Sample Cell

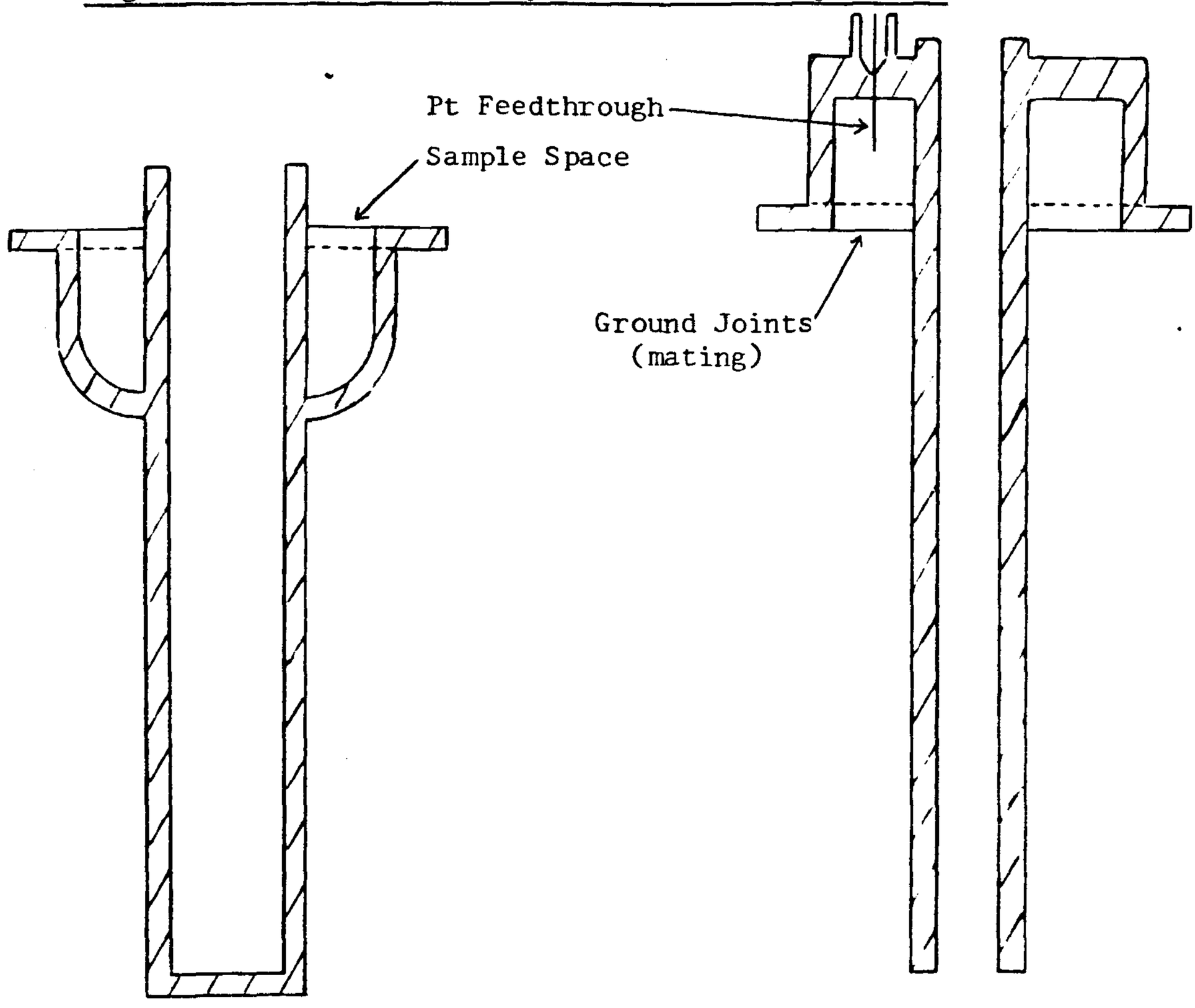

The pressure in the cell is then increased and the uptake of mercury by the sample is measured with increasing applied pressure. The uptake of mercury by the sample is usually measured electrically by a make or break contact probe, an example of which is shown in figure eleven. The experimental results from mercury porosimetry are usually presented in the form of a series of readings of applied pressure against the total volume of mercury uptake by the sample. Graphical plots of volume uptake against increasing applied pressure are called pressurising curves, and similarly plots of decreasing applied pressure against volume are called depressurising curves. Graphical integration of pressurising curves is used to obtain the pore size distributions for samples as well as their specific surface areas.

If the total volume of pores in a sample having radii between r and r + dr is dV, the relative pore frequency by volume is defined by.

$$D(r) = dV/dr$$

From the Washburn equation

$$0 = Pdr + rdP$$

Therefore

$$D(r) = (-P/r)\frac{dV}{dP}$$

$$= \frac{1}{r}\ \frac{dV}{d(\ln P)}$$

Therefore the total pore volume and the pore size distribution can be obtained from a graphical integration of a semi-log plot of mercury uptake against pressure. The surface area of the sample is given by (2) assuming that the values for the mercury contact angle of $140^{o}$ and the surface tension of 484 erg $cm^{-1}$ remain constant with increasing pressure.

$$S = 2{\cdot}645 \times 10^{-5}\int_{o}^{v} PdV\ (m^{2})$$

Pressure in $Kgm^{2}$

Volume in $cm^{3}$

The specific surface area for the sample can be obtained by dividing S by the degassed sample weight. The porosimeter used in this investig-ation was a Carlo Erba Strumentazione Porosimeter, Model M.O.D., situated at Brunel University, where all of the experimental work was carried out.

### 1.2.4. Mössbauer Spectroscopy

The Mössbauer effect is defined as the emission or absorbtion of a $\gamma$-ray by a nucleus without loss of energy due to the recoil of the nucleus and without thermal broadening. The importance of the effect is that it gives energy quanta of great precision which can be used to resolve minute energy differences, such as those which result from interactions between the nucleus and the electrons in an atom. Mössbauer spectro-scopy is thus concerned with the observation and measurement of the nuclear resonant absorbtion of $\gamma$-rays and associated fluorescence which result from the Mössbauer effect.

It was recognised by Kuhn[26] in 1927 that a $\gamma$-ray emitted during a nuclear transition should be capable of exciting a second ground state nucleus of the same isotope, thereby giving rise to nuclear resonant absorbtion and fluorescence. Unfortunately the high energy and momentum of the photon cause the nucleus to have a high recoil energy and so reduce the probability of detecting this resonant absorbtion to almost negligible proportions. A solution to this problem was discovered by R.L. Möss-bauer[27] in 1957. Under appropriate conditions in the solid state it was found to be possible to produce recoilless emission and absorbtion so the effect could easily be observed.

The $\gamma$-rays emitted in the recoilless events are an unusually good source of monochromatic radiation and have a spread in energy of $10^{-6}$KJ/mol.

In consequence it becomes possible to observe the weak interactions of the nucleus with its chemical enviroment. One of the unusual features of Mössbauer spectroscopy is the way in which these energy differences, of the order of 1 part in $10^{12}$, are measured. Such differences can be produced by the Doppler Effect. Thus if a $\gamma$-ray of energy E is emitted from a source moving with a relative velocity v the apparent energy is $(1 + (v/c))E$ , where c is the velocity of light. The emitting nuclei can therefore be moved in and out of resonance by merely a relative mechanical motion. A Mössbauer spectrum is therefore a record of the transmission rate of the resonant $\gamma$-rays as a function of the Doppler velocity between the source and the absorber.
A schematic diagram of a typical working Mössbauer spectrometer is shown in figure thirteen.

Figure Thirteen - A Mössbauer Spectrometer

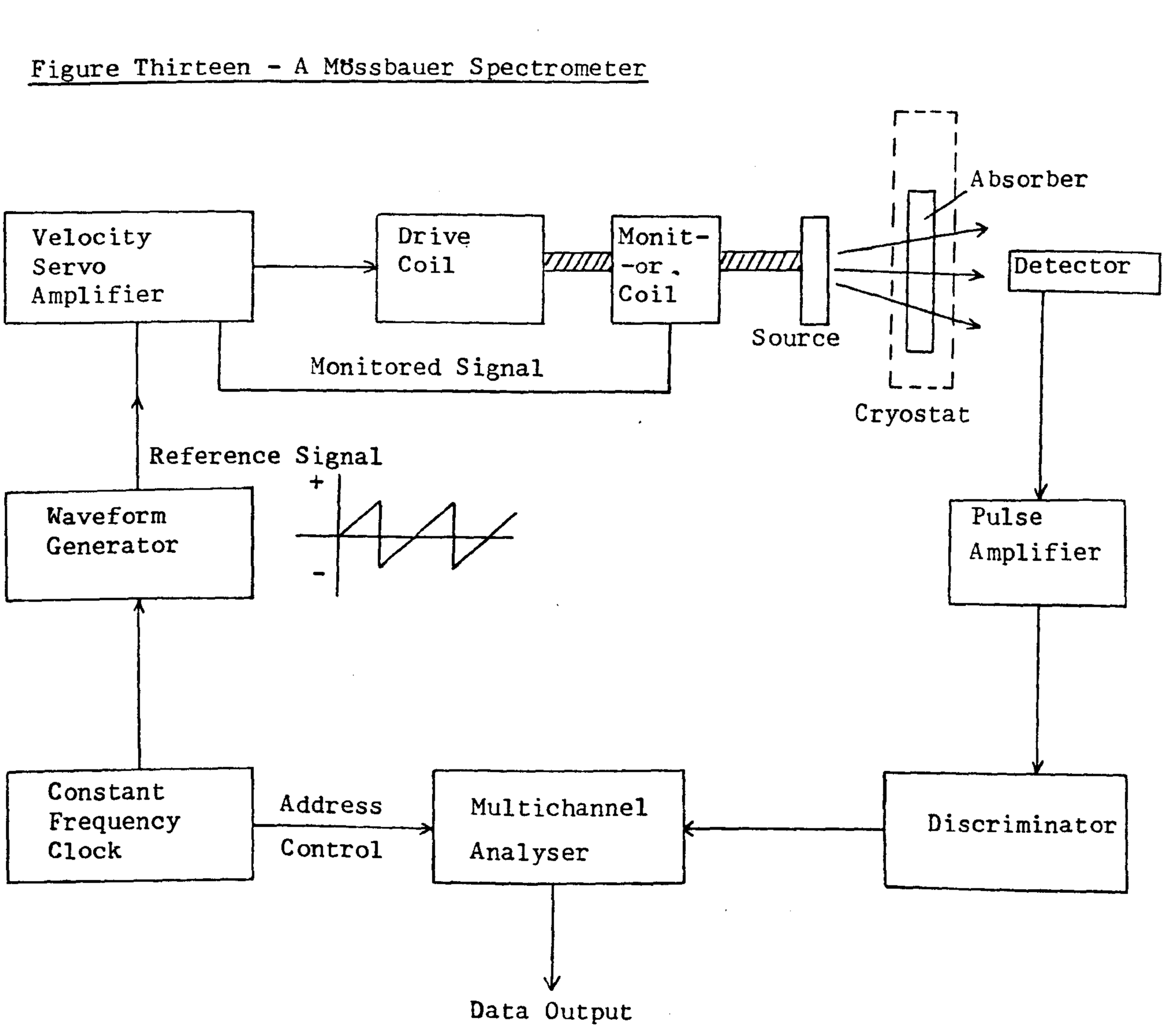

R.L. Mössbauer[27] found that by cooling the sample to liquid nitrogen temperatures in a cryostat the $\gamma$-ray absorbtion was maximised together with the nuclear recoil energy being minimised. The recording of a Mössbauer spectrum is usually acheived by mounting the source on a mechanical device so that the whole velocity range can be repeatedly scanned on a cyclical basis. The Mössbauer spectrum is then built up from a Fourier Transform analysis of the transmitted radiation over a period of time. The usefulness of the Mössbauer effect lies in the fact that the energy of a Mössbauer nucleus is influenced by its chemical environment and so by recording the Mössbauer spectrum of a nucleus its formal oxidation state and its symmetry may be determined.

The Hamiltonian describing the energy of the nucleus may be written as.

$$H = H_o + E_o + M_1 + E_2$$

$H_o$ = All terms except for hyperfine interactions with the environment.

$E_o$ = Coulombic interaction with electrons which gives rise to a separation of the ground and excited states of the nucleus and thus can cause a shift in the position of the resonance line. This is known as Chemical Isomer Shift.

$M_1$ = Interaction of nuclear spin with the magnetic field either intrinsic or extrinsic to the atom. The effect of the interaction is to split the resonance line into a multiplet line structure, this is known as Magnetic Hyperfine Splitting.

$E_2$ = Interaction of the nucleus'es quadrupole moment with the local electric field produced by the surrounding charge distribution. This also results in line splitting and is known as an Electric Quadrupole Interaction

Factors which influence the magnitude of the chemical isomer shift observed for a nucleus are;

(a) The 's' electron density at the nucleus

(b) p, d and f electron shielding

(c) Covalency effects

(d) $\sigma$ electron withdrawal due to electronegative groups

(e) Deshielding effects due to d$\pi$ backbonding

Of the above, the major factor influencing the magnitude of chemical isomer shift is the 's' electron density at the nucleus.

Observation of chemical isomer shifts, then, allows measurement of the s electron density which in turn gives an estimate of the bond character of atoms or ions chemically attached to the Mössbauer nucleus. Some chemical isomer shifts observed for tin species are given in table five.

Table Five - Chemical Isomer Shifts of $^{119}Sn$ Nuclei

| Tin Nuclei | Electronic Configuration | Chemical Isomer Shift $\delta$ / mm/sec |
|---|---|---|
| $Sn^{4+}$ | $5s^0$ | -6·0 |
| $SnO_2$ | | 0·0 |
| $SnCl_4$ | | +1·3 |
| $\alpha$ Sn | | +2·1 |
| $SnCl_2$ | | +3·5 |
| $Sn^{2+}$ | $5s^2$ | +6·0 |

The sign of the chemical isomer shift is dependant upon whether or not the radius of the excited state nucleus is larger or smaller than that of the ground state.

$$\text{Chemical Shift} = \text{Constant}\ (\rho^2_{ex} - \rho^2_{gs}) \left[\frac{R_{ex} - R_{gs}}{R_{gs}}\right]$$

Where $\rho$ = s electron densities of excited and ground state nuclei

and R = radii of excited and ground state nuclei.

For $^{119}Sn$ the value of $(R_{ex} - R_{gs})/R_{gs}$ is positive so a negative chemical isomer shift corresponds to a decrease in s electron density at the nuc--leus.

Electrical quadrupole splitting of Mössbauer resonance lines results from the interaction between the nuclear spin and the local electric field gradient. The majority of Mössbauer nuclei have non-zero spins and the spin of excited nuclei is invariably different from the spin of the nuclei in the ground state. Whenever a nuclear level has a spin of $I > \frac{1}{2}$ it will possess a nuclear quadrupole moment which can then interact with any non-zero electric field gradients across the nucleus to produce line splitting. For $^{119}Sn$ with nuclear spins of $I_{gs} = \pm\frac{1}{2}$ and $I_{ex} = \pm\frac{3}{2}$ this effect is shown in figure fourteen. The degree of electrical quadrupole splitting in a Mössbauer spectrum is therefore a measure of the symmetry of the electronic environment of a nucleus and relates directly to the electronic orbitals involved in bonding. Mössbauer spectra recorded for nuclei with $I > \frac{1}{2}$ which exhibit no quadrupole splitting indicate that those nuclei are in symmetrical environment.

Magnetic hyperfine interactions arise from magnetic flux at the nucleus causing the nuclear levels to split into $(2I+1)$ non-degenerate lines. No magnetic hyperfine interactions were observed in any of the Mössbauer spectra recorded in this work and no further treatment of the phenomenon is given here for that reason.

Mössbauer spectroscopy was used in this investigation to examine the thermal decomposition of indium tin benzoate, the thermal dehydration of metastannic acid and, tin oxide based semiconductors.

Figure Fourteen - Electrical Quadrupole Splitting in $^{119}Sn$ Nuclei

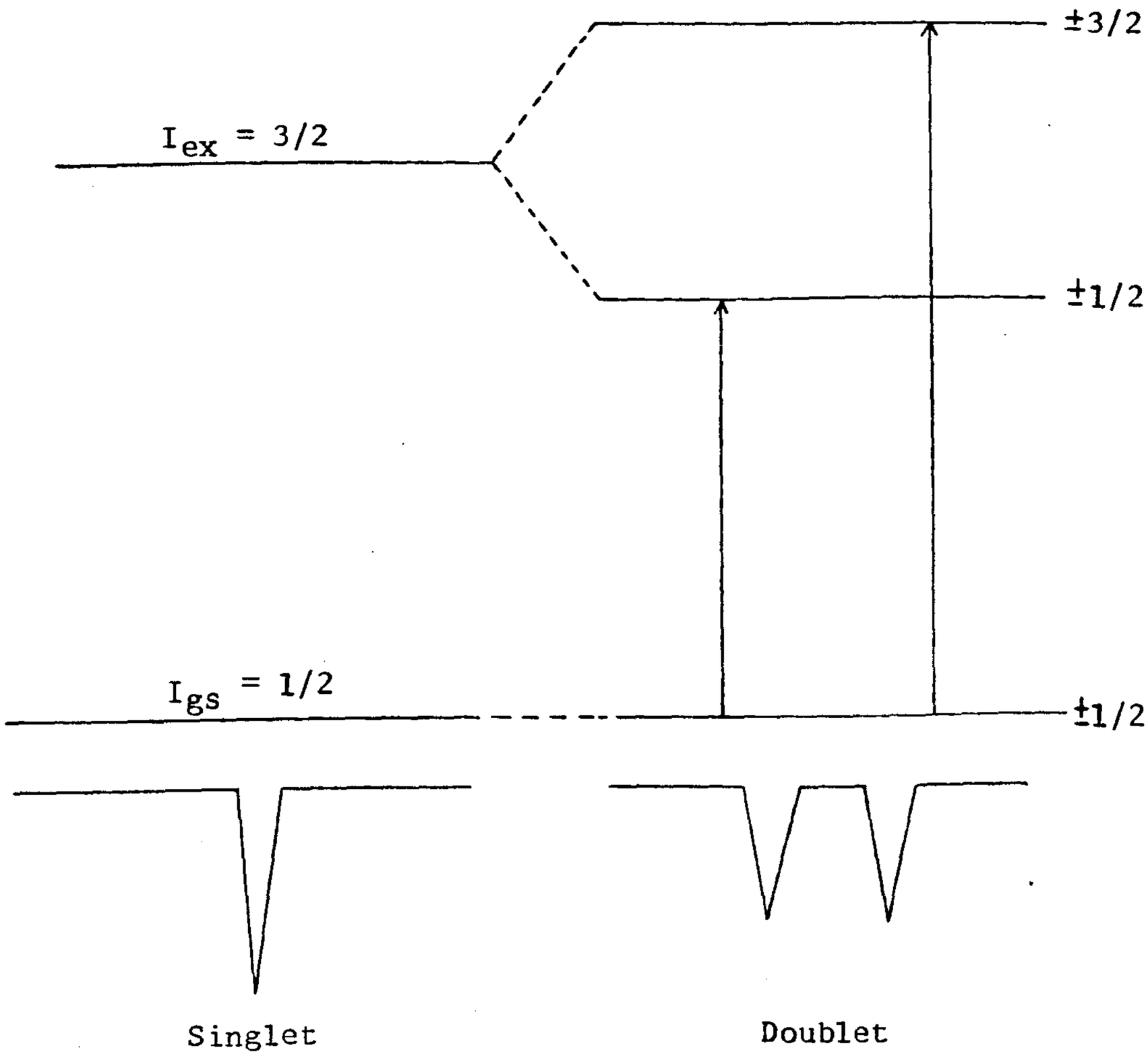


## 1.2.5. Powder X-Ray Diffraction

X-rays have wavelengths from 0·02 to 0·2nm. The shorter wavelengths are known as the harder and more penetrative x-rays; the longer wave--lengths are softer and more easily absorbed. For crystallographic studies wavelengths of about 0·1nm are used. X-rays are produced by a stream of electrons (cathode rays) bombarding an anode, or target. Just as light is diffracted from a grating of very closely spaced lines so x-rays are diffracted from the three dimensional array of equivalent points of the crystal lattice. In the diffraction of light each aper--ture in the grating functions as a new source of rays; so in the crystal each atomic electron cloud set into vibration by the x-rays acts as a source of secondary rays of the same wavelength.

W.L. Bragg[28] in 1912 showed that x-rays behaved in these circumstances exactly as if they had been reflected from the planes of atoms making up the crystal lattice. Figure fifteen shows a set of atomic planes together with a train of x-rays striking them at an angle $\theta$. The x-rays penetrate the layers, but are also reflected by them. The reflected rays from all planes of the set take the same direction, and if they are out of phase they will interfere with each other and be destroyed. Only if the difference in path between rays reflected from succesive planes is an integral number of wavelengths, will they reinforce each other and form a reflected beam. From figure fifteen the difference in path between rays reflected from succesive planes is ef + fg. Furthermore, ef = fg $=(\sin\theta)d$, hence the condition for succesful reflection is given by the Bragg Law.

$$n\lambda = 2d.\sin\theta$$

where n = any integer

d = interplanar spacing

$\theta$ = glancing angle of incidence

Thus, from the Bragg Law it becomes apparent that a set of planes of a particular spacing can reflect x-rays at one angle of incidence only. Therefore once the wavelength of x-rays incident on a crystal and the angle of reflectance are known, the interplanar spacing may be found.

Angular positions of the reflected x-rays are usually recorded in relation to the dircetion of the undeviated beam. Two types of methods are employed in x-ray crystallography for obtaining measurements of reflected rays from samples, one for single crystals and the other for powders. In this investigation all of the samples prepared were synthesised as powders and so the second technique proved to be most applicable to this work.

Figure Fifteen - The Bragg Angle of Reflection

(a) Condition for Reflection

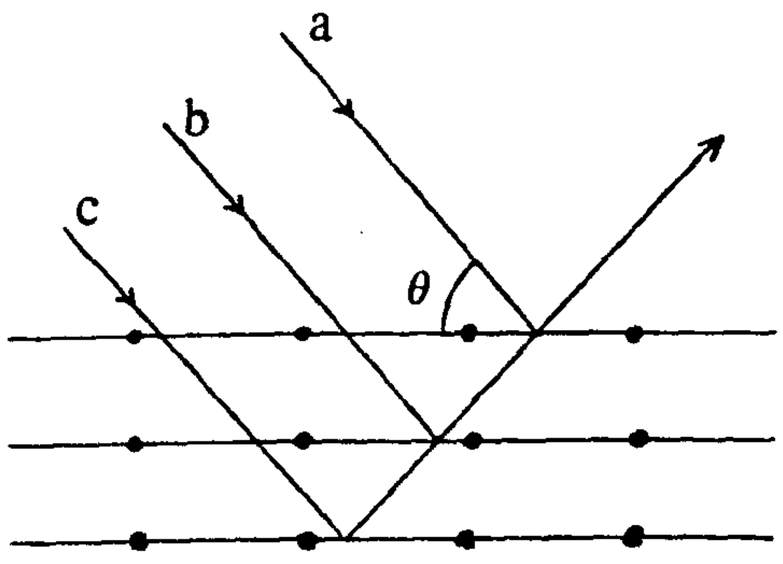


(b) Path Difference = $2d.\sin\theta$

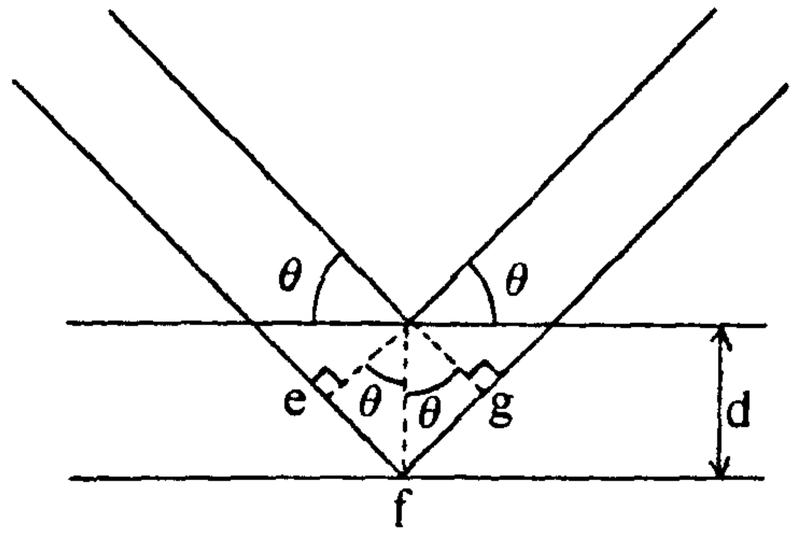


Figure Sixteen - The Counter Diffractometer

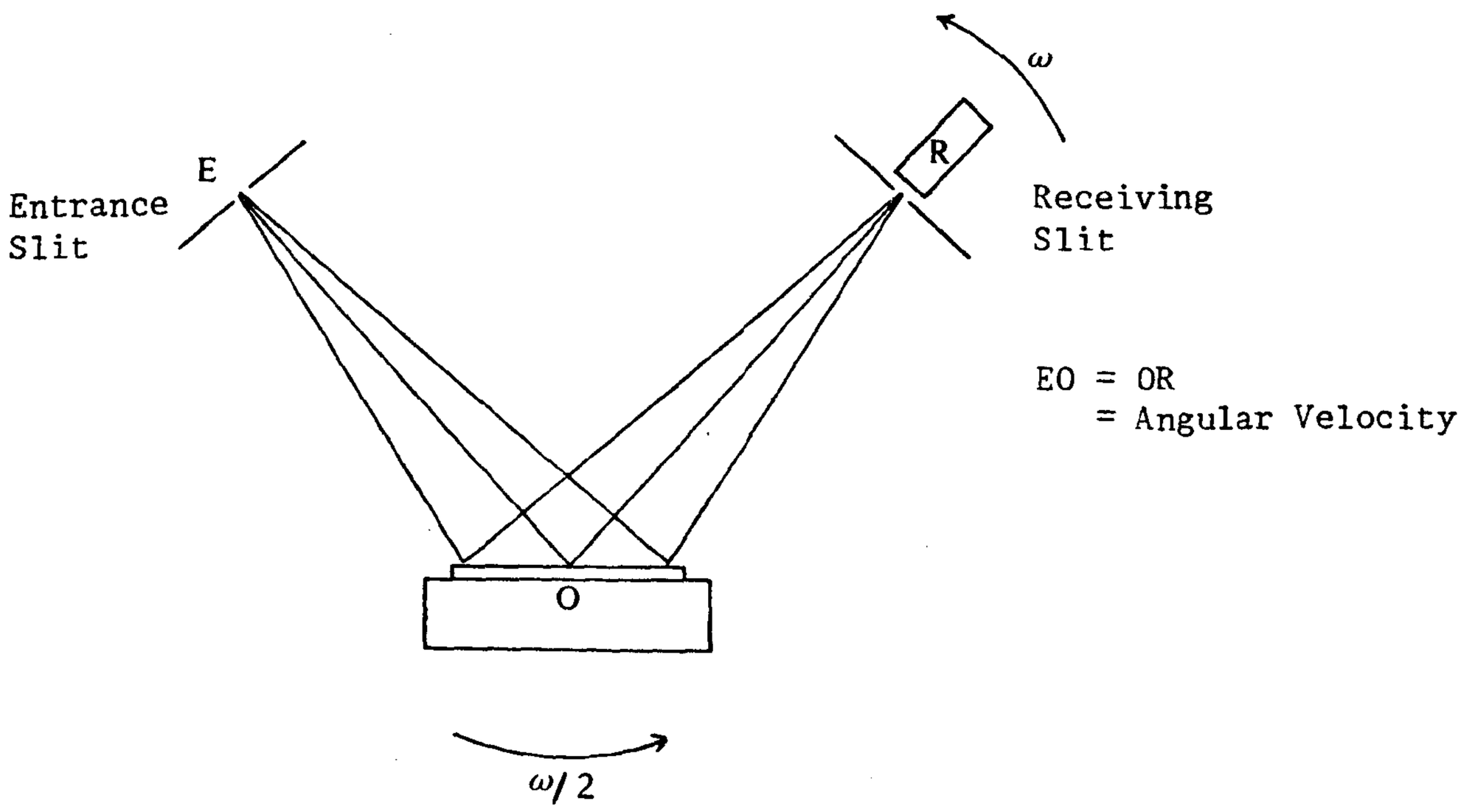

The ideal powder sample consists of an enormous number of very tiny crystals of size $10^{-3}$cm or smaller with completely random orientation. For any set of planes with spacing d(hkl), there are many crystals orientated so that their hkl planes make the correct Bragg angle $\theta$ with the primary beam. Since the correctly orientated crystals all have orientations about the primary beam, the diffracted beams form a cone of half apex angle $2\theta$ . For each planar spacing d(hkl) there is a cone of angle $2\theta$(hkl). Powder patterns are usually registered by film recording or by counter diffractometer, the diffractometer process is shown schematically in figure sixteen.

To obtain an x-ray diffractometer pattern the sample is usually prepared in the form of a flat plate placed upon a glass microscope slide. Care however has to be excercised in the preparation of a sample for analysis to ensure that the randomness of the crystallite orientation in the sample is not accidentally destroyed. The specimen once prep--ared is placed at the centre of rotation of the diffractometer on a mounting block, and must be accurately positioned so that it is tangent and parallel to the diffractometer's axis of rotation.

As every crystalline material produces a different characteristic powder pattern, due to variation in cell dimensions and types of atoms within the atomic planes, the immediate use of powder x-ray diffract--ion data is in material identification. A comprehensive index of powder patterns for crystalline substances is compiled by The American Society for Testing Materials,for the identification of crystals[29].

As atomic substitution into a crystal lattice results in small changes in unit cell dimensions and hence in the positions of powder lines. X-ray diffraction also provides a convenient method for the identific--ation of the presence of dopant and impurity species within a lattice. In this investigation powder x-ray diffraction techniques were used to follow the growth of crystalline phases from amorphous substrates at elevated temperatures and to identify the presence of dopant species in mixed metal oxide semiconductors. The instrumentation used in this investigation was a Phillips PW1010 X-Ray Diffractometer and the powder diffractograms were obtained using copper K$\alpha$ radiation.

### 1.2.6. Thermal Analysis

Thermal analysis is the name applied to a group of techniques with a common operating principle, viz as a sample is heated or cooled according to a predetermined programme, some physical property of the sample is recorded as a function of temperature on a thermal analysis curve. Therefore a thermal analyser is an instrument which enables a sample to be heated at a uniform rate whilst its temperature and one or more of its physical properties are being measured and recorded. To forfill this purpose such an instrument, must contain the following basic units;

(i) A measuring unit,

(ii) A temperature control unit and

(iii) A recording unit.

Two methods of thermal analysis were used in this investigation, thermal gravimeteric analysis and differential thermal analysis. A brief introduction to each is given overleaf.

(a) Thermal Gravimetric Analysis

As a material decomposes upon heating it loses volatile materials which escape from the sample so causing a decrease in weight. Thermal grav--imetric analysis is therefore the measurement of the weight changes which occur in a test sample upon heating or cooling. The results of thermal gravimetric analysis are usually plotted out in the form of a graph of percentage weight loss against temperature. A typical thermal gravimetric curve will show a series of sharp weight losses separated by plateaus of constant weight. In general since the rate of chemical reactions is temperature dependant weight losses do not occur at one temperature, but over a range and may even overlap. For this reason care must be excercised when attempting to interpret the results of thermal gravimetric data. In general thermal gravimetry can be used to follow reactions which conform to one or more of the three basic reaction schemes shown in (i) to (iii) below.

(i) $C_r \longrightarrow G_p$

(ii) $C_r \longrightarrow C_p + G_p$

(iii) $C_r + G_r \longrightarrow C_p$

Where C = solid and G = gas and the subscripts p and r indicate product and reactant respectively. Thermal gravimetry can be used to study chemical processes involving desolvation and thermal/thermo-oxidative degradation, the technique is also useful in the determination of mater--ial purity and in compound identification.

In this investigation thermal gravimetric analysis was performed along--side differential thermal analysis using a Stanton Redcroft STA 780 Simultaneous Thermal Analyser, which is described in the next section.

(b) Differential Thermal Analysis

Differential thermal analysis (D.T.A.) is a technique which involves heating or cooling a test sample and an inert reference sample under identical conditions and recording any temperature difference which develops between them. Thus a differential thermogram consists of a record of the difference in the sample and reference temperatures ($\Delta T$) plotted as a function of time, sample temperature, reference temperature or furnace temperature. In theory any transition or reaction which is accompanied by an absorbtion or emission of heat, or by a change in heat capacity can be followed by differential thermal analysis. Processes which involve a continuous change in heat cap--acity are known as first order transitions whereas processes which involve a discontinuous change in heat capacity are known as second order transitions. Some common causes of first order transitions are, melting and boiling points and crystalline rearrangements, common causes of second order transitions are, glass transitions in polymers and curie point transitions in magnetic materials.

A schematic diagram of a simultaneous thermal analyser of the type used in this investigation is shown in figure seventeen. When carrying out differential thermal analysis fine control over the atmosphere flow--ing through the furnace in the vicinity of the sample is essential in maintaining an even furnace temperature, the choice of an inert or reactive atmosphere is usually dependant upon the sample type and the purpose of the analysis. Static atmospheres have disadvantages in that they may allow decomposition products to condense on cooler parts of the instrument and that also they tend to promote secondary reactions between products and the residual sample.

Figure Seventeen - A Schematic Representation of a Simultaneous Thermal Analyser

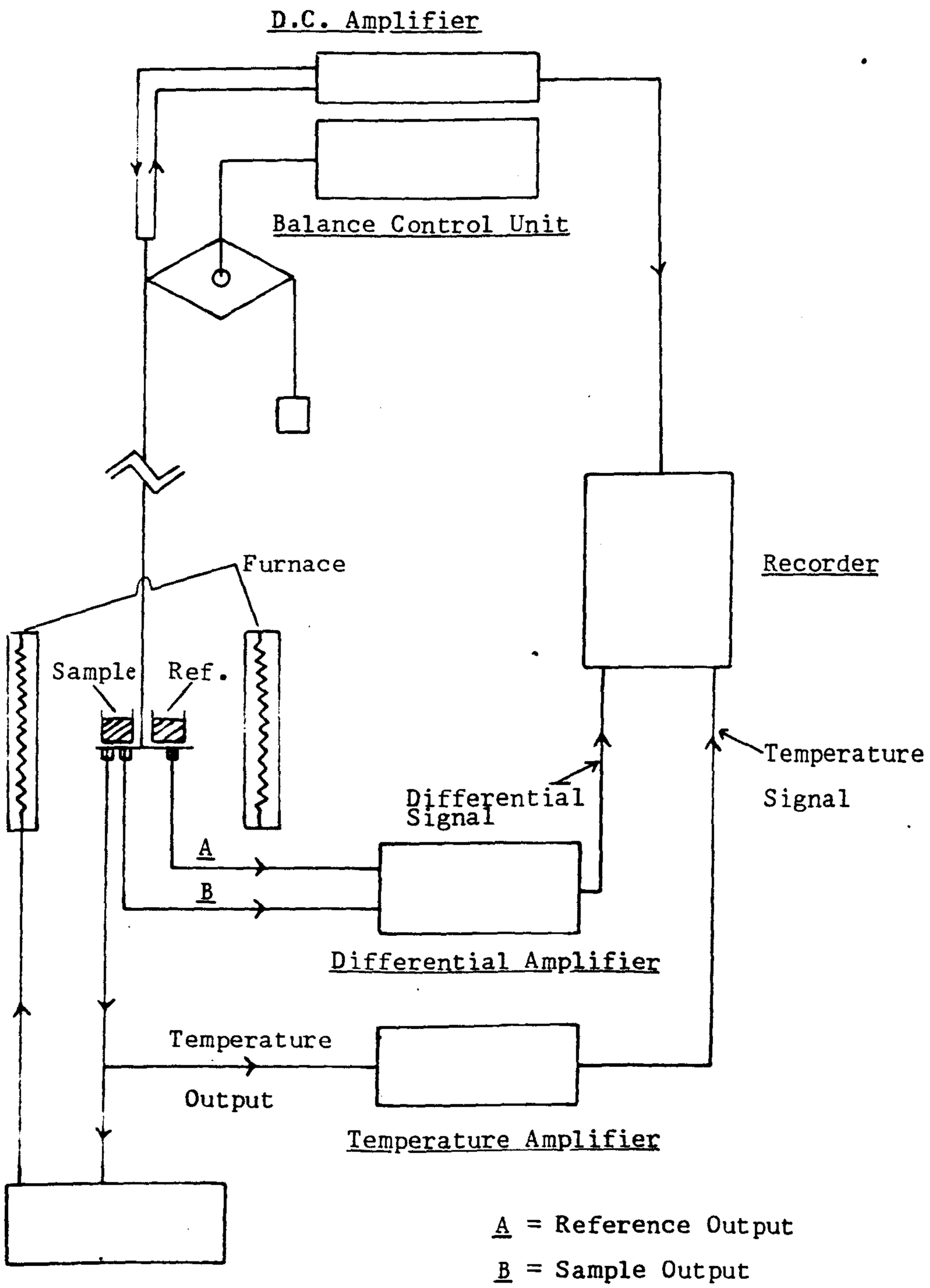

Any physical or chemical change which occurs within the test sample which involves evolution of heat will cause its temperature to rise temporarily above that of the reference sample and will result in an exothermic peak being recorded. Conversely any process which is accompanied by the absorbtion of heat will cause the temperature of the sample to lag behind that of the reference sample and will result in an endothermic peak being recorded.

As well as the peak type providing information about the test sample, the peak shape is also of analytical value, but the information it will yield is usually only of an empirical nature. Generally physical transitions give very sharp peaks, chemical reactions give broad peaks and irregular peaks are indicative of sample collapse. In addition, D.T.A. peaks need not be symmetrical as the conditions after the peak has been reached are quite different from the initial conditions, and often peaks may become superimposed.

References

1. E. Fremy, Compt. Rend., 1842, 14, 442.

2. A. Kleinschmidt, Monatsch, 1918, 39, 149.

3. J.M. Van Bemmellen, 'Die Absorption", T. Steinhopff, Dresden 1910.

4. A. Lorenz, Z. Anorg. Chem., 1895, 9, 369.

5. W. Meckelberg, Z. Anorg. Chem., 1909, 64, 368.

6. W. Meckelberg, Anales. Soc. Espan., Fis. Quim., 1911, 9, 261.

7. W. Meckelberg, Z. Anorg. Chem., 1911, 74, 207.

8. W. Meckelberg, Z. Anorg. Chem., 1913, 78, 242.

9. A.S. Menon, Kolloid-Z., 1937, 78, 242.

10. A.M. Babeshkin, P.B. Fabrichnyi and A.N. Neshmeinanov, Proc. Conf. Appl. Moss. Eff., (1969), Budapest 1971, page 319.

11. J.D. Donaldson and M.J. Fuller, J. Inorg. Nucl. Chem., 1968, 30, 1083.

12. M.J. Fuller, M.E. Warwick and A. Walton, J. Appl. Chem. Biotechnol., 1978, 28, 396.

13. J.F. Goodman and S.J. Gregg, J.C.S., 1960, part 1, 1162.

14. Literature Survey on Metastannic Acid, J.D. Donaldson, City University, London, 1980.

15. J. Knuckel, Voll. Standiges Laboratorium Chymicum, Berlin, 1716.

16. J. Berzelius, Ann. Chim. Phys., 1813, 1, 50.

17. C.R. Engel, Comptes. Rend., 1897, 124, 765.

18. C.R. Engel, Comptes. Rend., 1897, 125, 464.

19. A. Scheurer Kestner, Ann. Chim. Phys., 1816, 1, 40.

20. A. Neuman, Ber., 1904, 37, 3601.

21. J.L. Gay-Lusaac, Ann. Chim. Phys., 1816, 1, 40.

22. S. Kittaka, S. Kanemoto and T. Morimoto, J.C.S., Faraday Trans., 1978, 74, 676.

23. S. Oden, Kolloid-Z., 1916, 18, 33., 1919, 26, 100.

24. R.H. Berg, A.S.T.M., Publication No. 234 (1958).

25. S. Brunauer, P.H. Emmett and E. Teller, J. Am. Chem. Soc., 1938, 60, 309.

26. W. Khun, Phil. Mag., 1929, 8, 625.

27. R.L. Mossbauer, Z. Physik, 1958, 151, 124.

28. W.L. Bragg, Proc. Camb. Phil. Soc., 1912, 17, 43.

29. Standard X-Ray Diffraction Powder Patterns, National Bureau of Standards.

# Chapter Two - An Investigation into Hydrous Metal Oxide Chemistry

## Section 2.1 - The Stannic Acids

## Section 2.2 - Hydrous Metal Oxide Chemistry: A Comparative Study

## Chapter Two - An Investigation into Hydrous Metal Oxide Chemistry

### 2.1 The Stannic Acids

There are three forms of hydrous tin (IV) oxide, the so called ortho ($\alpha$)*, meta ($\beta$)* and para ($\gamma$)* stannic acids which are said to be formed from the hydrolysis of solutions of tin (IV) salts. Orthostannic acid can be formed from the slow, low temperature hydrolysis of any tin (IV) salt wheras metastannic acid can only be produced from the rapid, high temperature hydrolysis of tin (IV) nitrate which must be formed in situ by the action of nitric acid upon tin metal. The third form of hydrous tin oxide, parastannic acid, corresponds to an aged form of orthostannic acid which in its chemical and physical properties is very similar to metastannic acid. In fact meta and para stannic acids have often been mistaken for each other in the early literature, but the two materials can be shown to be quite different by thermal and x-ray analysis. Results of thermal gravimetric and differential thermal analysis on samples of the three stannic acids, are given in figures one to three and in table one, and show that all three of the materials lose water on heating and become completely dehydrated at around 600°C.

Table One - Thermal Analysis of $\alpha$, $\beta$ and $\gamma$ Stannic Acids

| Sample | Temp. at Which Water loss Starts / °C | Temp. of Max Rate of Water loss/ °C | Temp. at which Water loss ends /°C | Wt. $\%H_2O$ |
|---|---|---|---|---|
| $\alpha$ | 36 | 60 | 600 | 20 |
| $\beta$ | 50 (phys) | 105 (phys) | 157 (phys) | |
| | 157 (chem) | 200 (chem) | 600 (chem) | 11 |
| $\gamma$ | 70 | 94 | 600 | 10 |

* Alternative Notation

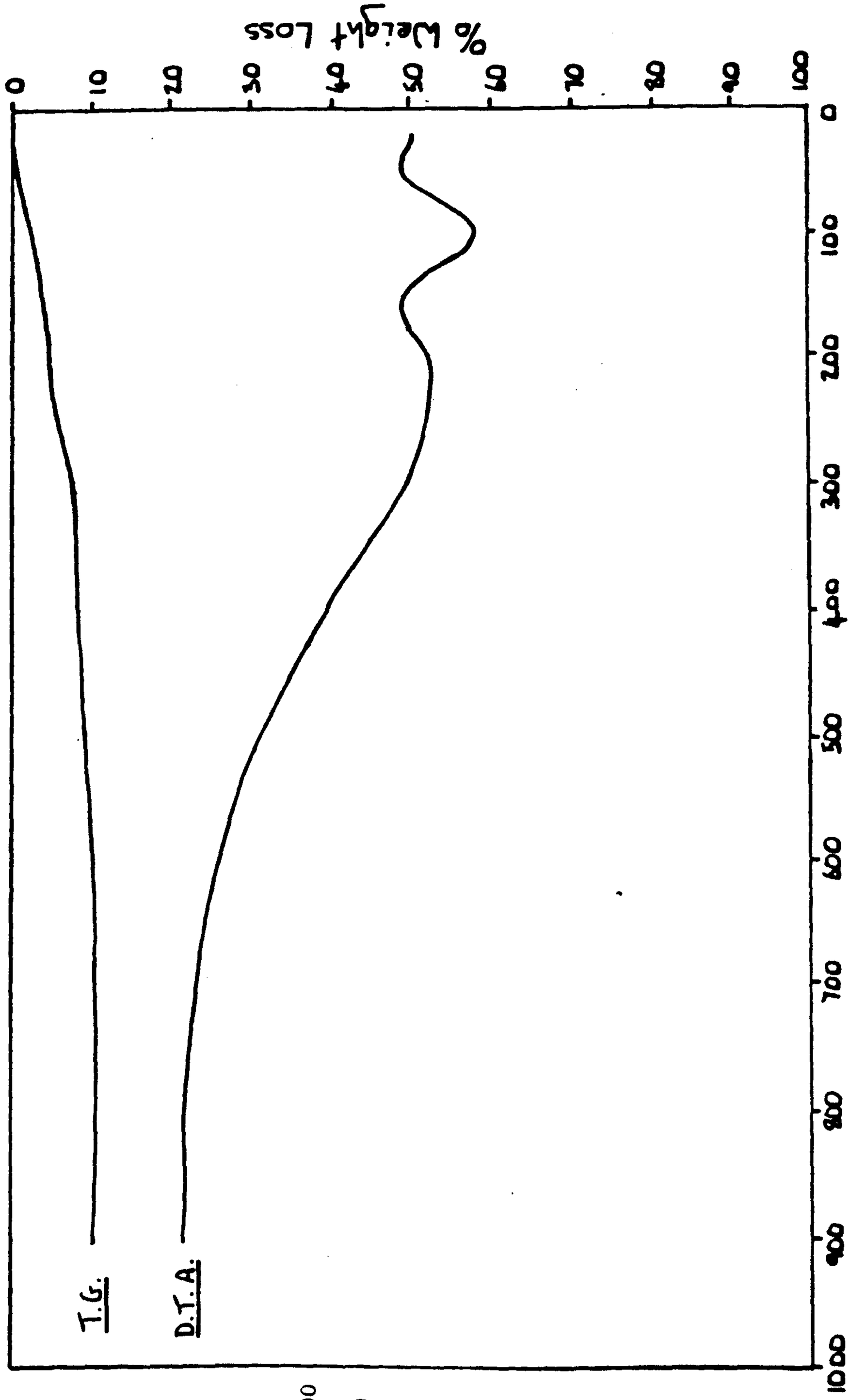


Figure One - Thermal Analysis of Metastannic Acid

PAGE
NUMBERS
CUT OFF
IN
ORIGINAL

A thermal analysis of an aged sample of metastannic acid, which had been boiled in aqueous solution for three hours, was found to be identical with that of the freshly precipitated material. The values for the percentage weight water content column in table one will vary from sample to sample as all three of the stannic acids may be prepared with varying amounts of water in the 'dried'materials. This observation justifies the use of the term 'hydrous' oxides in describing the mat--erials implying that water is bound both chemically and physically onto the surface of the material in non-stoichiometric proportions.

The effect of water loss on the structures of the hydrous oxides was investigated by x-ray powder diffraction studies on ortho, meta and para stannic acids, recorded for samples oven dried at 70$^{o}$C and thermally dehydrated at 600$^{o}$C are given in figures four to six, the diffraction data are in table two. A standard powder x-ray diffractogram for tin (IV) oxide is given in figure seven and the data are in table three. Tin (IV) oxide (stannic oxide), the parent species, occurs naturally as the mineral cassiterite with a tetragonal structure[1], though rhombic and hexagonal varieties of the material have also been reported[2,3].

The results of x-ray analysis show that whilst freshly precipiatated orthostannic acid is amorphous both meta and parastannic acids display residual rutile structure. All three stannic acids lose water upon calcination to give the parent tin (IV) oxide with crystal growth of the tetragonal rutile structure beginning at around 600$^{o}$C after water loss is complete.

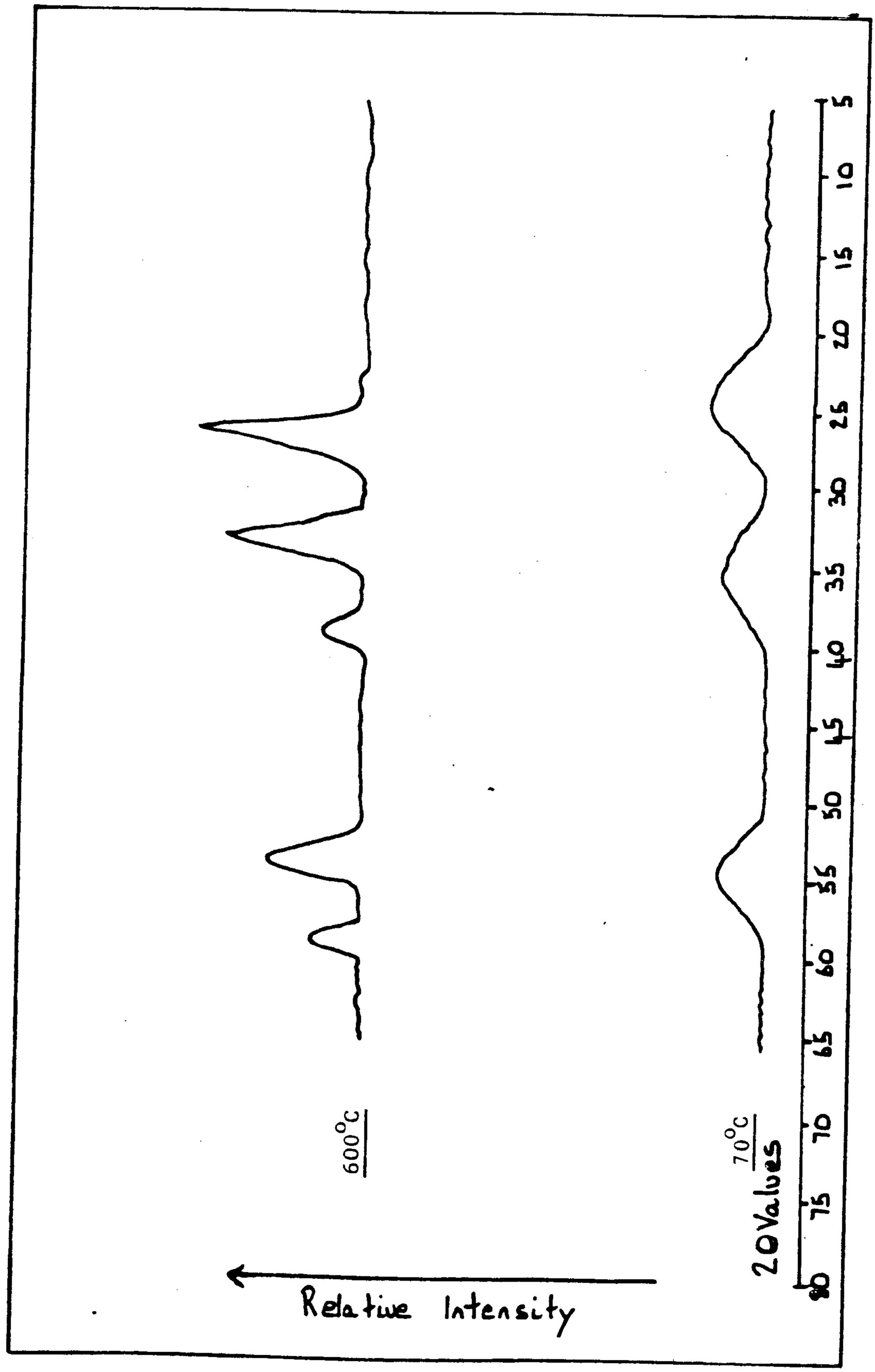


Figure Four - Powder X-Ray Diffractograms for Metastannic Acid

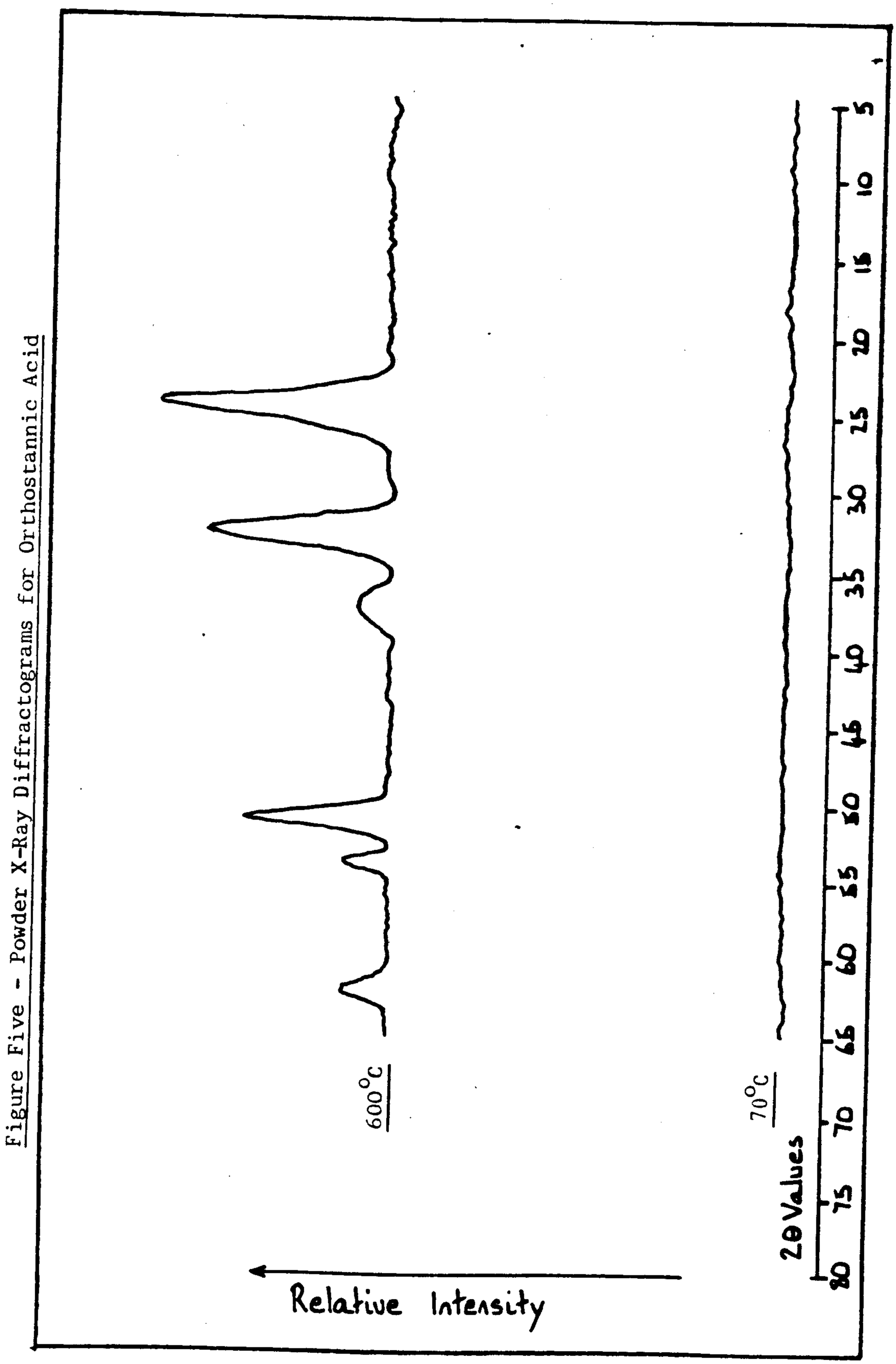


Figure Five - Powder X-Ray Diffractograms for Orthostannic Acid

Figure Six - Powder X-Ray Diffractograms for Parastannic Acid

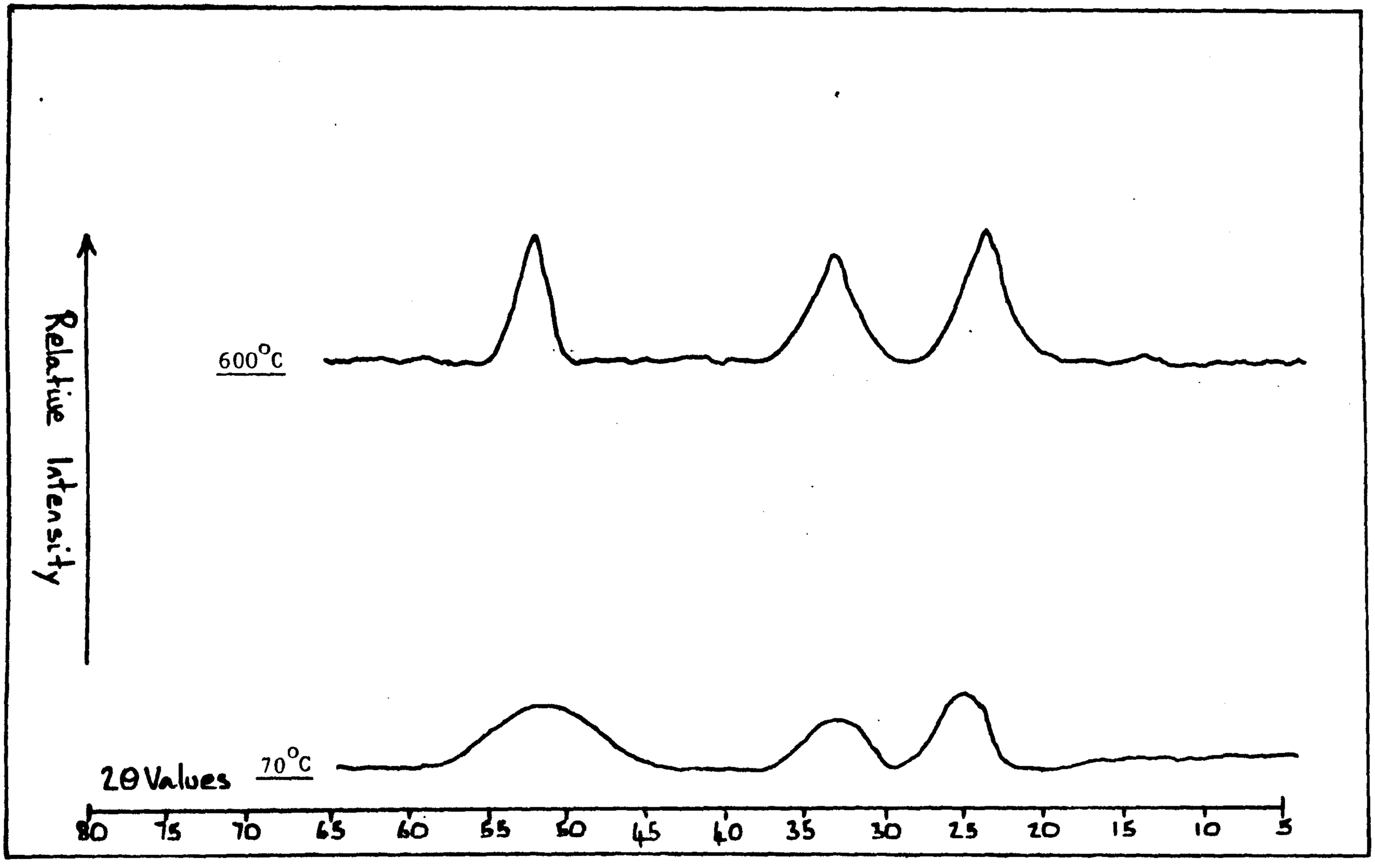

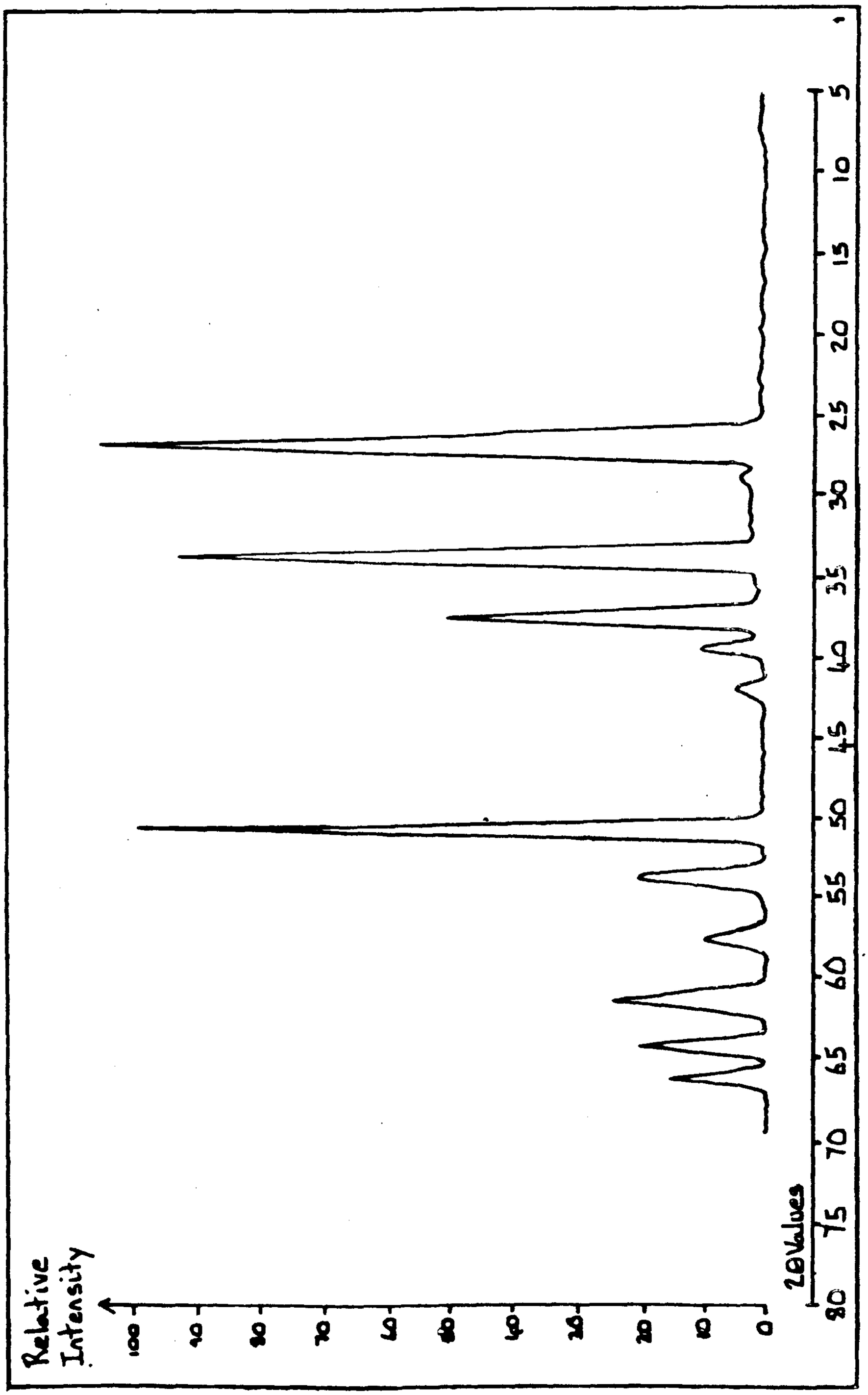


Figure Seven - Powder X-Ray Diffratogram of Tin (IV) Oxide

Table Two - Powder X-Ray Diffraction Data for $\alpha$, $\beta$ and $\gamma$ Stannic Acids

| $2\theta$ | $d_{spacing}$ | $I_{meas}$ | $I_{100}$ |
|---|---|---|---|
| $\alpha$Stannic Acid - 70°C | | | |
| | No Data - Amorphous | | |
| $\alpha$Stannic Acid - 600°C | | | |
| 26.6 | 3.3510 | 17.5 | 100.0 |
| 34.0 | 2.6367 | 14.5 | 82.8 |
| 37.9 | 2.3739 | 3.0 | 17.1 |
| 51.8 | 1.7649 | 13.0 | 74.3 |
| 54.6 | 1.6808 | 3.5 | 20.0 |
| 62.0 | 1.4968 | 3.0 | 17.1 |
| $\gamma$Stannic Acid - 70°C | | | |
| 26.4 | 3.3759 | 6.0 | 100.0 |
| 33.4 | 2.6827 | 4.0 | 66.7 |
| 51.9 | 1.7616 | 5.0 | 83.3 |
| $\gamma$Stannic Acid - 600°C | | | |
| 26.6 | 3.3510 | 11.0 | 100.0 |
| 33.9 | 2.6443 | 8.8 | 80.0 |
| 52.1 | 1.7554 | 9.0 | 81.8 |
| $\beta$Stannic Acid - 70°C | | | |
| 26.1 | 3.4141 | 11.0 | 100.0 |
| 33.0 | 2.7143 | 10.0 | 90.1 |
| 51.7 | 1.7681 | 6.0 | 54.5 |

| $2\theta$ | $d_{spacing}$ | $I_{meas}$ | $I_{100}$ |
|---|---|---|---|
| $\beta$Stannic Acid - 600°C | | | |
| 26.5 | 3.3634 | 27.0 | 100.0 |
| 33.7 | 2.6595 | 23.0 | 85.1 |
| 38.2 | 2.3539 | 8.0 | 29.6 |
| 52.7 | 1.7368 | 16.0 | 59.3 |
| 55.5 | 1.6557 | 8.0 | 29.6 |

Table Three - Powder X-Ray Diffraction Data for Tin (IV) Oxide

| $2\theta$ | $d_{spacing}$ | $I_{meas}$ | $I_{100}$ |
|---|---|---|---|
| 26.7 | 3.3387 | 111.0 | 100.0 |
| 28.7 | 3.1104 | 3.5 | 3.2 |
| 33.9 | 2.6443 | 109.0 | 98.2 |
| 37.8 | 2.3799 | 46.0 | 41.4 |
| 38.9 | 2.3151 | 7.5 | 6.8 |
| 42.6 | 2.1222 | 3.5 | 3.2 |
| 51.8 | 1.7649 | 26.0 | 23.4 |
| 54.7 | 1.6780 | 13.0 | 11.7 |
| 57.8 | 1.5951 | 11.5 | 10.4 |
| 61.9 | 1.4990 | 23.5 | 21.2 |
| 64.7 | 1.4407 | 23.0 | 20.7 |
| 65.0 | 1.4348 | 31.0 | 27.9 |

## 2.2. Hydrous Metal Oxides: A Comparative Study

Tin (IV) oxide is not unique amongst metal oxides in possessing a family of related hydrous oxides and similar systems are found in aluminium, boron, chromium, hafnium, magnesium, titanium and zirconium chemistry. In order to gain a better understanding of metal oxide/hydrous metal oxide chemistry especially in relation to tin (IV) oxide and the stannic acids a comparative study of other systems with chem--istry similar to tin was carried out.

From a knowledge of the peroidic table it was thought that germanium and lead chemistry might provide analogous hydrous metal oxide systems to tin. However this was not found to be the case.

Germanium dioxide ($GeO_2$) occurs in two crystalline modifications, one hexagonal and one tetragonal. The hexagonal form can easily be prep--ared from the hydrolysis of germanium (IV) chloride (c.f. orthostannic acid) and has a structure similar to that of low quartz, this modification is sometimes referred to as the soluble form as it dissolves in water to the extent of water to the extent of 4g/litre at 25°C. The second modification is the insoluble or tetragonal form which is prepared by hydrothermal conversion of the soluble form. The relationship between the different modifications of germanium dioxide is illustrated in figure eight and was established by Yamaguchi, Kotera and Asario[4]. However in direct contrast to the tin (IV) oxide system there is no evidence for hydrous (or hydrated) germanium dioxide, and in this respect the two materials are totally dissimilar.

Figure Eight - Germanium Dioxide Phases

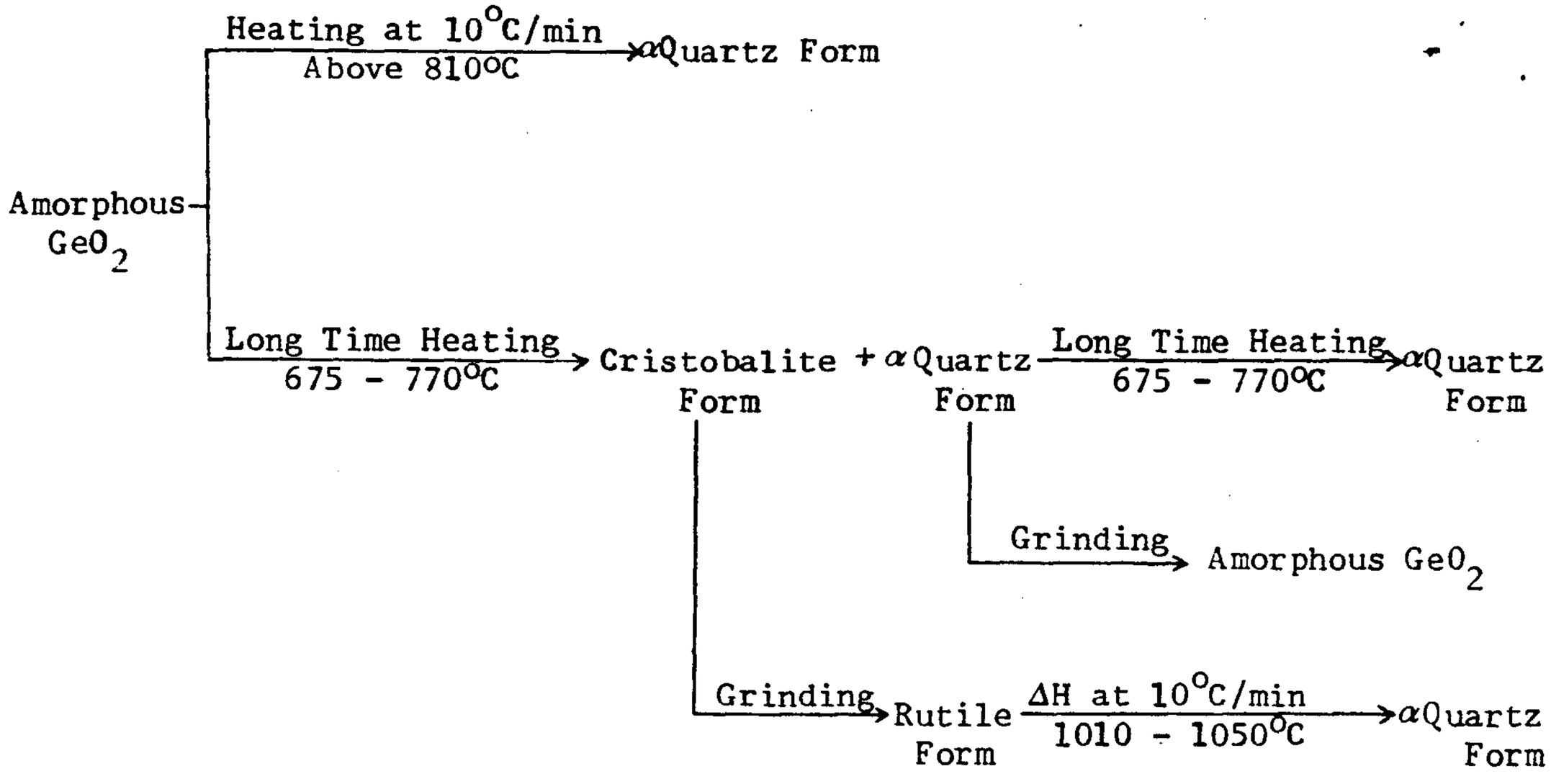


Lead (IV) oxide occurs naturally as the mineral plattnerite and is isomorphous with tin (IV) oxide (rutile). However lead dioxide unlike tin (IV) oxide is prepared by the hypochlorate oxidation of lead acetate or by the action of nitric acid upon $Pb_3O_4$. A true hydrous lead (IV) oxide has yet to be characterised although a series of plumbates $M^1_2PbO_3.3H_2O$ exist which contain discrete $Pb(OH)^{2-}_6$ ions which are analogous to the $Sn(OH)^{2-}_6$ ions in the hydroxostannates (IV), $M_2Sn(OH)_6$. The hydroxostannates and hydroxoplumbates are prepared by similar methods and this serves to highlight their chemical similarity.

Thus it would appear that tin is the only heavy element in main group IV of the periodic table that has extensive hydrous metal oxide chemistry (although the lighter element silicon does form hydrous oxides). Physical and chemical similarities between main group IV of the periodic table have been well documented, and it is in this group of elements that metals with hydrous oxides of the closest similarity to the stannic acids are found.

Titanium dioxide ($TiO_2$) exists in three different crystalline forms which all occur naturally - rutile (tetragonal), anatase (tetragonal) and brookite (orthorhombic) and two hydrous oxide species, orthotitanic acid and metatitanic acid have been reported. As with the stannic acids, both varieties of titanic acid may contain varying amounts of water, but convention gives them the formulae $Ti(OH)_4$ (ortho) and $TiO(OH)_2$ (meta)[5]. Titanic acids are precipitated when ammonia or an alkali hydroxide is added to a solution of titanium dioxide in hydro--chloric or sulphuric acid. When the starting solutions are cold and the rate of addition of alkali is slow orthotitanic acid is precipitated, but when the starting solutions are hot and the rate of addition of the alkali is fast then metatitanic acid is the product. Demoly[6] claimed that orthotitanic acid could be converted into metatitanic acid by boiling it in aqueous solution or by partial dehydration at elevated temperatures.

The surface hydroxyl/water groups on the surface of the titanic acids act as ion exchangers in a similar manner to those of the stannic acids and the use of metatitanic acid as a possible substrate for the extract--ion of uranium from seawater has been proposed[7].

The results of thermal analysis and powder x-ray studies on samples of ortho and meta titanic acids prepared in this work are shown in figures nine to twelve and tables four and five. The orthotitanic acid was prepared by precipitation with ammonia soution from a solution of titan--ium (IV) chloride, the product was washed by decantation with 50 volumes of water to remove excess chloride, filtered and vacuum dried over silica gel. The metatitanic acid used was prepared by boiling an aqueous sol--ution of orthotitanic acid for two hours until the precipitate became granular, the precipitate was filtered off and oven dried at 70°C.

Figure Nine - Thermal Analysis of Orthotitanic Acid

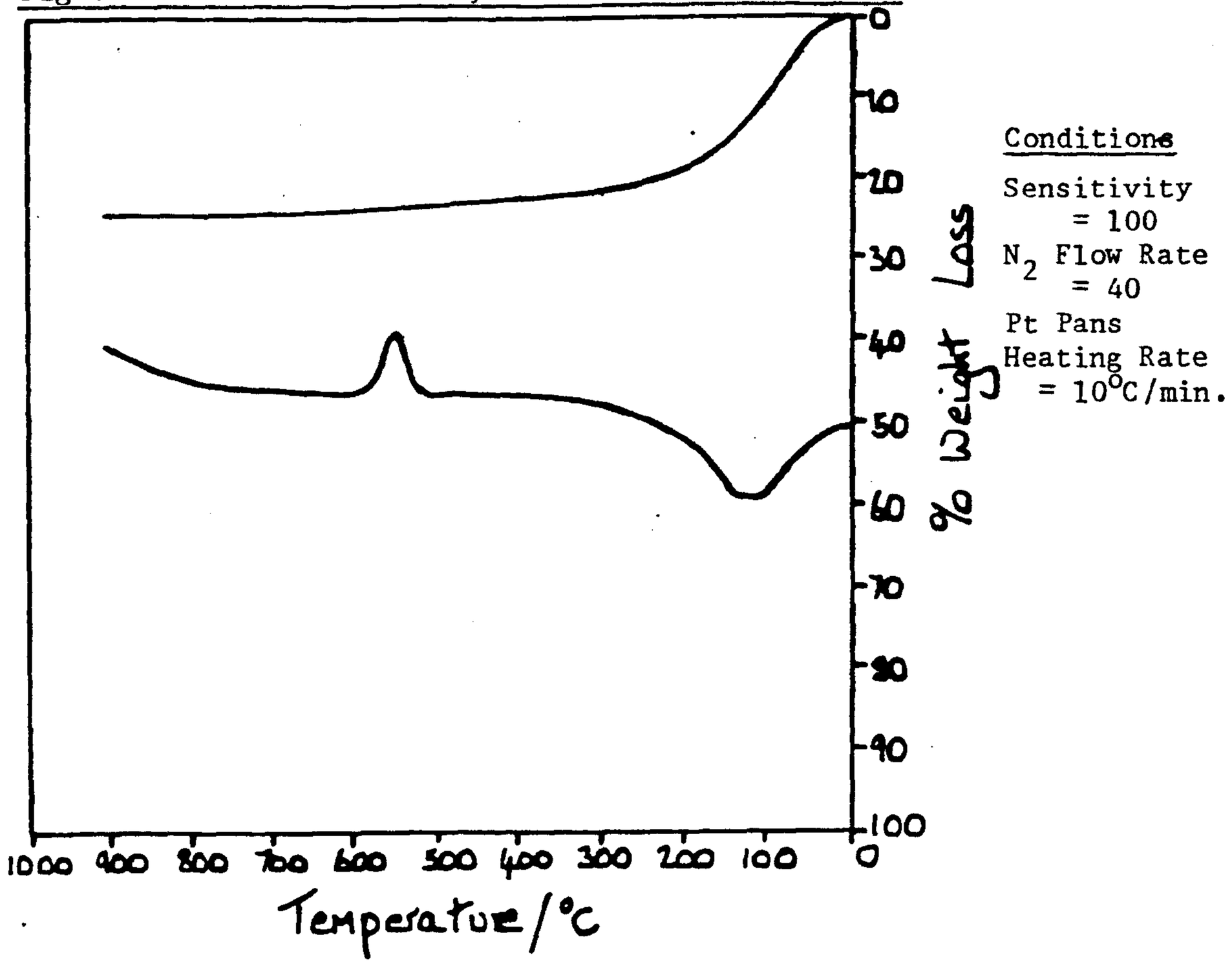


Figure Ten - Thermal Analysis of Metatitanic Acid

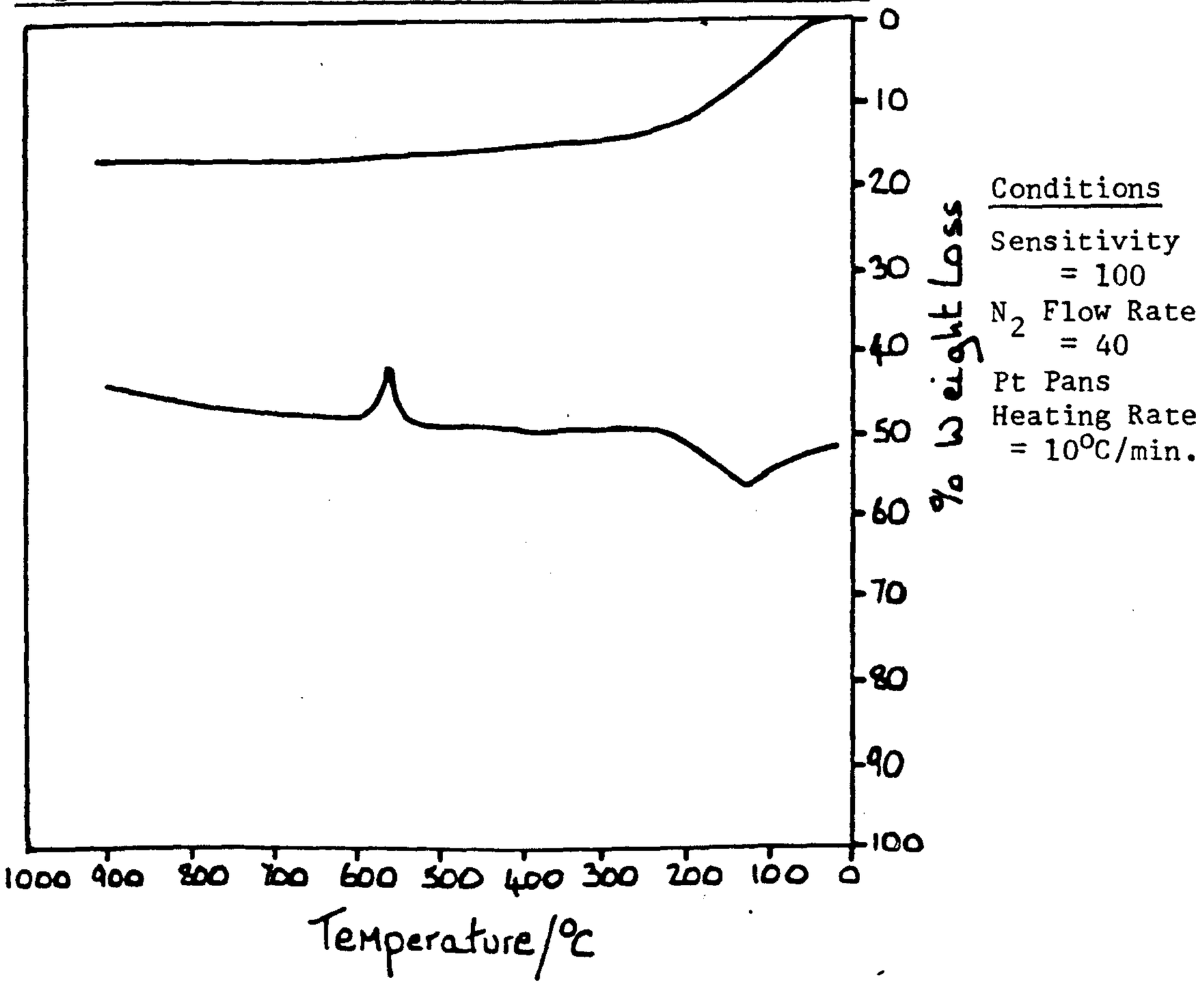

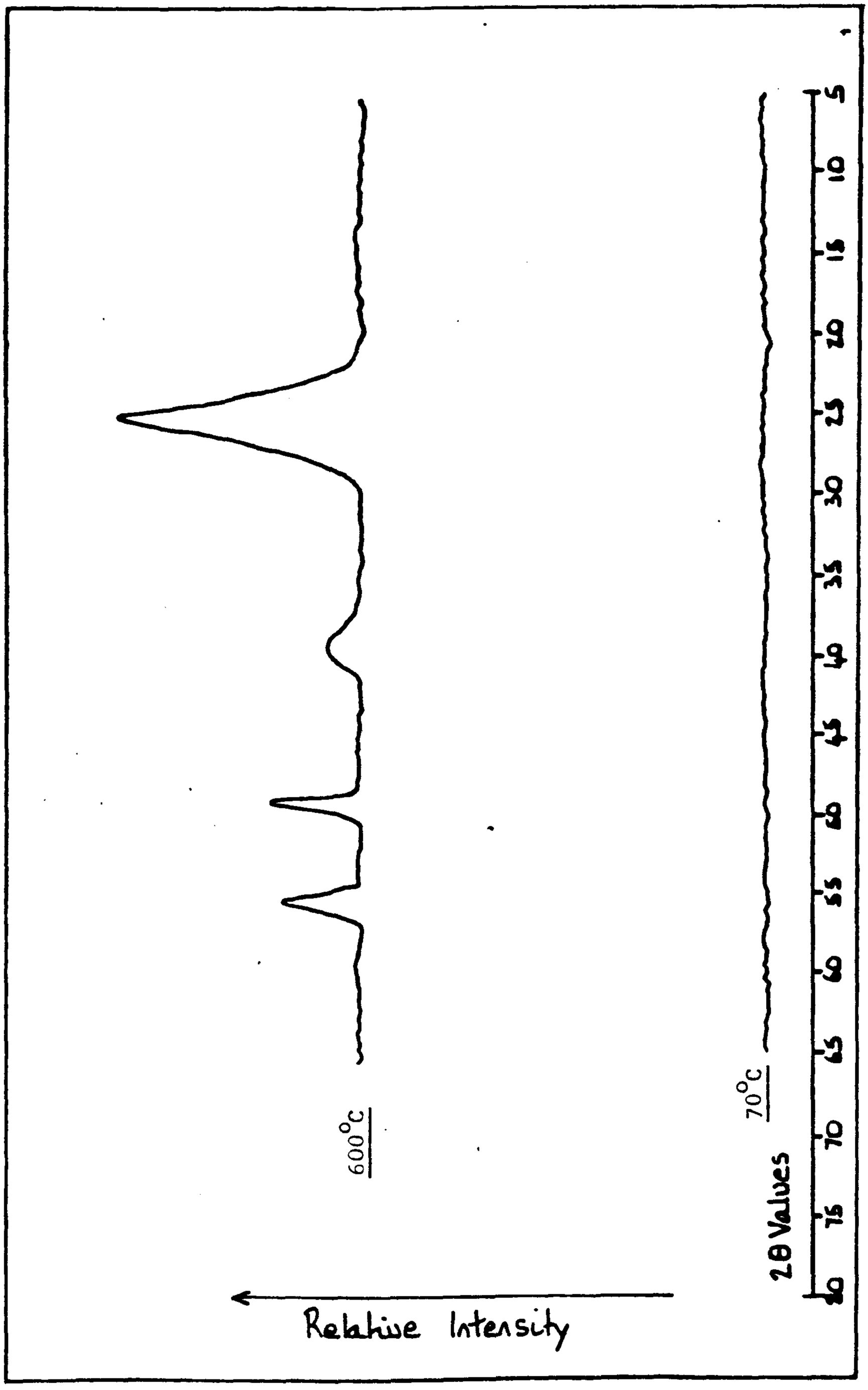


Figure Eleven - X-Ray Powder Diffractogram of Orthotitanic Acid

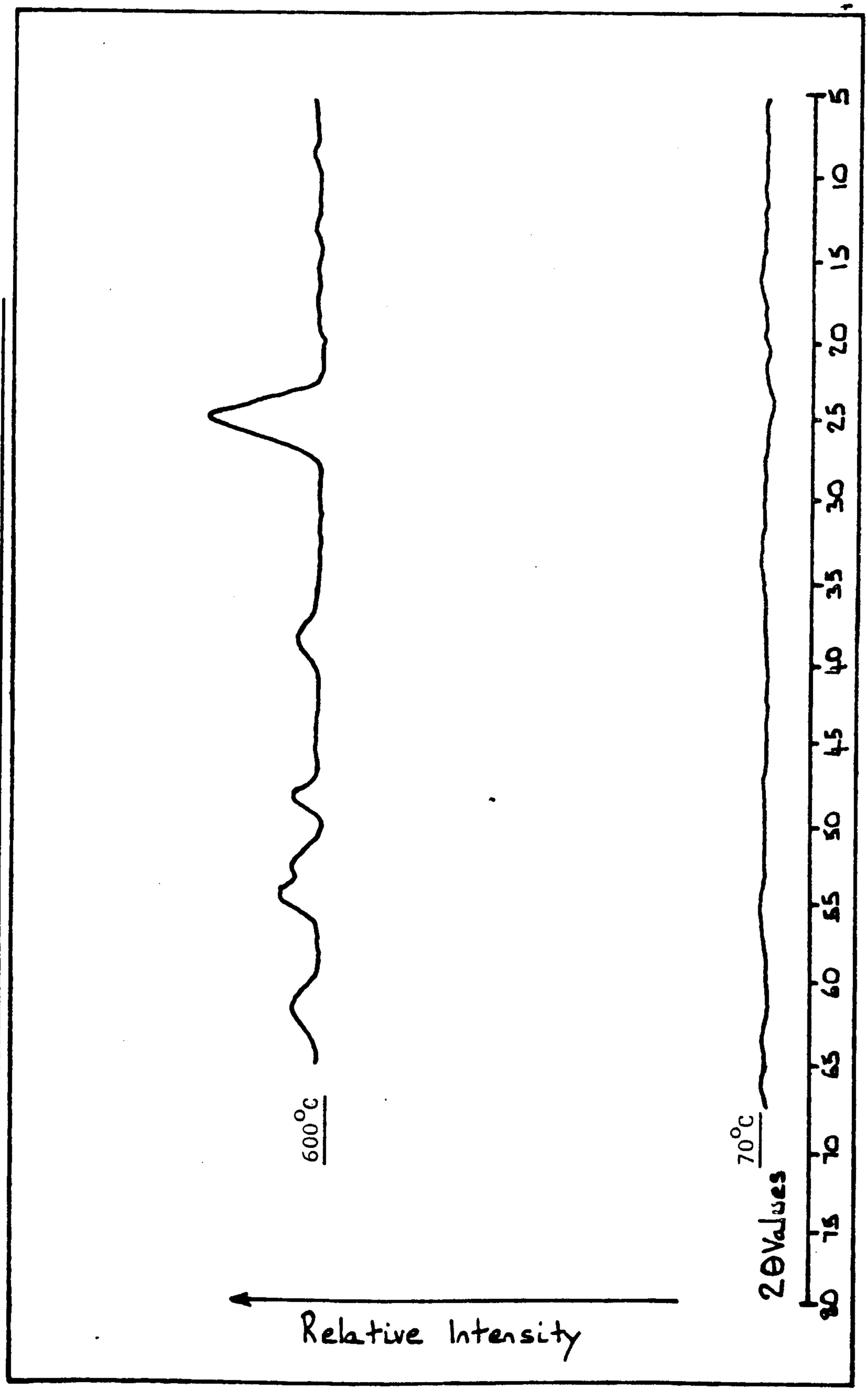


Figure Twelve - X-Ray Powder Diffractogram of Metatitanic Acid

Table Four - Results of Thermal Analyses of Ortho and Meta Titanic Acids

| Sample | Temp. at which Water loss Starts/$^{o}$C | Temp. of Max. rate of Water loss/$^{o}$C | Temp. at which Water loss Ends/$^{o}$C | Weight % Water | Temp. of Glow Exotherm |
|---|---|---|---|---|---|
| Ortho | 28 | 120 | 350 | 23 | 552 |
| Meta | 51 | 145 | 350 | 15½ | 570 |

The molecular formulae derived from the results of thermal analysis are, orthotitanic acid = $TiO_2.1{\cdot}3H_2O$ and metatitanic acid = $TiO_2.0{\cdot}8H_2O$. These results show that like the tin (IV) analogues, the hydrous titanium (IV) oxides contain non-stoichiometric amounts of water, with the molecular formulae of the materials depending upon the preparative conditions employed in the samples preparation. The differences between the meta and ortho-titanic acids are best accounted for in terms of grain size and crystal boundaries, as was found to be the case for the stannic acids.

The last column in table four refers to the Glow Temperature which is recorded as a sharp exothermic peak, called the Glow Exotherm, on the differential thermal analysis readout and represents a sudden change in phase from amorphous to crystalline in the test sample. The Glow Exotherm is attributed to the presence of small amounts of tenaciously held water in the material which prevent a smooth growth of the crystalline form. This in turn leads to a build up of internal stress which is released as heat energy when the amorphous solid suddenly changes into a crystalline form at the Glow Temperature. The Glow Exotherm is a common feature of hydrous metal oxide chemistry and is often visible to the unaided eye on heating a test sample in an open crucible. X-ray powder diffractograms were recorded for samples of hydrous titanium (IV) oxides above and below the Glow Temperature. Below the Glow Temperature both samples are amorphous, but above 650$^{o}$C the obtained diffractograms compare well with the literature standard data for anatase[8], one of the tetragonal forms of titanium (IV) oxide.

Table Five - X-Ray Powder Diffraction Data for Ortho and Meta Titanic Acids

| 2 values | $d_{spacing}$ | $I_{meas}$ | $I_{100}$ |
|---|---|---|---|
| Orthotitanic Acid - 70°C | | | |
| | No Data - Amorphous | | |
| Orthotitanic Acid - 600°C | | | |
| 25.4 | 3.5065 | 18½ | 100 |
| 38.0 | 2.3679 | 4 | 21.6 |
| 48.1 | 1.8916 | 6 | 32.4 |
| 54.6 | 1.6808 | 5½ | 29.7 |
| Metatitanic Acid - 70°C | | | |
| | No Data - Amorphous | | |
| Metatitanic Acid - 600°C | | | |
| 25.3 | 3.5202 | 10 | 100 |
| 37.8 | 2.3799 | 3 | 30 |
| 48.0 | 1.8953 | 3 | 30 |
| 53.9 | 1.7010 | 2½ | 25 |
| 55.0 | 1.6695 | 4 | 40 |
| 62.7 | 1.4817 | 2½ | 25 |

The relationship between the titanic acids and titanium dioxide thus established is shown in figure thirteen.

Figure Thirteen - Titanium Dioxide and the Titanic Acids

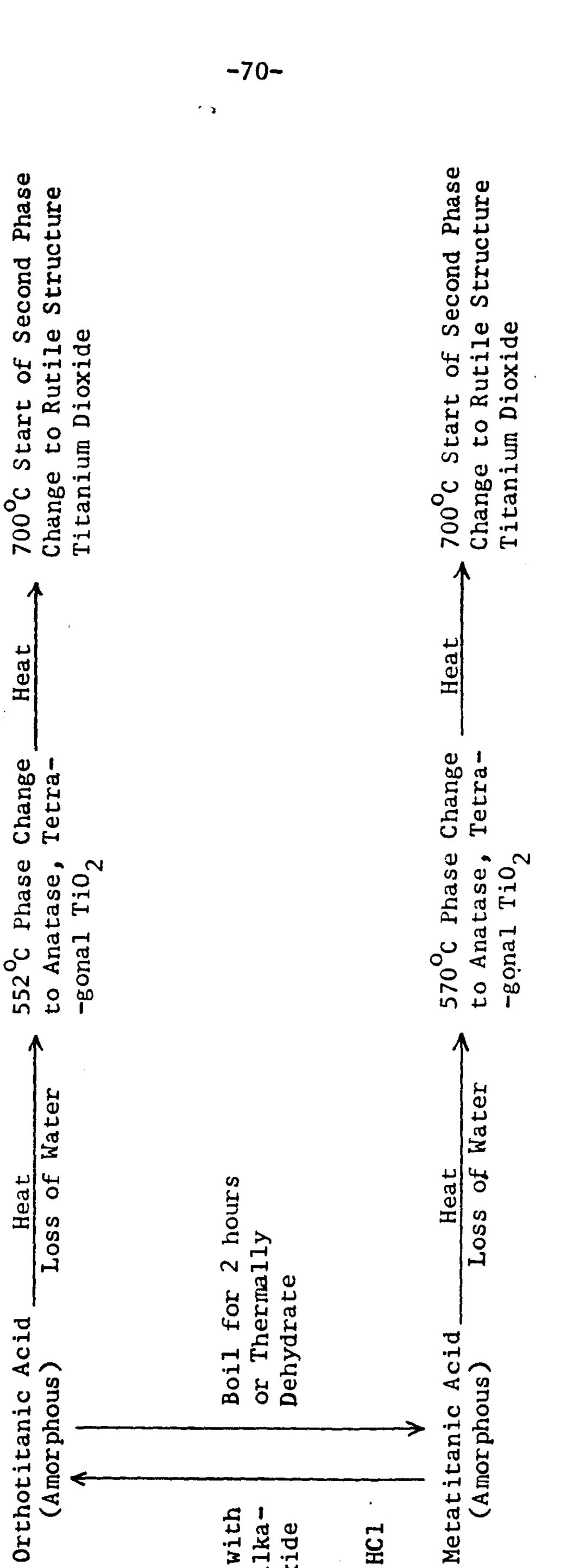

Zirconium dioxide ($ZrO_2$) can exist in three crystalline forms monoclinic, cubic and tetragonal, of these modifications only the monoclinic variety is found in nature where it occurs as the mineral baddeleyite. Three hydrous zirconium (IV) oxide gels, the $\alpha$, $\beta$ and $\gamma$ zirconic acids have also been reported[8]. These three hydrous zirconium gels which can be obtained by the addition of alkalis to solutions of zirconium (IV) salts have been the subject of much controversy in the literature. Tradit-ionally the hydrous oxides had been regarded as being non-stoichiometric with the formula $ZrO_2.nH_2O$. However Zaitsev[9] claims on chemical grounds that three distinguishable hydroxides exist. The $\alpha$ hydroxide, which can be obtained by slow controlled precipitation from cold solutions as the compound $Zr(OH)_4.nH_2O$, which Zaitsev formulated as a cyclic structure $Zr_4(OH)_8^t(OH)_8^b(H_2O)_x$ containing bridging $(OH)^b$ and terminal $(OH)^t$ groups. This compound ages or may be converted into the $\gamma$ hydrous oxide commonly known as zirconyl hydroxide by boiling. The $\gamma$ hydrous oxide was form-ulated by Zaitsev as $Zr_4O_4(OH)_8^t(H_2O)_y$ and was said to contain oxo bridges in place of hydroxo bridges in the $\alpha$ form. The intermediate $\beta$ form, can only be prepared by precipitation from zirconium nitrate in aqueous meth-anolic solution and was formulated as $Zr_4O_2(OH)_8^t(OH)_4^b(H_2O)_q$.

Zaitsev's work on the classification of hydrous zirconium oxides assumes the presence of cyclic ring structures in the solid materials. The ring structures are also assumed to be similar to the tetramers which have been identified in basic zirconium chloride solutions[10] - viz figure fourteen.

However Zaitsev's work has recently been challenged by Gimblett, Rahman and Sing[11] who report that Infra-red spectroscopy, magnetic susceptab-ility measurements, gas absorption and thermal studies all show a comp-lete absence of hydrates and they advance the general formula $ZrO_2.nH_2O$ for all three zirconic acids.

Figure Fourteen - The $Zr(OH)_8(H_2O)_{16}^{8+}$ unit in $ZrOCl_2(H_2O)_8$

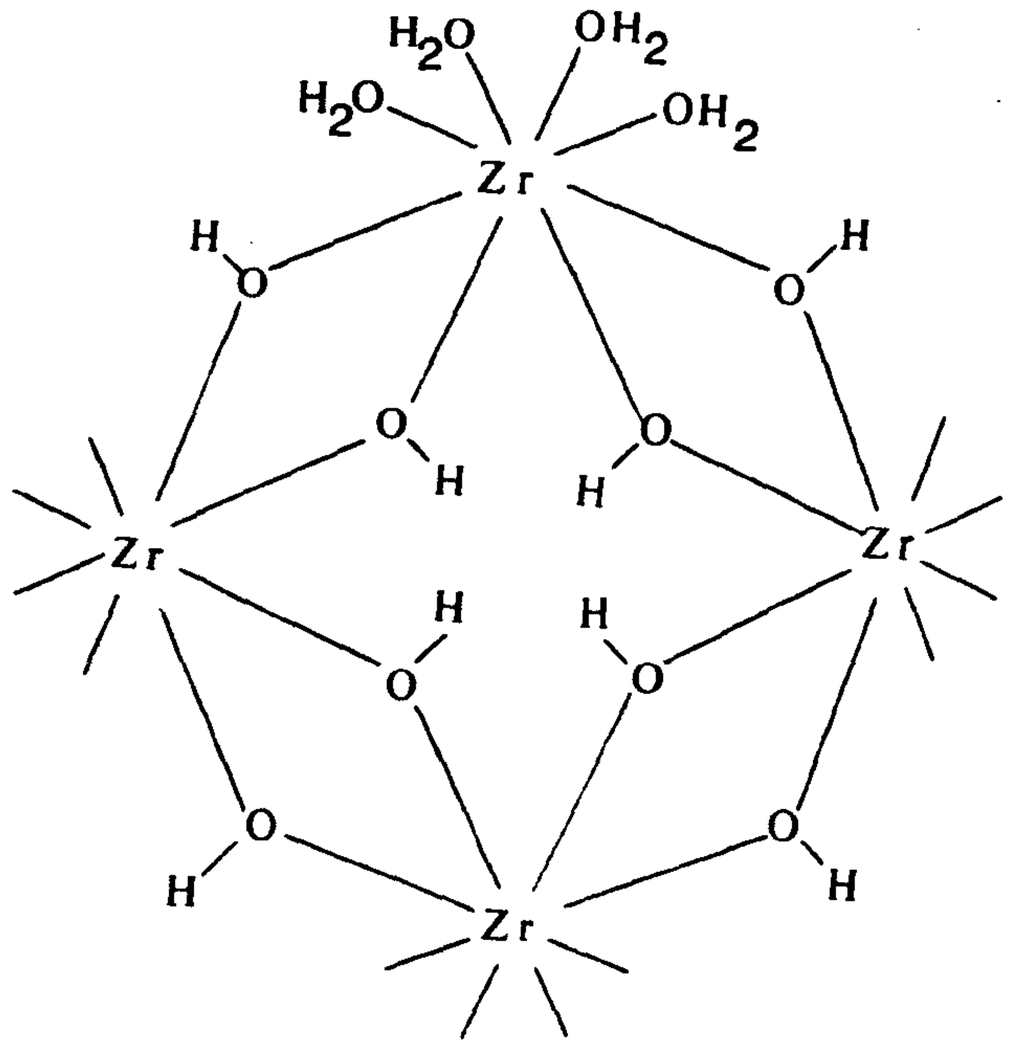


Thermal analysis of $\alpha$, $\beta$ and $\gamma$ zirconic acids prepared in this work was carried out on samples prepared as follows:

$\alpha$ zirconic acid was prepared by addition of aqueous sodium hydroxide solution to a cold solution of zirconium oxychloride in hydrochloric acid. The precipitated gel was then washed with approximately 50 volumes of water, filtered and dried at 65°C.

$\beta$ zirconic acid was prepared by precipitation from an aqueous methanolic solution of zirconium and zirconyl nitrates, which had been prepared in situ from the action of nitric acid (conc.) on zirconium metal at 0°C

$\gamma$ zirconic acid was prepared by boiling a suspension of $\alpha$ zirconic acid in water for c2 hours, followed by washing and drying.

The results of thermal analysis on these three samples are given in figures fifteen to seventeen and also in table six.

Figure Fifteen - Thermal Analysis of $\alpha$ Zirconic Acid

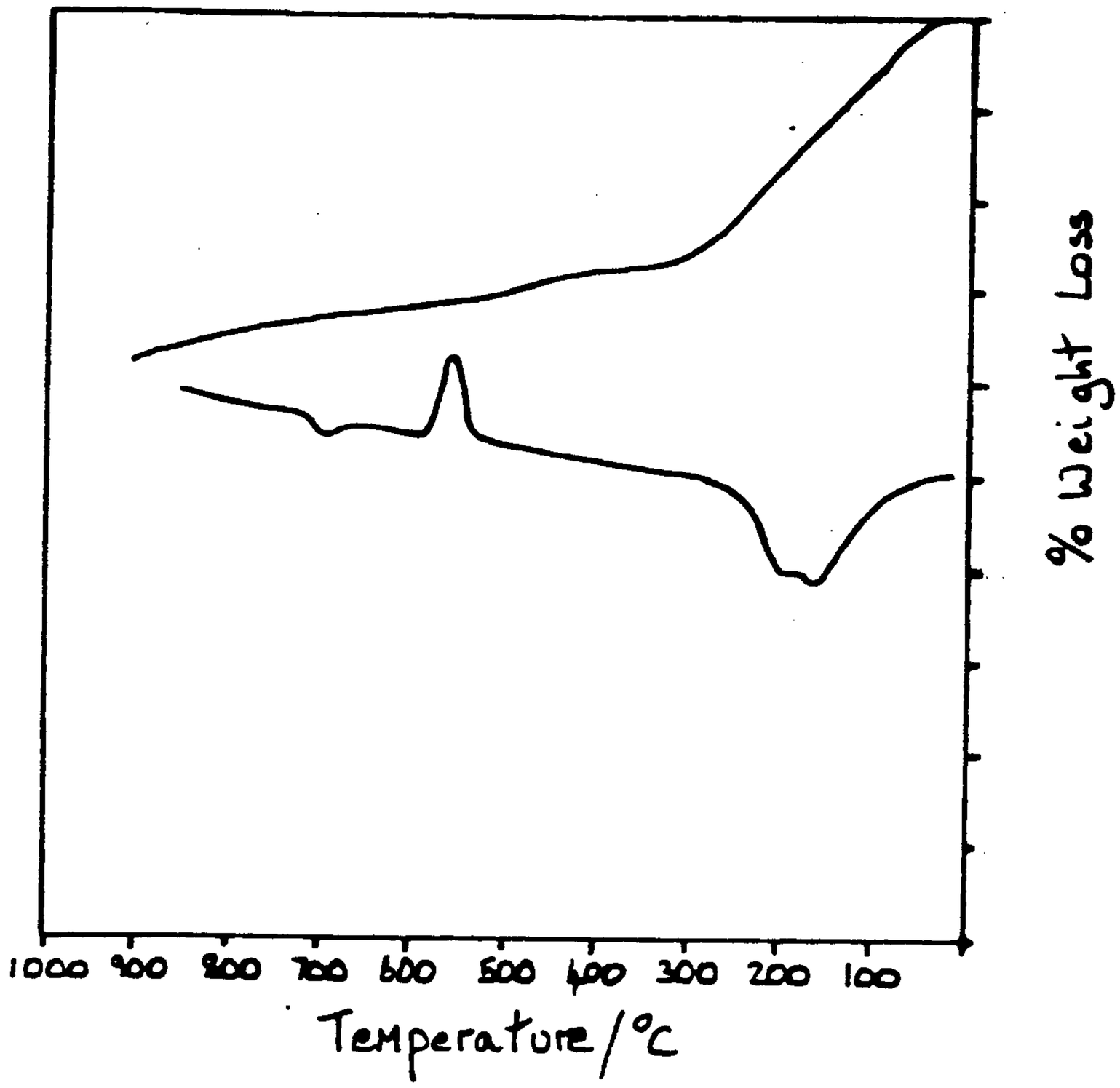


Figure Sixteen - Thermal Analysis of $\beta$ Zirconic Acid

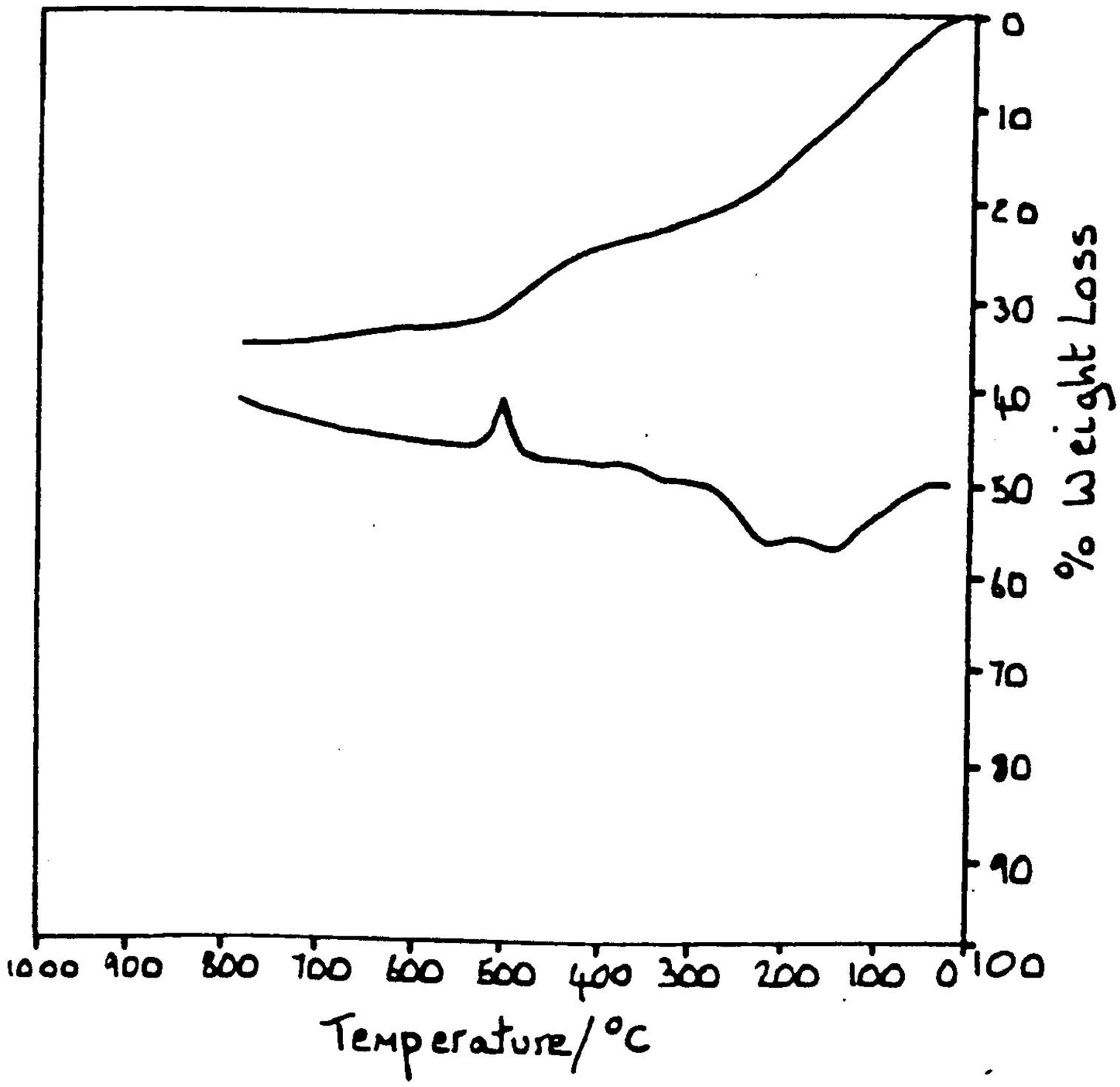

Figure Seventeen - Thermal Analysis of γZirconic Acid

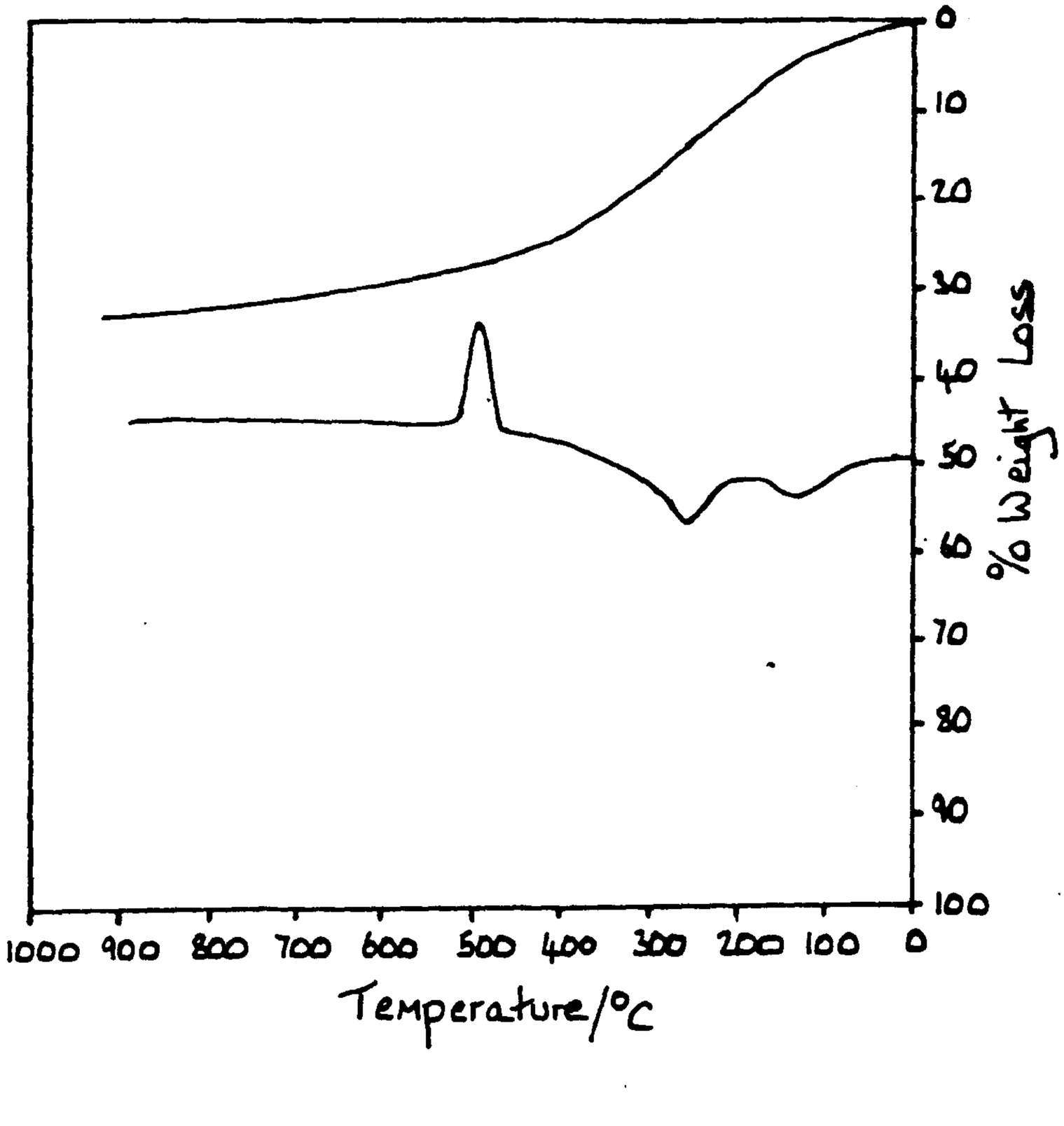

Table Six - Thermal Analysis of $\alpha$, $\beta$ and $\gamma$ Zirconic Acids

| Sample | Temperature at Which Water Loss Starts /°C | Temperature of Max. Rate of Water Loss /°C | Temperature at Which Water Loss Ends /°C | Weight % Water | Temp. of Glow Exo. -therm /°C |
|---|---|---|---|---|---|
| $\alpha$ | 70 - Phys<br>170 - Chem | 180 | 170 - Phys<br>380 - Chem | 27 | 547 |
| $\beta$ | 69 - Phys<br>180 - Chem | 258 | 180 - Phys<br>382 - Chem | 32 | 555 |
| $\gamma$ | 35 - Phys<br>215 - Chem | 258 | 180 - Phys<br>400 - Chem | 31 | 500 |

The molecular formulae derived from the results of thermal analysis are; $\alpha$ zirconic acid = $ZrO_2.2{\cdot}5H_2O$, $\beta$ zirconic acid = $ZrO_2.3{\cdot}2H_2O$ and $\gamma$ zirconic acid = $ZrO_2.2{\cdot}4H_2O$. Again it is found that formulae for the zirconic acids are preparation dependant and do not give good agreement with the cyclic unit models. The best description of the zirconic acids is as hydrous zirconium oxides of general formula $ZrO_2.nH_2O$.

The effects of heating and associated water loss on the structure of the zirconic acids has been investigated by Gimblett, Rahman and Sing[11] who found the changes shown in figure eighteen to occur in thermally treated samples.

Figure Eighteen - Phase Changes in Zirconic Acid Heated Samples

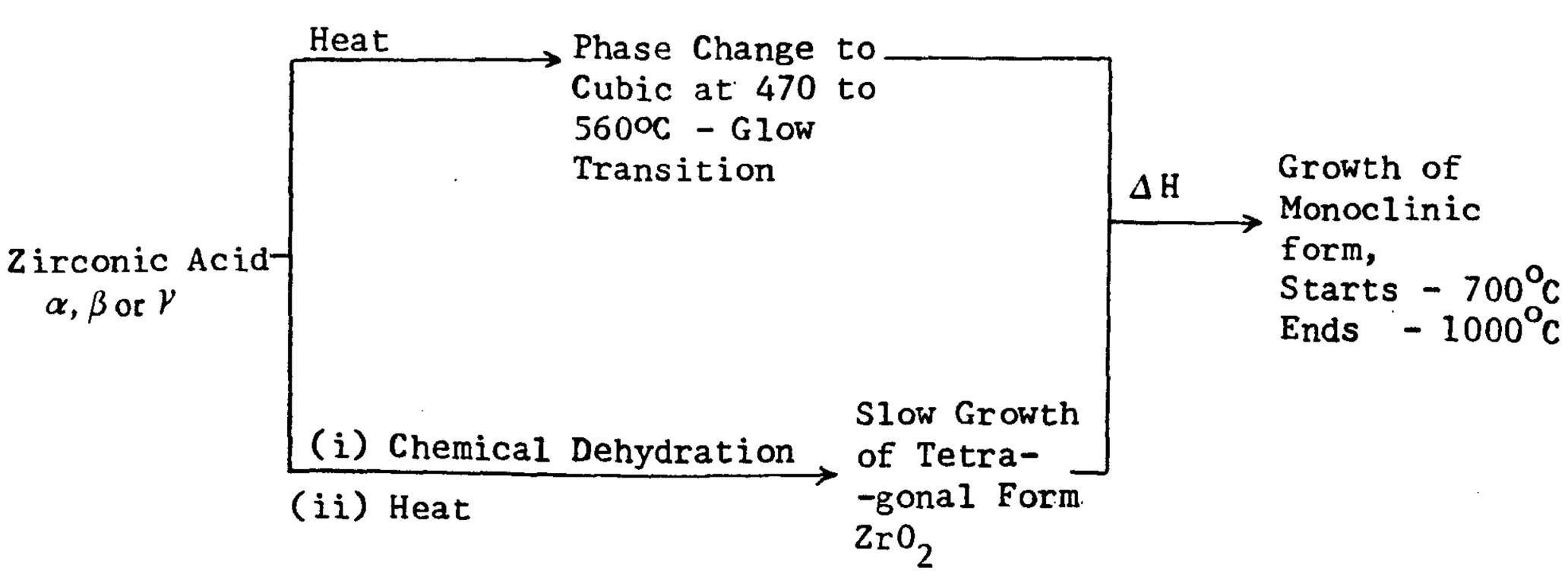

The presence of the glow exotherm in zirconic acids is accounted for in terms of residual water molecules being present in the structure at elev-ated temperatures which prevents a smooth growth of the tetragonal form of zirconium dioxide. This leads to a build up of internal stress within the material which is released at the glow temperature when the solid und-ergoes a phase change from amorphous to the metastable cubic form. Further heating of cubic or tetragonal zirconium dioxide results in form-ation of a monoclinic form which is the most stable phase, and is the variety found in nature.

In marked contrast to zirconium dioxide the literature on hafnium oxide and hydrous hafnium oxide species is sparse. Due to the effects of the lanthanide contraction zirconium and hafnium are chemically very similar and generally effects observed for zirconium chemistry will be true for the corresponding hafnium system. An infra-red and thermal study of hafnium oxide gels (hafnic acids) was carried out by Vivien, Livage and Maziries[12] who concluded that definate hydrated species with the structures $HfO_{2-x}(OH)_{2x}.yH_2O$ exist, in which hydroxide groups are directly bonded to the metal atom and in which water molecules are bonded in some way to the surface of the material.

In conclusion to this section of the project it can be stated that there appear to be many analoges to ortho and para stannic acids in the hydrous oxide chemistry of metals other than tin. However there is no chemically analogous hydrous oxide to metastannic acid. Metastannic acid is unique in that it can be prepared by direct oxidation of the metal with nitric acid and also that once prepared the material is insoluble in acidic sol-utions (except for HCl). Metastannic acid is not interchangeable with the other forms of stannic acid wheras the ortho and para modifications of hydrous tin (IV) oxide and their analoges are. Orthotitanic acid and $\alpha$zirconic acid exhibit similar properties to orthostannic acid.

Orthotitanic acid and $\alpha$zirconic acid also can easily be converted into metatitanic acid and $\gamma$zirconic acid respectively by boiling or by thermal dehydration as can the ortho and para stannic acids. All three of the aged hydrous oxide forms of zirconium, titanium and tin exhibit the same change in properties upon conversion in being generally less reactive towards acids and bases and having lower water contents.

$\beta$zirconic acid like metastannic acid does not fit into the general pattern of hydrous oxide chemistry and similarly to metastannic acid, is not inter--changable with other hydrous oxide modifications. However here the sim--ilarity ends and $\beta$zirconic acid and $\beta$stannic acid are so completely diff--erent in both their methods of preparation and properties that they both must be regarded as being unrelated, unique materials.

References

1. Standard X-Ray Diffraction Powder Patterns, N.B.S. Monograph 25, Section 7, page 52, 1969.

2. A. Daubrees, Ann. Mines, 1849, 16(4), 137

3. A. Michel Levy and L. Bourgeois, Compt. Rend., 1882, 94, 1365.

4. O. Yamaguchi, K. Kotera and M. Asario, J.C.S. Dalton Trans., 1982, 10, 1907.

5. Kirk-Othmer, Encyclopedia of Chemical Technology, Second Edition, Volume 20, page 391, Interscience, U.S.A., 1969.

6. A. Demoly, Recherchen sur le titane et ses combinations, Paris, 1849.

7. R.V. Davies, Nature, 1964, 203, 1110.

8. Standard X-Ray Diffraction Powder Patterns, N.B.S. Monograph 25, Section 7, page 85, 1969

9. L.M. Zaitsev, Russ. J. Inorg. Chem., 1966,11, 900.

10. L.M. Zaitsev and G.S. Bochkarev, Russ. J. Inorg. Chem., 1962, 7, 411.

11. G. Gimblett, A.A. Rahman and K.S.W. Sing, J. Appl. Chem. and Biotechnol., 1980, 30, 51.

12. D. Vivien, J. Livage and C. Mazieres, J. Chim. Phys. Physiochim. Biol., 1970, 67(1), 199.

# Chapter Three - The Manufacture of Metastannic Acid

## Chapter Three - The Manufacture of Metastannic Acid

### 3.1. Introduction and Objectives

Traditionally metastannic acid has been manufactured by Keeling and Walker Ltd. for use in the ceramic industry as a base for the production of glazes, and ceramics still represent the largest tonnage market for the material. In recent years newer markets for metastannic acid have developed and a number of potential industrial uses have been considered. These possible future applications include those as:

a) A flame retardent and smoke suppressor in fabrics[1,2,3].

b) A low temperature converter of carbon monoxide to carbon dioxide for automobile exhaust fumes[4,5].

c) An ion exchanger in H.P.L.C. columns[6,7].

d) A catalyst for the manufacture of acrolein or methacrolein from prop-ylene or isobutane repectively[8,9,10].

e) A gas sensitive electrode in monitering equipment[11,12].

f) A component in the manufacture of semiconducting binary metal oxides with antimony and indium (antimony tin oxide is the material used to make glass melting electrodes).

Many of these applications require the availability of a product with consistent physical and chemical properties. In general it is the particle size of the product obtained from the reaction between nitric acid and tin, rather than the water content which is critical in defining the properties of the material. The current commercial metastannic acid varies in particle size and distribution greatly from one batch to the next and so it becomes impossible to standardise downstream processing procedures when particle size is an important controlling factor.

The control of particle size becomes even more important in the synth--esis of metastannic acid based semiconductors as the resistivity in the product bears a direct relationship to the particle size of the start--ing material.

The plant used at present by Keeling and Walker consists of three, one--kettle, semi-batch reactors that are capable of producing about 800Kg of product per working week but the average particle size of the meta--stannic acid does vary from batch to batch. The aims of the present work are three-fold; (i) todetermine the factors controlling the reaction between tin metal and nitric acid, (ii) to determine which of these factors are important in controlling the particle size of the product and (iii) to consider the design of a plant capable of producing samples of metastannic acid of controlled (usually small) particle size in comm--ercially appropriate tonnages. At the very start of the project emph--asis was placed upon trying to achieve the first and second of the objectives outlined above and the experimental work and results are des--cribed in the next section of this chapter.

## 3.2. Small Scale Preparations of Metastannic Acid

As described in chapter one, section 1.1.1. metastannic acid can be prepared as a white precipitate from the action of concentrated nitric acid on tin metal and the product particle size appears to be a direct consequence of the reaction conditions used. The initial stages of the project were concerned with gaining an understanding of how the various reaction parameters contribute to determining the nature of the reaction and the product particle size.

The information from these studies on the optimum conditions for the production of particles of a desired range was used subsequently so that the reaction, with certain modifications, could be scaled up to plant size. The initial studies on the preparative conditions consisted of a systematic series of 27 experiments on 100g scale syntheses to investigate the following seven parameters which could influence particle size.

(i) The nitric acid concentration.

(ii) The reaction operating temperature.

(iii) The nitric acid to tin metal volume to weight ratio.

(iv) The physical form of the tin metal used.

(v) The degree of agitation in the reaction medium.

(vi) The washing and drying procedures

(vii) Addition of wetting agents and/or catalysts to the reaction medium.

The apparatus used, figure one, consisted of a two litre flanged flask fitted with a motorised paddle stirrer, a thermometer and a scrubber column. The reaction operating temperature was controlled by means of an external heating mantle and a cooling loop situated inside the the reaction vessel and through which ice-cold water could be passed. In all work carried out using this apparatus the nitric acid was added to the reaction vessel first followed by controlled addition of tin metal in order to regulate the reaction temperature. After completion of a reaction the lower half of the flanged flask could be unclipped to enable the unused nitric acid to be decanted off leaving the meta-stannic acid as a white precipitate. Material processing of the product prior to analysis was carried out in the same manner for all samples of metastannic acid prepared.

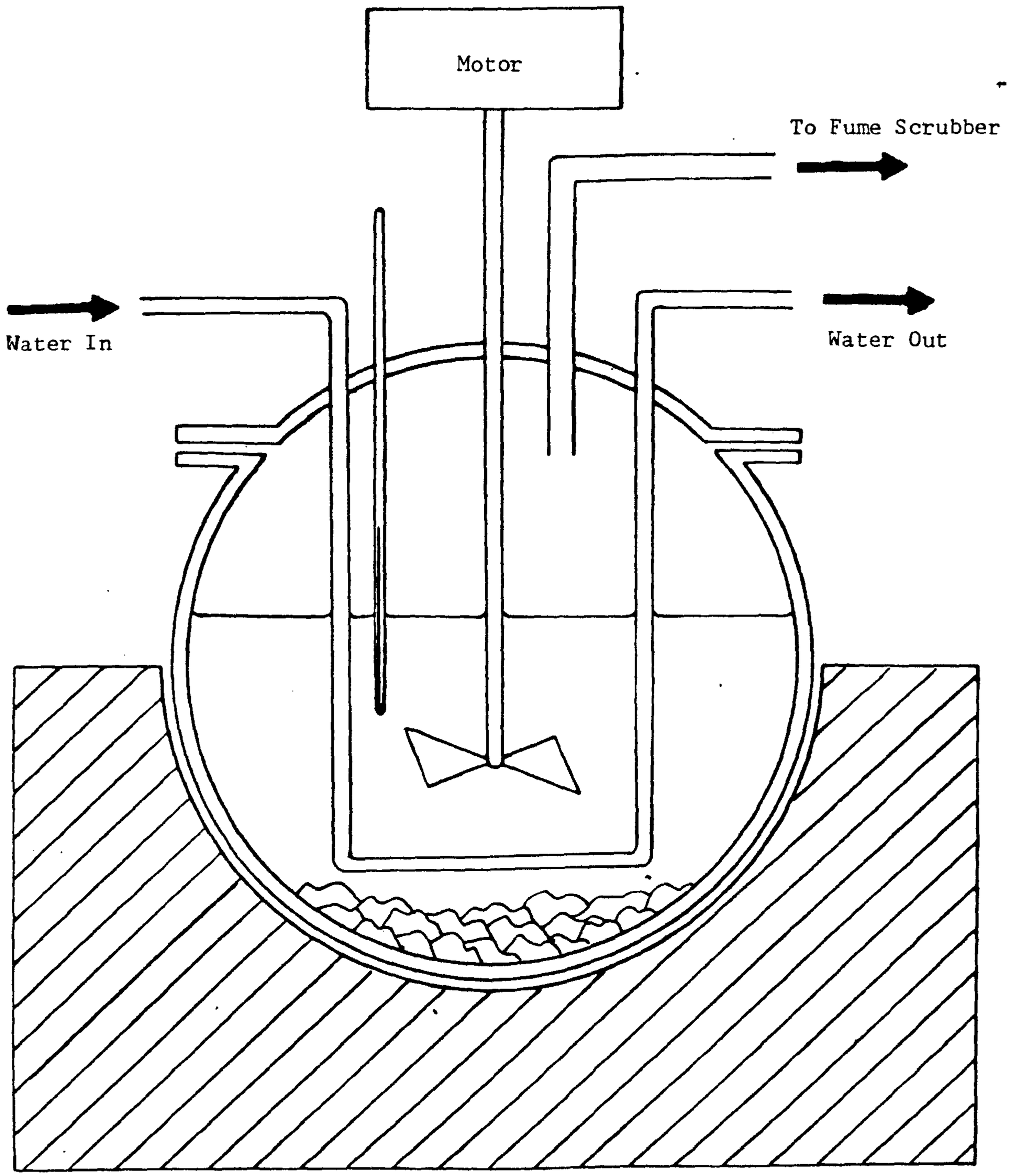


Figure One - The Apparatus used for the Small Scale Preparation of Metastannic Acid

This involved extensive washing of the precipitate with water by decant--ation to remove any adsorbed nitric acid from the surface of the product. All samples were washed till the pH of the liquor was greater than 4·5 and were then oven dried at 95°C. Particle size analysis was carried out using a Model D (Industrial) Coulter Counter fitted with a 200$\mu$m aperture. Details of the 27 reactions carried out in this part of the investigation are given below.

(i) <u>Investigation into the effects of nitric acid concentration upon particle size.</u>

Earlier preliminary experiments carried out upon gram quantities of material showed that the lowest workable concentration of nitric acid which will give metastannic acid from tin metal is 32%. Samples pre--pared from nitric acid of concentrations of lower than 32% were found to be discoloured due to the presence of minute particles of unreacted tin metal. Four experiments (C1 to C4) were carried out in this series using nitric acid of concentrations 32%, 37%, 42% and 47%. The results of these experiments together with the experimental conditions used are in table two.

(ii) <u>Investigation into the effects of the reaction operating temperature on particle size.</u>

In order to investigate the dependency of the product particle size upon the reaction temperature four experiments (T1 to T4) were carried out with reaction temperatures between 40 and 80°C being controlled by means of the heating mantle and a cooling loop. The reaction between tin metal and nitric acid is itself very exothermic and a source of heat input into the reaction system. For this reason use of the cooling loop was found to be most effective in controlling the reaction temp--erature.

The results of these experiments together with the relevant experi--mental conditions are in table two.

(iii) Investigation into the effects of the nitric acid to tin metal volume to weight ratio on particle size.

The effects of the ratio of nitric acid to tin metal, volume to weight, in the range 1:3·2 to 1:45 on the particle size of the product was investigated in eight experiments (V1 to V8) and results together with the relevant experimental conditions are in table two.

(iv) Investigation into the effects of the physical form of the tin metal on particle size.

The tin metal used in all of the other experimental series described in this work was granulated metal supplied by Keeling and Walker Ltd. It was assumed this form of the metal provided a constant surface area to weight ratio for the initial tin sample prior to treatment with nitric acid. In this initial study the reaction was carried out using powdered (S1) and cast tin (S3) as well as with the granulated tin (S2) to investigate what effects, if any, the surface area of the reacting tin metal has on the particle size of the product. The specific sur--face areas of the forms of tin metal used in this investigation are given in table one in which the surface factor column refers to the relative increase in surface area upon granulation or powdering cast tin i.e. conversion of 1g of cast tin into 1g of granulated tin results in a 22-fold increase in surface area. The results of these experi--ments together with experimental conditions used are in table three.

Table One - Specific Surface Areas of Different Tin Forms

| Experiment | Tin Form | Specific Surface Area/$m^2g^{-1}$ | Surface Factor |
|---|---|---|---|
| S1 | Powder | $2.8 \times 10^{-3}$ | 67 |
| S2 | Granulated | $9.3 \times 10^{-4}$ | 22 |
| S3 | Cast | $4.2 \times 10^{-5}$ | 1 |

(v) Investigation into the effects of agitating the reaction medium on particle size.

There are two reasons for agitating the reaction medium during the manufacturing process. Firstly to ensure that the granulated tin in the reaction vessel does not become surrounded with spent acid which would cause the reaction to become diffusion controlled and secondly to remove product metastannic acid from the tin surface to prevent the surface from becoming passivated with a layer of insoluble oxide. Agitation of the reaction medium was effected in all experiments by means of a paddle stirrer rotating at constant speed. To investigate the effects of agitation upon particle size two series of experiments were carried out using conventional and ultrasonic methods.
Reaction A1 was carried out using no external stirring, the only agit--ation being that occurring naturally in the vessel from convection currents and gas evolution. A second reaction A2 was carried out using a paddle stirrer rotating at a setting of 20 on the motor cont--roller and a third reaction A3, with the stirrer at a setting of 40 on the controller.

It is difficult to quantify the actual degree of agitation in the reaction medium for each case as this is dependent upon many factors which vary from one system to another.

However in order to gain a general insight into the effects of agitation it can be assumed that the degree of agitation in each reaction can be given by

$$A3 = A2 \times 2 \gg A1$$

Ultrasonic waves are known to produce many unusual chemical and physical phenomenon. Practically all of the observed chemical effects of ultra-sonics in liquid systems have been attributed to cavitation i.e. the formation and violent collapse of small bubbles or cavities in the liquid as a result of pressure changes. Cavitation is said to promote the rate of a chemical reaction by the electrolytic action brought about by the appearance of equal and opposite free electrical charges at opp-osite ends of bubbles and also the enormous local increases of pressure and temperature when the bubbles collapse and the release of energy from the bubbles when resonating with the ultrasonic waves. Two experi-ments were carried out to investigate the effect of ultrasound on the reaction on a 50g scale. Reaction U1 was carried out without ultra-sonic stirring but with a paddle stirrer rotating at a constant speed of 10. Reaction U2 was carried out with the paddle at speed 10 but also with the reaction vessel immersed in an ultrasonic bath which produced pulsed ultrasound at about 20KHz. The results of these experiments together with experimental details are given in table four.

(vi) <u>Investigation into the effects of washing and drying proc e dures on particle size.</u>

It was found experimentally that the washing and drying stages used in processing freshly prepared metastannic acid had little or no effect on the materials primary particle size. This is understandable since the material is produced as a hard, white, abrasive precipitate from the tin - nitric acid reaction and as a consequence is very resistant to further processing.

One problem which is however encountered when oven drying the washed metastannic acid gel is that of granular agglomeration. This arises because of the formation of liquid bridges when the voids between particles become partly filled with saddle shaped water droplets. Once a liquid bridge becomes established (in this case during the wash-ing process) any evaporation of liquid from the bridge reduces the radii of curvature of the liquid/gas interface and thus increases the forces holding the particles together, so that they approach each other more closely. The extent of liquid bridging can also be increased if there is a possible interaction between a polar bridging medium and surface groupings on the particle i.e. in this case water with the surface hydroxyl groups on the metastannic acid. The forces involved in liquid bridging are of the order of 100 atmospheres pressure and one process for the formation of liquid bridges is shown in figure two. However it should be noted that the problem of agglomeration does not affect the size of the metastannic acid primary particles produced from the tin-nitric acid reaction and so is extraneous to the present investigation.

(vii) <u>Investigation into the effects of wetting agents and catalysts on particle size.</u>

The use of vanadium pentoxide as a possible catalyst for the manufac-ture of metastannic acid has been reported in the literature[13]. In order to investigate this claim an experiment was carried out using vanadium pentoxide (5g) with tin metal (100g) and nitric acid ( 700ml, 60%). The metastannic acid prepared from this reaction was found to have a strong yellow/brown discolouration due to the incorporation of vanadium impurities in the material. For this reason no further use was made of vanadium pentoxide as a possible catalyst for the metastannic acid reaction in this work.

Figure Two - The Formation of Metastannic Acid Agglomerates

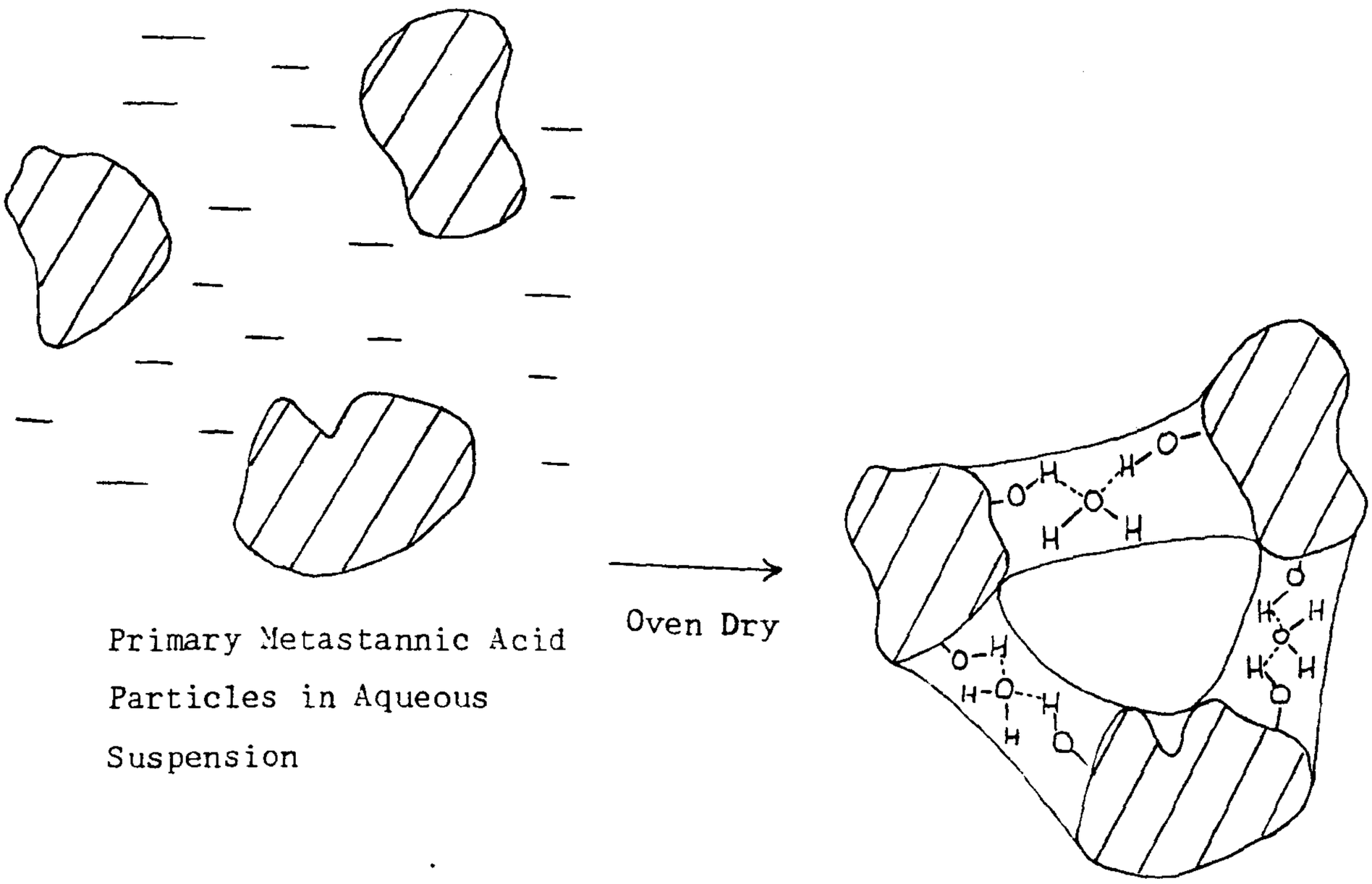


The addition of wetting agents to the tin/nitric acid reaction medium was also investigated in this part of the work and a detergent supplied by Universal Matthey (UMS13RM) was tested for its effect on particle size. It was hoped that the addition of a suitable detergent to the reaction mixture would lower the surface tension of the nitric acid and so enable it to react with the tin metal at a faster rate. Two experiments, D1 and D2, were carried out in this investigation and the results are given in table five.

Table Two - Particle Size Data for Metastannic Acid from Acid Concentration, Reaction Temperature and Volume to Weight Ratio Investigative Experiments

| Experimental Conditions | | | Results (Temp. Uncorrected) | | | Results (Temp. Corrected) | | |
|---|---|---|---|---|---|---|---|---|
| Experiment | Acid Conc$^{n}$ | Sn:Acid | Temp./$^{o}$C | $\bar{x}/\mu m$ | $\sigma/\mu m$ | Temp./$^{o}$C | $\bar{x}/\mu m$ | $\sigma/\mu m$ |
| C1 | 32 | 1:18·5 | 32 | 3·4 | 2·7 | 45 | 3·3 | 2·6 |
| C2 | 37 | 1:18·5 | 51 | 2·9 | 2·1 | 45 | 3·2 | 2·3 |
| C3 | 42 | 1:18·5 | 57 | 2·8 | 2·0 | 45 | 3·1 | 2·2 |
| C4 | 47 | 1:18·5 | 57 | 2·6 | 1·4 | 45 | 3·0 | 1·8 |
| V1 | 40 | 1:3·2 | 101 | 3·2 | 2·6 | 45 | 3·9 | 3·0 |
| V2 | 40 | 1:5·0 | 97 | 2·9 | 2·3 | 45 | 3·5 | 2·6 |
| V3 | 40 | 1:7·5 | 94 | 1·6 | 0·7 | 45 | 2·2 | 1·0 |
| V4 | 40 | 1:10·0 | 93 | 1·9 | 0·9 | 45 | 2·6 | 1·2 |
| V5 | 40 | 1:15·0 | 67 | 2·1 | 0·9 | 45 | 2·7 | 1·2 |
| V6 | 40 | 1:25·0 | 60 | 2·9 | 2·1 | 45 | 3·1 | 2·3 |
| V7 | 40 | 1:35·0 | 35 | 3·7 | 1·8 | 45 | 3·5 | 1·6 |
| V8 | 40 | 1:45·0 | 27 | 4·5 | 1·4 | 45 | 4·1 | 1·0 |
| T1 | 40 | 1:20·0 | 40 | 5·4 | 2·8 | 45 | 4·5 | 1·9 |
| T2 | 40 | 1:20·0 | 45 | 4·5 | 1·9 | 45 | 4·5 | 1·9 |
| T3 | 40 | 1:20·0 | 67 | 3·5 | 1·8 | 45 | 4·5 | 1·9 |
| T4 | 40 | 1:20·0 | 80 | 2·1 | 1·3 | 45 | 4·5 | 1·9 |

Table Three - Particle Size Data for Metastannic Acid from Surface Area Investigative Experiments

| Experimental Conditions | | | Results (Temp Uncorrected) | | | Results (Temp Corrected) | | |
|---|---|---|---|---|---|---|---|---|
| Expt. | Acid Conc$^{n}$ | Sn:Acid | Temp/$^{o}$C | $\bar{x}/\mu$m | $\sigma/\mu$m | Temp/$^{o}$C | $\bar{x}/\mu$m | $\sigma/\mu$m |
| S1 | 40 | 1:20 | 29 | 3·6 | 2·7 | 45 | 3·4 | 2·5 |
| S2 | 40 | 1:20 | 45 | 4·5 | 1·9 | 45 | 4·5 | 1·9 |
| S3 | 40 | 1:20 | 40 | 3·3 | 2·6 | 45 | 2·9 | 2·2 |

Table Four - Particle Size Data for Metastannic Acid from Agitation Investigative Experiments

| Experimental Conditions | | | Results (Temp Uncorrected) | | | Results (Temp Corrected) | | |
|---|---|---|---|---|---|---|---|---|
| Expt. | Acid Conc$^{n}$ | Stirrer | Temp/$^{o}$C | $\bar{x}/\mu$m | $\sigma/\mu$m | Temp/$^{o}$C | $\bar{x}/\mu$m | $\sigma/\mu$m |
| A1 | 40 | 0 | 70 | 3·7 | 2·5 | 45 | 4·1 | 2·0 |
| A2 | 40 | 20 | 45 | 4·5 | 1·4 | 45 | 4·5 | 1·4 |
| A3 | 40 | 40 | 40 | 3·1 | 2·3 | 45 | 2·9 | 1·4 |
| U1 | 40 | 10 | 65 | 3·0 | 3·5 | 45 | 3·3 | 3·8 |
| U2 | 40 | 10 + Ultrasd | 60 | 3·0 | 2·6 | 45 | 3·2 | 2·9 |

Table Five - Particle Size Data for Metastannic Acid from Detergent Additive Investigative Experiments

| Expt. | Acid Conc$^{n}$. | Stirrer | Temp/$^{o}$C | Wt. Detergent Added/% | Median $\mu$m | % Above 10$\mu$m | % Below 1$\mu$m |
|---|---|---|---|---|---|---|---|
| D1 | 60 | 20 | 85 | 0 | 2·1 | 2·0 | 25 |
| D2 | 60 | 20 | 85 | 5 | 2·6 | 4·0 | 20 |

Figure Three - Plot of Metastannic Acid Particle Size Against Nitric Acid Concentration

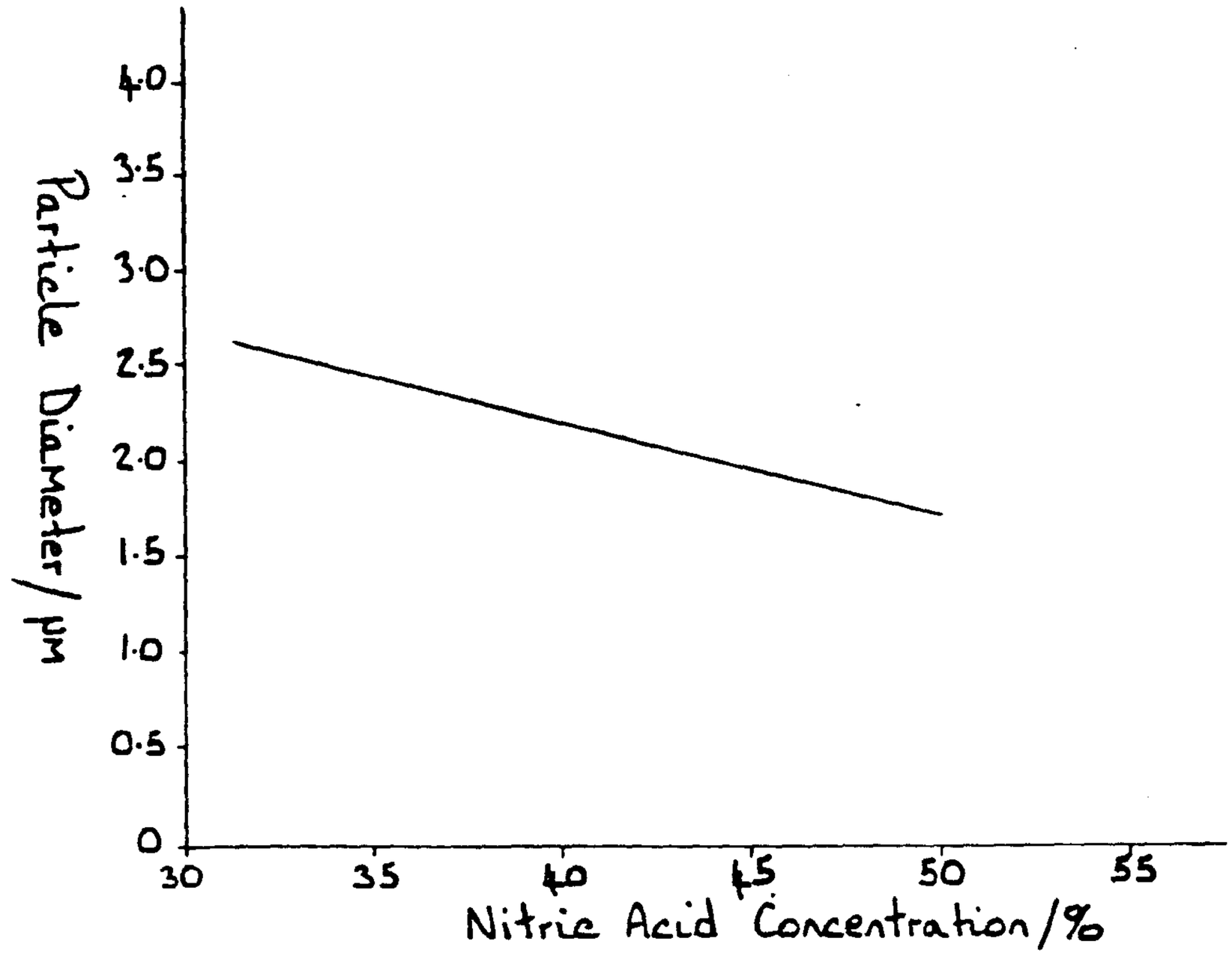


Figure Four - Plot of Metastannic Acid Particle Size Against Reaction Temperature

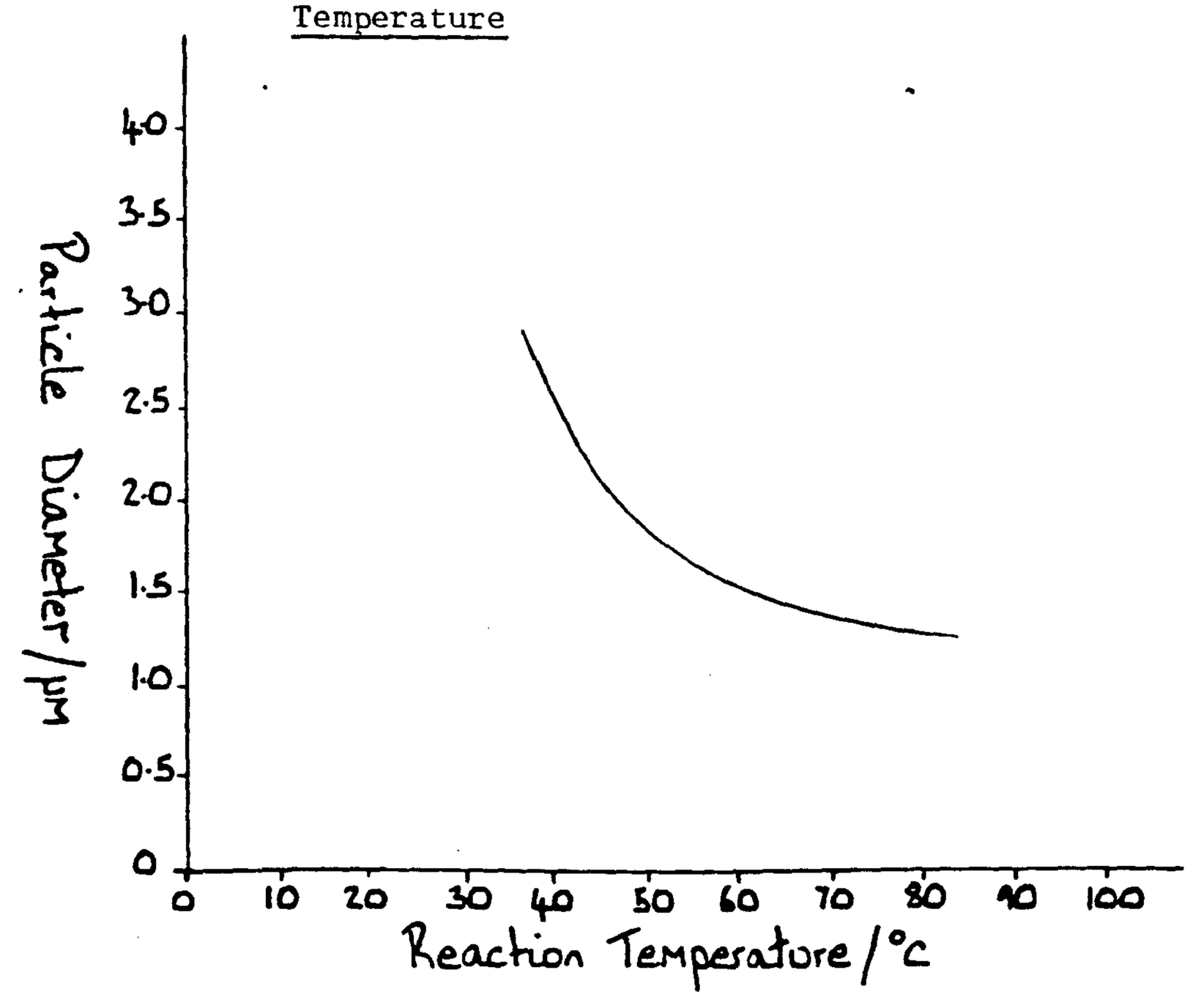

From the results of particle size analyses in tables two to five it can be seen that the reaction temperature and the acid concentration are the two most important factors in controlling the metastannic acid - particle size. The effects of these two parameters are shown in figures three and four and it can be seen that a high reaction temperature and a high nitric acid concentration are conducive to the preparation of fine particles. The nitric acid to tin ratio (volume to weight) was considered only to be of secondary importance in the reaction in main--taining the reaction temperature and the acid concentration. A tin to nitric acid ratio of between 1g:4ml and 1g:7ml was found to be most effective in this respect.

The results also show that increasing the extent of agitation up to a point is helpful in decreasing the product particle size, but that excessive agitation above this point has little effect on the particle size.

Experiments carried out on tin in varying degrees of subdivision showed that the most effective way of presenting tin to the reaction medium, was in the form of granulated metal. Lastly work carried out on the addition of wetting agents and catalysts to the reaction medium proved unsuccessful and their use was abandoned in further experimentation.

Thus from the results of the 27 experiments carried out on the preparation of metastannic acid the reaction conditions selected as the most appropriate for the production of fine particles were those given in table six. These conditions were used in two reactions carried out on a 100g ($\theta 1$) and 300g ($\theta 2$) scale. The particle size characteristics of the metastannic acid produced from these two reactions were;

Table Six - Optimum Conditions for the Preparation of Fine Particles of Metastannic Acid on a Small Scale

| Parameter | Optimum Conditions |
|---|---|
| Nitric Acid Concentration | 62%(1·38sg) |
| Tin : Nitric Acid Ratio | 1g : 7ml |
| Reaction Temperature | 105°C (boiling) |
| Degree of Agitation | High |

| Reaction | Scale | Median/$\mu$m | % Above 10$\mu$m | % Below 1$\mu$m |
|---|---|---|---|---|
| $\theta$1 | 100g | 1·8 | 5 | 34 |
| $\theta$2 | 300g | 2·3 | 7 | 23 |

## 3.3. The Preparation of Metastannic Acid on an Intermediate Scale

The results obtained from the small scale preparations described in the previous section would seem to indicate that the conditions most conducive to the production of metastannic acid of fine particle size from the reaction between nitric acid and tin metal are those given in table six. In order to try to approximate these reaction conditions to those of an industrial pilot plant the scale of the reaction was increased to kilogramme preparative batches. Three basic types of chemical manufacturing processes are suitable for the type of reaction involved in metastannic acid production.

### Type One - The Batch Reactor

All of the reactants are mixed together in a vessel at an instant in time. The reaction proceeds quickly at first because of the high initial concentrations of reactants but slows down as the reaction proceeds.

Figure Five - The Batch Reactor

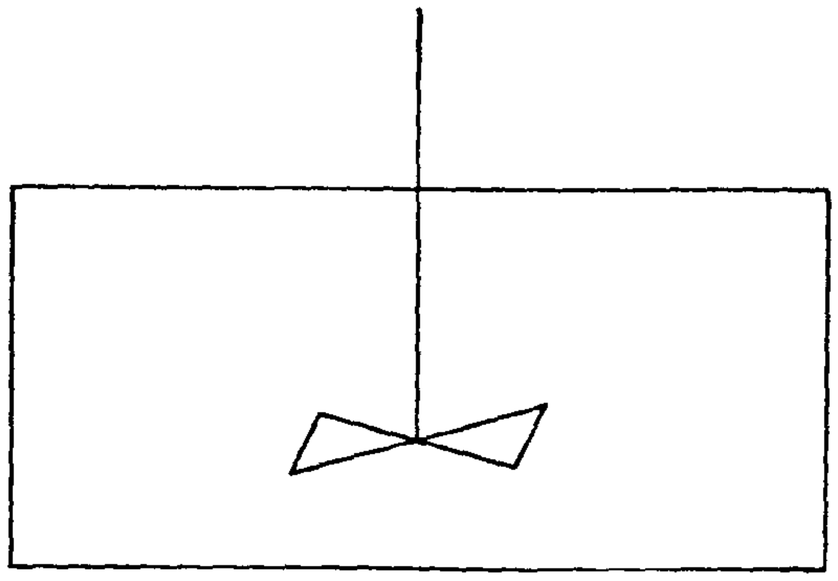

Figure Six - The Semi-Batch Reactor

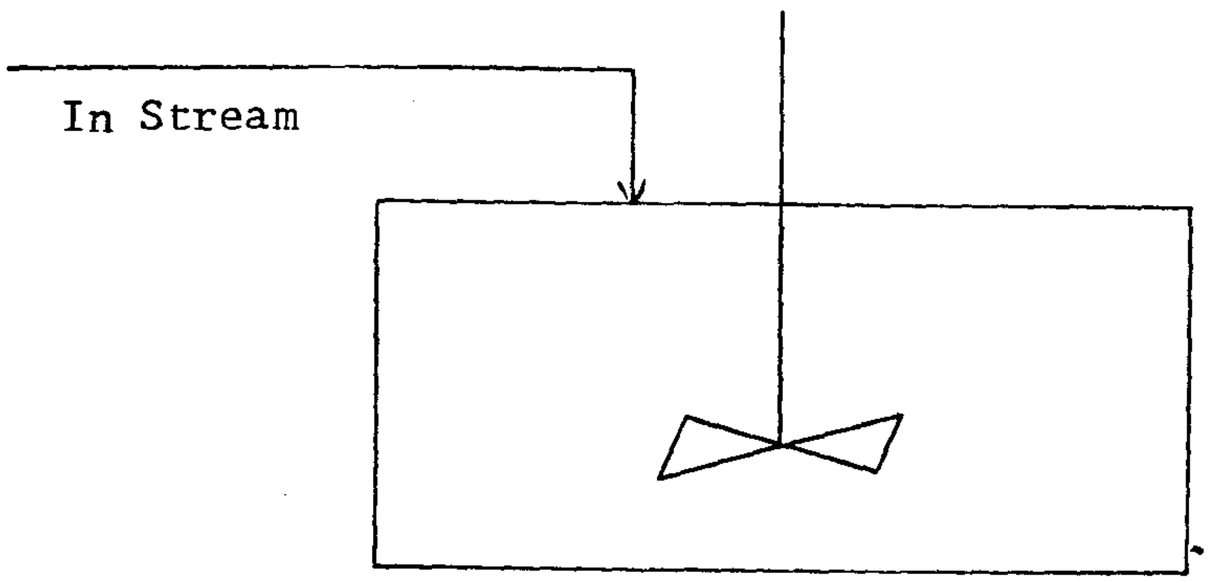


Figure Seven - The Continuous Reactor

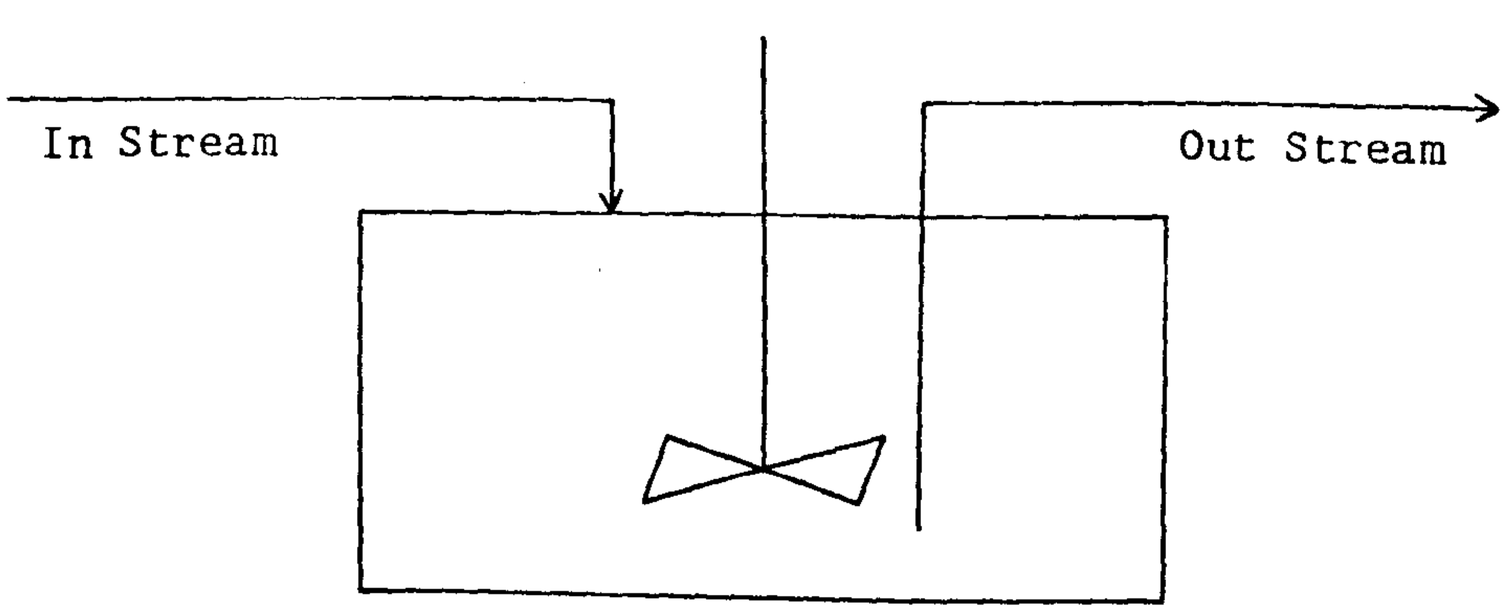

Type Two - The Semi-Batch Reactor

An initial charge of reactants is used to start the reaction and the other reactants are added during the course of the process. The Semi-Batch process is preferred to the Batch process if the initial reaction rates are too high causing uncontrollable temperature changes and/or uncontrollable gas evolution.

Type Three - The Continuous Stirred Tank Reactor

Reactants are added and products removed from the reaction vessel continuously and at identical rates so that their tank volume remains constant. The rate of flow of reactants and products define the tank residence time in that particular vessel. A typical chemical manu-facturing process may use several Continuous Stirred Tank Reactors in series.

The Batch, Semi-Batch and Continuous Stirred Tank Reactors are shown schematically in figures five, six and seven.

Seven, one kilogramme batches of metastannic acid were prepared in this investigation, using the three chemical manufacturing processes outlined above. The experimental conditions and details for the seven reactions are given below.

Reaction B1 was carried out as a Batch Reaction, using minimal agit-ation of the reaction medium. The reaction conditions were;

| | | |
|---|---|---|
| Weight of Tin Metal used | = | 1 Kilogramme |
| Volume of Nitric Acid used | = | 7 Litres |
| Initial Acid Concentration | = | 60% |
| Reaction Temperature at Equilibrium | = | $65^{o}C$ |

Total Reaction Time = 2½ Hours

400g of tin metal was added initially to the reaction vessel which upon reacting raised the temperature of the nitric acid to 65°C. This equilibrium temperature was then maintained throughout the course of the reaction by slow controlled addition of the rest of the tin metal. Stirrer agitation was applied to the reaction mixture for the first 70 minutes of the reaction only, the last 30 minutes of the reaction were carried out with no externally applied agitation.

Reaction B2 was carried out as a Batch reaction with conditions similar to reaction B1 except that the reaction was carried out with continu-ous agitation. The reaction conditions were;

| | | |
|---|---|---|
| Weight of Tin Metal used | = | 1 Kilogramme |
| Volume of Nitric Acid used | = | 7 Litres |
| Initial Acid Concentration | = | 60% |
| Reaction Temperature at Equilibrium | = | 70°C |
| Total Reaction Time | = | 2¼ Hours |

Reaction B3 was carried out as a Batch reaction with all of the tin metal and nitric acid being added to the reaction vessel at the start of the reaction. The reaction conditions were;

| | | |
|---|---|---|
| Weight of Tin Metal used | = | 500g |
| Volume of Nitric Acid used | = | 4 Litres |
| Initial Acid Concentration | = | 60% |
| Reaction Temperature at Equilibrium | = | 86°C |
| Total Reaction Time | = | 2 Hours |

Reaction B4 was carried out as a Semi-Batch reaction in three stages.

The reaction conditions were;

| | | |
|---|---|---|
| Stage One | Addition to Reaction Vessel of | 0·3Kg Tin Metal |
| t = 0mins | | 2·5Litres of 1·48sg Nitric Acid |
| | | 1Litre of Water |
| Stage Two | Addition to Reaction Vessel of | 0·2Kg Tin Metal |
| t = 30mins | | 1·5Litres of 1·48sg Nitric Acid |
| | | 0·5Litres Water |
| Stage Three | Addition to Reaction Vessel of | 0·2Kg Tin Metal |
| t = 60mins | | 1·5Litres of 1·48sg Nitric Acid |
| | | 0·5Litres of Water |

Averaged Reaction Equilibrium Temperature = 67 - 70°C

Total Reaction Time = 2 Hours

Reaction B5 was carried out as a Semi-Batch reaction in five stages.

The reaction conditions were;

| | | |
|---|---|---|
| Stage One | Addition to Reaction Vessel of | 0·14Kg Tin Metal |
| t = 0mins | | 0·7Litres of 1·42sg Nitric Acid |
| | | 0·7Litres of 1·3sg Nitric Acid |
| Stage Two | Repeat of Addition of Stage One | |
| t = 15mins | | |
| Stage Three | Repeat of Addition of Stage One | |
| t = 30mins | | |
| Stage Four | Addition to Reaction Vessel of | 0·14Kg Tin Metal |
| t = 45mins | | 1Litre of 1·42sg Nitric Acid |

| | | |
|---|---|---|
| Stage Five | Addition to Reaction Vessel of | 0·14Kg Tin Metal |
| t = 60mins | | 1·4Litres of 1·42sg Nitric Acid |

Averaged Reaction Equilibrium Temperature = 75 - 80°C

Total Reaction Time = 1 Hour, 50 Minutes

Reaction B6 was carried out as a Continuous reaction with experimental conditions as follows;

| | | |
|---|---|---|
| Stage One | Addition to Reaction Vessel of | 0·2Kg Tin Metal |
| t = 0mins | | 2·0Litres of 1·35sg Nitric Acid |
| Stage Two | Addition to Reaction Vessel of | 0·2Kg Tin Metal |
| t = 20mins | | 2·0Litres of 1·35sg Nitric Acid |
| | Removal From Vessel of | 2Litres of Reaction Medium @2ml/min. |
| Stage Three | Addition to Reaction Vessel of | 0·2Kg Tin Metal |
| t = 40mins | | 2·0Litres of 1·35sg Nitric Acid |
| | Removal From Vessel of | 2Litres of Reaction Medium @2ml/min. |
| Stage Four | Addition to Reaction Vessel of | 0·2 Kg Tin Metal |
| t = 60mins | | 2·0Litres 1·42sg Nitric Acid |
| | Removal From Vessel of | All of Reaction Medium at Pumping Rate of 1ml/min. |

Averaged Equilibrium Temperature = 80 - 90°C

Total Reaction Time = 1 Hour, 40 Minutes

Reaction B7 was carried out as a Semi-Batch reaction in seven stages.

The experimental conditions were;

| | | |
|---|---|---|
| Stage One | Addition to Reaction Vessel of | 0·1Kg Tin Metal |
| t = 0mins | | 1·0Litres of 1·36sg Nitric Acid |
| Stage Two | Addition to Reaction Vessel of | 0·1Kg Tin Metal |
| t = 12mins | | 1·0Litre of 1·36sg Nitric Acid |
| Stage Three | Addition to Reaction Vessel of | 0·1Kg Tin Metal |
| t = 24mins | | 1·0Litre of 1·36sg Nitric Acid |
| Stage Four | Addition to Reaction Vessel of | 0·1Kg Tin Metal |
| t = 36mins | | 1·0Litre of 1·36sg Nitric Acid |
| Stage Five | Addition to Reaction Vessel of | 0·1Kg Tin Metal |
| t = 48mins | | 1·0Litre of 1·42sg Nitric Acid |
| Stage Six | Addition to Reaction Vessel of | 0·1Kg Tin Metal |
| t = 60mins | | 1·0Litre of 1·42sg Nitric Acid |
| Stage Seven | Addition to Reaction Vessel of | 0·1Kg Tin Metal |
| t = 72mins | | 1·0Litre of 1·42sg Nitric Acid |

Average Equilibrium Temperature = 80 - 85$^{o}$C

Total Reaction Time = 1 Hour, 35 Minutes

The apparatus used for all seven experiments consisted of a scaled up version of the equipment used in the work described in the previous section, the two litre flanged flask being replaced by a 20litre one. A schematic representation of the apparatus used in this section of the work is shown in figure eight.

Sedigraph particle size analyses of the metastannic acid produced from reactions B1 to B7 are shown in figures nine to seventeen and the coll-ected data relating to particle diameters and interdecile deviations are-given in table seven.

Table Seven - Results of Sedigraph Analyses of Metastannic Acid

| Sample | Median/$\mu$m | Wt% Above 10$\mu$m | Wt% Below 1$\mu$m |
|---|---|---|---|
| B1 | 3·1 | 10 | 22 |
| B2 | 3·0 | 5 | 23 |
| B3 | 6·0 | 27 | 6 |
| B4 | 5·6 | 27 | 8 |
| B5 | 2·4 | 2 | 19 |
| B6 | 2·9 | 6 | 18 |
| B7 | 2·3 | 3 | 21 |
| $\theta 1^{*}$ | 1·8 | 5 | 34 |
| $\theta 2^{**}$ | 1·6 | 4 | 37 |

* = Best result obtained from small scale preparations of metastannic acid.

** = Keeling and Walkers commercial grade metastannic acid after jet milling.

From table seven it can be seen that the material with the most satis-factory particle size was that produced from reaction B7. The cond-itions employed in the manufacture of this batch of metastannic acid would thus appear to have the greatest potential for transfer to work on a larger scale i.e. the proposed pilot plant would operate as a Semi-Batch process using a high nitric acid concentration, a high degree of agitation and a high operating temperature.

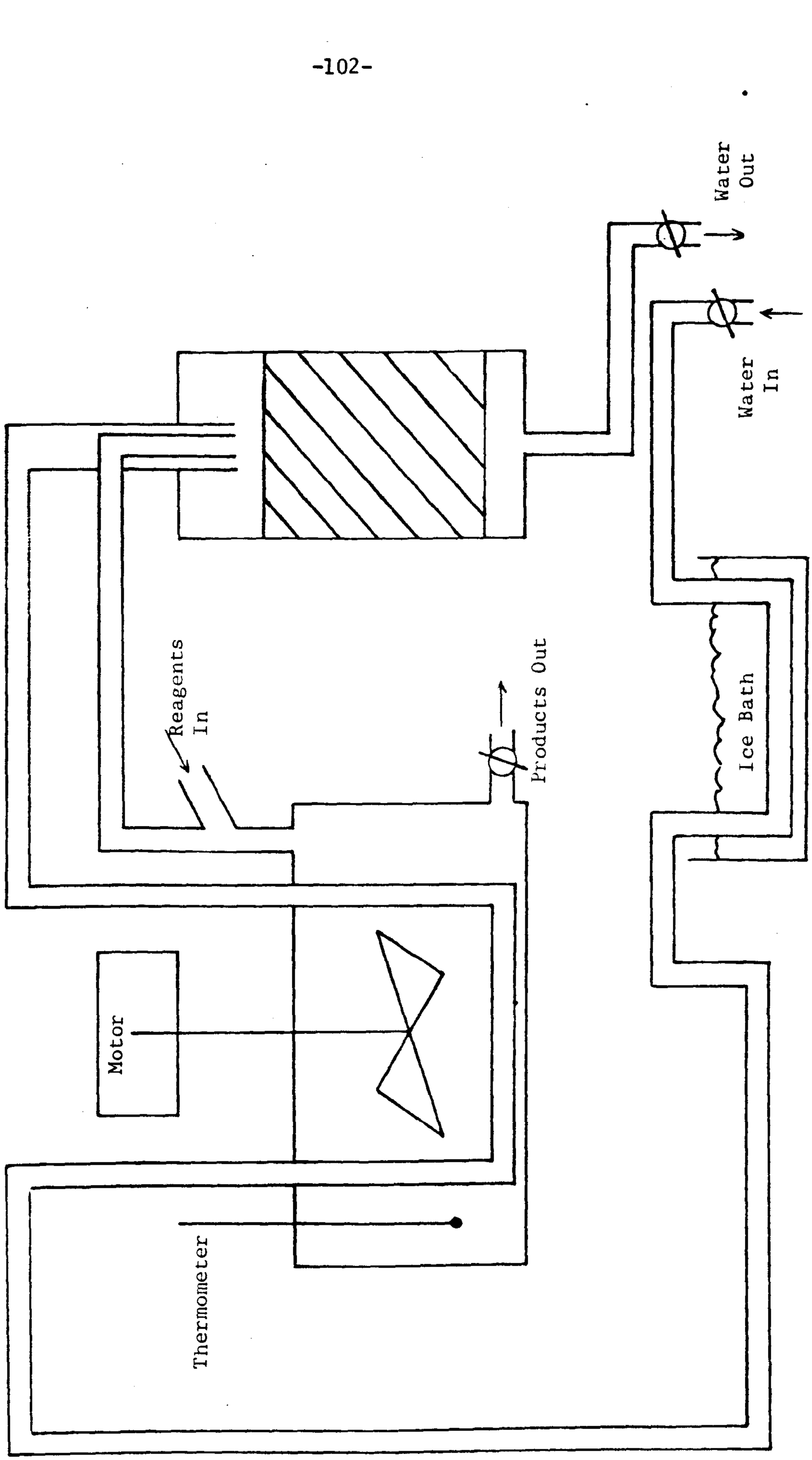


Figure Eight - Schematic Representation of the Equipment used to Prepare Metastannic Acid

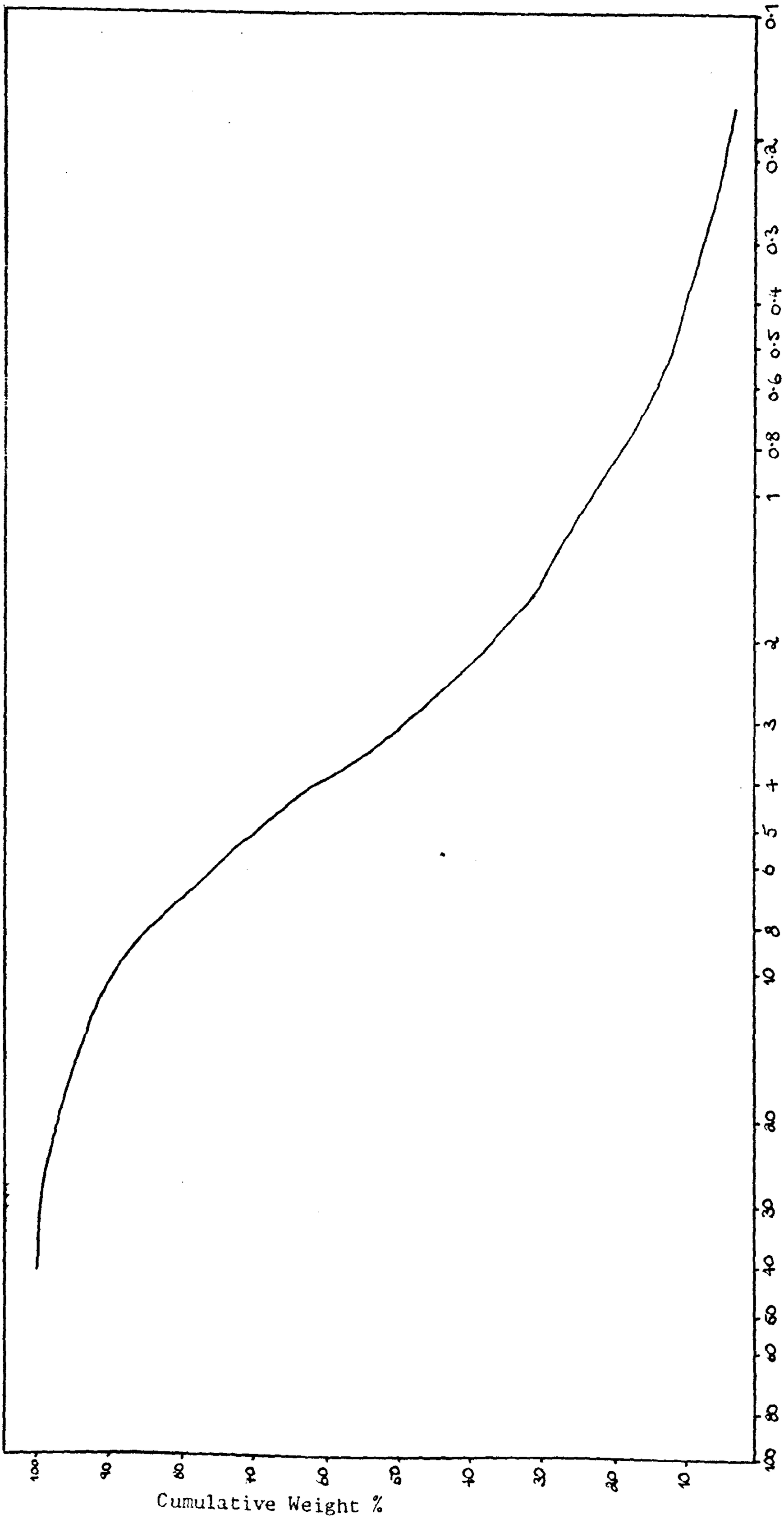


Figure Nine - Sedigraph Analysis of Metastannic Acid B1

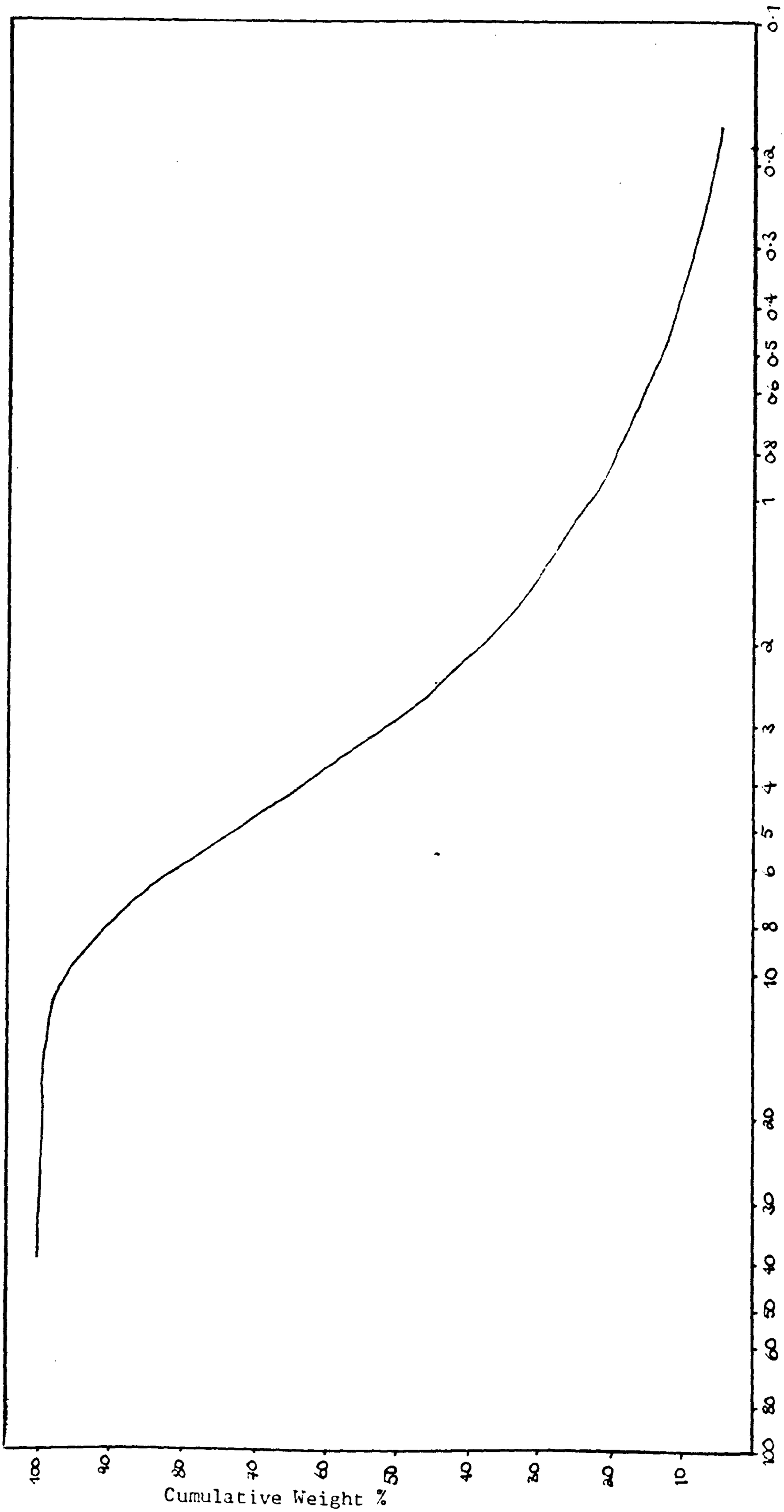


Figure Ten - Sedigraph Analysis of Metastannic Acid B2

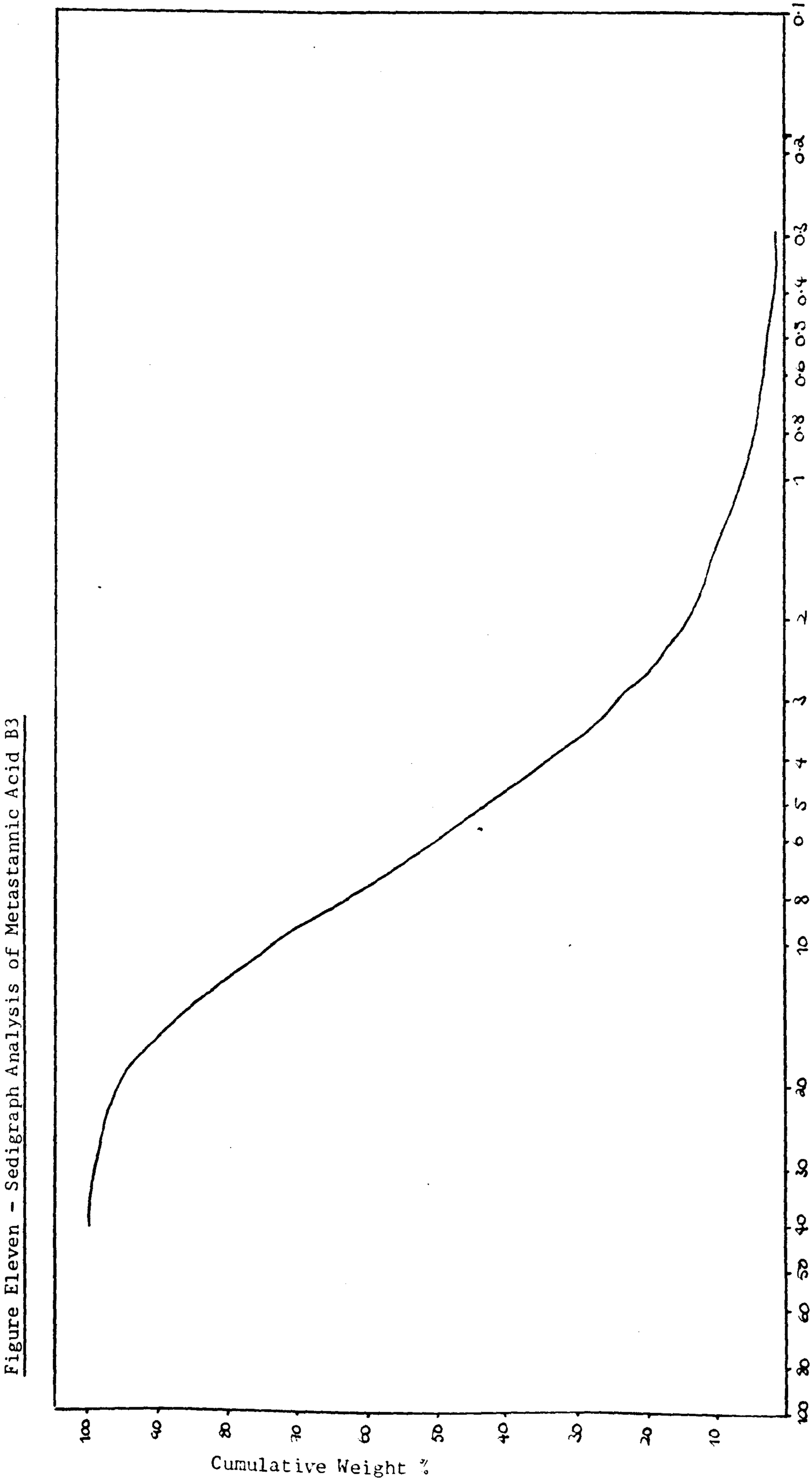


Figure Eleven - Sedigraph Analysis of Metastannic Acid B3

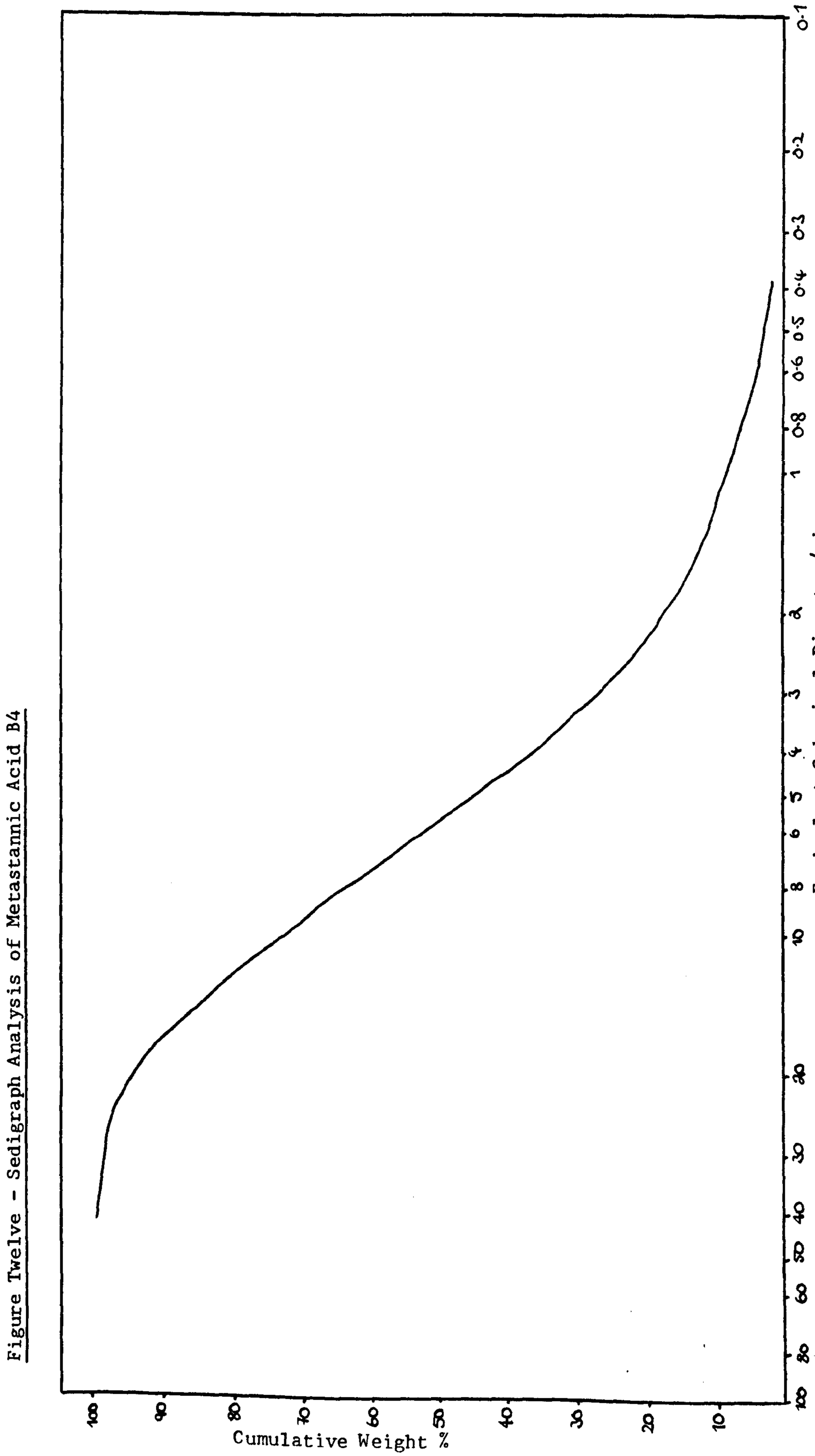


Figure Twelve - Sedigraph Analysis of Metastannic Acid B4

Figure Thirteen - Sedigraph Analysis of Metastannic Acid B5

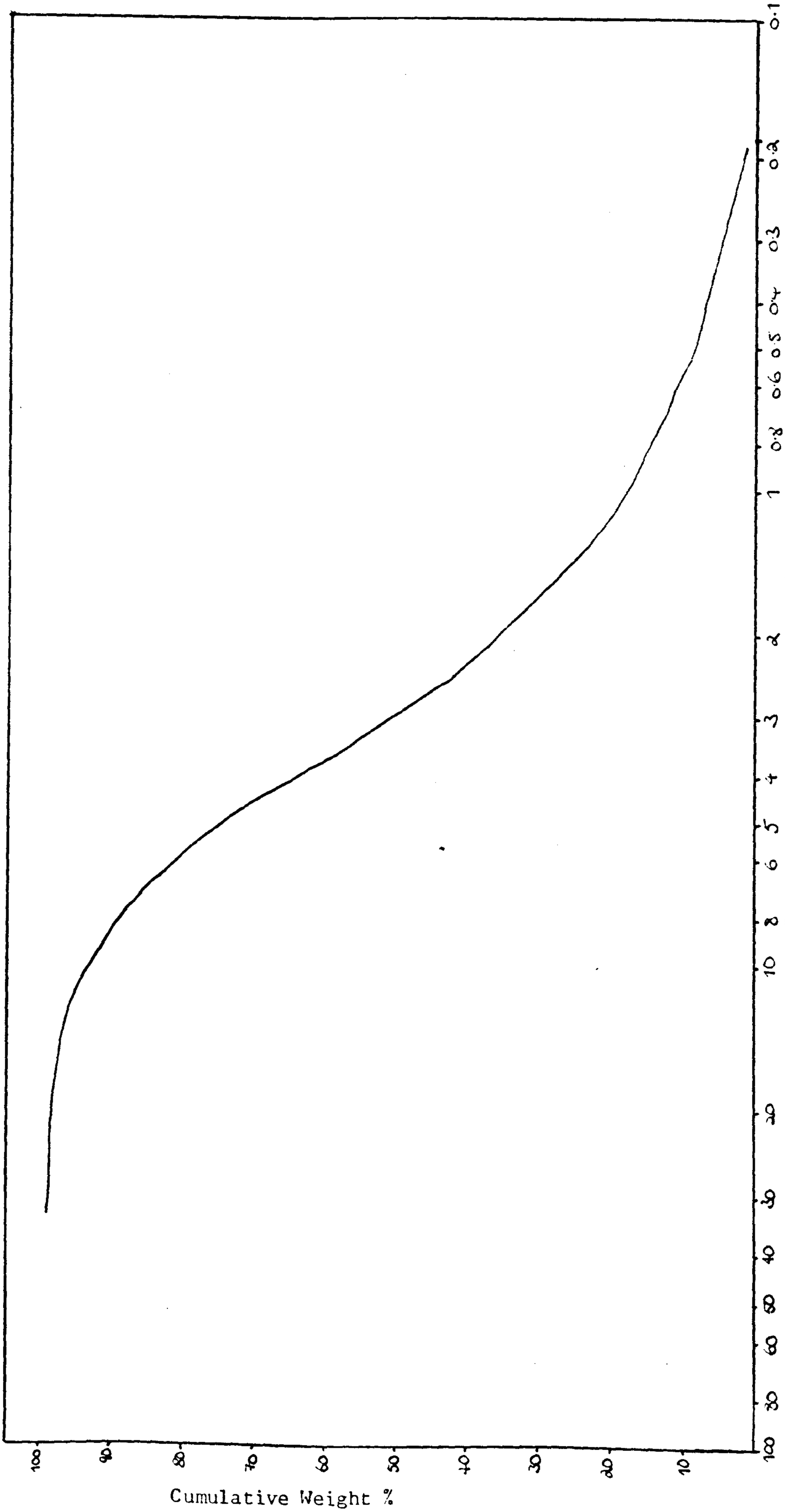


Figure Fourteen - Sedigraph Analysis of Metastannic Acid B6

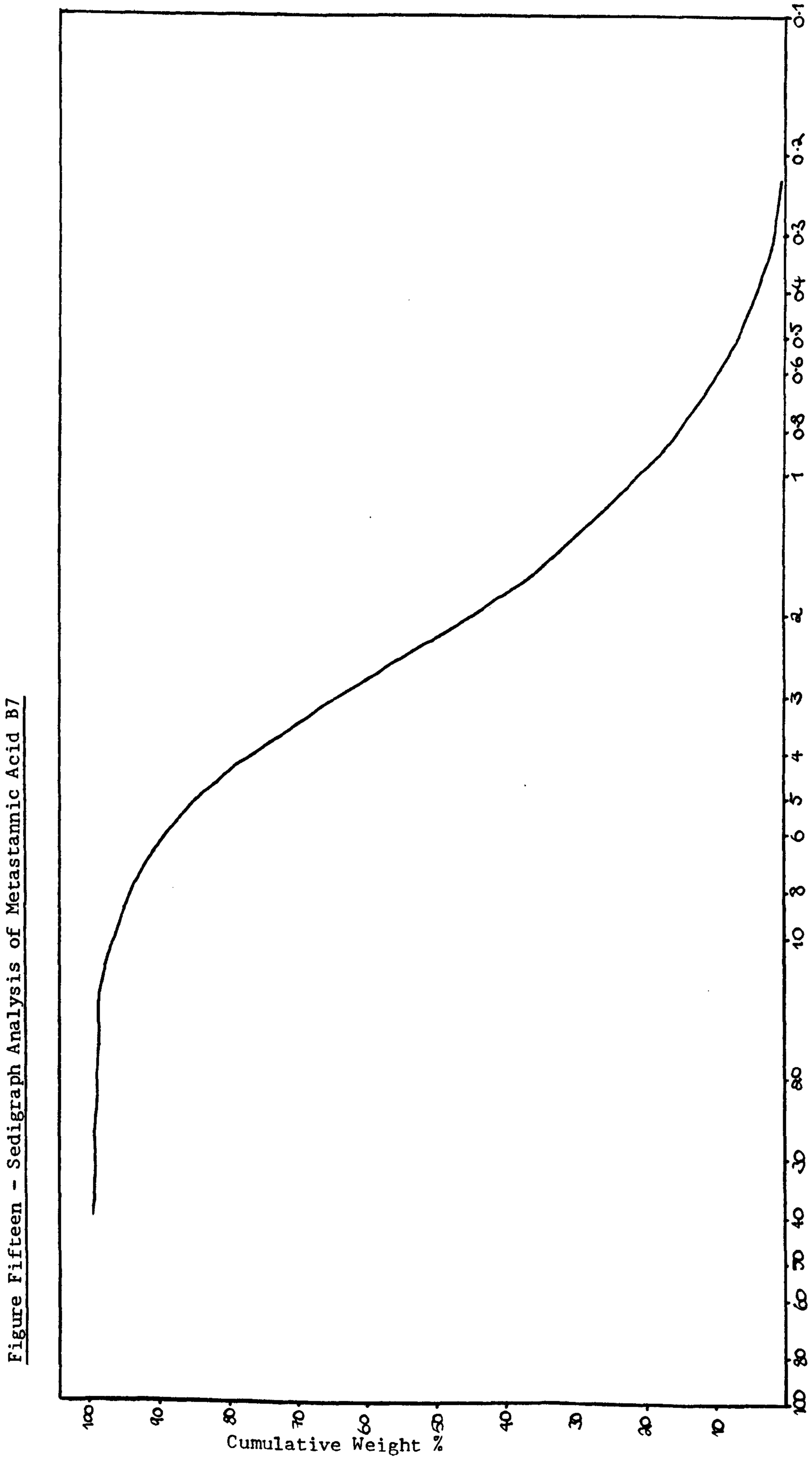


Figure Fifteen - Sedigraph Analysis of Metastannic Acid B7

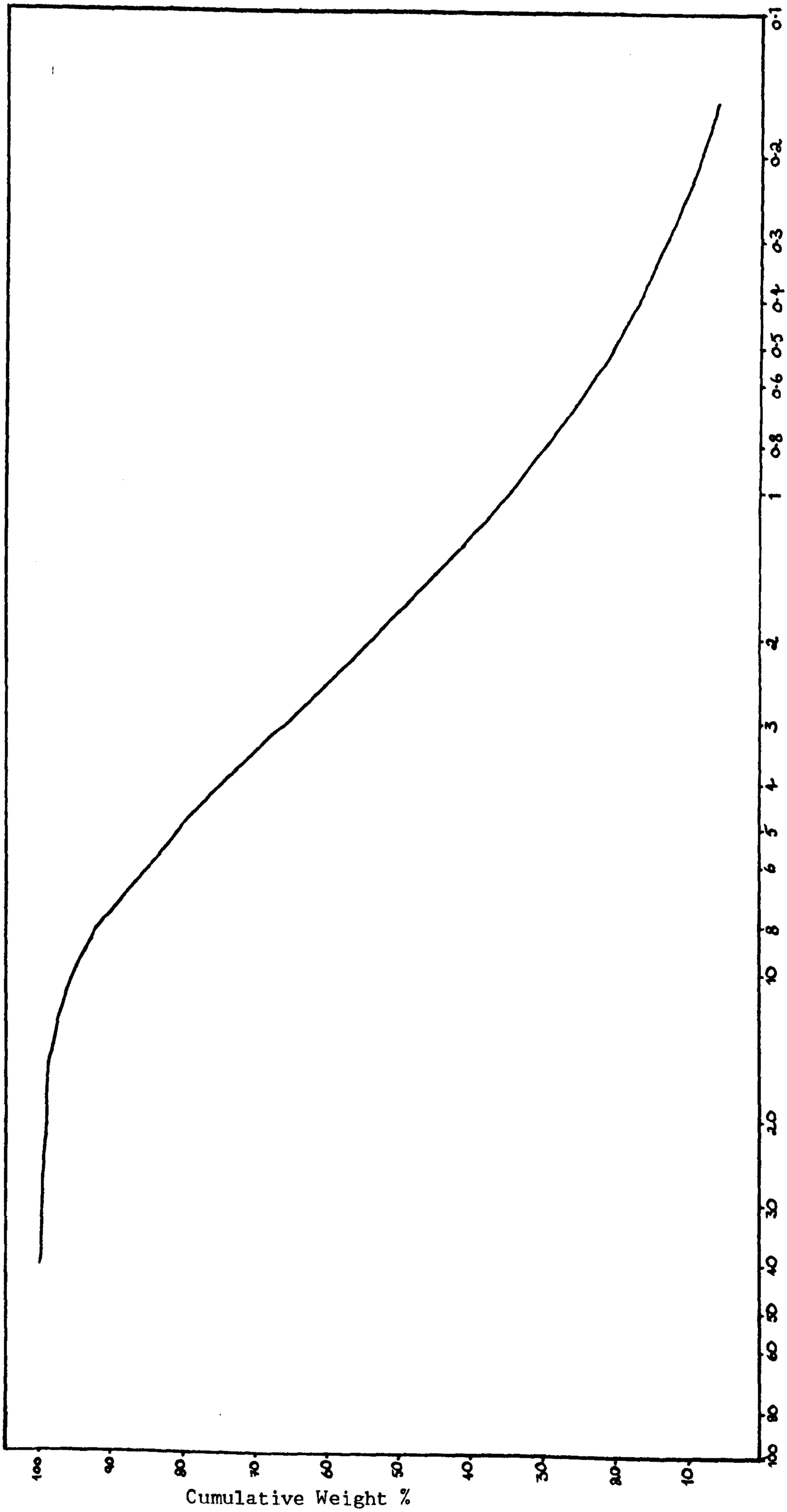


Figure Sixteen - Sedigraph Analysis of Metastannic Acid θ1

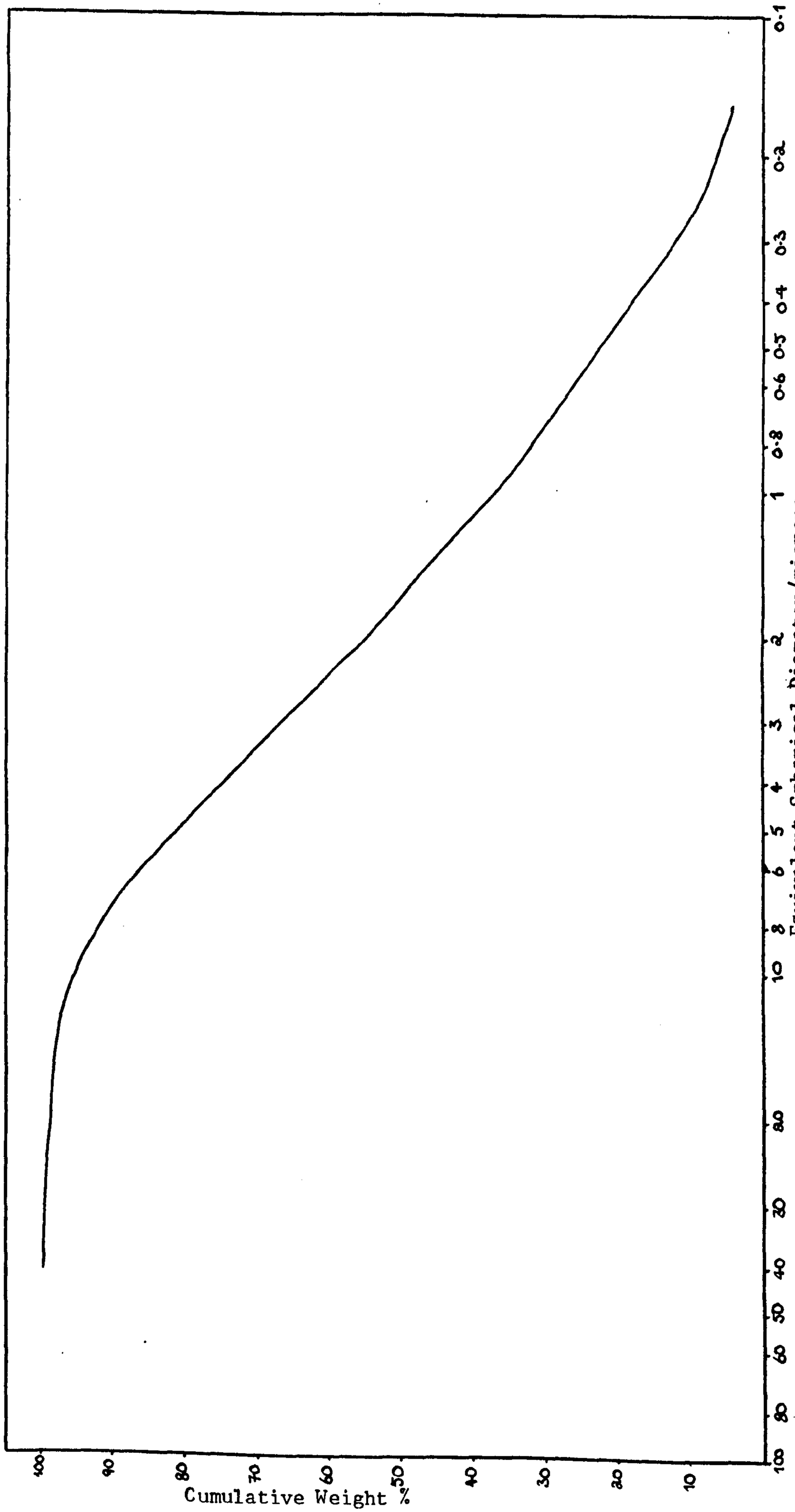


Figure Seventeen - Sedigraph Analysis of Metastannic Acid θ2

Scaling up of the reaction from 1Kg was carried out at Keeling and Wal--ker's plant at Stoke-on-Trent. Details of work carried out on the large scale manufacture of metastannic acid are given in the next section of this chapter.

## 3.4. The Preparation of Metastannic Acid on a Large Scale

Preliminary experiments on a kilogramme scale described in the previous section suggested that the reaction conditions most likely to result in the controlled production of small particles were those realised in exp--eriment B7. It was hoped that data transfer of these reaction cond--itions onto a larger scale (with slight modifications due to equipment parameters) would enable the production of fine particles of metastannic acid on an industrially viable scale.

The experimental details of the two reactions carried out 'on site' at Keeling and Walker Ltd., denoted Y1 and Y2, are given as follows.

### Experiment Y1

| | |
|---|---|
| Stage One | Loading of Reaction Vessel With; |
| t = 0mins | 1001, 70% Nitric Acid |
| | 401 Water at Room Temp. |
| | 20Kg Tin Metal @ Feed Rate = 1Kg/2 minutes |
| | Cooling Loop on |
| Stage Two | Pumping off from Reaction Vessel of; |
| t = 85mins | 301 of Reaction Medium |
| | Load Reaction Vessel With; |
| | 701, 70% Nitric Acid |
| | 7Kg Tin Metal @ Feed Rate = 1Kg/2 minutes |

| | |
|---|---|
| Stage Three | Pumping off from Reaction Vessel of; |
| t = 110mins | 25l of Reaction Medium |
| | Load Reaction Vessel with; |
| | 25l, 70% Nitric Acid |
| | 9Kg Tin Metal @ Feed Rate = 1Kg/2 minutes |
| | Reaction left to completion |
| Overall | Addition of 235l of 58% Nitric Acid |
| | and 36Kg of Granulated Tin Metal. |
| | Ratio = 1 : 6·5 |

The reaction temperature in the vessel was measured every 15 minutes and the reaction temperature profile is shown in figure eighteen.

Experiment Y2

| | |
|---|---|
| Stage One | Loading of Reaction Vessel With; |
| t = 0mins | 150l, 70% Nitric Acid |
| | 70l Water preheated to 80$^{o}$C |
| | 30Kg of Tin Metal @ Feed Rate = 1Kg/3 minutes |
| | Cooling Loop off. |
| Stage Two | Cooling Loop Switched on |
| t = 30mins | |
| Overall | Addition of 150l of 60·7% Nitric Acid |
| | and 30Kg of Granulated Tin Metal. |
| | Ratio = 1 : 5 |

The reaction temperature in the vessel was measured every 15 minutes and the reaction temperature profile is given in figure eighteen.

Sedigraph particle size analysis was carried out upon three samples of metastannic acid taken from the two reactions carried out,

Sample MSA - SL - 1A = First pump-off from Reaction Y1

Sample MSA - SL - 1B = Second and Third pump-offs combined from Reaction Y1

Sample MSA - SL - 2 = From Reaction Y2

The results of sedigraph analysis are given in table eight and in figures nineteen, twenty and twenty one.

Figure Eighteen - Temperature Profiles of Reactions Y1 and Y2

A = Sample MSA-SL-1A Taken Here

B = Sample MSA-SL-1B Taken Here

C = Sample MSA-SL-2 Taken Here

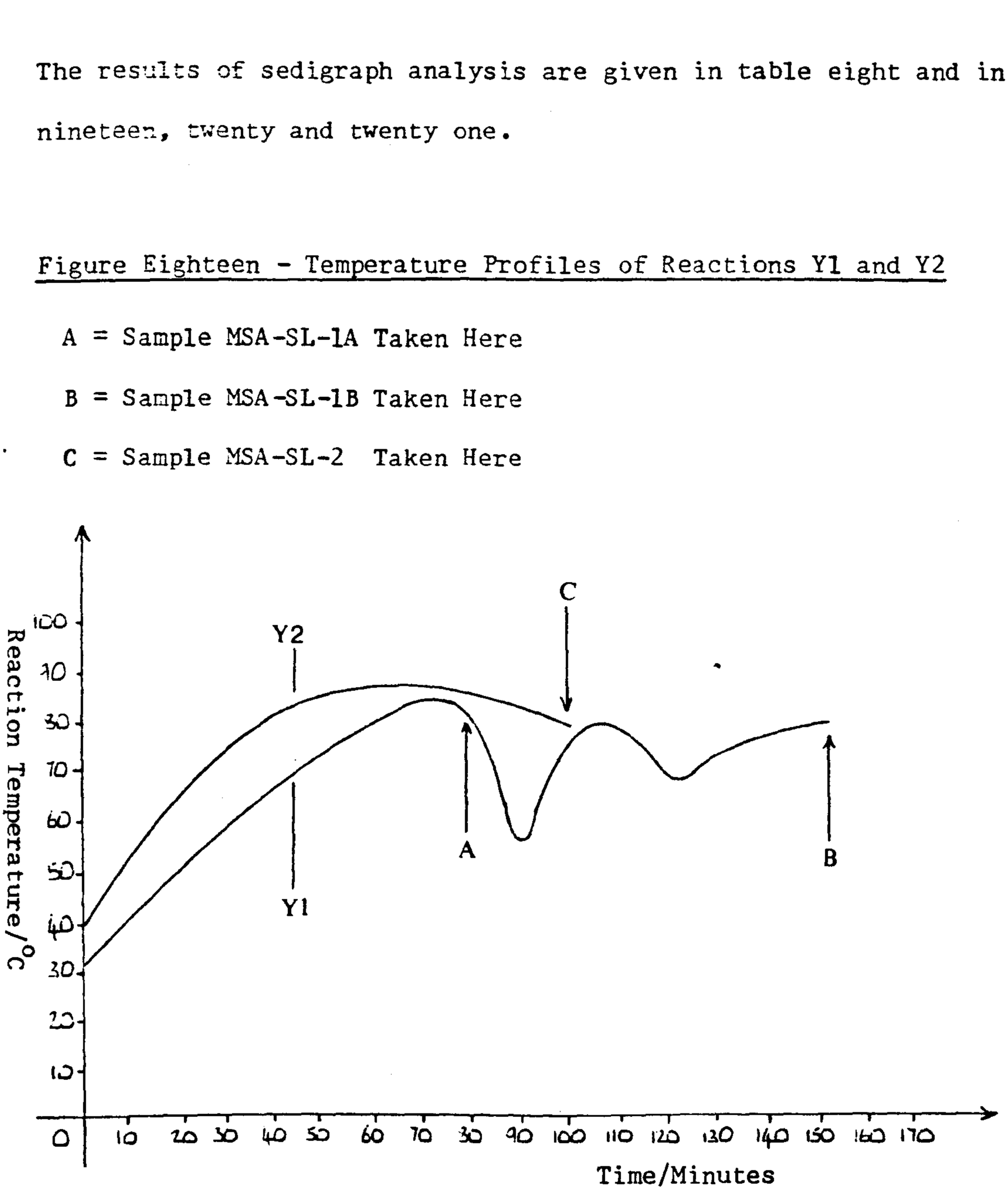

Figures Nineteen Twenty and Twenty One - Sedigraph Analyses of Metastannic Acid

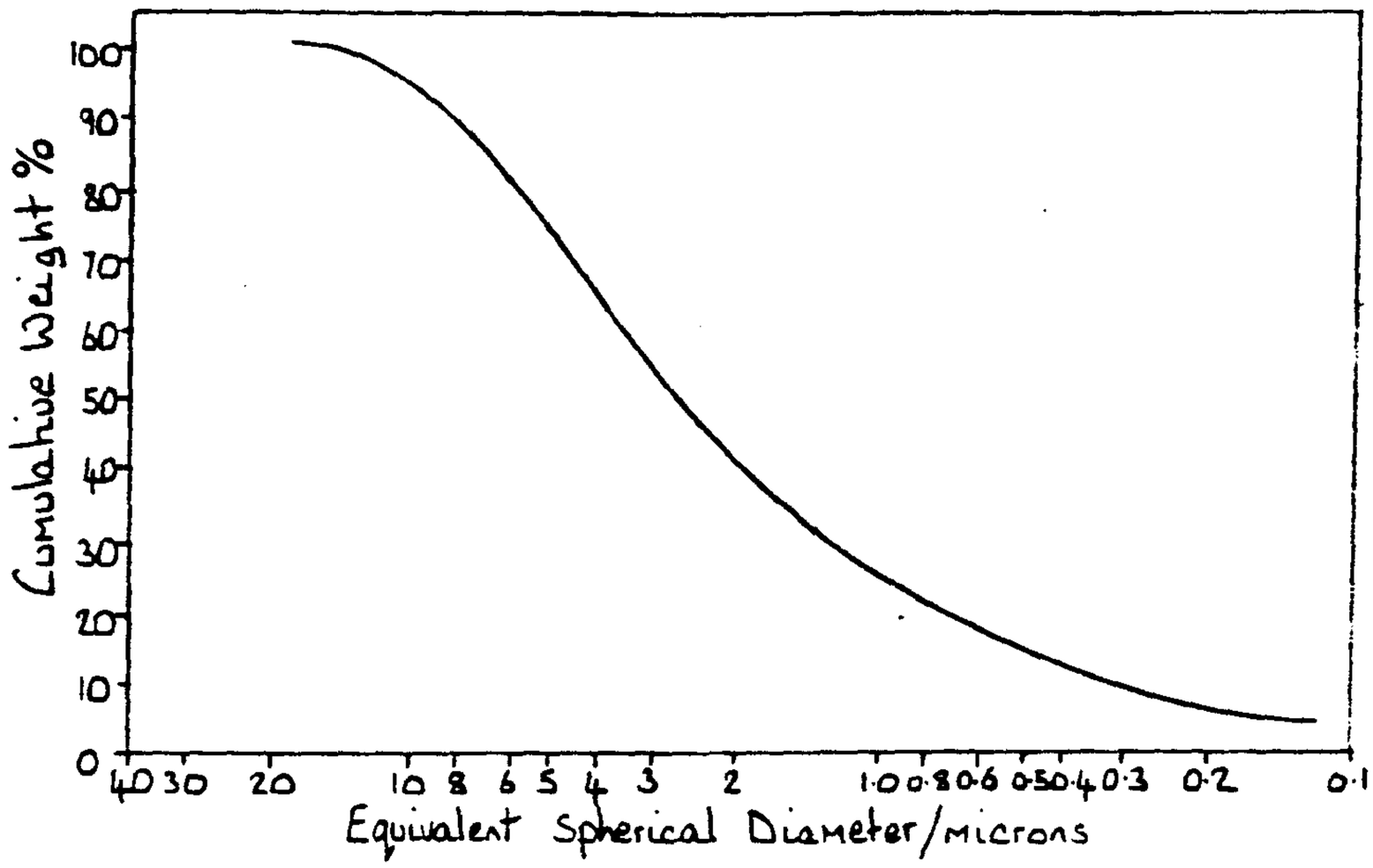


MSA-SL-1A

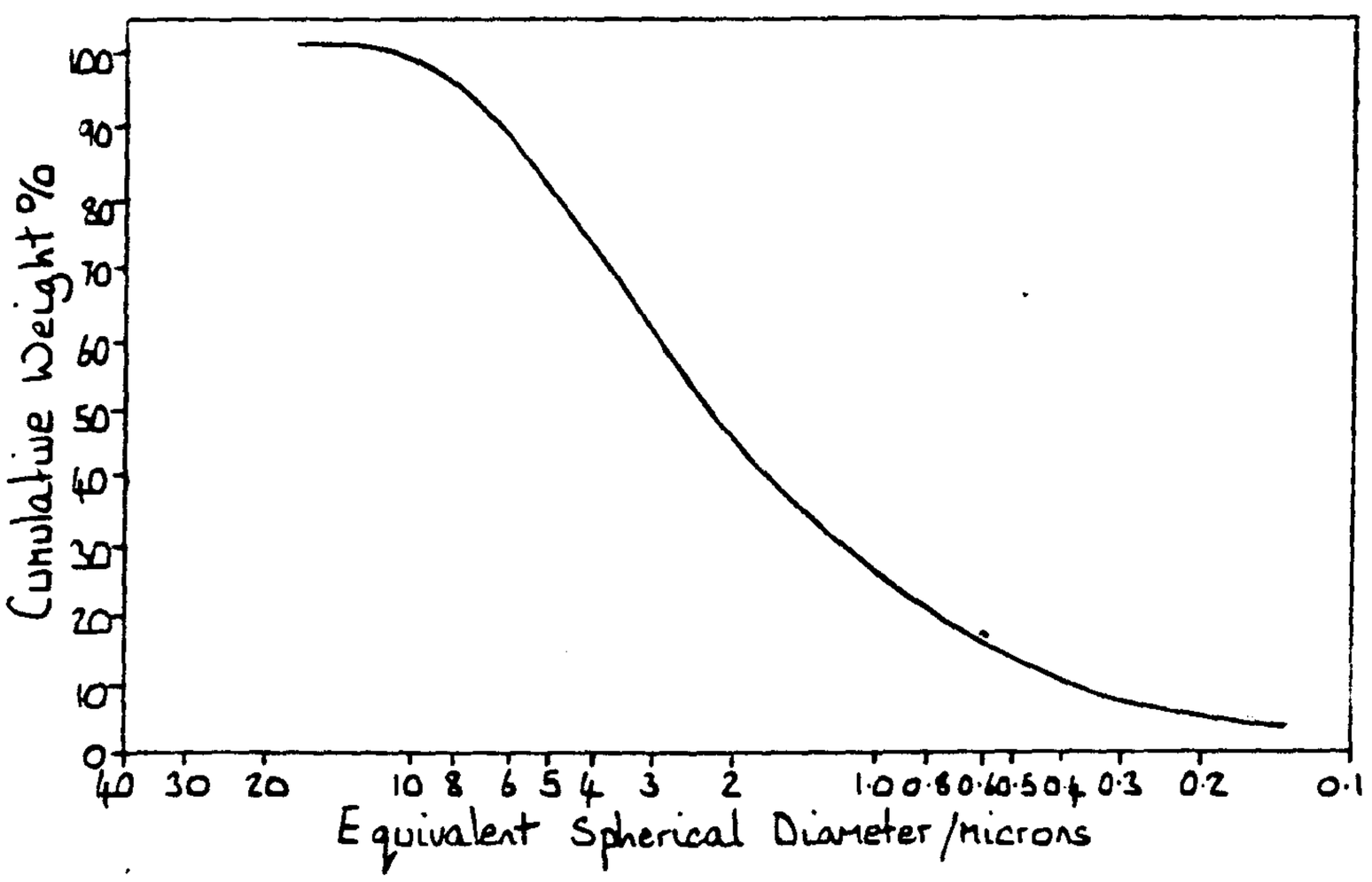


MSA-SL-1B

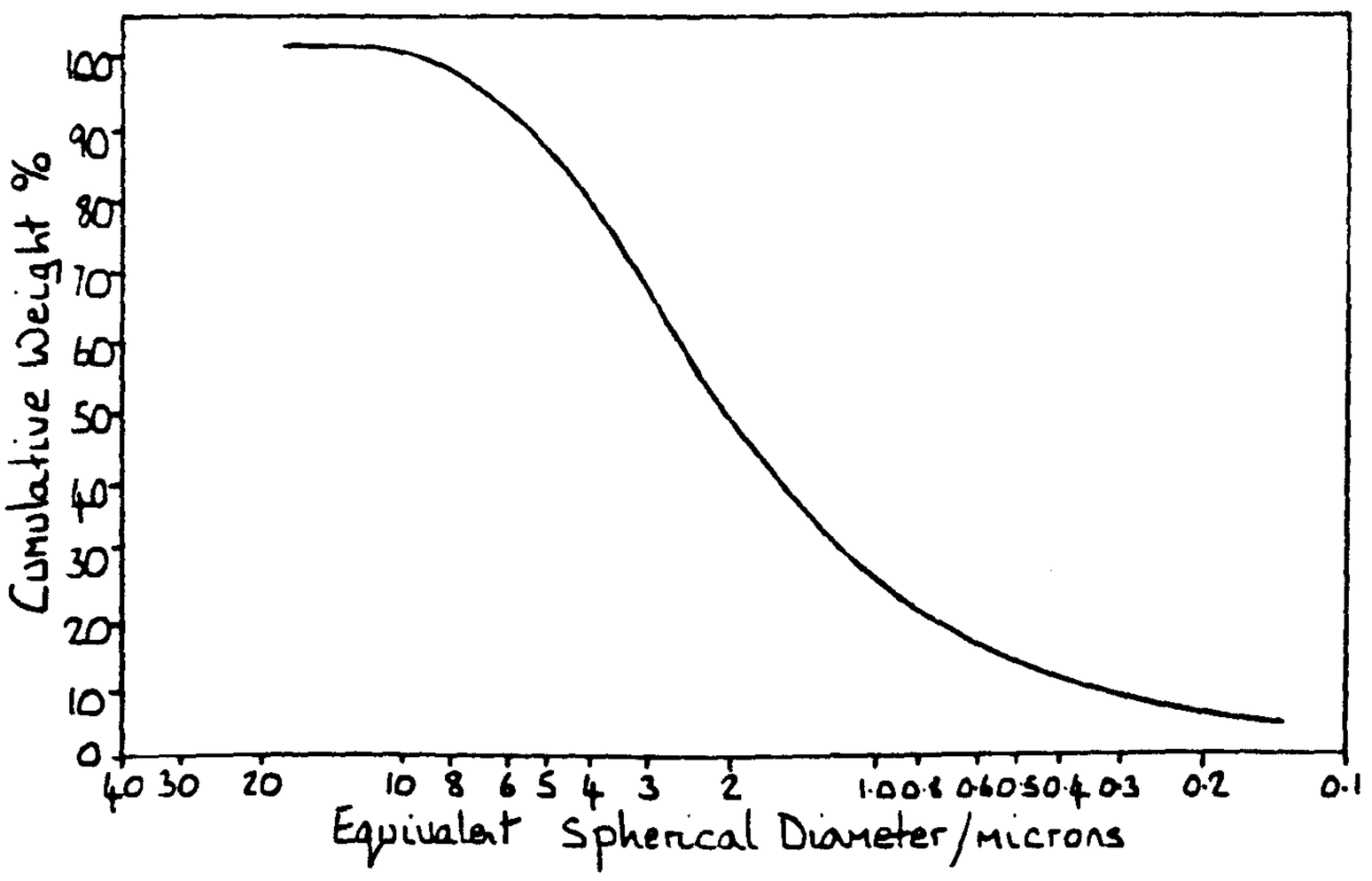


MSA-SL-2

The results in table eight indicate that the reaction conditions most conducive to the controlled production of fine particles are firstly a high operating temperature and secondly a high nitric acid concentration. In addition it was found that to control the reaction in such a way as to give consistent production of a large percentage of small particles in the product the temperature profile curve should approximate to the shape shown in figure twenty two. The nearer the experimental temperature profile is to this theoretical profile the nearer will be the particle size of the product to that desired. The production equipment at Keeling and Walker was not designed for operation at high temperatures in excess of 75-80$^{o}$C and so the temperature profile of experiment Y2 most probably represents the best possible reaction conditions which can be realised on the existing plant.

Design defects identified in the plant which prevented its operation at temperatures in excess of 80$^{o}$C were.

(i) An inadequate scrubbing system for the removal of nitrogen dioxide fumes.

(ii) The tin metal entry port was prone to blocking with feed and also its design enabled nitrogen dioxide gas to escape from the reaction vessel into the working environment without passing through a fume scrubber

(iii) The stirrer speed was too slow to keep the reaction medium homo--geneous and so maintain a constant rate of reaction.

Special attention was given to rectify these points in the outline for the pilot plant design given in the next section of this chapter.

Table Eight - Sedigraph Particle Size Analyses of Metastannic Acid Produced from Experiments Y1 and Y2.

| Reaction | Sample | % Under 10$\mu$m | % Under 1$\mu$m | Median/$\mu$m |
|---|---|---|---|---|
| Y1 | MSA-SL-1A | 95 | 23 | 2·7 |
| Y1 | MSA-SL-1B | 99 | 23 | 2·4 |
| Y2 | MSA-SL-2 | 99 | 23 | 2·3 |

## 3.5. Pilot Plant Design

Keeling and Walker's original specifications for a new metastannic acid plant were for two reactors which would produce 100 tonnes of metastan--nic acid per year i.e. one reactor to produce 50 tonnes of metastannic acid per year. Assuming that the plant was to operate for 47 weeks of the year on a four day week (one day per week for maintenance and prep--aring for the next weeks operation) one reactor would then have to pro--duce 0·27 tonnes of metastannic acid per day.

Since metastannic acid (= $SnO_2.nH_2O$ where typically n = 0·93) contains 71% tin by weight.

0·3 tonnes of metastannic acid contain 0·21 tonnes of tin metal.

Therefore to produce 0·3 tonnes of metastannic acid each reactor will require 213 Kg tin metal feed per day (1 tonne = 1000 Kg).

Results obtained from the large scale manufacture of metastannic acid showed that the finest particles of material were produced when the temperature of the reaction mixture was above 90$^{o}$C. An ideal temper--ature profile for the production of fine particles of metastannic acid is shown in figure twenty two. Whilst obviously this profile could never be experimentally realised a temperature profile for a real sys--tem which gives a good approximation to the theoretical optimum is shown in the same figure.

Figure Twenty Two - Temperature Against Time for Proposed and Ideal Metastannic Acid Production Cycles

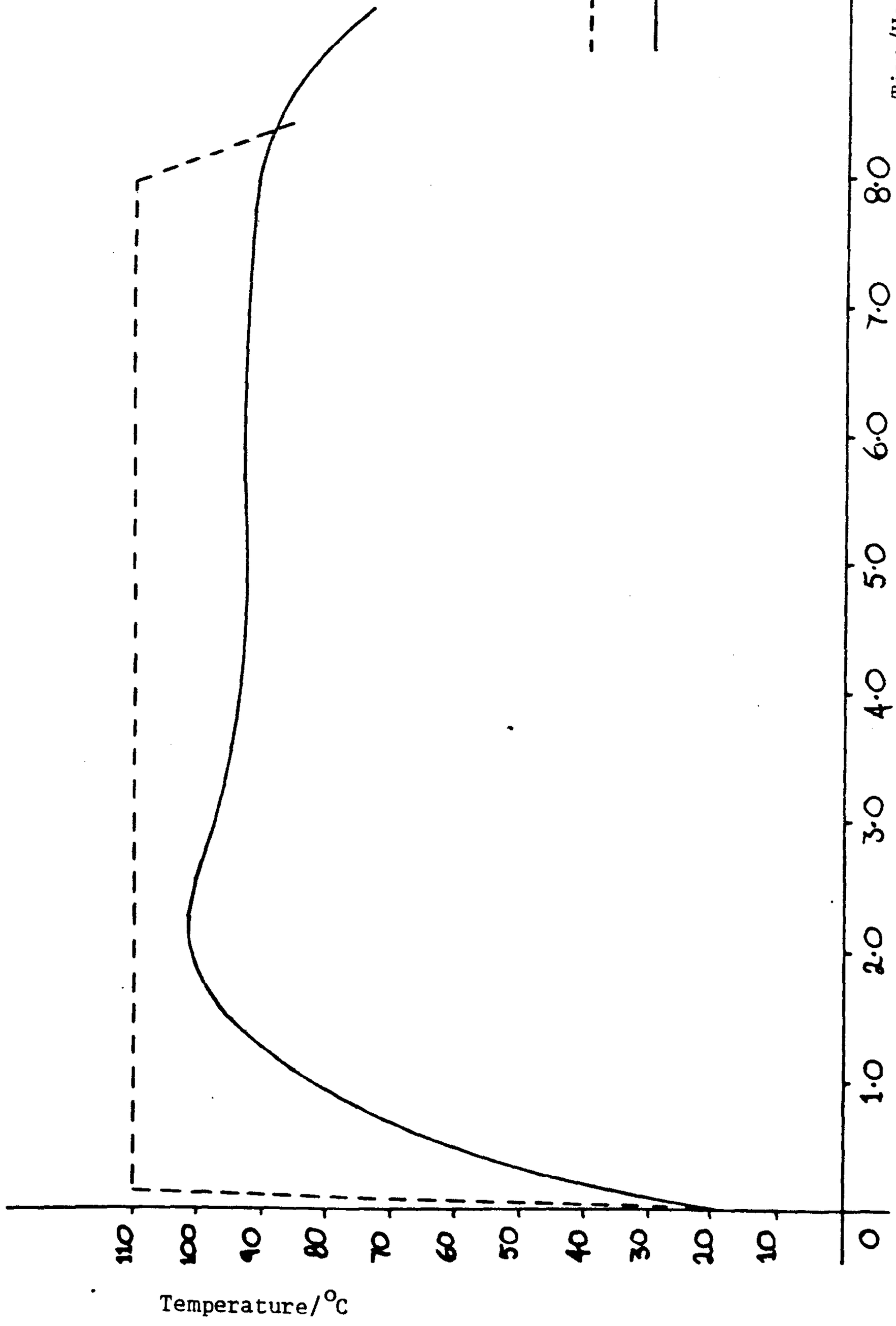

The reaction procedure which would give rise to this temperature profile is given below.

| | | |
|---|---|---|
| <u>Step One</u> | Load Reactor With | 90 Kg granulated tin metal |
| time = 0 Hours | | @ feed rate 3 Kg/4 minutes |
| | | 630 Litres, 60% nitric acid |
| | | (550 Litres stock, 70% acid |
| | | + 80 litres water) |
| <u>Step Two</u> | Pump off from Reactor | 120 litres reaction solution |
| time = 2 Hours | | |
| | Load Reactor With | 41 Kg granulated tin metal |
| | | @ feed rate 1 Kg/2½ minutes |
| | | 100 litres, 70% nitric acid |
| <u>Step Three</u> | Pump off from Reactor | 120 litres reaction solution |
| time = 4 Hours | | |
| | Load Reactor With | 41 Kg granulated tin metal |
| | | @ feed rate 1 Kg/2½ minutes |
| | | 100 litres, 70% nitric acid |
| <u>Step Four</u> | Pump off from Reactor | 120 litres reaction solution |
| time = 6 Hours | | |
| | Load Reactor With | 41 Kg granulated tin metal |
| | | @ feed rate 1 Kg/2½ minutes |
| | | 100 litres, 70% nitric acid |
| <u>Step Five</u> | Pump out Reaction Vessel | |
| time = 8 Hours | | |

Overall Addition of 213 Kg granulated tin metal

850 litres, 70% nitric acid

80 litres water

In order to calculate heat and mass balances for the pilot plant reactor operating on the proposed production cycle it was necessary to make three assumptions as to how the metastannic acid reaction would behave on such a large scale. The first assumption was that the reaction mixture con--tained in the vessel would be homogenous at all times, such that any processes occuring in any one part of the reaction medium could be taken as being representative of the whole of the reaction medium.
This assumption is of course not true for real systems as in any reaction containing two or more components the effect of gravity will cause sedi--mentation of the heavier elements in the reaction vessel, this first assumption also does not allow for any 'wall effects' occurring at the sides of the reaction vessel. The second assumption made was that on addition or removal of any material of any phase from the reaction vessel the reaction media would immediately attain a new equilibrium. This second assumption completely ignores any thermodynamic and kinetic considerations that the reaction might have, but like the first assump--tion it can be justified by the results obtained from its usage in these circumstances. The third assumption was that the pilot plant reactor and the existing metastannic acid reactor at Keeling and Walker would be similar. From a chemical engineering viewpoint two objects are said to be similar if there exists a frame of reference with respect to which the behaviour of both objects appears identical. If two systems are similar data transfer is simple as the behaviour of the experimental system will be described by means of relationships which will also hold for the ind--ustrial system.

Therefore assuming that the size and shape of the two different reactors has no effect upon the reaction, direct data transfer may be carried out.

Mass Balance

When working upon 35 Kg preparative batches of metastannic acid on Keel-ing and Walker's plant it was observed that one kilogramme of tin metal will react with 3200 ml of 70% nitric acid leaving 20% nitric acid.

If the assumption is made that the acid volume remains approximately con-stant during the reaction then 1 gram of tin metal will react completely with 0·84g of nitric acid. Thus the steady state of the reaction may be written as follows.

$$Sn + 4HNO_3 \longrightarrow Sn(NO_3)_4 + 2H_2$$

$$Sn(NO_3)_4 \longrightarrow SnO_2 + 4NO_2 + O_2$$

Overall

$$Sn + 4HNO_3 \longrightarrow SnO_2 + 4NO_2 + 2H_2O$$

1g 2·12g 1·27g 1·55g 0·3g

Therefore 2·12 - 0·84 = 1·28g of nitric acid must be regenerated during the course of the reaction at steady state.

$$2H_2O + 4NO_2 \longrightarrow 3HNO_3 + \tfrac{1}{2}H_2O + \tfrac{1}{2}NO$$

$$\tfrac{1}{2}NO \xrightarrow[\text{Oxygen}]{\text{Atmospheric}} \tfrac{1}{2}NO_2$$

Therefore 1g of tin metal will react with nitric acid to yield 1·41g of metastannic acid and 0·194g of nitrogen dioxide.

Thus, 213 Kg Tin Metal ⟶ 300·3 Kg Metastannic Acid

41·3 Kg Nitrogen Dioxide

(26·1$m^3$ of Nitrogen Dioxide)

Where tin is the limiting reagent.

## Acid Balance

### Stage One

Initial Acid Strength = 630 litres, 60% Acid = $\rho$ = 1·37

Final Acid Strength = 630 litres, 42% Acid = $\rho$ = 1·26

Average Acid Strength = 630 litres, 51% Acid = $\rho$ = 1·32

### Stage Two

Initial Acid Strength = 610 litres, 46·6% Acid = $\rho$ = 1·29

Final Acid Strength = 610 litres, 36·7% Acid = $\rho$ = 1·22

Average Acid Strength = 610 litres, 41·5% Acid = $\rho$ = 1·26

### Stage Three

Initial Acid Strength = 590 litres, 49·3% Acid = $\rho$ = 1·31

Final Acid Strength = 590 litres, 35·2% Acid = $\rho$ = 1·21

Average Acid Strength = 590 litres, 40·7% Acid = $\rho$ = 1·25

### Stage Four

Initial Acid Strength = 570 litres, 49·3% Acid = $\rho$ = 1·31

Final Acid Strength = 570 litres, 25·1% Acid = $\rho$ = 1·14

Average Acid Strength = 570 litres, 33·7% Acid = $\rho$ = 1·20

Heat Balance

When working on a 35 Kg preparative batch of metastannic acid it was found that addition of 10 Kg of tin metal to 150 litres of 60% nitric acid caused a rise in temperature of the reaction medium of 34°C over 30 minutes.

The specific heat capacity of 12M nitric acid was taken to be 332·1 joules/deg.C/Kilogramme.

Stage One

Reaction Starting Temperature = 18°C.

The addition of 90 Kg of tin metal to 630 litres of acid will create a rise in temperature of +72·9°C.

Therefore after two hours the reaction temperature = 100·9°C

Stage Two

Pump off 120 litres from the reaction vessel. Assuming no further reaction the remaining 510 litres of reaction solution will have cooled down to 45°C after 2 hours.

Heat Output = $E_1$ = 332·1 x (100·9-45) x (510x1·26)

= 11929477 joules

Now the addition of 41 Kg of tin metal to 100 litres of nitric acid will generate a rise in temperature of + 209·1°C.

Heat Input = $E_2$ = 332·1 x 209·1 x (1·42x100)

= 9860779·6 joules

Heat Balance for stage two $E_2 - E_1$ = -2068697·4 joules

$$T = \frac{-2068697 \cdot 4}{332 \cdot 1 \times 1 \cdot 26 \times 610} = -8 \cdot 1^{\circ}C$$

Reaction Temperature Falls to 92·8°C after 4 hours

Stage Three

Pump off 120 litres from reaction vessel. Assuming no further reaction the remaining 490 litres of reaction solution will have cooled down to $43 \cdot 5^{o}C$ after two hours.

Heat Output = $E_3$ = 332·1 x (92·8 - 43·5) x (490 x 1·22)

= 9787498·4 joules

Heat Input = $E_2$ = 9860779·6 joules

Heat Balance for Stage Three = $E_2 - E_3$ = -73281·2 joules

$$T = \frac{-73281 \cdot 2}{332 \cdot 1 \times 590 \times 1 \cdot 25} = -0 \cdot 31^{o}C$$

Reaction Temperature falls to $92 \cdot 5^{o}C$ after 6 hours

Stage Four

Pump off 120 litres of reaction solution. Assuming no further reaction the remaining 470 litres of solution will have cooled down to $40 \cdot 2^{o}C$ after 2 hours.

Heat Output = $E_4$ = 332·1 x (92·5 x 40·2) x (470 x 1·22)

= 9926633·7 joules

Heat Input = $E_2$ = 9860779·6 joules

Heat Balance for Stage Four = $E_2 - E_4$ = -65854·1 joules

$$T = \frac{-65854 \cdot 1}{332 \cdot 1 \times 570 \times 1 \cdot 2} = 0 \cdot 29^{o}C$$

Reaction Temperature falls to $92 \cdot 2^{o}C$ after 6 hours.

A schematic representation of the proposed metastannic acid manufacturing plant to operate on the high temperature production cycle outlined earl-ier is shown in figure twenty three.

Figure Twenty Three - Schematic Representation of the Pilot Plant

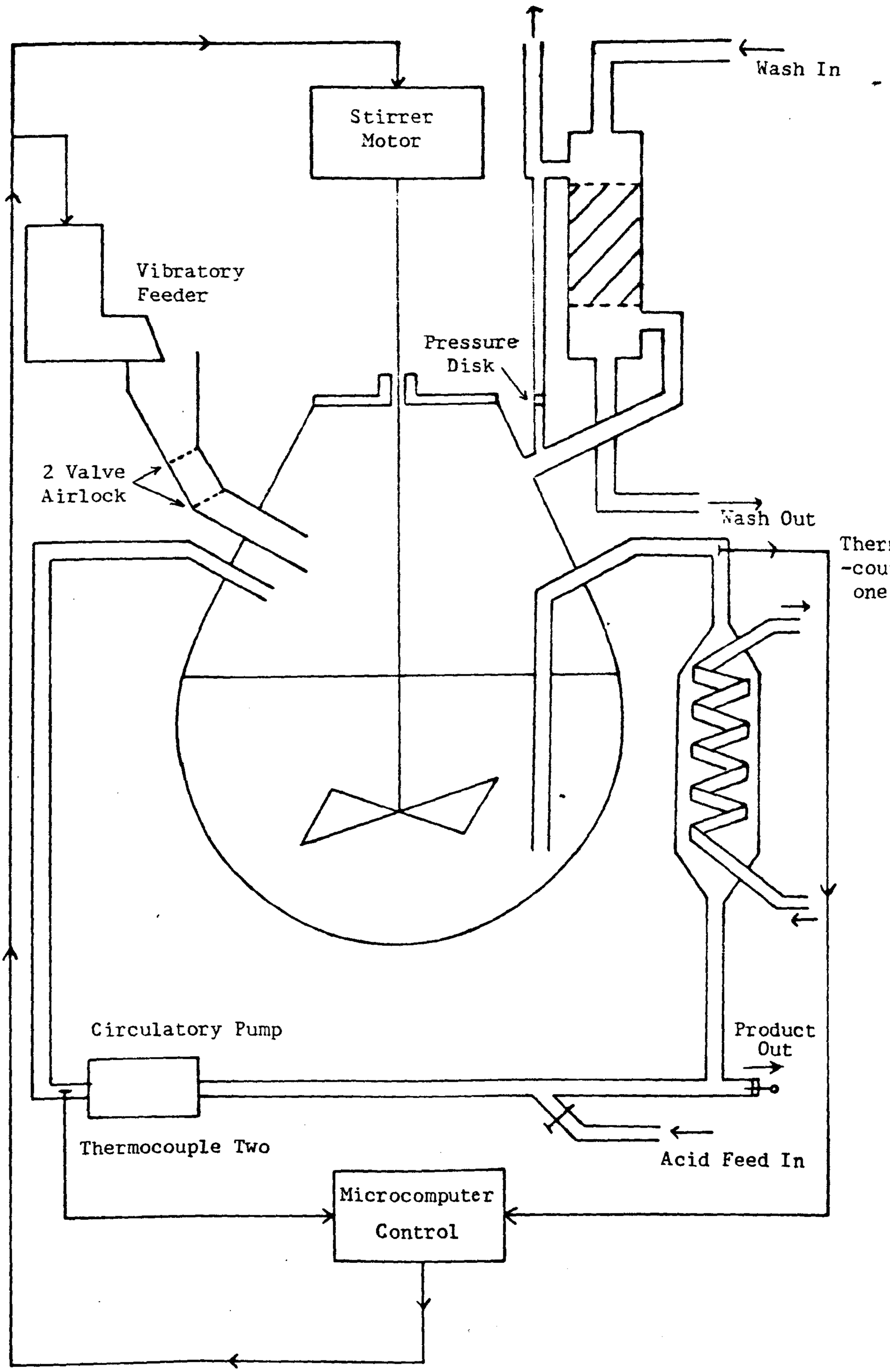

Table Four - Results of Mercury Porosimetric Analysis on Metastannic Acid

| Characteristic | Sample One | Sample Two |
|---|---|---|
| Mean Particle Diameter/$\mu$m | 2•9 | 4•5 |
| Standard Deviation of Particle Diameter/$\mu$m | 2•1 | 0•1 |
| Surface Area/$m^2g^{-1}$ | 0•86 | 0•67 |
| Pore Volume/$cm^3g^{-1}$ | 0 | 0 |
| Intrusion Volume/$cm^3g^{-1}$ | 0•23 | 0•17 |

At an applied pressure of about $100Kg/m^2$ all of the interparticular voids become filled and further increases in pressure do not result in any further uptake of mercury in non-porous samples, normally this region of the mercury uptake curve (region 2) would represent uptake of mercury by a porous sample. Therefore the results of mercury porosimetric analysis would indicate that the samples are non-porous or that any pores in the material are blocked to the mercury probe. This second explanation would seem to be most likely as Fuller, Warwick and Walton[12] reported that their degassed metastannic acid analysed by B.E.T. was highly porous and had a specific surface area of around $100m^2g^{-1}$. The failure of the mercury porosimeter to detect any pore structure can be accounted for by hydroxyl groups on the material's surface sterically blocking any pore openings and so excluding the mercury probe. These hydroxyl groups may be removed by heating as is carried out in the B.E.T. degassing treatment prior to analysis and this would explain Fuller etal's identification of pore structure in metastannic acid.

The analyses performed by mercury porosimetry show specific surface areas of below $1m^2g^{-1}$ which is exactly what would be expected for a material comprised of hard spheres and of a mean particle size of a few microns.

The plant consists of a 1000 litre glass reactor vessel equiped with a cooling loop, a scrubbing column and an agitator. Some modifications on the old plant included in the new plant design are.

(i) A microcomputer to control the reaction temperature in the vessel by adjusting the rate of tin metal feed to the reactor and the sp--eed of the stirrer agitating the reaction medium.

(ii) A new high torque stirrer motor able to rotate the paddle stirrer at a variable speed. Due to the high operating temperature of the reaction polypropylene would be unsuitable as a construction material for the stirrer blades and the use of flame coated metal is recommended.

(iii) A tin metal entry port with the inlet tube terminating above the level of the reaction medium in the vessel and fitted with a dou--ble valve airlock to eliminate fume problems. A sidearm fitted with a pressure disk was also included in the design to cope with any sudden pressure build-ups in the reaction vessel.

(iv) An alkali wash scrubber system to reduce the concentration of nitrogen dioxide fumes passed into the environment to below 0·1% in air.

Although the exact particle size specifications of the metastannic acid manufactured by such a plant would be very much dependant upon many equip--ment parameters a mean particle size of 1·8 to 2·0$\mu$m with some 30 Wt.% of particles below one micron diameter would not be inconsistent with the results of this work.

## References


1. I. Touval, J. Fire Flamm., 1972, 3, 130.
2. Jpn. Kokai Tokkyo Hoho, 80,075,45.
3. J. D. Donaldson, J. F. Donbavand, M. M. Hirschler, Eur. Polym. J., 1984, 20, 4.
4. M. J. Fuller, M. E. Warwick, J.C.S. Chem. Comm., 1973, 210.
5. G. C. Bond, C. R. Molloy, M. J. Fuller, J.C.S. Chem Comm., 1975, 796.
6. J. D. Donaldson, M. J. Fuller, J. Inorg. Nucl. Chem., 1968, 30, 1083.
7. J. D. Donaldson, M. J. Fuller, J. N. Price, J. Inorg. Nucl. Chem., 1968, 30, 2841.
8. U. K. Patent, 902952.
9. U. K. Patent, 864666.
10. M. J. Fuller, M. E. Warwick, A. Walton, J. Appl. Chem., Biotechnol., 1978, 28, 396.
11. Jpn. Kokai Tokkyo Hoho, 80, 832, 02.
12. Jpn. Kokai Tokkyo Hoho, 80, 838, 42.
13. A. Neuman, Ber., 1904, 37, 3601.

# Chapter Four - The Synthesis and Properties of Indium Tin Oxides

# Chapter Four - The Synthesis and Properties of Indium Tin Oxides

## 4.1. Introduction

One of the possible future commercial outlets for metastannic acid may be as a material for use in the synthesis of semiconducting metal oxide materials containing tin. There are at present two commerci-ally available conducting mixed oxide phases containing tin (IV) viz. antimony tin oxide and indium tin oxide. At present tin antimony oxide is manufactured by Keeling and Walker as a dark grey/blue powder with a resistivity of between 1·0Ωcm and 0·1Ωcm depending on the particle size of the metastannic acid used in its manufacture.
The current major commercial outlet for tin antimony oxide is in the glass manufacturing industry where it is used to make glass melting electrodes for the production of lead crystal glass. A large potential future market for tin antimony oxide, however, may involve its use as a conductive filler in plastic antistatic coatings. One drawback associated with the use of tin antimony oxide in this area is, however, its high chromophoric character and any plastic doped with the material takes on a strong blue/grey colouration which is undesirable in many uses·including mixed metal oxide doped plastics for sprayed antistatic coatings on carpets and mattings for domestic use.
Although indium tin oxide is a considerably more expensive material than tin antimony oxide due to the relative difference in prices between indium and antimony metals, it has the advantage of having only a slight green colouration and therefore being less chromophoric than tin antimony oxide. For this reason indium tin oxide appears to be an ideal material for use in specialised antistatic plastics in place of the highly coloured tin antimony oxide.

The objective of the work described in this chapter of the thesis was;

(i) to study the resistivities of various indium tin oxides and

(ii) to find a synthetic route for the preparation of low resistivity (c0·2 Ωcm) indium tin oxide that could be used effectively on a commer--cial scale.

Antimony tin oxide and indium tin oxide are both classified as being semiconducting binary metal oxide systems and have resistivities more or less midway between those of metals ($10^{-6}$ Ωcm) and insulators ($10^{8}$--$10^{10}$ Ωcm). Although there are large differences in the scale of electrical conductivity between metals and semiconductors there are many features in the conduction processes which are common to both types of material and which may be explained by use of the free elec--tron model, a brief treatment of which is given below.

The free electron model starts with two basic assumptions. Firstly that the conduction electrons behave towards one another as uncharged particles and secondly that the potential within a crystal is essen--tially uniform. Although these assumptions appear at first glance to be rather crude they are justified by their successful applications in explaining real systems.

The first assumption appears unrealistic in the light of the mutual electrostatic repulsive forces between like charged species such as electrons, however in solids electrons are held together against mu--tual coulombic repulsion by the greater coulombic attraction from positive ions within the material. This then enables electrons to be treated as single uncharged species.

The second assumption also appears unrealistic as it might be supposed that a row of positive ions would lead to a row of deep potential wells each of which would bind an electron to secure neutrality as illustrated in figure one. This problem however never really arises because, when atoms bind together to form solids, the outer electron energy levels overlap and broaden into energy bands and in the solid state this pro-
-cess is repeated throughout the material. Consequently the wavefunc-
-tions corresponding to the highest energy electrons can spread and mix throughout the material and are no longer confined to the potential wells. It is the electrons in these higher levels which act as conduction elec-
-trons. In a crystal of N atoms the same effect takes place. As N atoms are brought together to form the crystal each atomic energy state splits into N levels and the average energy decreases until the atoms are at their equilibrium separation $R_o$. When N becomes very large these levels merge into one another to form a band of allowed energies and are in general separated from neighbouring bands by a forbidden band of energies. This process is illustrated diagramatically in figures two to four.

One consquence of the free electron model is that the principal differ-
-ence between metals and insulators can be defined in terms of the occupation of the highest energy bands. Under normal conditions the electrons in insulators can be defined in terms of the occupation of the highest energy bands. At sufficiently high temperatures however the electrons in insulators can be excited from the valence band over the energy gap and into the conduction band. In this way insulators become ideal or intrinsic semiconductors and the incompletely filled energy bands (valence and conduction) give rise to electronic conduc-
-tion.

Figure One- Electronic Wavefunctions Generated by a Unidimentional Row of Positive Ions.

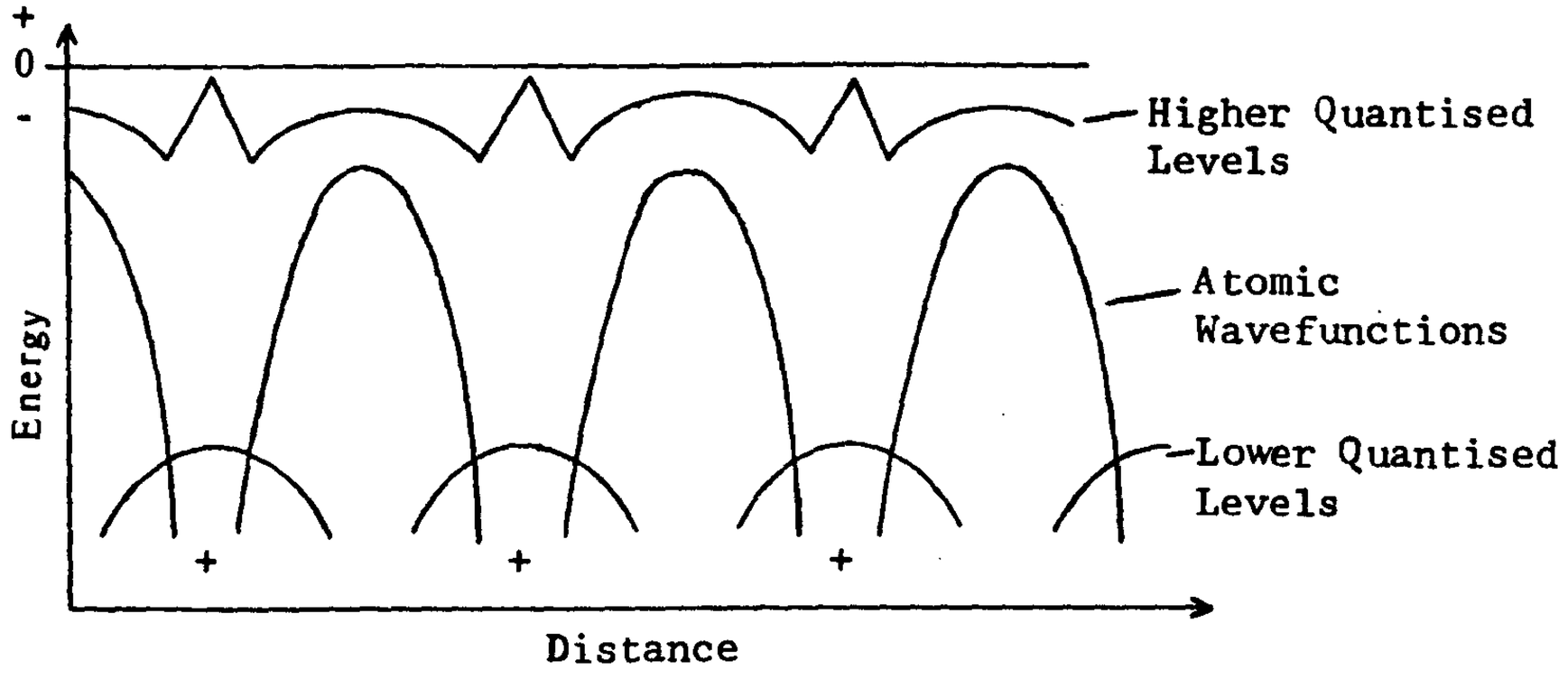


Figures Two, Three and Four - The Formation of Electronic Energy Bands in Solids from Overlapping Individual Wavefunctions.

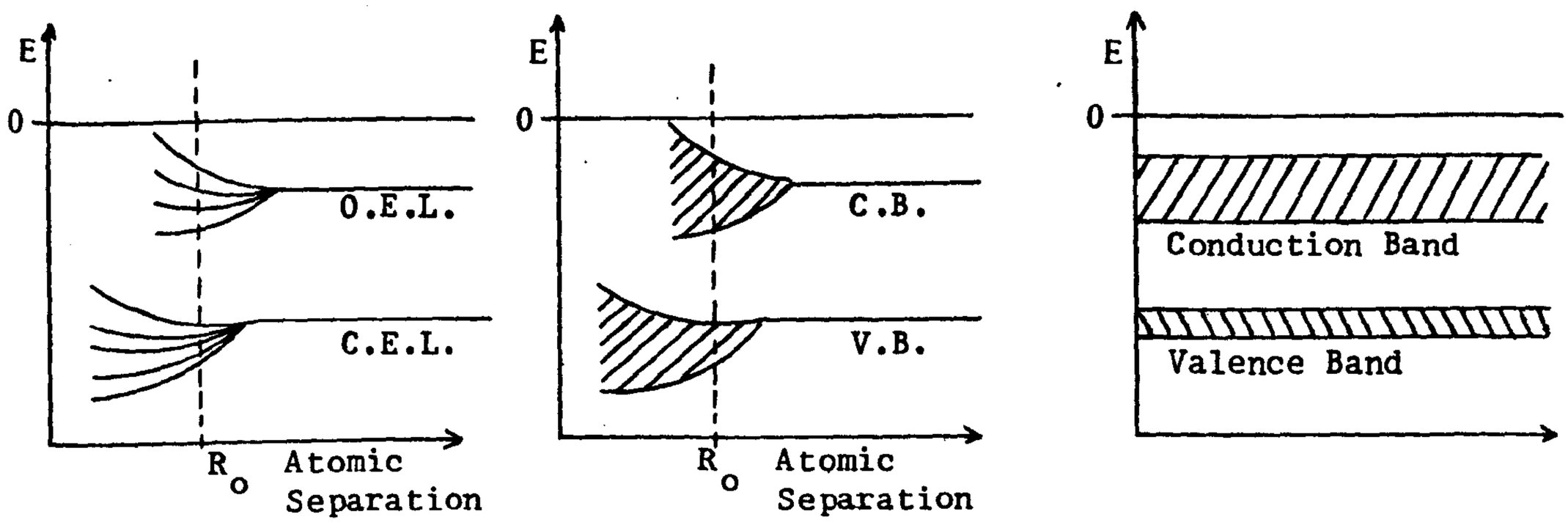


O.E.L. = Outer Electron Levels

C.E.L. = Core Electron Levels

C.B. = Conduction Band

V.B. = Valence Band

An intrinsic (or ideal) semiconductor is one in which the electrical properties are determined by the host material.

Inevitable imperfections in crystals, such as impurities and lattice defects lead to additional allowed energy levels in the energy gap between the valence and conduction bands. Excitation of electrons from the valence band to unoccupied defect levels or from occupied defect levels to the conduction band leads to incompletely filled en--ergy bands which permit electrical conduction. Semiconductors dis--playing this type of conductivity are called extrinsic or impurity semiconductors. An extrinsic semiconductor is one in which the cond--uctivity is governed by chemical or physical impurities.

The energy band diagrams corresponding to metals, insulators and semi--conductors are shown in figure five.

Figure Five - Energy Band Diagrams for Metals, Semiconductors and Insulators.

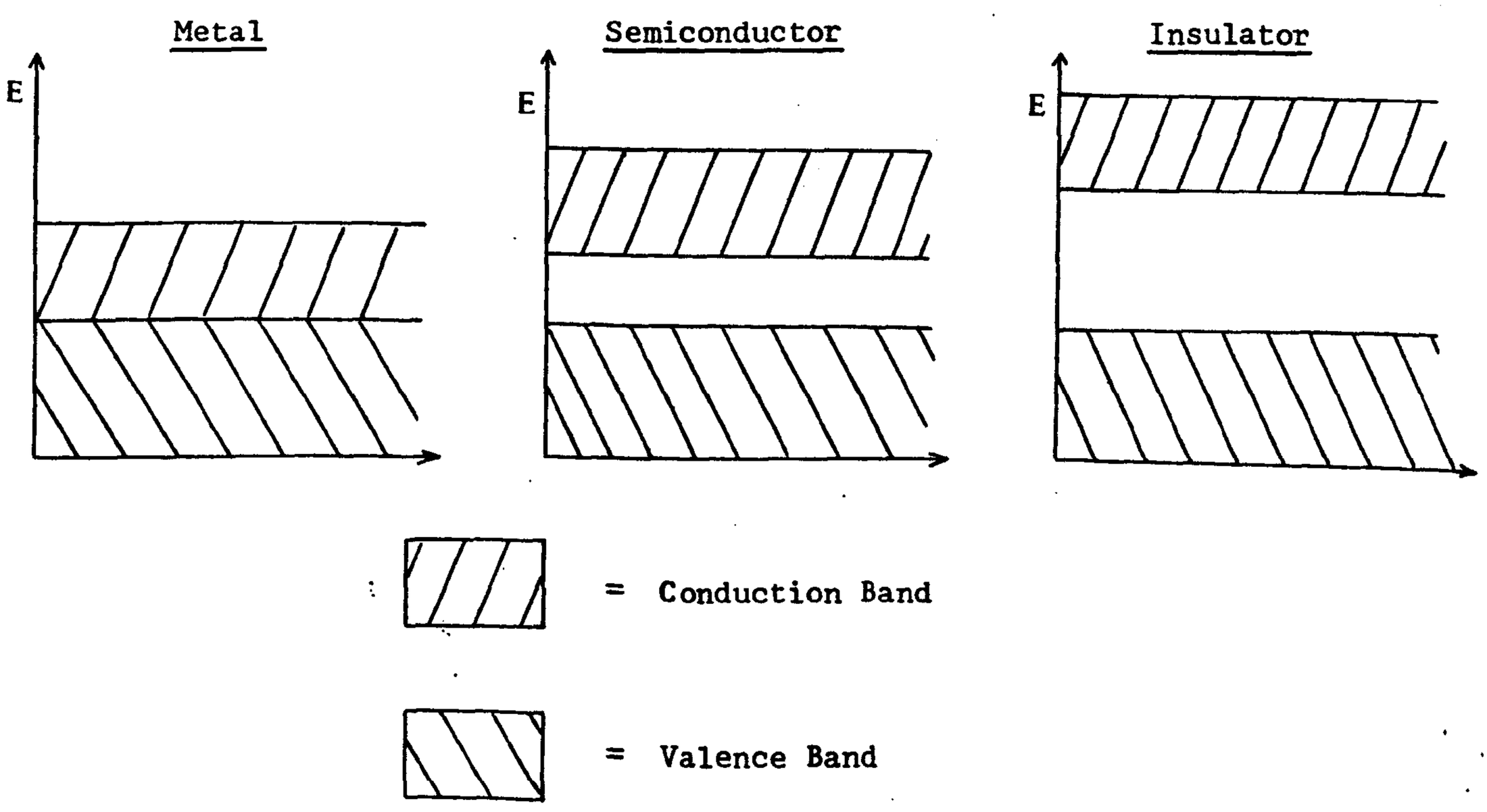

Chemical imperfections may be achieved artificially in materials by incorporating foriegn atoms at lattice sites or interstitial positions within the host sructure. The catagory of extrinsic semiconductors may be subdivided into two further types which are.

n-type in which conductivity arises from an excess of negative charges. This can be illustrated by the replacement of one atom in a germanium crystal with an antimony atom, the crystal will then contain on substit--ution one more electron than is necessary to satisfy covalent bonding requirements and which may then become a conduction electron at quite low temperatures. Doping of this kind leads to an energy diagram of the type shown in figure six.

Figure Six - Effects of Antimony Doping in a Germanium Crystal

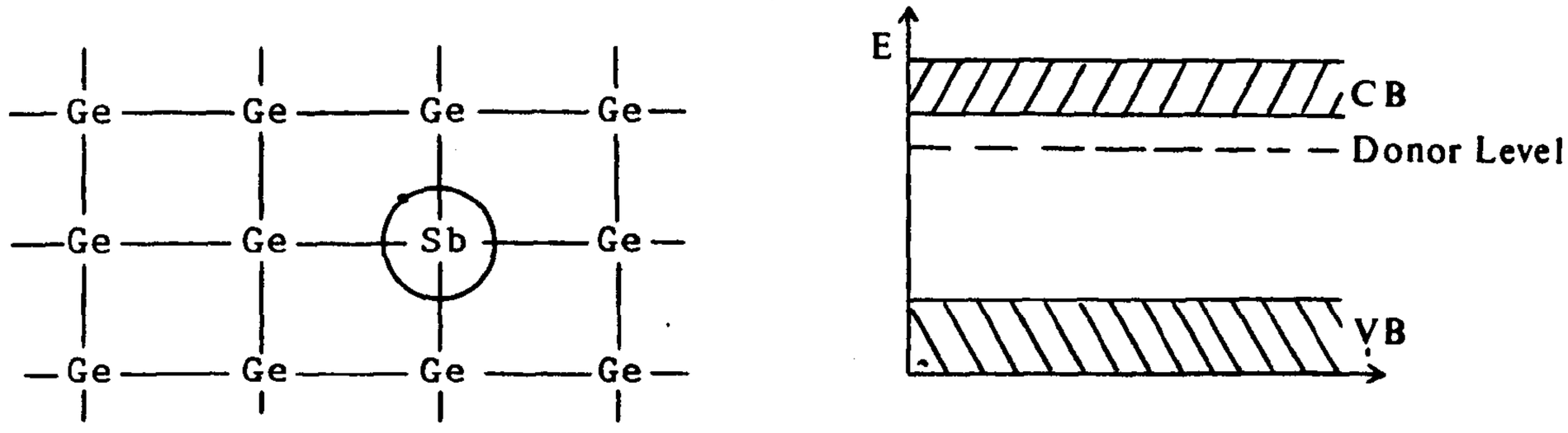


In the example each impurity atom donates one electron into the pool of conduction electrons, the impurity energy levels are known as donor lev--els At high concentrations of dopant species dopant impurity bands are formed which give rise to a number of useful characteristics.

p-type in which conductivity arises from an excess of positive carriers. This can be illustrated by the replacement of one atom in a germanium crystal by an indium atom. In this case the crystal will contain one electron fewer than the number usually participating in the covalent bonds.

There is therefore a tendency for this atom to attract electrons, so that it effectively acts as a source of electron holes, this is shown in the form of an energy band diagram in figure seven.

Figure Seven - Effects of Indium Doping in a Germanium Crystal

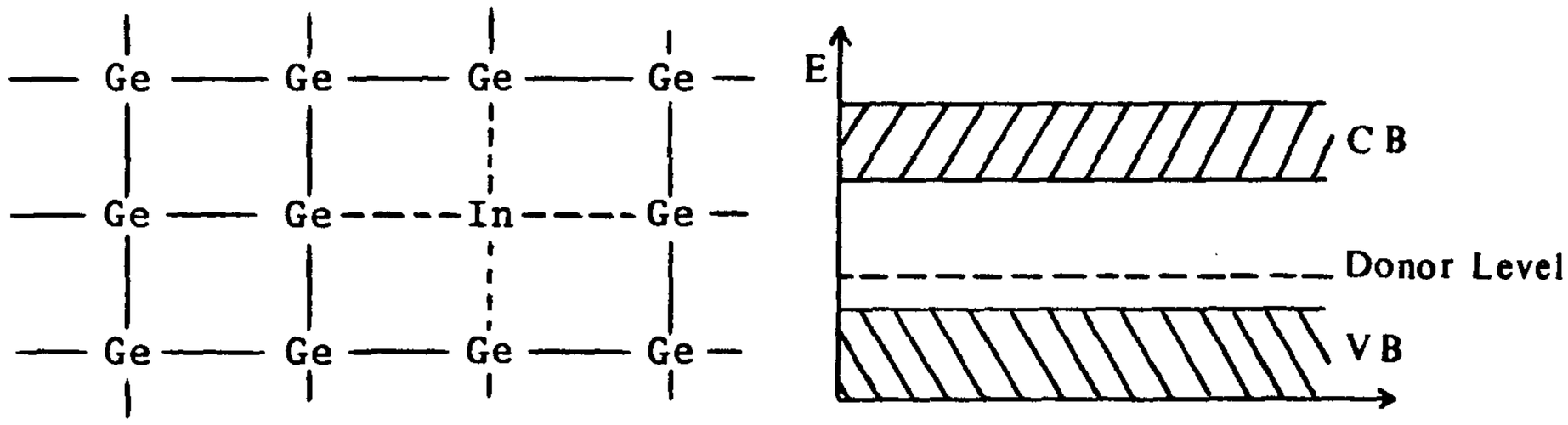


The theories relating semiconductor electrical conductivity in element-al materials can equally well be applied to compound semiconductors of which binary metal oxide systems are one example.

Little is known about the basic physical properties of tin (IV) oxide and its band structure. On the basis of electrical conductivity and Hall Effect measurements tin (IV) oxide was found to be an n-type semi-conductor like natural cassiterite[1]. The structure of native defects in tin (IV) oxide is still uncertain although electrical conductivity measurements would seem to imply that oxygen vacancies are present in the material as the predominant defect[1,1a]. The mechanism of the interaction of native defects and foriegn atoms and the scattering mech-anisms in tin (IV) oxide remain to be investigated.

The effects of doping single crystals of tin (IV) oxide with antimony oxide have been investigated by many workers[2,3,4,5]. Pyke, Reid and Tilley[6] reported that the blue/grey crystals of antimony tin oxide represent the phase $SnO_2.nSb_2O_4$.

Pyke, Reid and Tilley[6] also attribute the materials blue colouration to charge transfer between $Sb^{3+}$ and $Sb^{5+}$ cations as Robin and Day[7] do not list any blue or grey $Sn^{2+}/Sn^{4+}$ mixed oxidation state systems in their tabulation. However, in order for charge transfer of this type to take place it would be necessary for both cations to be in close proximity in geometrically similar sites. One way in which this could be achieved would be by introducing $Sb^{3+}$ and $Sb^{5+}$ cations into the latt-ice occupying interstitial octahedral sites to form an oxide of comp-osition $Sb_x^{3+}Sb_x^{5+}SnO_2$ or alternatively by substituting into tin posi-tions to form an oxide of formula $(Sb_x^{3+}Sb_x^{5+})Sn_{1-2x}O_2$. Mössbauer spectroscopic studies carried out by Alapin etal[3] suggested that antim-ony was present in the bulk phase of the material.

There are however two drawbacks to this simple model, firstly that $Sb^{3+}$ cations do not normally have octahedral co-ordination and secondly that the lattice parameters of tin (IV) oxide and antimony tin oxide are identical. Optical microscopy revealed that the blue colouration of these crystals was not homogeneous and electron microscopy showed the crystals to possess a variable microstructure[6]. Thus the antimony cat-ions would not appear to be uniformly distributed throughout the cry-stal lattice. In terms of microstructure the noticeable difference between doped and pure tin (IV) oxide crystals was found to be the presence of twins[4,5,6] in the antimony containing oxides. Twinning is usually a form of stress relief in crystals, but it also provides a means of changing the anion to cation stoichiometry and so providing sites with different co-ordination to the normal crystal matrix.
As $Sb^{3+}$ ions do not favour octahedral symmetry in oxide lattices due to the lone pair of electrons on the cation and also as the twin bound-aries seem to be associated with the presence of antimony in the cry-stal, it is possible that the twin boundaries are important in deter-mining the properties of the material.

Any $Sb^{3+}$ ions segregated at the twin boundaries would have negligible influence upon the lattice parameter of the crystal and such a segrega--tion would put some or all of the $Sb^{3+}$ ions into more favourable sites from a crystal-chemical viewpoint. One possible mechanism by which $Sb^{3+}$ ions could be incorporated into a tin (IV) oxide rutile lattice structure is shown in figure eight and was proposed by Pyke, Reid and Tilley[6].

Pyke, Reid and Tilleys' proposals as to the nature of the structure of the material were confirmed by more recent work carried out by Porte--faix etal[4] and Herman etal[5] who reported that the calcination of homo--geneous samples of tin antimony oxide at temperatures in excess of 800°C causes demixing of the oxides and flat bidimentional sheets of antimony tetraoxide ($Sb_2O_4$) were positively identified in the bulk phase of the material by X-ray crystallographic methods.

The $^{119}Sn$ transmission mössbauer spectrum of a conductive tin antimony oxide (90% $SnO_2$, 10% $Sb_2O_5$) has been recorded by Berry and Greaves[8] and was found to consist of a single resonance line corresponding to Sn (IV). The transmission mössbauer spectrum of Keeling and Walker's conductive tin antimony oxide species (KW175, 93·5% $SnO_2$/6·5% $Sb_2O_{5-y}$) was recorded as part of the present investigation and is shown in figure nine. Like Berry and Greaves'es spectrum,figure nine shows a single resonance line with a chemical shift of $\delta$ = 0·09mmsec$^{-1}$ from tin (IV) oxide, thus it would appear that the tin oxide species present in tin antimony oxide is chemically indistinguishable from tin (IV) oxide.

The mechanism by which dopant tin ions combine with the indium oxide host lattice to form indium tin oxide is at present uncertain and many conflicting postulates have been put forward.

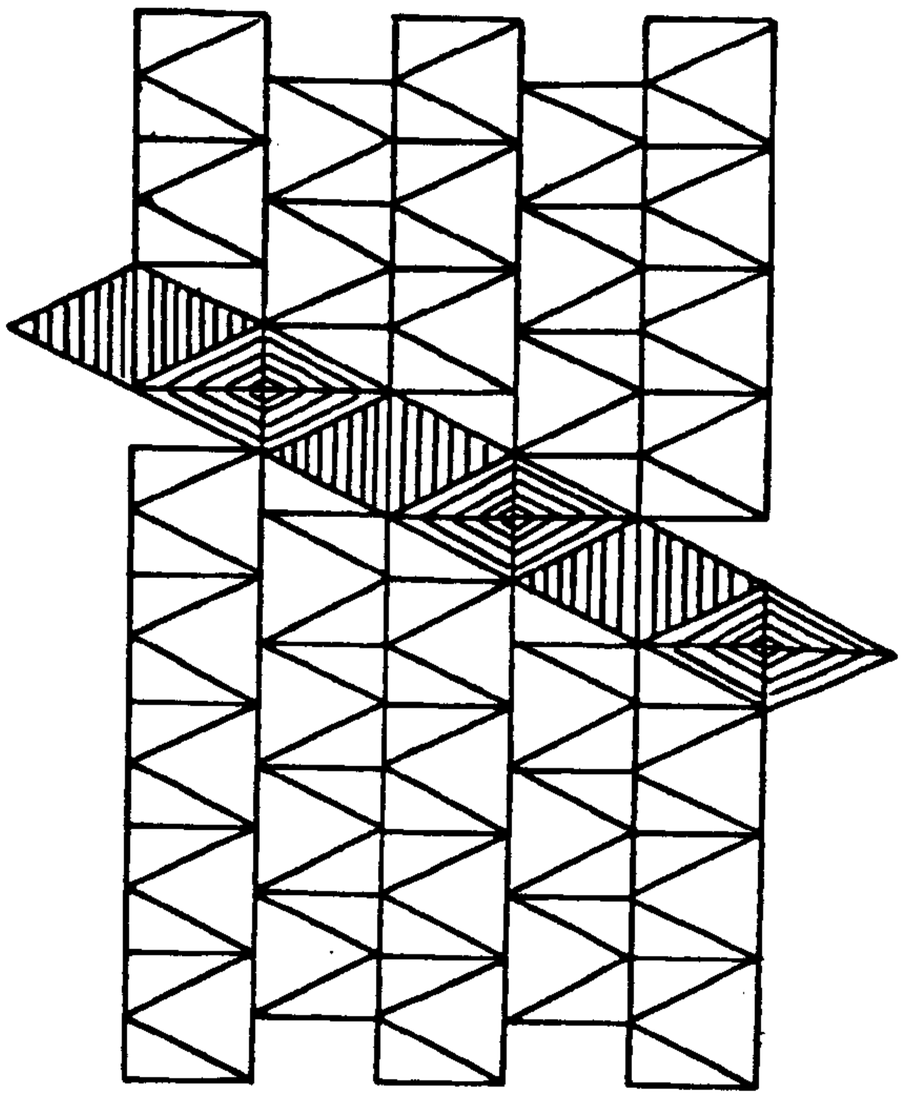


(c)

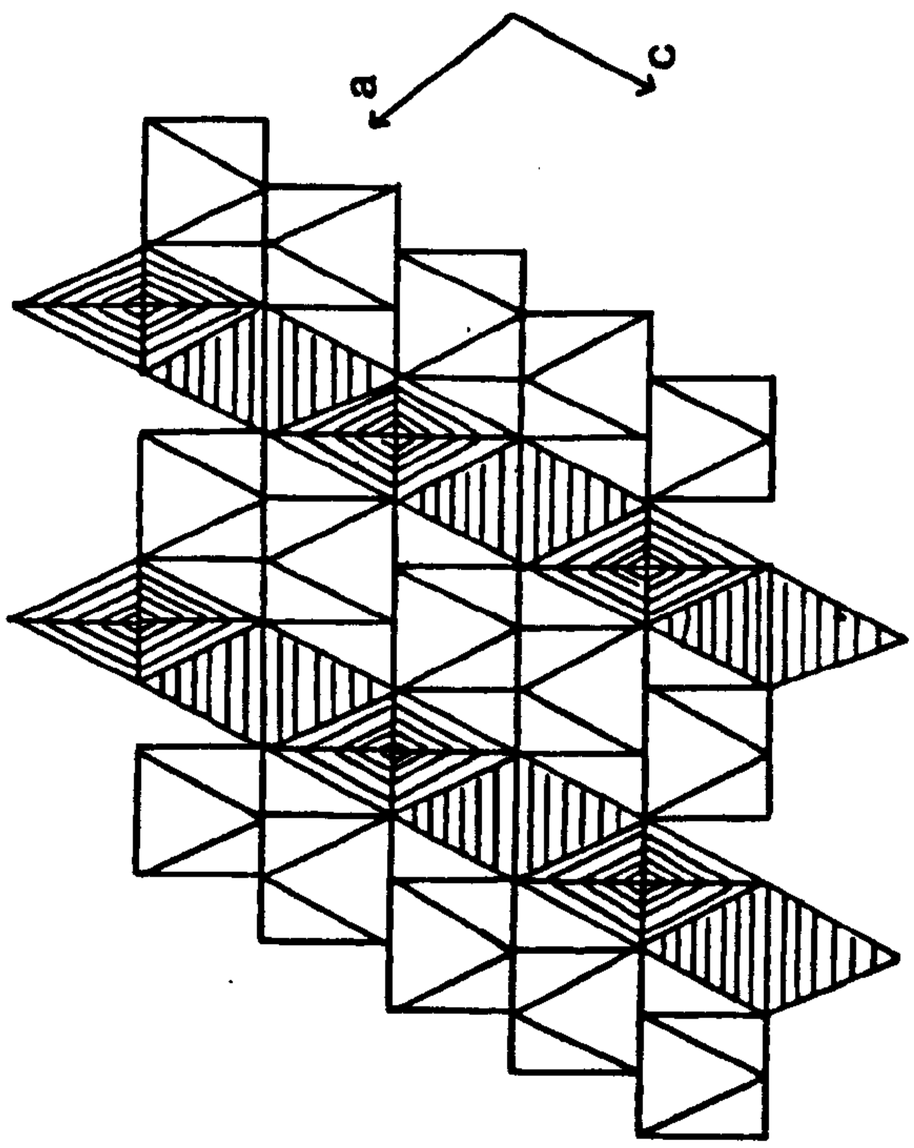


(b)

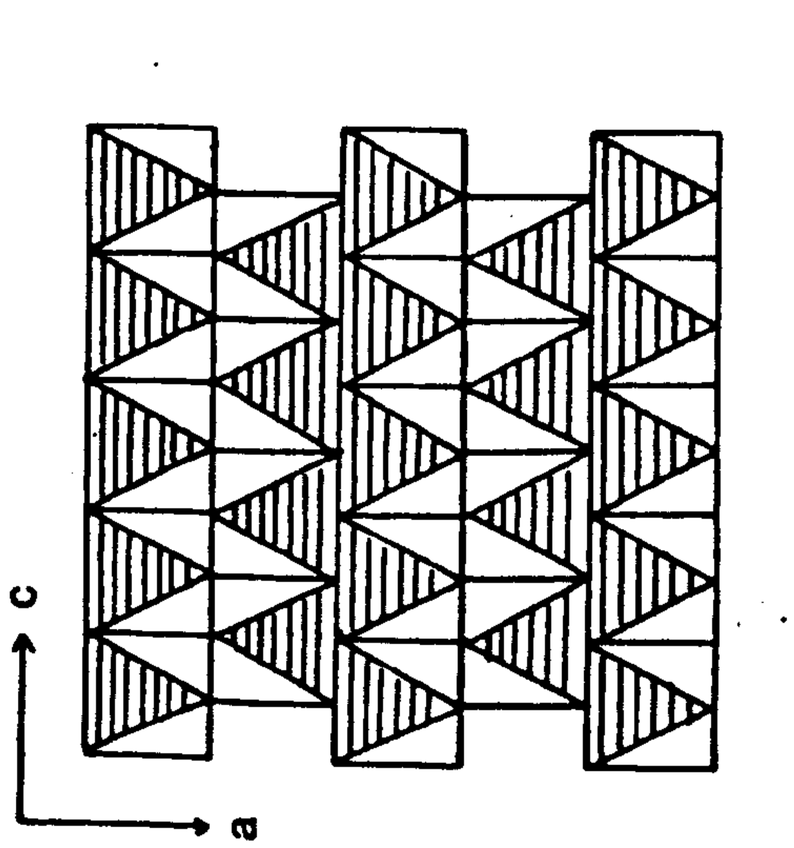


(a)

Figure Eight - (a) ac projection of the rutile structure, (b) ac projection of the $Sb_2O_4$ structure containing polyhedra of Sb containing one isolated lamella of Sb containing polyhedra, equivalent to an intergrowth between $Sb_2O_4$ and rutile. All structures are slightly idealised in these representations

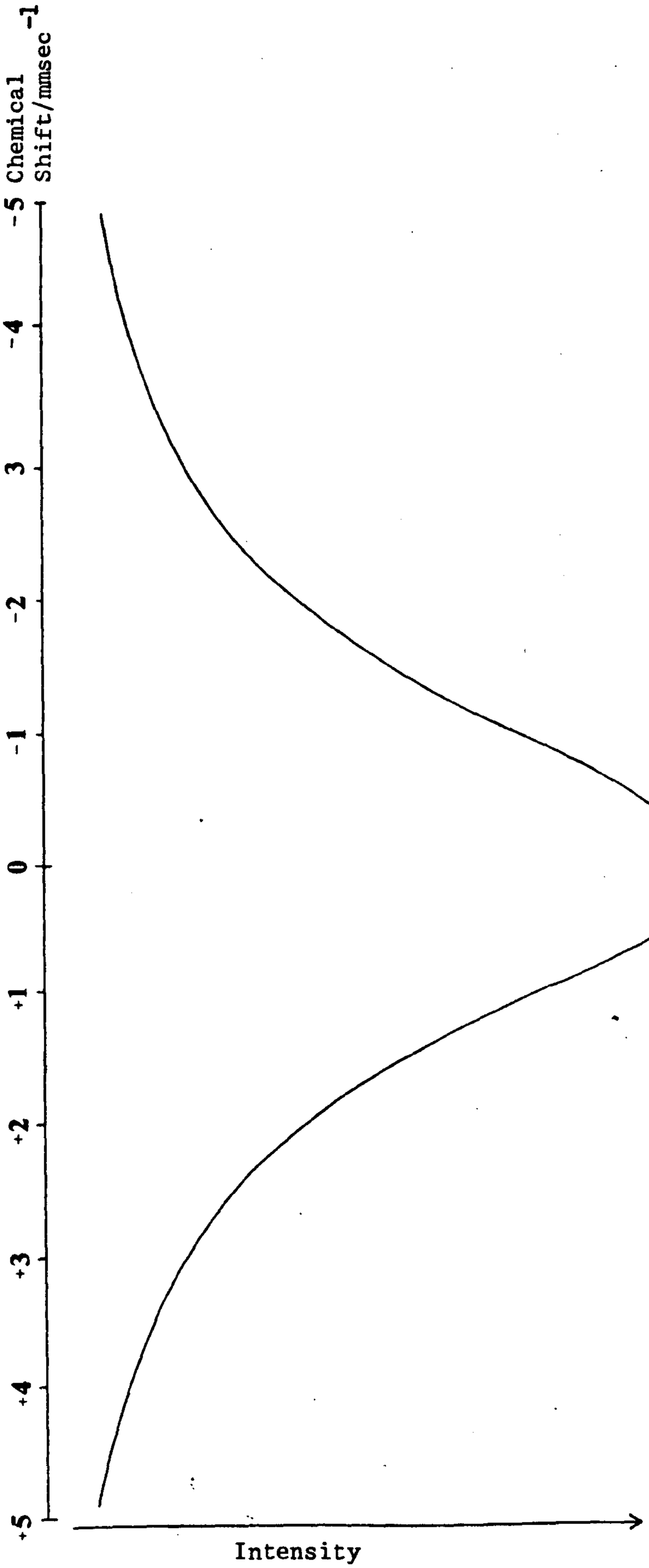


Figure Nine - $^{119}$Sn Mössbauer Spectrum of Tin Antimony Oxide

Frank, Kostlin and Rabenau[9] were able to show, using X-ray diffraction techniques, that at concentrations of 6 atom % or less of tin in ind--ium oxide a single solid phase was formed on calcination. The tin atoms in the single phase occupying indium lattice sites. At concen--trations of above 6 atom % in indium oxide the tin atoms begin to occupy interstitial positions in the lattice of tetragonal symmetry, in addition to indium lattice sites, so forming a second solid phase within the material. Frank etal[9] found that X-ray diffractograms of indium tin oxides containing 6 atom % of tin or less showed only lines due to cubic indium oxide, whereas at tin concentrations of above 6 atom % the diffractograms showed additional lines attributable to tetra--gonal tin (IV) oxide. The ability of $Sn^{4+}$ ions to substitute into $In^{3+}$ ion lattice sites was attibuted to a similarity in the size of the ionic radii of the two ions ($Sn^{4+}$=0·71Å and $In^{3+}$ = 0·81Å). In order to preserve electrical neutrality, four $In^{3+}$ ions were consid--ered to be equivalent to three $Sn^{4+}$ ions, thus for every three dopant tin atoms in the indium tin oxide lattice there would be one associated indium vacancy.

The free elctron density for indium tin oxide containing 6 atom % tin was determined by Frank etal[9] as 1·7 x $10^{21}$ $cm^{-3}$, this was the highest value recorded for a series of indium tin oxides of different composit--ions. Mizuhashi[10] found indium tin oxide to be an n-type semicond--uctor and reported that samples of the composition 9 Wt.% $SnO_2$/ 91 Wt. % $In_2O_3$ had the highest conductivity values. In contrast BoHyun, Young and Jeong[11] have reported that 15 mol.% $SnO_2$ in indium oxide gives the best conducting oxide.

Morriss[12] found that indium tin oxides of the composition by weight of $90In_2O_3/10SnO_2$ possessed the best conductivity when compared against other oxide compositions.

This weight composition may also be expressed approximately as the molar ratio of $1SnO_2:10InO_{1\cdot5}$ (5 moles $In_2O_3$ = 10 moles $InO_{1\cdot5}$). Thus if one mole in eleven moles of indium oxide is replaced by tin (IV) oxide a simple calculation shows that the resulting oxide must be oxygen deficient, viz.

$$110 \text{ moles of } InO_{1\cdot5} = In_{110}O_{165}$$

Now if 10 moles of $InO_{1\cdot5}$ are replaced by 10 moles of $SnO_2$.

$$100 \text{ moles of } InO_{1\cdot5} = In_{100}O_{150}$$

$$10 \text{ moles of } SnO_2 = Sn_{10}O_{20}$$

$$\rightarrow In_{100}Sn_{10}O_{170}$$

Thus in the example above the $In_2O_3$ bixtite structure contains 5 too few oxygen atoms to enable the tin and/or indium ions to maintain their formal oxidation states, so the material must of necessity contain metal(s) in mixed valence states. All of the four processes shown bel-low, A to D, would serve to accomodate the oxygen deficiency in indium tin oxide.

A. $In_2O_3 \longrightarrow In_2O + O_2^{\cdot}$

B. $In_2O_3 \longrightarrow 2In + 1\frac{1}{2}O_2$

C. $SnO_2 \longrightarrow SnO + \frac{1}{2}O_2$

D. $SnO_2 \longrightarrow Sn + O_2$

The reduction potentials associated with these processes are given be-low, (i) to (iv) and show that $In^{3+}$ is less susceptable to reduction than $Sn^{4+}$.

| | | | Reduction Potential/volts |
|---|---|---|---|
| (i) | $In^{3+} + 2e^- \longrightarrow In^+$ | | -0·40 |
| (ii) | $In^{3+} + 3e^- \longrightarrow In$ | | -0·338 |
| (iii) | $Sn^{4+} + 2e^- \longrightarrow Sn^{2+}$ | | +0·15 |
| (iv) | $Sn^{2+} + 2e^- \longrightarrow Sn$ | | -0·1364 |

Groth[13] has suggested that the indium oxide host lattice structure in indium tin oxide phases is so stable that any conduction electrons present in the material must be originating from the dopant tin ions. Groth's work has, however, recently been challenged by many workers. Solov'eva, Zhdanov,Markov and Shvangiradze[14] reported an observation of mixed indium oxidation states in samples of indium tin oxide which had been heated to 1200°C in air or to 900°C in vacuo, to which they assigned the formula $In^{III}_{2-x}\ In^{I}_{x}\ O_{3-2x}$. The existance of indium in oxidation states other than $In^{3+}$ in indium tin oxide has also been reported by Fraser and Cook[15], Pan and Ma[16] and Holland[17]. The pres--ence of $In^{I}_{2}O$ phases in samples of indium oxide and indium tin oxide has also been shown by Burrel, Kaller and Armstrong[18] who used Auger spectroscopy to positively identify indium (I) ions. Further evid--ence for the presence of indium in a low oxidation state in indium oxide has been reported by Ovadyahnu, Ovryn and Kramer[19] who used X-ray flourescence spectroscopy and X-ray diffraction techniques to identify indium (I) and indium (III) in samples of indium oxide and indium (I), indium (III), tin (II) and tin (IV) in samples of indium tin oxide. Ovadyahnu <u>etal</u> predicted a value of $c10^{22}cm^{-3}$ for the free electron density of indium oxide on the basis that between five and six oxygen atoms left each unit cell each leaving behind two electrons which could then enter the conduction band of the material. However Ovadyahnu <u>etal</u>[19] experimentally determined a value of $10^{20}cm^{-3}$ for the free elec--tron density of the material and they concluded that in each unit cell some indium ions must possess a valency other than three in order to preserve electrical neutrality. In this case it becomes natural to assume that the basic conduction mechanism involves charge transfer between indium atoms of different valencies.

Analyses of diffraction patterns of indium tin oxide samples by dark field imaging techniques carried out by Ovadyahnu etal[19] revealed the presence of an additional quasi amorphous tin phase in the material which they attributed as $Sn_3O_4$. However samples which contained this phase usually also exhibited high resistivities together with low opt--ical transmission coefficients and only small volumes of this phase in indium tin oxide were found to have a large detrimental effect on the properties of the material. The presence of $Sn_3O_4$ in samples of thermally treated tin (IV) oxide has also been reported by Lawson[20] and Bonchev and Manushev[21].

The results of Mössbauer spectroscopic analyses of 90/10 indium tin oxide phases in this investigation show that the tin species present in indium tin oxide is indistinguishable from tin (IV) oxide. Trans--mission and conversion electron (surface) Mössbauer data for 90/10 indium tin oxide are given in table one.

Table One - Mössbauer Spectral Data for Indium Tin Oxide

| Spectrum Type | Peak Type | Chem. Shift $\delta$/mm/sec | ½ Width $\Gamma$/mm/sec | Residual |
|---|---|---|---|---|
| Transmission | Singlet | 0·04±0·08 | 1·17 | 150 |
| Conversion Electron | Singlet | 0·13±0·08 | 1·19 | 2713·6 |

Thus the mechanism of tin doping in indium tin oxide would appear to be direct substitution of tin (IV) ions into indium (III) ion lattice sites, together with one associated indium vacancy for every three tin substituted indium positions in order to preserve electrical neu--trality. The presence of an anion vacancy together with an associa--ted electron in the solid state of a material is called an F centre.

Some possible mechanisms by which tin doping in indium oxide may give rise to F centres are shown below in equations (v) and (vi).

$$(v)\quad In_2O_3 \xrightarrow[10\%SnO_2]{\text{Calcine}} In^{III}_{2-x}\, In^{I}_{x}\, O_{3-2x} \longrightarrow$$

$$In^{III}_{2-x}\, In^{I}_{x}\, O_{3-2x-q} + q(\square + 2e^-) + (q/2)O_2$$

$$(vi)\quad SnO_2 \xrightarrow[90\%\ In_2O_3]{\text{Calcine}} Sn^{IV}_{1-x}\, Sn^{II}_{x}\, O_{2-x} \longrightarrow$$

$$Sn^{IV}_{1-x}\, Sn^{II}_{x}\, O_{2-x-p} + p(\square + 2e^-) + (p/2)O_2$$

Where $q \gg p$. The conductivity of indium tin oxide thus arises from a function,

$$\sigma = F(p) + F(q) + F(In^{3+}/In^{+}) + F(Sn^{4+}/Sn^{2+})$$

Where F(p) is a function of the total number of vacant oxygen sites arising from tin species,

F(q) is a function of the total number of vacant oxygen sites arising from indium species,

$F(In^{3+}/In^{+})$ is a function of the degree of charge transfer between indium ions of different valencies and

$F(Sn^{4+}/Sn^{2+})$ is a function of the degree of charge transfer between tin ions of different valencies.

## 4.2. The Preparation of Indium Tin Oxide: Small Scale

The objective of this part of the investigation was twofold. Firstly to prepare a range of samples of indium tin oxide of different percent-age compositions to investigate the effects upon resistivity, so that the optimum rate of indium oxide to tin oxide for low resistivity could be found. Secondly to find a suitable synthetic route for the large scale manufacture of low resistivity indium tin oxide of the ratio found in part one of the work.

Results reported in the literature state that for a product of low res-istivity the optimum weight ratio tin (IV) oxide to indium oxide is 1:10[10,13,18]. In order to verify this result a series of conductivity trials were carried out upon composite materials containing indium ox-ide to tin (IV) oxide in different proportions. Samples were prepared by milling together the appropriate quantities of materials and then calcining the mixture of preparation using the following experimental method.

Indium oxide (Xg) and tin (IV) oxide (Yg:10-X=Y) were ball milled to-gether in ethanol for 20 minutes until a homogeneous mixture was obtain-ed. The wet material was then oven dried at 105$^{o}$C to remove ethanol and the dry powder was calcined (1050$^{o}$C,2½Hours) in a silica crucible, to yield green indium tin oxide (10g). The cooled product was ball milled for a second time in ethanol for 20 minutes and oven dried at 105$^{o}$C to prepare a homogeneous sample for resistivity testing.

Fifteen samples were prepared in this series and the electrical resis-tivity results are given in table two and illustrated graphically in figure ten as a semi-log plot of resistivity against composition.

Table Two - Results of Resistivity Trials upon Indium Tin Oxides

| Weight % of Indium Oxide | Weight % of Tin Oxide | Resistivity / Ω cm | $\log_e \rho$ |
|---|---|---|---|
| 100 | 0 | $3 \cdot 0 \times 10^6$ | 14·9 |
| 95 | 5 | 28·6 | 3·3 |
| 92 | 8 | 2·1 | 0·7 |
| 90 | 10 | 1·1 | 0·1 |
| 88 | 12 | 1·8 | 0·6 |
| 80 | 20 | 13·4 | 2·6 |
| 70 | 30 | 278·4 | 5·6 |
| 60 | 40 | 1078·1 | 7·0 |
| 50 | 50 | 2102·0 | 7·7 |
| 40 | 60 | 7315·0 | 8·9 |
| 30 | 70 | $2 \cdot 1 \times 10^4$ | 10·0 |
| 20 | 80 | $5 \cdot 8 \times 10^4$ | 11·0 |
| 10 | 90 | $9 \cdot 2 \times 10^4$ | 11·4 |
| 5 | 95 | $4 \cdot 1 \times 10^3$ | 8·3 |
| 0 | 100 | $5 \cdot 5 \times 10^5$ | 13·2 |

These data show that the optimum composition of indium tin oxide for low resistivity is 10% weight tin (IV) oxide to 90% weight indium oxide in agreement with the literature results.

Powder resistivity measurements were carried out using the specially designed cell shown in figure eleven. The electrode end plugs were constructed from beryllium aluminium alloy (Beral) and the housing from 'Nylon'. The optimum loading of indium tin oxide for the cell was found to be 0·8g and all measurements were carried out at one ton/$cm^2$ pressure.

Figure Ten - $\log_e$ Resistivity Against Weight % Tin(IV)Oxide in Indium Tin Oxide Phases

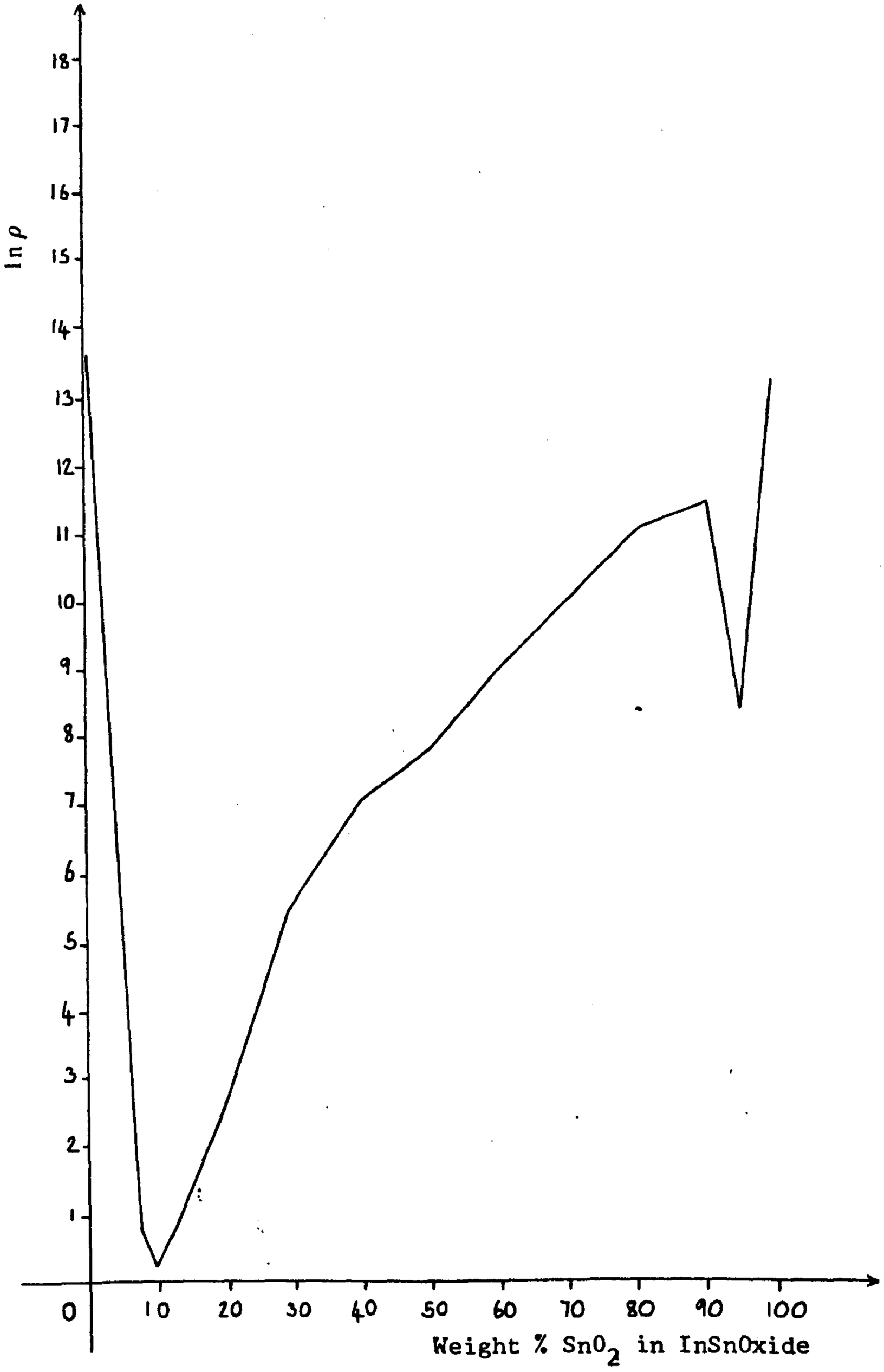

Figure Eleven - The Powder Conductivity Cell

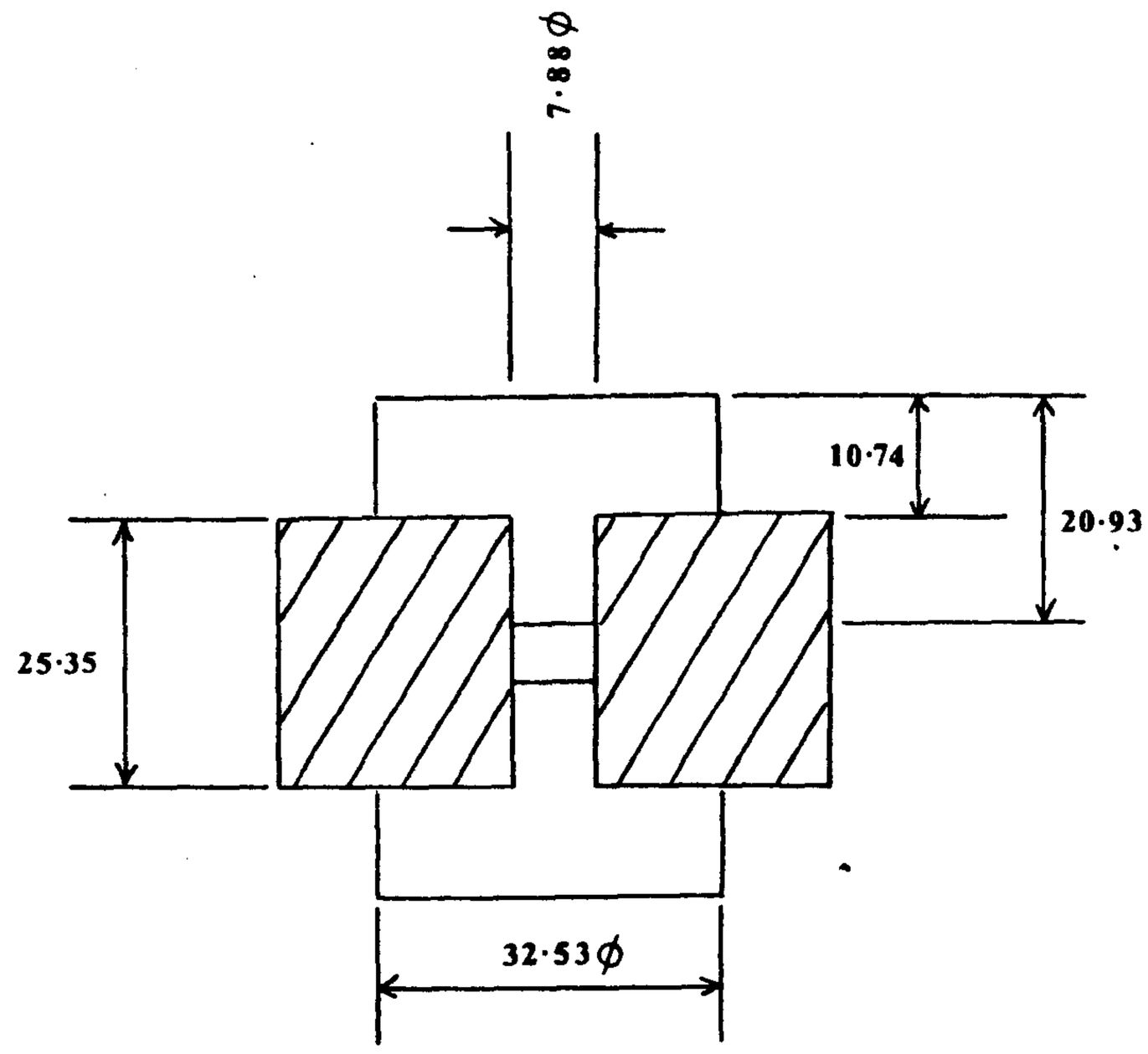


All Dimensions Given in Millimetres

In the course of the present work it was found that the resistivity of indium tin oxide was pressure sensitive. An example of this pres--sure dependance is shown in the data for a sample of 90/10 indium tin oxide in figure twelve and given in table three.

Table Three - The Measured Resistivity of an Indium Tin Oxide Sample With Increasing Applied Pressure.

| Applied Pressure $Ton/cm^2$ | 0·1 | 0·5 | 1·0 | 1·5 | 2·0 | 3·0 | 4·0 | 5·0 | 6·0 | 7·0 | 8·0 | 9·0 | 10·0 |
|---|---|---|---|---|---|---|---|---|---|---|---|---|---|
| Measured Resistivity $\Omega cm$ | 27·4 | 3·0 | 1·1 | 0·7 | 0·4 | 0·2 | 0·1 | 0·1 | 0·2 | 0·3 | 0·4 | 0·6 | 0·9 |

The resistance of the indium tin oxide sample in the cell was measured using a digital electrometer and the measured resistance was converted into resistivity using equation (i)

(i) $$\rho = \frac{R \times A}{t}$$

Where $\rho$ = Resistivity in Ohmcm

R = Resistance of Powder Bed in Ohms

A = Cross Sectional Area of Powder Bed in $cm^2$

t = Thickness of Powder Bed in cm

The initial decrease in resistivity which is observed on first applying pressure to the sample arises from an improved contact between the elec--trodes and the particles. The initial increase in pressure also helps to squeeze out moist air which fills the interparticular voids and which is responsible for a residual amount of the materials resistivity at atmospheric pressure. Once the optimum pressure has been reached for particle contact, further increases merely lead to compaction processes resulting in a loss of sample surface area and which serve to raise slight--ly the value of the measured resistivity.

Figure Twelve - Measured Resistivity Against Applied Pressure for Indium Tin Oxide Test Samples

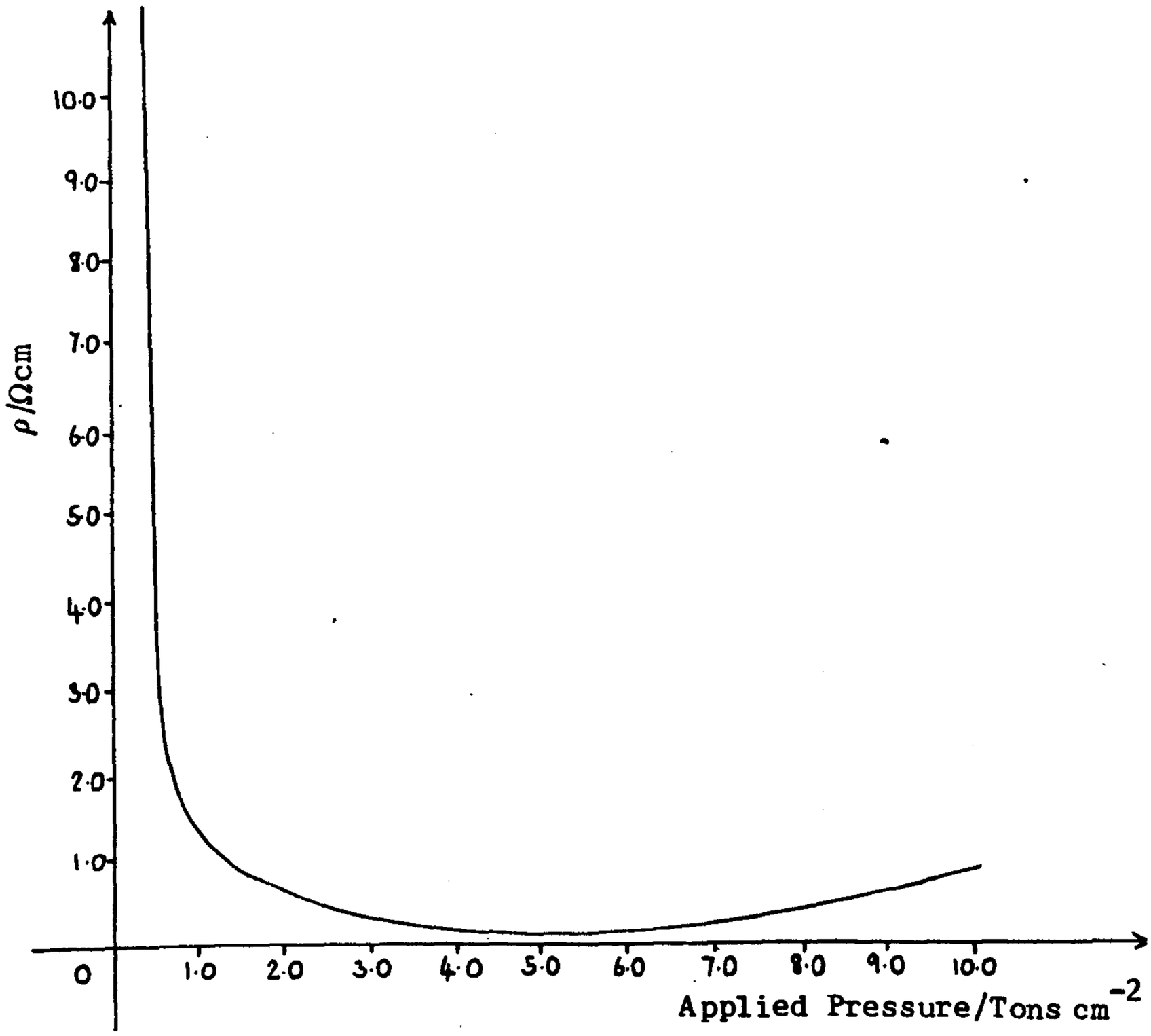

Resistivity measurements were carried without proir degassing of the test samples. Measurements carried out on samples which had been de--gassed in dry nitrogen for five hours prior to testing showed little or no difference when compared with results from samples of the same materials which had not been subjected to this treatment. A compar--ison of the results obtained from the gassed and degassed samples is given in table four.

Table Four - Resistivities of Indium Tin Oxide and Tin Antimony Oxide in Different Atmospheres

| Sample | Atmosphere | $\rho$ ($\Omega$ cm) at Applied Pressure (tons/cm$^2$) | | | |
|---|---|---|---|---|---|
| | | 0·1 | 0·5 | 1·0 | 2·0 |
| Tin Antimony Oxide | Air | 3·8 | 1·9 | 0·3 | 0·1 |
| | Nitrogen | 8·8 | 4·0 | 0·3 | 0·1 |
| Indium Tin Oxide | Air | 27.4 | 3·0 | 1·1 | 0·4 |
| | Nitrogen | 91·4 | 6·9 | 1·1 | 0·4 |

Calcination of the indium oxide/tin oxide milled samples is necessary to incorporate the dopant species into the host crystal lattice,by a mechanism of crystal growth which occurs in the sample at elevated temperatures. Prior to calcination the samples are simple mixtures of host and dopant species, and it is during the calcination treatment that the amorphous particles of material anneal together to form a coherent structure. It is only after calcination that the dopant species becomes fully incorporated into the crystal lattice and pro--cesses giving rise to semiconduction can operate.

An investigation into the effect of different calcination treatments upon indium tin oxide by Solov'eva and Zhdanov[22] showed that the res--istivity of the calcined product was closely related to the calcin--ation temperature and furnace times used in processing the material. Morriss[23] also reported similar observations and found a calcination temperature of 1060°C gave the lowest resistivity indium tin oxide.

In order to fully investigate the effects of the calcination treat--ment on the resistivity of indium tin oxide samples two experimental series were carried out. The first series used different calcination temperatures at fixed times and the second different times at a fixed temperature. The 90/10 indium tin oxide used in these trials was prepared by milling and the powder resistivity measurements were made on the cell shown in figure ten. The results of these two sets of trials are given in tables five and six and show that the conditions most conducive to the preparation of low resistivity indium tin oxides are a calcination temperature of 1050°C and a furnace time of two hours. From the results it is most likely that furnace times of under two hours at 1050°C are not sufficient for the dopant tin (IV) oxide species to be fully incorporated in the indium oxide host crystal structure, and furn--ace times of over two hours at this temperature result in the onset of a collapse of the internal structure of the sample. Similar effects to these were observed by Morriss[24] in the processing of tin antimony oxides.

The results from this part of the investigation show that the chemical composition of indium tin oxides and the calcination treatment used in processing them are important in defining product resistivity.

A chemical composition of 90:10, indium oxide to tin (IV) oxide and a calcination treatment of two hours at 1050°C were found to be most effect--ive in preparing low resistivity oxides.

Table Five - Effects of Calcination Temperature upon the Resistivity of Indium Tin Oxides at Constant Time

| Calcination Temperature/$^{o}$C (80 minutes at max temp) | Resistivity/$\Omega$ cm |
|---|---|
| 900 | 74·1 |
| 1000 | 0·9 |
| 1050 | 0·6 |
| 1100 | 1·0 |
| 1200 | 2·3 |
| 1300 | 6·7 |

Table Six - Effects of Calcination Time upon the Resistivity of Indium Tin Oxides at Constant Temperature

| Calcination Time/minutes (1050$^{o}$C Temp.) | Resistivity/$\Omega$ cm |
|---|---|
| 15 | 2·4 |
| 30 | 1·7 |
| 60 | 0·8 |
| 90 | 0·6 |
| 120 | 0·5 |
| 150 | 1·1 |
| 180 | 1·6 |

Following on from the results of the preliminary work, fifteen novel synthetic routes leading to 90/10 indium tin oxides were studied as potential methods for the commercial synthesis of low resistivity ind--ium tin oxides. These experiments are described in (a) to (n) as follows.

(a) <u>From Indium Nitrate and Orthostannic Acid (A Route)</u>

Indium metal (7·43g) was added to a beaker containing nitric acid (120ml, 52%) at 45°C and was left to react until the metal had completely dis--solved leaving a green solution of indium nitrate. The reaction sol--ution was then diluted to 250ml with distilled water and tin metal(0·79g) was added to the diluted solution which reacted with the nitric acid to produce tin (IV) nitrate. After the reaction was complete, aqueous ammonia solution was added to the solution of mixed nitrates to precip--itate out indium hydroxide and hydrous tin (IV) oxide. The resulting precipitate was washed with water by decantation to pH 7 and then filt--ered and oven dried at 105°C to yield a glassy granular dried gel. The dried material was calcined (1050°C for 2 Hours) to yield indium tin oxide as a green powder (10g). The cooled product was ball milled in acetone for 15 minutes and then oven dried at 75°C to give a homogen--ous sample for resistivity analysis.

<u>Product Resistivity = 20·2Ω cm</u>

(b) <u>From Indium Nitrate and Metastannic Acid (BRoute)</u>

Indium Metal (7·43g) was added to a beaker containing nitric acid (120ml, 52%) at 45°C and was left to react completely leaving a clear green sol--ution of indium nitrate. Tin metal (0·79g) was then added to this sol--ution and reacted with it to produce a colloidal suspension of metastannic acid.

After the reaction was complete the reaction mixture was diluted to 500cc with distilled water and the pH of the solution was adjusted to a pH>5 by the addition of aqueous ammonia solution. This had the effect of precipitating out indium hydroxide and of floculating the colloidal suspension of metastannic acid. The resulting precipitate was then washed with water by decantation to pH 7 filtered and oven dried at 105°C to give a glassy granular solid. The dried material was calcined (1050°C, 2hours) to give indium tin oxide as a green pow--der (10g). The cooled product was ball milled in acetone for 15 min--utes and then oven dried at 75°C to produce a homogeneous sample of indium tin oxide for resistivity analysis.

Product Resistivity = 0·9Ω cm

(c) From Mixed Sulphates

Solid hydrated indium sulphate (150g) was prepared by dissolving indium metal (64g) in sulphuric acid (250ml, 50%) and evaporating off the mother liquor on a rotary evaporator. The hydrated sample prepared analysed as $In_2(SO_4)_3.2{\cdot}1H_2O$.

Tin (II) sulphate (14·7g) was prepared by refluxing a mixture of tin metal (10·0g, granulated), copper sulphate (9·7g) and sulphuric acid (200ml, 0·05M) for two hours until the solution was colourless, the reaction mixture was then filtered and the product was left to crys--tallise out by evaporation.

Indium tin oxide was prepared from solutions of mixed sulphates by the pH precipitation and spray drying methods which are described below.

(i) pH Precipitation

Indium sulphate (64·8g) was added to a solution of tin (II) sulphate (5·1g) in water (700ml, 35°C). The pH of this solution was raised to pH 8 by the addition of aqueous ammonia solution to precipitate out a mixed indium hydroxide/hydrous tin (IV) oxide gel. The gel was then washed with water by decantation to a pH of 7, filtered and oven dried at 105°C to give a glassy granular solid gel. The dried material was calcined (1050°C, 2hours) to give indium tin oxide (36g) as a green powder, the cooled product was ball milled in acetone for 15 minutes and then oven dried at 75°C to yield a homogenised sample of indium tin oxide for resistivity analysis.

Product Resistivity = 1·2 Ωcm

(ii) By Spray Drying

Indium sulphate (80g) and tin (II) sulphate (6·3g) were dissolved in warm water (100ml, 35°C). The pH of the solution was adjusted with ammonia solution (aqueous, 220w/v) to the point where a permanent pre--cipitate was just beginning to form. The solution was then spray dried using a lab plant spray drier (model one) using the following conditions.

| | | |
|---|---|---|
| Spray Nozzle | = | 1·0mm diameter |
| Inlet Temp. | = | 180°C |
| Outlet Temp. | = | 90°C |
| Feed Pump Rate | = | 6·7cc/minute |
| Yield of Dried Material | = | 42g |

The spray dried product was calcined (1050°C, 2hours) to give 10·3g of green indium tin oxide (experimental yield = 23·2%).

The cooled product was ball milled in acetone for 15 minutes and then oven dried at 75°C to prepare a homogenised sample for resistivity analysis.

Product Resistivity = 18·0 Ωcm

Particle size analyses carried out on the pH precipitated and spray dried materials by coulter counter showed the pH precipitated material to be finer, the measured values being 4·0 and 4·5 microns respectively.

(d) From tin (II) oxide and indium (III) nitrate

Tin (II) oxide (4·47g) was added to a beaker containing nitric acid (100ml, d=1·42) and left to react completely to give a clear yellow solution. Indium metal (37·2g) was then added slowly to this solution keeping the temperature of the reaction media to below 25°C. The pH of the resulting solution of mixed nitrates was then adjusted to greater than 8 with aqueous ammonia solution to precipitate out a mixture of indium (III) hydroxide and hydrous tin (IV) oxide. The precipated gel was washed with water by decantation to pH 7 and then filtered and oven dried to yield a glassy granular gel. The dried material was calcined (1050°C, 2hours) to give 50g of indium tin oxide which had a grey col--ouration. The cooled material was ball milled in acetone for 15 minutes and oven dried at 75°C to give a homogenous sample for resist--ivity analysis.

Product Resistivity = $7 \times 10^4$ Ωcm

(e) From Mixed Nitrates using Acetylacetone

Indium metal (38·1g) was added to nitric acid (500ml, d=1·48) and was left to react completely to give a clear green solution of indium (III) nitrate. Nitric acid (68ml, d= 1·48) and acetylacetone (50g) were added to a beaker and the mixture was cooled to 0°C in an ice salt bath. Tin metal (3·85g) was then added very slowly to the cooled solution with care being taken to keep the temperature of the reaction solution below 15°C. The tin metal reacted with the nitric acid to give a clear yellow/green solution of tin(IV) nitrate. This solution was then added to the indium (III) nitrate solution. The mixed solution was diluted with water to make up one litre and the pH of the solution was adjusted to a pH >8 by addition of aqueous ammonia solution to precipitate out indium hydroxide and hydrous tin (IV) oxide. The precipitated gel was washed with water by decantation to pH 7, filtered and oven dried at 105°C to give a glassy granular precipitate. The dried material was then calcined (1050°C, 2hours) to give green indium tin oxide (50g). The cooled material was ball milled with acetone for 15 minutes and then oven dried at 75°C to prepare a homogenised sample for resistivity analysis.

Product Resistivity = 70 Ωcm

(f) From Mixed Nitrates using Pyridine

Indium metal (15·2g) and tin metal (1·54g) were added to a beaker containing nitric acid (240ml, d=1·48) and pyridine (40g). The mixture reacted to give a clear green solution of mixed nitrates which was diluted with water (750ml) and the resulting solution was taken to a pH>8 by the addition of aqueous ammonia solution to precipitate out indium hydroxide and hydrous tin (IV) oxide. The precipitated gel was washed with water by decantation to pH 7, filtered and dried at 105°C to give a glassy granular precipitate.

The dried material was then calcined (1050°C, 2hours) to give indium tin oxide (20g) as a green (20g) as a green powder. The cooled mat-erial was ball milled in acetone and oven dried at 75°C to prepare a homogenised sample for resistivity analysis.

Product Resistivity = 0·32 Ω cm

(g) From Indium Tin Alloy and Nitric Acid

Indium tin alloy (54·2g, granulated) was prepared by melting tin metal (5·2g) and indium metal (49·0g) in a plumbago crucible and the pouring the molten alloy into a large beaker containig cold water. The alloy was then added to another beaker containing nitric acid (550ml, d=1·42) to give a clear green solution of indium and tin nitrates. This sol-ution was diluted to one litre with distilled water and the pH of the solution raised to pH 8 by the addition of aqueous ammonia solution, to precipitate out indium hydroxide and hydrous tin (IV) oxide.

The precipitated gel was washed with water by decantation to pH 7, fil-tered and oven dried at 105°C to yield a glassy granular gel. The dried gel was calcined (1050°C, 2hours) to give 65·6g of green indium tin oxide. The product was ball milled in acetone for 15 minutes and then oven dried at 75°C to yield a homogenous sample for resistivity analysis.

Product Resistivity = 0·3 Ω cm

(h) From Indium (III) Hydroxyformate and Tin (II) Formate

Tin (II) formate (9·4g) was prepared by refluxing a mixture of tin (II) oxide (10g) with formic acid (70ml, 90%) and water (30ml) under nitrogen for 1½ hours. After the reaction was complete the solution was filtered and cooled to give white crystals of tin (II) formate which were filtered off and dried.

Indium hydroxyformate (18·5g) was prepared by refluxing a mixture of indium hydoxide (15g) and formic acid (150ml, 90%) for 1½ hours. After the reaction was complete the reaction solution was filtered and reduced to half of its original volume on a rotary evaporator. Upon cooling what was assumed to be indium (III) hydroxyformate pre-cipitated out from the reaction solution, which was then filtered off and dried.

The supposed indium (III) hydroxyformate (13·56g) and tin (II) formate (1·39g) were ball milled in ethanol for 20 minutes and then oven dried at 70°C to yield a pink homogenous mixed indium tin formate. This mixed formate was then converted into indium tin oxide by heating it in a pyrex tray to 375°C. The oxide product then calcined (1050°C, 2hours) to give indium tin oxide (10g) as a green powder. The cooled material was ball milled in acetone for 15 minutes and then oven dried at 75°C to yield a homogenous sample for resistivity determination.

Product Resistivity = 3·0Ωcm

(i) From Indium (III) Hydroxyacetate and Tin (II) Acetate

Tin (II) acetate (14·7g) was prepared by refluxing tin (II) oxide (10g) with acetic acid (100ml, 50%) under nitrogen for two hours. After this time the solution was filtered and reduced to dryness on a rotary evaporator. The precipitated tin (II) acetate was then collected and stored under vacuo until required.

Indium (III) hydroxyacetate (70·1g) was prepared by refluxing indium (III) hydroxide (50g) in acetic acid (200ml) for 1½ hours. After the reflux the solution was filtered and cooled to give white crystals of what was assumed to be indium (III) hydroxyacetate.

The supposed indium (III) hydroxyacetate (61·5g) and tin (II) acetate (7·9g) were ball milled in ethanol for 20 minutes and then oven dried at 75°C to give a homogenous mixed indium tin acetate. This mixed acetate was converted into indium tin oxide by heating the mixture at 375°C on a pyrex plate. The oxide was calcined (1050°C, 2hours) to give indium tin oxide (42·2g) as a green powder. The cooled material was ball milled in acetone for 15 minutes and then oven dried at 75°C to give a homogenous sample for resistivity analysis.

Powder Resistivity = 0·9 Ω cm

(j) From Indium (III) Hydroxyacetate and Tin (IV) Acetate

Tin (IV) acetate (7·5g) was prepared by refluxing tin (IV) bromide (15g) in a mixture of acetic acid (75ml, glacial) and acetic anhydride (75ml) for three hours. After the reflux period the solution was vacuum fil-tered, whilst still hot, through a sintered glass crucible and the filtrate was left to cool. Tin (IV) acetate crystallised out from the solution as orange/yellow crystals which were filtered off and stored under vacuum to prevent hydrolysis occuring from contact with atmospheric moisture.

Indium (III) hydroxyacetate (61·5g) was prepared as described in section (i) of this section.

Tin (IV) acetate (5g) and indium (III) hydroxyacetate (34·8g) were ball milled in ethanol for 20 minutes and then oven dried at 70°C to yield a pink homogenous mixed indium tin acetate. The mixed acetate was then converted into an indium oxide/tin oxide mixture by drying it on a pyrex plate at 375°C. The oxide was then calcined (1050°C, 2hours) which gave indium tin oxide (20g) as a green powder.

The cooled material was ball milled in acetone for 15 minutes and then oven dried at 75°C to give a homogenised sample for resistivity anal--ysis.

Product Resistivity = 0·1 Ω cm

(k) From Indium Tin Alloy and Acetic Acid

Indium tin alloy (20g, 94·3g:10g) was added to a solution of acetic acid (150ml, glacial) and acetic anhydride (50ml) and the mixture was refluxed for 18 hours (this was the time taken for all of the alloy to react with the acetic acid). White crystalline catenae of indium tin acetate crystallised out from the cooled solution and were filtered off under suction and dried over silica gel in vacuo. The indium tin acetate was ball milled in ethanol for 15 minutes and was then convert--ed into indium tin oxide by heating on a pyrex tray at 375°C. The oxide was then calcined (1050°C, 2hours) to yield indium tin oxide (24g) as a green powder. The cooled material was ball milled in ace--tone for 15 minutes and oven dried at 75°C to give a homogenised sample for resistivity analysis.

Product Resistivity = 0·13 Ω cm

(l) From Indium Tin Alloy and Dichloroacetic Acid

Indium tin alloy (21·2g, 94.3g:10g) was added to dichloroacetic acid (230ml) in a round bottomed flask and the reaction mixture was refluxed for 1½ hours. After the reaction time had elapsed the reaction mixture was left to cool and a black precipitate (71g) was filtered off . An attempted calcination of this material resulted in comp--lete volatilisation of the product without formation of indium tin oxide.

(m) From Indium Tin Alloy and Phenylacetic Acid

Indium tin alloy (10g, 94·3g:10g) and phenylacetic acid (50g) were refluxed in a round bottomed flask for 5 hours. After this period it was found that there had been a complete polymerisation of mater--ials in the reaction flask and a solid black tar was left as the reaction product. This tar exploded upon heating and so the syn--thetic procedure was abandoned as a possible route to indium tin oxide.

(n) From Indium Tin Alloy and Benzoic Acid

Indium tin alloy (25g, 94·3g/10g) was added to a round bottomed flask containing benzoic acid (120g) and the reaction mixture was refluxed for 5 hours on a heating mantle. After this period the reaction mixture was allowed to cool leaving the reaction products and reagents to set solid. Excess benzoic acid was dissolved from the product in cold methanol which was filtered off under vacuum suction to leave the indium tin benzoate as a white powder. The indium tin benzoate was converted into oxide by burning the material in a silica crucible over a bunsen flame. The oxide produced was calcined (1050$^{o}$C, 2hours) to yield indium tin oxide (26·7g) as a green powder. The cooled material was ball milled in acetone for 15 minutes and oven dried at 75$^{o}$C to give a homogenous sample for resistivity analysis.

Product Resistivity = 0·3 Ωcm

The resistivities of the fifteen, 90/10 indium tin oxide samples pre--pared from the experimental trials carried out in this series were determined using the powder cell described in section 5.1 with a stand--ard pressure of 1 ton/cm$^{2}$ being applied to each test sample.

Table Seven - The Results of Small Scale Preparations of Indium Tin Oxide

| Prep. | Synthetic Route | Product Resistivity Ω/cm |
|---|---|---|
| (a) | From Indium (III) Nitrate and Orthostannic Acid | 20•2 |
| (b) | From Indium (III) Nitrate and Metastannic Acid | 0•9 |
| (c) | From Mixed Sulphates (i) By pH Precipitation | 1•2 |
| | (ii) By Spray Drying | 18•0 |
| (d) | From Tin (II) Oxide and Indium (III) Nitrate | $7 \times 10^4$ |
| (e) | From Mixed Nitrates using Acetylacetone | 70•0 |
| (f) | From Mixed Nitrates using Pyridine | 0•32 |
| (g) | From Indium Tin Alloy and Nitric Acid | 0•3 |
| (h) | From Indium (III) Hydroxyformate and Tin (II) Formate | 3•0 |
| (i) | From Indium (III) Hydroxyacetate and Tin (II) Acetate | 0•9 |
| (j) | From Indium (III) Hydroxyacetate and Tin (IV) Acetate | 0•1 |
| (k) | From Indium Tin Alloy and Acetic Acid | 0•13 |
| (l) | From Indium Tin Alloy and Dichloroacetic Acid | - |
| (m) | From Indium Tin Alloy and Phenylacetic Acid | - |
| (n) | From Indium Tin Alloy and Benzoic Acid | 0•3 |

The criterion used for determining succesful synthetic routes at this stage was that the resistivity of the indium tin oxide sample produced by a particular route should be below 0·5Ωcm. From table seven, which is a collation of the results obtained from resistivity trials on the indium tin oxides prepared in this section, the 0·5Ωcm criter-ion immediately eliminates ten synthetic routes as being unworthy of further investigation. The suitability of the remaining five routes, (f), (g), (j), (k) and (n) for application to large scale work is discussed in the next section of this chapter.

## 4.3. The Preparation of Indium Tin Oxide : Large Scale

In the previous section, of the fifteen synthetic routes to 90/10 indium tin oxide only five proved to be sucessful in preparing low resistivity oxides. Each of these five selected processes is exam-ined in this section for suitability to the manufacture of indium tin oxide on a large scale.

Route (f), which involved precipitation of a mixed indium (III) hydrox-ide/hydrous tin (IV) oxide gel from a solution containing nitric acid and pyridine was eliminated from the investigation at this stage because of the health and safety measures which would have to be implemented when working with pyridine on a large scale, which would make the process too expensive when compared with other synthetic routes.

Route (j) was also eliminated from the investigation at this stage because of the difficulties which would be associated with the prep-aration and the storage of large quantities of tin (IV) acetate, required for this sythetic route.

Thus the three synthetic routes to indium tin oxide which had not been rejected at this stage were,

(g) the synthesis from indium tin alloy and nitric acid,

(k) the synthesis from indium tin alloy and acetic acid and

(n) the synthesis from indium tin alloy and benzoic acid.

At this stage in the investigation Keeling and Walker felt that it would be in the best interests of the project if the synthetic routes (k) and (n) were examined further for commercial viability at City University as part of this work. This section therefore contains work carried out at City University on the large scale manufacture of 90/10 indium tin oxide by the acetate and benzoate routes.

(a) The Acetate Route

Work carried out on the preparation of indium tin oxide by the acetate route in this part of the project has concentrated upon the manufac--ture of two separate batches of material for evaluation.

The experimental conditions and subsequent analysis carried out for each of the two preparations, BA1 and BA2, is given below.

BA1

Weight of Indium Tin Alloy used = 1135g

Volume of Acetic Acid used = 2900ml

Volume of Acetic Anhydride used = 600ml

The reaction solution was refluxed for 52 hours at 118°C

The residue of undissolved alloy after 52 hours = 125·2g

After refluxing the mixture for 52 hours the solution obtained was allowed to cool, to precipitate out white catenae of indium tin ace--tate.

The product acetate was filtered off and was converted into indium tin oxide by heating it to 375°C. Calcination of this first batch of material (1050°C, 3 hours) at City University yielded approximately one kilogramme of indium tin oxide which had a measured resistivity of 0·8 Ωcm.

BA2

Weight of Indium Tin Alloy used = 1112·9g

Volume of Acetic Acid used = 2750ml

Volume of Acetic Anhydride used = 500ml

Reaction was refluxed for 46·5 hours at 118°C

Residue of undissolved alloy = 252g

After refluxing the mixture for 46½ hours the solution obtained was allowed to cool to precipitate out white catenae of indium tin acetate. The product was filtered off and converted into indium tin oxide by heating at 375°C. This second batch of material was then forwarded to Keeling and Walker for calcination (8 hour heating and cooling cycle with 3 hours at maximum temperature of.1050°C). Resistivity measurements carried out on calcined samples of this second batch of material showed it to possess a high resistivity. The results of different calcination trials carried out on 30g samples of the oxide are given in table eight. Partly as a response to the disappointing resistivity results obtained from this second batch of material and also in an attempt to gain an understanding of the physical and chem-ical backgrounds to the acetate route, a further investigation into this synthetic route was carried out. In particular this investigation was carried out in order to try to identify factors which might oper-ate giving rise to a high resistivity in the product.

Table Eight - Results of Calcination Trials carried out upon Indium Tin Oxide from Batch BA2

| Calcination Temp./$^{o}$C | Time Held at Max Temp./min | Product Resistivity/$\Omega$ cm |
|---|---|---|
| 800 | 180 | 13·3 |
| (i) 1040 (ii)1080 | (i) 180 (ii) 180 | 4·7 |
| 1140 | 180 | 8·1 |
| 1050 | 8 Hour Cycle with 180 mins at Max Temp. | 1500 |

The acetate route may be represented schematically as follows

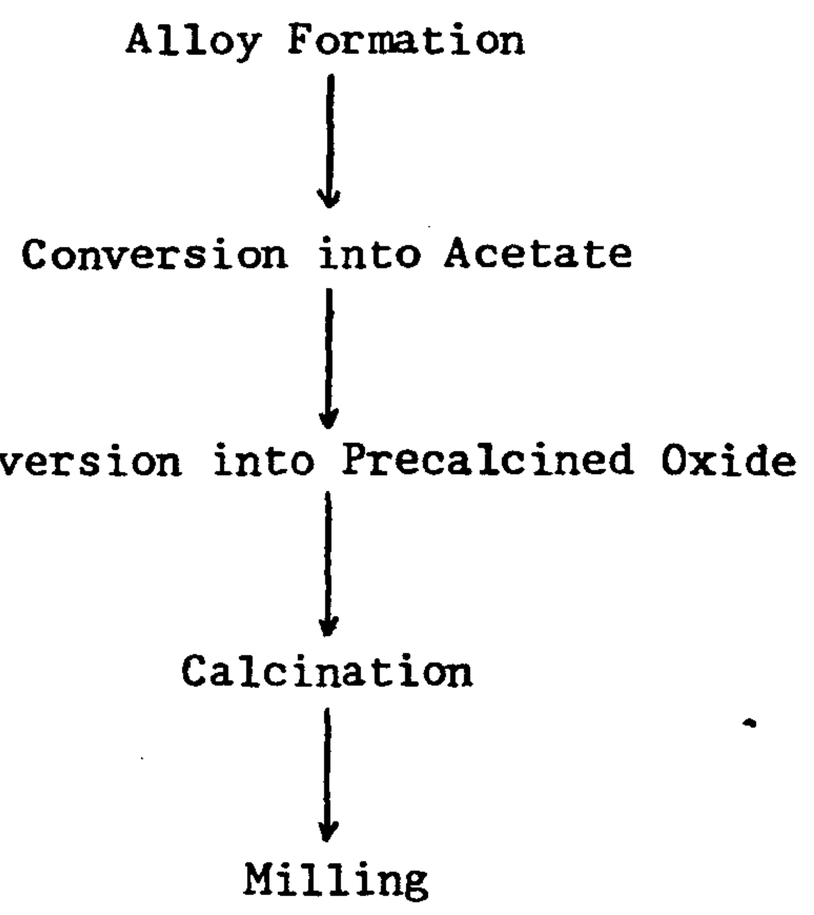


At the start of this investigation it was assumed that the formula of indium tin acetate prepared from 89·8/10·2 indium tin oxide was, $In(CH_3CO_2)_3.0{\cdot}11Sn(CH_3CO_2)_2$, this would give the following elemental percentage composition.

Carbon = 24·3%

Hydrogen = 3·0%

Oxygen = 32·6%

Indium = 36·4%

Tin = 3·7%

Empirical Formula = $In_{1\cdot0}Sn_{0\cdot11}C_{6\cdot3}H_{9\cdot4}O_{6\cdot4}$

A comparison of the theoretical and experimentally derived empirical formulae for indium tin acetate shows the indium tin acetate prepared from reaction BA2 to be tin deficient, containing approximately only 25% of the quantity of tin which would be required to successfully prepare 90/10 indium tin oxide. Thermal analysis carried out on a sample of indium tin acetate from reaction BA2 (figure 13) showed that the material decomposed upon heating to 400°C to leave a 55% residue of 90/10 indium tin oxide. This figure is some 6% too high to be consistent with the theoretical value.

$$\underset{100}{In(CH_3CO_2)_3.0\cdot11Sn(CH_3CO_2)_2} \xrightarrow{\Delta H} \underset{48\cdot9}{InSn_{0\cdot11}O_{1\cdot7}}$$

However, the experimentally determined thermal decomposition residue weight is reasonably consistent with the formula derived from the elemental analysis assuming that the material decomposes as follows.

$$\underset{100}{In_{1\cdot0}Sn_{0\cdot025}C_{4\cdot4}H_{7\cdot4}O_{6\cdot1}} \longrightarrow \underset{53}{In_{1\cdot0}Sn_{0\cdot025}O_{1\cdot55}}$$

$In_{1\cdot0}Sn_{0\cdot025}O_{1\cdot55}$ analyses as 97·3% $In_2O_3$ : 2·6% $SnO_2$.

When preparing indium tin acetate from indium tin alloy and acetic acid, after refluxing the reaction solution for 46·5 hours there re-mained 252g of unreacted alloy left in the reaction vessel. It had been assumed initially that the composition of this residual alloy would be identical to that of the freshly prepared alloy at the start of the reaction. However from the results of analyses carried out in this investigation, which showed the indium tin acetate from BA2 to be tin deficient, it was predicted that the residual indium tin alloy would analyse as being high in tin.

Figure Thirteen - Thermal Analysis of Indium Tin Acetate BA2

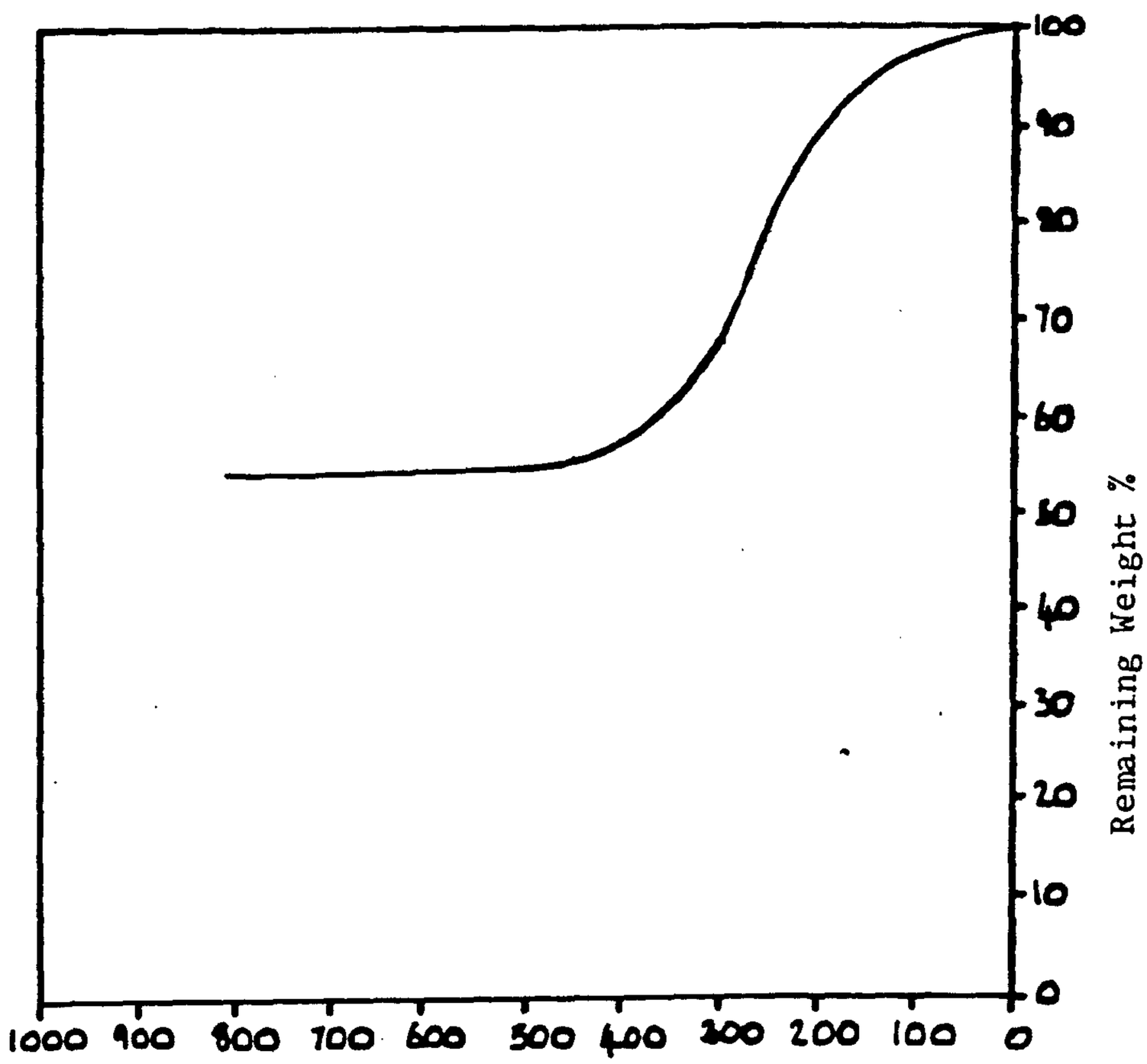


Heating Rate = 10°C/min.

Nitrogen Flow = 30

Pt Pans

$Al_2O_3$ Reference used

Samples of new and residual indium tin alloy were analysed for tin content by titration against cerium (IV) sulphate solution.

A piece of the alloy under test (c0·3g) was added to hydrochloric acid (10ml, conc.) and was left to dissolve to give a clear solution. This solution was then made up to 50cc in a volumetric flask with distilled water. Aliquots (10cc) from this solution were then tit-rated against a standardised solution of cerium (IV) sulphate held in a burette using ferrous indicator (red to blue).

$$Sn^{2+} \longrightarrow Sn^{4+} + 2e^-$$

$$2Ce^{4+} + 2e^- \longrightarrow 2Ce^{3+}$$

$$2Ce^{4+} + Sn^{2+} \longrightarrow Sn^{4+} + 2Ce^{3+}$$

$$Sn^{2+} \longrightarrow Sn^{4+} + 2e^-$$

$$2(Fe^{3+} + e^-) \longrightarrow 2Fe^{2+}$$

$$2Fe^{2+} \longrightarrow 2(Fe^{3+} + e^-)$$

$$2(Ce^{4+} + e^-) \longrightarrow 2Ce^{3+}$$

The percentage of tin (X) in the analyte is calculated from

$$X = \frac{118{\cdot}7}{2} \text{ x Molarity of Ceric Sulphate x Vol. used x } 10^{-3} \text{ x } \frac{100}{\text{Sample Wt.}}$$

Where the sample weight is in grams and the volume of $Ce^{4+}$ solution is in millilitres.

Analysis of New Alloy

Sample Weight = 0·3872g (÷5 for one aliquot)

Titration Volume = 1·12cc

Molarity of Solution = 0·1018M

%Tin = 8·73

Analysis of Alloy Residue

Sample Weight = 0·2575g (÷ 5 for one aliquot)

Titration Volume = 2·74ml %Tin = 32·78

Molarity of $Ce^{4+}$ Solution = 0·1018M

New alloy was prepared with the ratio 10·2% Sn : 89·8% In

Experimental value obtained for new alloy = 8·73% Sn

Error in Value = 14%

Alloy Residue contains 32·8(±4·6)% Tin

Now the initial 'new' alloy weight was 1135g = 115·77g Tin

Residual alloy weight was 252g = 102·56g Tin

Tin Uptake = 13·21g

Therefore, assuming complete decomposition of indium tin acetate to give oxide, the oxide composition is 1·3(±1)% $SnO_2$/98·7(±1)% $In_2O_3$. This thus accounts for the high resistivity of indium tin oxide samples prepared from BA2.

Finally a sample of the residual indium tin alloy from reaction BA2 (10g) was converted into indium tin oxide by dissolving it in nitric acid, precipitating with ammonia, washing, drying and then calcining (2 hours, 1050°C). The resistivity of the indium tin oxide prepared from this residual alloy was 240Ωcm.

From analyses carried out it would appear that during the reaction between indium tin alloy and acetic acid, indium metal is leached out of the alloy in preference to the tin which is left behind. Thus the alloy composition varies during the course of the reaction with the tin weight percentage increasing as the reaction proceeds.

In the first experiment, BA1, the reaction was carried out to virtual completion and only a small amount of alloy was left in the reaction vessel so that the greater proportion of the tin metal had reacted and had been converted into acetate. In the second experiment this was not the case and the greater proportion of the tin metal was left in the unreacted alloy residue. A sample of indium tin oxide (100g) from BA2 was adjusted to the correct composition for low resistivity (90/10) by the addition of tin (IV) oxide (9g). After milling and recalcining (2 hours, 1050°C) the recovered material was found to have a resistivity of 0·53Ωcm. Therefore in order to successfully prepare 90/10 indium tin oxide by the acetate route it is obviously necessary to allow the reaction to reflux for a much longer period to enable all of the tin metal to react with the acetic acid. A third experiment in this series was then carried out which was denoted BA3 and which is detailed below.

BA3

| | | |
|---|---|---|
| Weight of Indium Tin Alloy used | = | 914g |
| Volume of Acetic Acid used | = | 3500ml |
| Volume of Acetic Anhydride used | = | 750ml |
| Reflux Time | = | 75 hours (+ 84 hours) |
| Weight of Alloy Residue | = | 90g |

After refluxing for 75 hours the reaction mixture was allowed to cool which precipitated out white catenae of indium tin acetate. Upon filtration of the indium tin acetate it was found that there was still indium tin alloy (92g) left in the reaction vessel. This unreacted indium tin alloy was then refluxed in a fresh solution of acetic acid (500ml) and acetic anhydride (20ml) for a further 84 hours,which had little effect upon the alloy residue.

The remaining weight of alloy residue was now 90g. At this stage the reaction was aborted and the prepared indium tin acetate was forwarded to Keeling and Walker for calcination (3 hours, 1060°C). After calcination the product resistivity was found to be 0·7Ω cm. This resistivity value was too high to meet with Keeling and Walker's approval and so this synthetic route was abandonned as a viable route for the large scale manufacture of indium tin oxide.

(b) The Benzoate Route

Work carried out on the preparation of indium tin oxide by the benz--oate route in this part of the project has concentrated upon the manufacture of a 200g batch of material for evaluation. The experi--mental conditions employed in the reaction (BB1) and the subsequent product analysis are described below.

BB1

Weight of 10·2/89·8 Indium Tin Alloy used = 202·5g

Weight of Benzoic Acid used = 1·0Kg

Reflux Time = 38 Hours at 248°C

After refluxing for 38 hours the reaction mixture was allowed to cool and before setting hard, the solid product was removed from the reaction vessel whilst still soft with the aid of a scoop. The solid mixture of indium tin benzoate and benzoic acid obtained from the reaction was then separated by washing the material with cold methanol which dissolved the unreacted benzoic acid leaving behind the indium tin benzoate which was filtered off. The indium tin benzoate once extrac--ted was converted into indium tin oxide, batchwise, by burning 30g lots in a nickel crucible held over a bunsen flame in a fume cupboard.

The indium tin benzoate burnt with a black flame and yielded 235·3g of black residue which comprised of indium tin oxide and carbon. This material was forwarded to Keeling and Walker for calcination. After calcination (3 hours, 1060°C) this material yielded 192·4g of indium tin oxide which upon cooling and milling was found to have a resistivity of 0·35Ωcm.

Expected Theoretical Yield from 202·5g Alloy = 246·0g

Actual Yield = 192·4g

Percentage Yield of Product = 78·2%

The indium tin oxide produced from reaction BB1 met with Keeling and Walker's criteria for low resistivity and a further investigation into the manufacturing process was called for, to determine the physical/chemical background to the benzoate route. At the start of the investigation it was assumed that the formula of the indium tin benz--oate prepared from 89·8/10·2 indium tin alloy would be $In(C_6H_5CO_2)_3 \cdot 0{\cdot}11Sn(C_6H_5CO_2)_2$. However analysis of the prepared benzoate by trans--mission mössbauer spectroscopy showed tin (IV) and not tin (II) to be the tin species present in the solid state of the material. Thus the formula of the prepared indium tin benzoate was assumed to be $In(C_6H_5-CO_2)_3 \cdot 0{\cdot}11Sn(C_6H_5CO_2)_4$, which gave the following elemental percentage composition.

Indium = 21·1%

Tin = 2·4%

Carbon = 53·1%

Hydrogen= 3·2%

Oxygen = 20·2%

Empirical Formula

$= In_{9{\cdot}1}Sn_{1{\cdot}0}C_{219}H_{158{\cdot}4}O_{62{\cdot}5}$

Molecular Weight = 544·2

Experimentally it was found that the material contained 49% carbon and 3·3% hydrogen, however it was not possible to find a suitable solvent for the material and so indium and tin analyses could not be carried out. The results of elemental carbon and hydrogen analyses are not inconsistent with the theoretical values for these elements and are within the limits of experimental error.

The thermal decomposition of indium tin benzoate was investigated by mössbauer spectroscopy and thermal gravimetric analysis as part of this project and the results of these analyses are given in table nine and figure fourteen respectively.

Table Nine - Mössbauer Spectroscopic Analysis of the Thermal Decomposition of Indium Tin Benzoate.

| Temp./°C | Sample | No. of Peaks | Type | Chem.Shift δ mm/sec | | Residual |
|---|---|---|---|---|---|---|
| -195 | In Sn Benzoate | 1 | Singlet | 0·04 | 0·04 | 137 |
| 475 | In Sn Oxide | 2 | Singlet | 0·07 | 0·01 | 139 |
| | | | Singlet | 2·59 | 0·02 | |
| 1050 | In Sn Oxide | 1 | Singlet | 0·13 | 0·08 | 150 |

The $^{119}Sn$ transmission mössbauer spectra in table nine show that indium tin benzoate and the sample of indium tin oxide which had been calcined to 1050°C contain tin exclusively as tin (IV) and that the indium tin oxide prepared from the thermal decomposition of the benzoate at 475°C contains tin (IV) and tin metal. Examination of the oxide prepared from the benzoate at 475°C showed the material to contain c5% elemental carbon so it would seem likely that the tin metal present in the mat-erial arises from the following reaction processes.

$$SnO_2 + C \longrightarrow Sn + CO_2$$

$$SnO_2 + 2C \longrightarrow Sn + 2CO$$

It is also highly probable that indium (III) oxide is similarly reduced to indium (I) oxide and indium metal by the same process.

In addition to mössbauer spectroscopy the thermal decomposition of ~~indium tin benzoate~~ was also investigated in air and ~~nitrogen by ther-~~ -mal gravimetric analysis. Results of the analyses show that indium tin benzoate decomposes leaving a 44 weight % residue in air and a 27·5 weight % residue in nitrogen. The thermal gravimetric analysis shown in figure fourteen displays a five stage decomposition process which was interpreted as follows.

Stage One - Decomposition occurs 105°C to 155°C.

5½% weight loss corresponds to loss of moisture and decomp-osition of tin (IV) benzoate

$$Sn(C_6H_5CO_2)_4 \longrightarrow SnO(C_6H_5CO_2)_2$$

Stage Two - Decomposition occurs 155°C to 210°C.

4½% weight loss corresponds to second stage decomposition of tin (IV) benzoate

$$SnO(C_6H_5CO_2)_2 \longrightarrow SnO_2$$

Stage Three - Decomposition occurs 155°C to 265°C (max. 247°C).

11% weight loss corresponds to loss of unreacted benzoic acid from the sample. Benzoic acid boiling point = 249°C.

Stage Four - Decomposition occurs 265°C to 456°C.

42% weight loss corresponds to decomposition of indium (III) benzoate. Elemental carbon was only found in samples which had been heated to 320°C or above.

$$In(C_6H_5CO_2)_3 \longrightarrow InO_{1.5} \text{ (+carbon)}$$

Figure Fourteen - Thermal Gravimetric Analysis of Indium Tin Benzoate

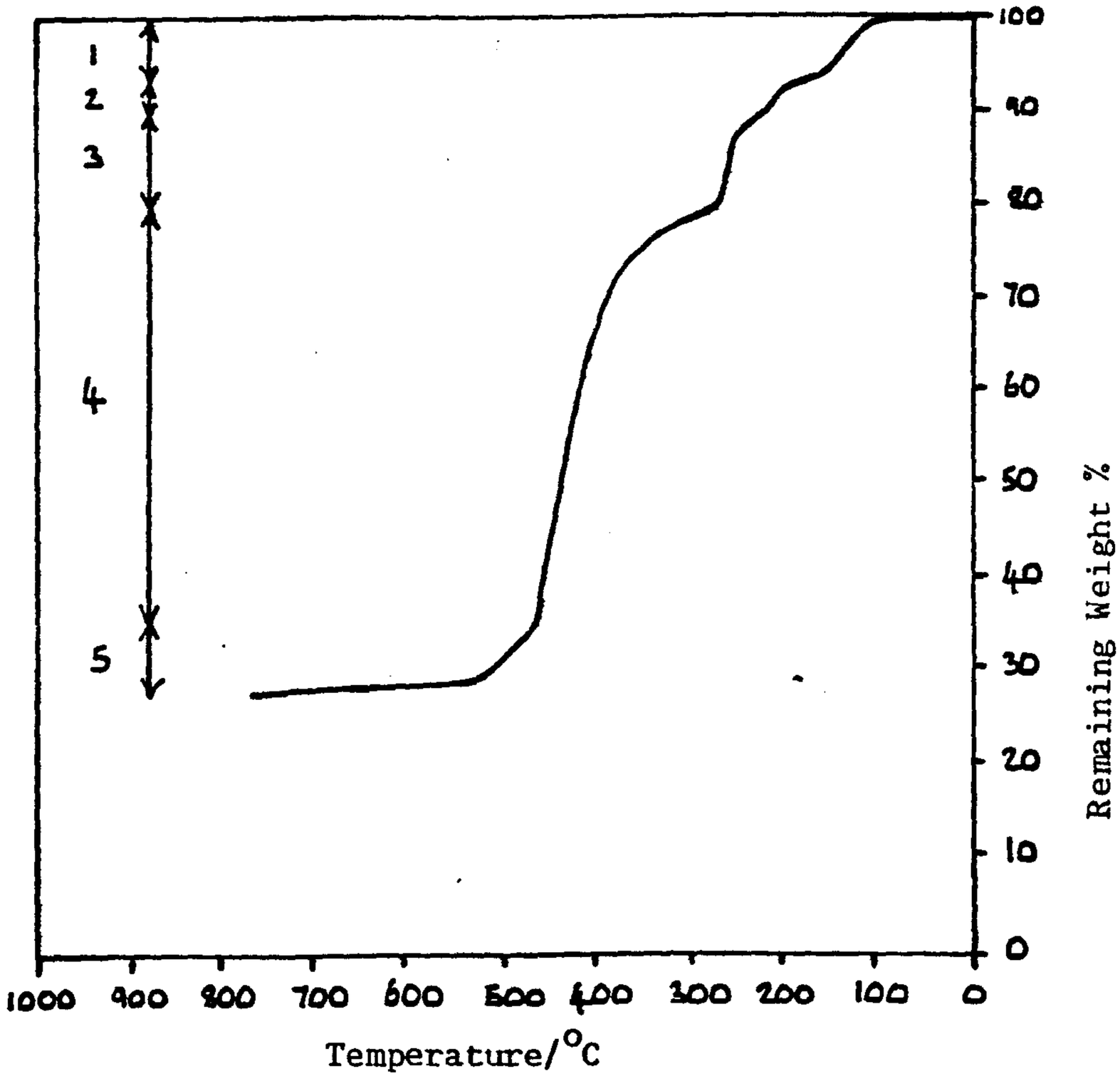


Heating Rate = 10°C/min.

Nitrogen Flow = 0·5cm$^3$min$^{-1}$

Pt pans

$Al_2O_3$ Reference

Stage Five - Decomposition occurs 456°C to 950°C.

9½% weight loss corresponds to reduction(s)

$$Sn^{IV}O_2 \xrightarrow{\Delta H, C} Sn^{o}$$

$$In_2^{III}O_3 \xrightarrow{\Delta H, C} In_2^{I}O/In^{o}$$

of indium and tin oxides by carbon. Any $Sn^{II}O$ formed at this elevated temperature would be highly susceptable to dissociation into $Sn^{IV}O_2$ and $Sn^{o}$ viz.

$$2SnO \longrightarrow SnO_2 + Sn$$

As a result of this investigation, the benzoate synthetic route to indium tin oxide can be represented by the following reaction sequence.

(i) $In + 0{\cdot}11Sn \longrightarrow InSn_{0{\cdot}11}$

(ii) $InSn_{0{\cdot}11} + 3{\cdot}4C_6H_5CO_2H \xrightarrow{\text{Reflux}} In(C_6H_5CO_2)_3.0{\cdot}11Sn(C_6H_5CO_2)_4$

(iii) $In(C_6H_5CO_2)_3.0{\cdot}11Sn(C_6H_5CO_2)_4 \xrightarrow{320^{o}C} InO_{1{\cdot}5} + 0{\cdot}11SnO_2 + nC$

(iv) $InO_{1{\cdot}5} + 0{\cdot}11SnO_2 + nC \xrightarrow[450^{o}C]{\Delta H} In^{III}O_{1{\cdot}5}/In_2^{I}O/In^{o} + Sn^{IV}O_2/Sn^{o}$

$$\xrightarrow[950^{o}C,\ Air]{\text{Calcine}} In_{1{\cdot}0}Sn_{0{\cdot}11}O_{1{\cdot}72-X}$$

Pan and Ma[16] reported that samples of indium tin oxide which they analysed as containing slight amounts of indium metal usually possess-ed a high conductivity. The presence of carbon in the sample during calcination is therefore most probably beneficial in preparing a pro-duct of low resistivity as the carbon maintains the sample in a red-ucing enviroment which helps to stabilise mixed oxidation states in the calcined material.

Conclusion

Of all the synthetic pathways to 90/10 indium tin oxide investigated in this part of the work, the benzoate route appears to be the most suitable for application to large scale production.

From a chemical viewpoint the benzoate route is simply a synthetic homologue of the acetate route, which was investigated earlier on in this section, but with benzoic acid replacing acetic acid as the react--ion medium. The reaction between 89·8/10·2 indium tin alloy and benzoic acid proceeds at a much faster rate than the corresponding reaction with acetic acid. This is attributed to the higher boiling point and the higher acidity of benzoic acid compared with acetic acid.

| | Boiling Point /°C | $pK_a$ |
|---|---|---|
| Benzoic Acid | 249 | 4·2 |
| Acetic Acid | 118 | 4·75 |

As a synthetic route the benzoate route has one further advantage over the acetate route in that the presence of carbon, generated in situ from the thermal decomposition of indium tin benzoate, helps to main--tain a reducing environment so stabilising any mixed metal valence states present in the material. Two disadvantages of the benzoate route are; (i) low experimental yields (78%) and (ii) strong product colouration which results from the presence of carbon in the calcined material. However the final decision on whether or not to adopt the benzoate route as a synthetic route for the large scale manufacture of indium tin oxide must rest, for the present, with Keeling and Walker Ltd.

References

1. M. Nagasawa, S. Shionoya, S. Makishima, J. Phys. Soc. Japan, 1965, 20, 1093.

1a. Z.M. Jarzebski, J.P. Martin, J. Electrochem. Soc., 1976, 123, 299C.

2. M.K. Paria, M.S. Maiti, J. Mater. Sci., 1982, 17(11), 3275.

3. B.G. Alapin, D. Degtyarev, V.I. Drozd, N.V. Gul'ko, S.V. Lysak, Izv. Akad. Nauk. S.S.S.R., Neorg. Mater., 1981, 17(5), 923.

4. J.L. Portefaix, P. Bussiere, J.P. Forisser, J.M. Friedt, J.P. Sanchez, F. Theobald, J.Chem. Soc., Faraday Trans. 1, 1980, 76(8), 1652.

5. J.M.J. Herman, J.L. Portefaix, M. Forisser, F. Figueras, P. Pichat, J. Chem. Soc., Faraday Trans. 1, 1979, 75(6), 1346.

6. D. Pyke, R. Reid, R.J.D. Tilley, J. Solid State Chem., 1978, 25, 231.

7. M.B. Robin, P. Day, Adv. Inorg. Radio. Chem., 1967, 10, 247.

8. F.J. Berry, C. Greaves, J.C.S. Dalton Trans., 1981, 12, 2447.

9. G. Frank, H. Kostlin, A. Rabenau, Phys. Stat. Sol. (A), 1979, 52, 231.

10. M. Mizuhashi, Asahi Garasu Kenkyu Hokoko, 1980, 30(2), 89.

11. C. BoHyun, P.H. Young, K.H. Jeong, New Phys.(Korean Phys. Soc.), 1982, 22(1), 31.

12. H. Morriss, Personal Communication.

13. R. Groth, Phys. Status Solidi, 1966, 14, 69.

14. A.E. Solov'eva, V.A. Zhdanov, V.L. Markov, R.R. Shvangiradze, Izv. Akad. Nauk. S.S.S.R., Neorg. Mater., 1982, 18(5), 825.

15. D.B. Fraser, H.D. Cook, J. Electrochem. Soc., 1972, 119, 1368.

16. C.A. Pan, T.P. Ma, Appl. Phys. Lett., 1980, 37, 163.

17. L. Holland, "Vacuum Deposition of Thin Films", p466, John Wiley + Sons Inc., New York, 1961.

18. M.C. Burrel, R.S. Kaller, N.R. Armstrong, Anal. Chem., 1982, 54, 2511.

19. Z. Ovadyahnu, B. Ovryn, H.W. Kraner, J. Electrochem. Soc., 1983, 130(4), 917.

20. F. Lawson, Nature, 1967, 215, 955.

21. Ts. Bonchev, B. Manushev, God. Sofii. Univ. Fiz. Fak., 1974 - 1975, (publ. 1978), 66, 11.

22. A.E. Solov'eva, V.A. Zhdanov, Teplofiz. Vys. Temp., 1983, 21(3), 609.

23. H. Morriss, Personal Communication.

24. H. Morriss, Personal Communication.

# Chapter Five - Mixed Metal Oxide Semiconductors

## Section 5.1 - Introduction

## Section 5.2 - Diluants in Indium Tin Oxide Systems

5.2.1. - An Investigation into the Effects of Impurities on the Resistivity of Indium Tin Oxide

5.2.2. - An Investigation into the Effects of Diluants on the Resistivity of Indium Tin Oxide.

## Section 5.3 - Mixed Metal Oxides

# Chapter Five - Mixed Metal Oxides

## 5.1. Introduction

The work described in this chapter is concerned with the attempted preparation of conducting metal oxides combining the desirable resist-ivities of antimony tin oxide or indium tin oxide with low chromo-phoric character and/or lower cost. The work undertaken in this chapter fell into two sections outlined below.

(i) The first part of the investigation was an attempt to try to improve the commercial viability of indium tin oxide by mixing it with small quantities of a more expensive material which would further reduce the resistivity and chromophoricity of the product.

(ii) The second part of the investigation was an attempt to prepare other mixed metal oxide semiconductors to replace tin antimony and indium tin oxides.

The incorporation of foriegn atoms into a crystal is accompanied by the appearance of energy levels in a forbidden energy gap. The loca-tion of these levels depends upon the type of foreign atoms and the nature of the matrix components of the lattice. A general discussion of these effects is included in Chapter 4, section 1 of this thesis. For indium tin oxide, which is an n-type semiconductor, a plot of electron states as a function of electron energy E will be of the form shown in figure one. If $E_g$ is the energy gap between the valence and the conduction band and $E_f$ is the fermi level, which is defined as the level below which all electron states are occupied at absolute energy.

Fermi statistics show that the concentration of electrons in the cond-uction band of a material is related to the position of the Fermi level in the material by the equation

$$n_e = \text{Constant} \times T^{3/2} \times \exp\left[(-E_g - E_f)/KT\right]$$

where K is the Boltzman constant and T is the absolute temperature.

Figure One - Electronic Levels in an n-type Semiconductor

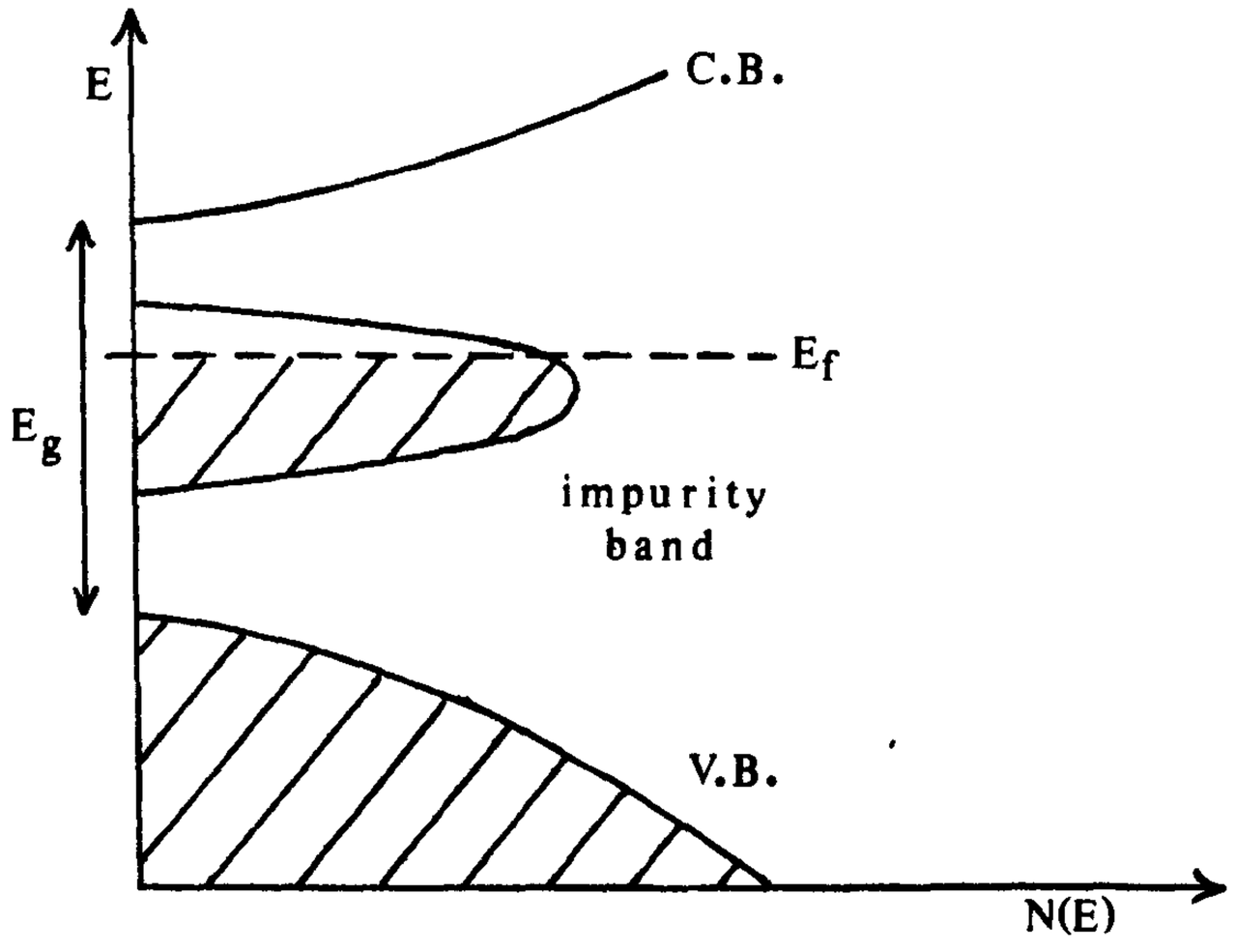


For an intrinsic semiconductor the total conductivity, $\sigma_{tot}$, is the sum of that due to electrons, $\sigma_e$, moving within the energy restrictions of the valence band.

$$\sigma_{tot} = \sigma_h + \sigma_e$$

$$= n|e|\mu_e + p|e|\mu_h$$

where n and p are the numbers of electrons and holes and $\mu_e$ and $\mu_h$ are their respective mobilities.

Now $$\mu = \text{Constant} \times T^{-3/2}$$

and for an intrinsic semiconductor $E_f = \frac{1}{2}E_g$

Therefore $$\sigma_I = \sigma_{OI} \exp(-E_g/2KT)$$

For an extrinsic semiconductor the excitation of carriers from impur--ity levels has to be allowed for. If the impurity level excitation energy is $E_i$, then.

$$\sigma_E = \sigma_{OE} \exp(-E_i/KT)$$

where $\sigma_{OE}$ is a constant and $\sigma_E$ is the extrinsic contribution to the conductivity of the material due to the presence of an impurity. Thus the total conductivity is defined by an equation.

$$\sigma_{tot} = \sigma_{OI} \exp(-E_g/2KT) + \sigma_{OE} \exp(-E_i/KT)$$

Further terms may be added to this equation if necessary to account for the presence of several impurity donors in a material i.e.

$$\sigma_{tot} = \sigma_1 + \sigma_{E_2} + \sigma_{E_3} + \ldots\ldots \sigma_{E_n}$$

The conductivity of a semiconductor may thus be increased by heating, by the application of radiant energy, by the addition of appropriate impurities or by any combination of these three methods. In this investigation the addition of impurities to intrinsic and extrinsic semiconductors was investigated in a series of experiments in an attempt to prepare low resistivity, novel oxide semiconducting mat--erials.

## 5.2. Diluants in Indium Tin Oxide Systems

### 5.2.1. An Investigation into the Effects of Impurities on the Resistivity of Indium Tin Oxide

Experimental trials carried out in the preparation of tin antimony oxide electrodes for use in glass melting furnaces showed the presence of copper to be advantageous in preparing a low resistivity material. Following on from this observation a series of experiments were carr--ied out in the present work to study the effects of further dopants on the resistivity of 90/10 indium tin oxide. The experimental pro--cedure adopted was as follows:

Indium tin oxide (90/10, 9·7g) was ball milled for 15 minutes in ethanolic media with a dopant material (0·3g) and then dried in an oven at 95°C. The dried material was then calcined (2 hours, 1050°C) in a silica crucible to incorporate the dopant species into the host lattice structure. The calcined material was cooled, ball milled a second time in ethanol and oven dried to obtain a homogenous sample for analysis.

The results obtained for eight dopant species in indium tin oxide at a 3 weight % level are given in table one.

Table One - Resistivities of Doped Indium Tin Oxides

| Dopant Material (3 Wt. %) | Resistivity/Ω cm |
|---|---|
| Control | 128 |
| Iron Oxide ($Fe_3O_4$) | 1410 |
| Zinc Oxide | 243 |
| Copper (II) Oxide | 900 |
| Cadmium (II) Oxide | 54 |
| Lead Oxide ($Pb_3O_4$) | 2040 |
| Cobalt Oxide | 513 |
| Cerium Oxide | 1217 |
| Cadmium Flouride | $1·7 \times 10^{10}$ |

The control sample of indium tin oxide used in the above trials came from one of Keeling and Walkers batches of rejected samples. The results show that cadmium oxide is the only one of the dopant materials that is effective at the 3 weight % level in reducing the resistivity of indium tin oxide. Cadmium oxide as a dopant was also found to change the colour of the product from green to light beige.

Further experimentation in this area showed that 3 weight % cadmium oxide was the optimum dopant loading in indium tin oxide for a low resistivity product. When using the same control sample of indium tin oxide,doping with 1 weight % cadmium oxide gave a product with resistivity 115 Ω cm and doping with 5 weight % cadmium oxide gave a product with resistivity 118·5 Ω cm. A similar experiment on the addition of 3 weight % of cadmium oxide to a more conducting indium tin oxide (resistivity 1·0 Ω cm) resulted in a reduction of the resist-ivity of 0·3 Ω cm.

### 5.2.2. An Investigation into the Effects of Diluants on the Resistivity of Indium Tin Oxide

The objective of this part of the investigation was to find an inexpen-sive, inert, white filler which could be sucessfully blended with 90/10 indium tin oxide to yield a new composite material of low resist-ivity. In total the effects of eleven diluants were investigated over a range of all possible compositions. The experimental procedure adopted was as follows.

Indium tin oxide (90/10, (10-X)g) was ball milled in ethanolic solution with a diluant (Xg) for 15 minutes and was then dried at 100°C in an oven. The dried material was calcined (2 hours, temp. depending on the sample - see table fourteen) in a silica crucible to aid the form-ation of any new phases in the material. After calcination the mixed oxide was cooled, ball milled for a second time for 15 minutes in ethanol and oven dried to prepare a homogenous sample for resistivity analysis.

The indium tin oxide used in these experimental trials came from several batches of Keeling and Walkers rejected samples and it should be noted

that the resistivity of the initial 100 weight % indium tin oxide sample is different for each of the experimental trials.

The results obtained for the eleven experimental series studied in this investigation are given in figures two to twelve and in tables two to twelve. A summary of the results obtained together with the calcination temperatures used in the preparations is given in table thirteen.

Table Two - Resistivities of Titanium Dioxide doped Indium Tin Oxide Phases

| Wt. % $TiO_2$ | Wt. % In Sn Oxide | Resistivity/$\Omega$ cm |
|---|---|---|
| 0 | 100 | 6·0 |
| 5 | 95 | 9·2 |
| 10 | 90 | 54·0 |
| 20 | 80 | $4 \cdot 3 \times 10^{5}$ |
| 30 | 70 | $5 \cdot 4 \times 10^{5}$ |
| 40 | 60 | $1 \cdot 8 \times 10^{3}$ |
| 50 | 50 | $2 \cdot 7 \times 10^{4}$ |
| 60 | 40 | $8 \cdot 9 \times 10^{5}$ |
| 70 | 30 | $7 \cdot 3 \times 10^{7}$ |
| 80 | 20 | $5 \cdot 5 \times 10^{10}$ |
| 90 | 10 | $8 \cdot 6 \times 10^{7}$ |
| 95 | 5 | $8 \cdot 0 \times 10^{6}$ |
| 100 | 0 | $1 \cdot 0 \times 10^{7}$ |

Table Three - Resistivities of Zirconium Dioxide doped Indium Tin Oxide Phases

| Wt. % $ZrO_2$ | Wt. % In Sn Oxide | Resistivity/$\Omega$ cm |
|---|---|---|
| 0 | 100 | 18·2 |
| 5 | 95 | 18·5 |
| 10 | 90 | 19·2 |
| 20 | 80 | 19·6 |
| 30 | 70 | 31·8 |
| 40 | 60 | 38·7 |
| 50 | 50 | 154·0 |
| 60 | 40 | 400·0 |
| 70 | 30 | $7·1x10^4$ |
| 80 | 20 | $8·5x10^5$ |
| 90 | 10 | $8·7x10^6$ |
| 95 | 5 | $8·8x10^7$ |
| 100 | 0 | $1·2x10^6$ |

Table Four - Resistivities of Aluminium Trioxide doped Indium Tin Oxide Doped Phases

| Wt. % $Al_2O_3$ | Wt. % In Sn Oxide | Resistivity/$\Omega$ cm |
|---|---|---|
| 0 | 100 | 18·2 |
| 5 | 95 | 19·0 |
| 10 | 90 | 21·0 |
| 20 | 80 | 24·2 |
| 30 | 70 | 34·9 |
| 40 | 60 | 41·1 |
| 50 | 50 | 148·0 |
| 60 | 40 | 812·0 |
| 70 | 30 | 8955·0 |
| 80 | 20 | $5·5x10^6$ |
| 90 | 10 | $9·5x10^9$ |
| 95 | 5 | $7·1x10^6$ |
| 100 | 0 | $1·2x10^8$ |

Table Five - Resistivities of Zinc Oxide Doped Indium Tin Oxide Doped Phases

| Wt. % ZnO | Wt. % In Sn Oxide | Resistivity/Ω cm |
|---|---|---|
| 0 | 100 | 18·2 |
| 5 | 95 | 25·0 |
| 10 | 90 | 184·0 |
| 20 | 80 | 855·0 |
| 30 | 70 | $6·2x10^4$ |
| 40 | 60 | $1·0x10^7$ |
| 50 | 50 | $1·5x10^5$ |
| 60 | 40 | $3·1x10^5$ |
| 70 | 30 | $4·7x10^5$ |
| 80 | 20 | $3·4x10^6$ |
| 90 | 10 | $5·1x10^5$ |
| 95 | 5 | $1·1x10^5$ |
| 100 | 0 | $1·9x10^6$ |

Table Six - Resistivities of Silicon Dioxide Doped Indium Tin Oxide Phases

| Wt. % $SiO_2$ | Wt. % In Sn Oxide | Resistivity/$\Omega$ cm |
|---|---|---|
| 0 | 100 | 9·8 |
| 5 | 95 | 13·0 |
| 10 | 90 | 15·5 |
| 20 | 80 | 17·2 |
| 30 | 70 | 19·5 |
| 40 | 60 | 29·0 |
| 50 | 50 | 66·1 |
| 60 | 40 | 210·3 |
| 70 | 30 | $9·9 \times 10^4$ |
| 80 | 20 | $1·2 \times 10^7$ |
| 90 | 10 | $2·7 \times 10^8$ |
| 95 | 5 | $1·9 \times 10^7$ |
| 100 | 0 | $2·3 \times 10^6$ |

Table Seven - Resistivities of Rasorite Doped Indium Tin Oxide Phases

| Wt. % Rasorite | Wt. % In Sn Oxide | Resistivity/$\Omega$ cm |
|---|---|---|
| 0 | 100 | 9·8 |
| 5 | 95 | 10·0 |
| 10 | 90 | 11·0 |
| 20 | 80 | 18·2 |
| 30 | 70 | 40·4 |
| 40 | 60 | 164·0 |
| 50 | 50 | $2·5x10^{4}$ |
| 60 | 40 | $7·1x10^{6}$ |
| 70 | 30 | $9·1x10^{7}$ |
| 80 | 20 | $2·0x10^{8}$ |
| 90 | 10 | $5·9x10^{8}$ |
| 95 | 5 | $5·4x10^{9}$ |
| 100 | 0 | $1·8x10^{8}$ |

Table Eight - Resistivities of Cryolite Doped Indium Tin Oxide Phases

| Wt. % Cryolite | Wt. % In Sn Oxide | Resistivity/Ω cm |
|---|---|---|
| 0 | 100 | 9·8 |
| 5 | 95 | 194·6 |
| 10 | 90 | 360·0 |
| 20 | 80 | 413·0 |
| 30 | 70 | 651·0 |
| 40 | 60 | 1535·0 |
| 50 | 50 | 3100·0 |
| 60 | 40 | $7·5x10^4$ |
| 70 | 30 | $6·7x10^6$ |
| 80 | 20 | $1·8x10^7$ |
| 90 | 10 | $1·7x10^8$ |
| 95 | 5 | $2·3x10^8$ |
| 100 | 0 | $3·6x10^6$ |

Table Nine - Resistivities of Tungsten (VI) Oxide Doped Indium Tin Oxide Phases

| Wt. % $WO_3$ | Wt. % In Sn Oxide | Resistivity/$\Omega$ cm |
|---|---|---|
| 0 | 100 | 9·8 |
| 5 | 95 | 25·4 |
| 10 | 90 | 71·8 |
| 20 | 80 | 763·0 |
| 30 | 70 | $2·6x10^5$ |
| 40 | 60 | $8·5x10^5$ |
| 50 | 50 | $1·1x10^7$ |
| 60 | 40 | $2·2x10^7$ |
| 70 | 30 | $6·4x10^7$ |
| 80 | 20 | $1·0x10^8$ |
| 90 | 10 | $8·3x10^6$ |
| 95 | 5 | $1·6x10^6$ |
| 100 | 0 | $1·8x10^7$ |

Table Ten - Resistivities of Molybdenum (VI) Oxide Doped Indium Tin Oxide Phases

| Wt. % $MoO_3$ | Wt. % In Sn Oxide | Resistivity/Ω cm |
|---|---|---|
| 0 | 100 | 9·8 |
| 5 | 95 | 1256·0 |
| 10 | 90 | $3·4x10^4$ |
| 20 | 80 | $2·8x10^5$ |
| 30 | 70 | $1·6x10^7$ |
| 40 | 60 | $3·1x10^7$ |
| 50 | 50 | $1·2x10^9$ |
| 60 | 40 | $1·4x10^9$ |
| 70 | 30 | $3·2x10^8$ |
| 80 | 20 | $1·9x10^7$ |
| 90 | 10 | $5·0x10^6$ |
| 95 | 5 | $1·1x10^7$ |
| 100 | 0 | $9·3x10^7$ |

Table Eleven - Resistivities of Talc Doped Indium Tin Oxide Phases

| Wt. % Talc | Wt. % In Sn Oxide | Resistivity/Ω cm |
|---|---|---|
| 0 | 100 | 9·8 |
| 5 | 95 | 43·0 |
| 10 | 90 | 2454·0 |
| 20 | 80 | 9120·0 |
| 30 | 70 | $3 \cdot 1 \times 10^{4}$ |
| 40 | 60 | $4 \cdot 0 \times 10^{4}$ |
| 50 | 50 | $6 \cdot 0 \times 10^{4}$ |
| 60 | 40 | $9 \cdot 0 \times 10^{6}$ |
| 70 | 30 | $2 \cdot 5 \times 10^{7}$ |
| 80 | 20 | $2 \cdot 9 \times 10^{7}$ |
| 90 | 10 | $3 \cdot 4 \times 10^{8}$ |
| 95 | 5 | $1 \cdot 2 \times 10^{8}$ |
| 100 | 0 | $1 \cdot 2 \times 10^{9}$ |

Table Twelve - Resistivities of Zircon Sand Doped Indium Tin Oxide Phases

| Wt. % $ZrSiO_4$ | Wt. % In Sn Oxide | Resistivity/Ω cm |
|---|---|---|
| 0 | 100 | 9·8 |
| 5 | 95 | 25·4 |
| 10 | 90 | 29·8 |
| 20 | 80 | 37·1 |
| 30 | 70 | 43·4 |
| 40 | 60 | 45·6 |
| 50 | 50 | 46·2 |
| 60 | 40 | 198·2 |
| 70 | 30 | 625·9 |
| 80 | 20 | $1·6x10^5$ |
| 90 | 10 | $8·7x10^5$ |
| 95 | 5 | $6·3x10^6$ |
| 100 | 0 | $1·3x10^7$ |

Figure Two - $\log_e$ Resistivity v. Composition of $TiO_2$/In Sn Oxide Phases

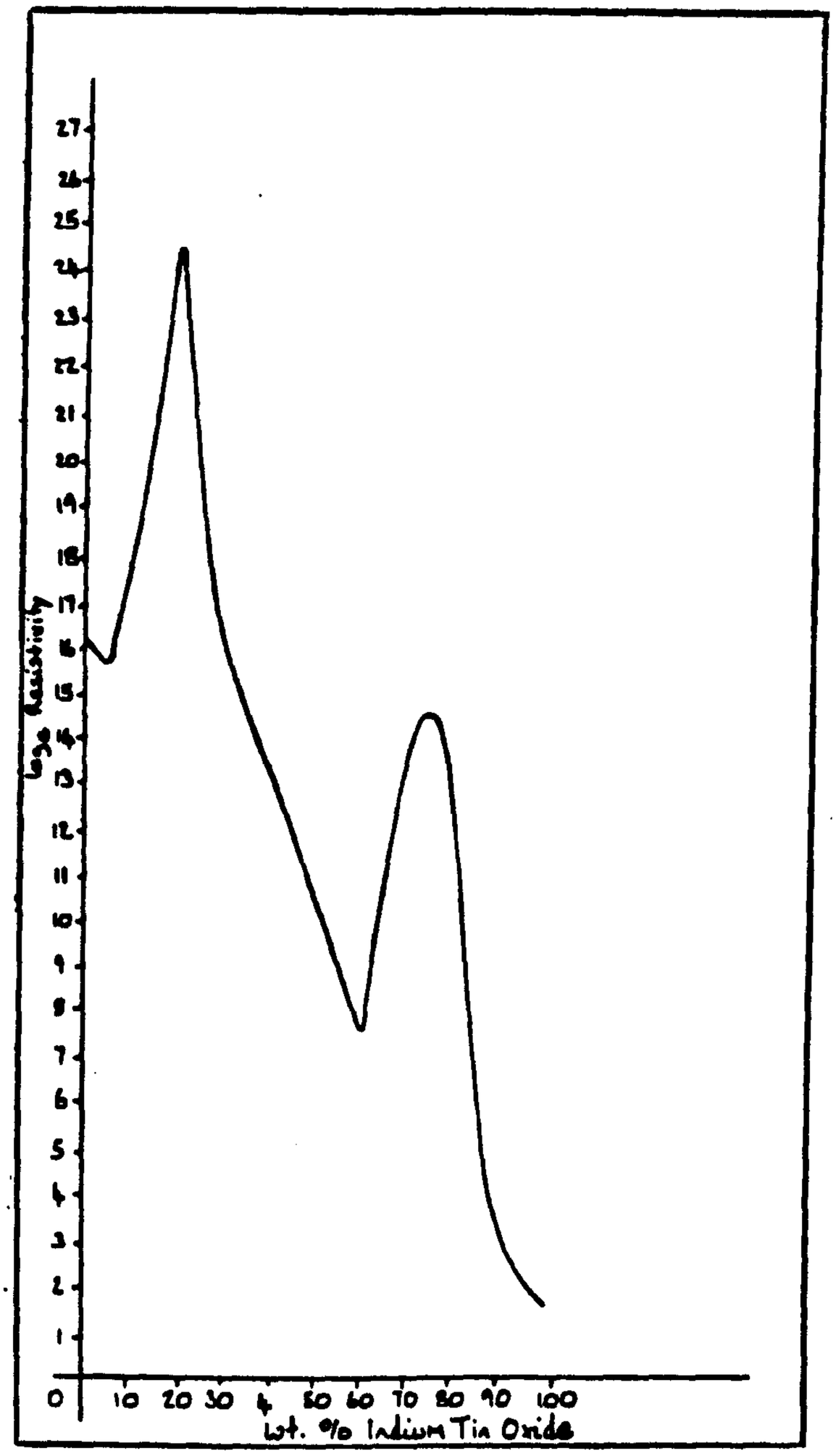

Figure Three - $\log_e$ Resistivity v. Composition of $ZrO_2$/In Sn Oxide Phases

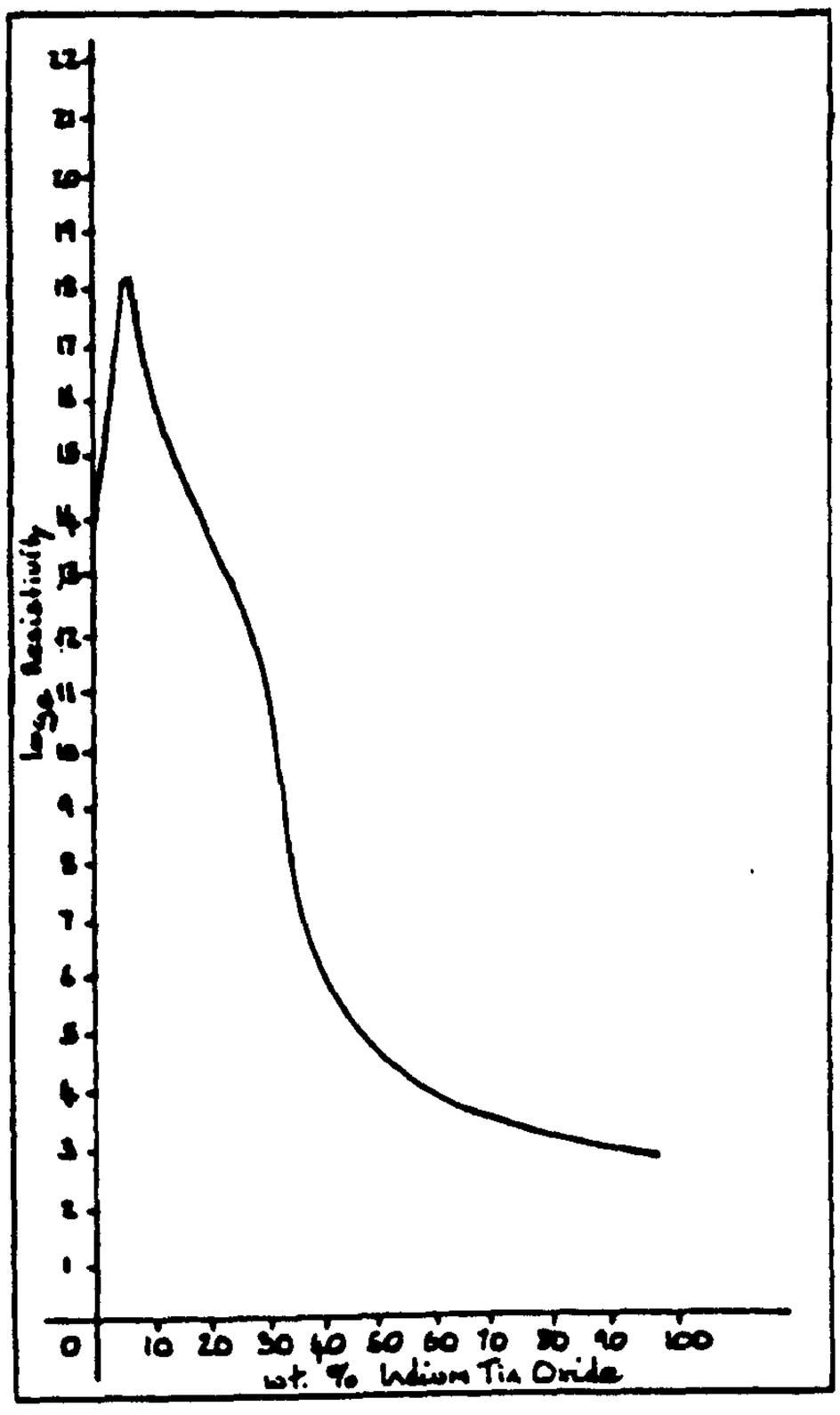


Figure Four - $\log_e$ Resistivity v. Composition of $Al_2O_3$/In Sn Oxide Phases

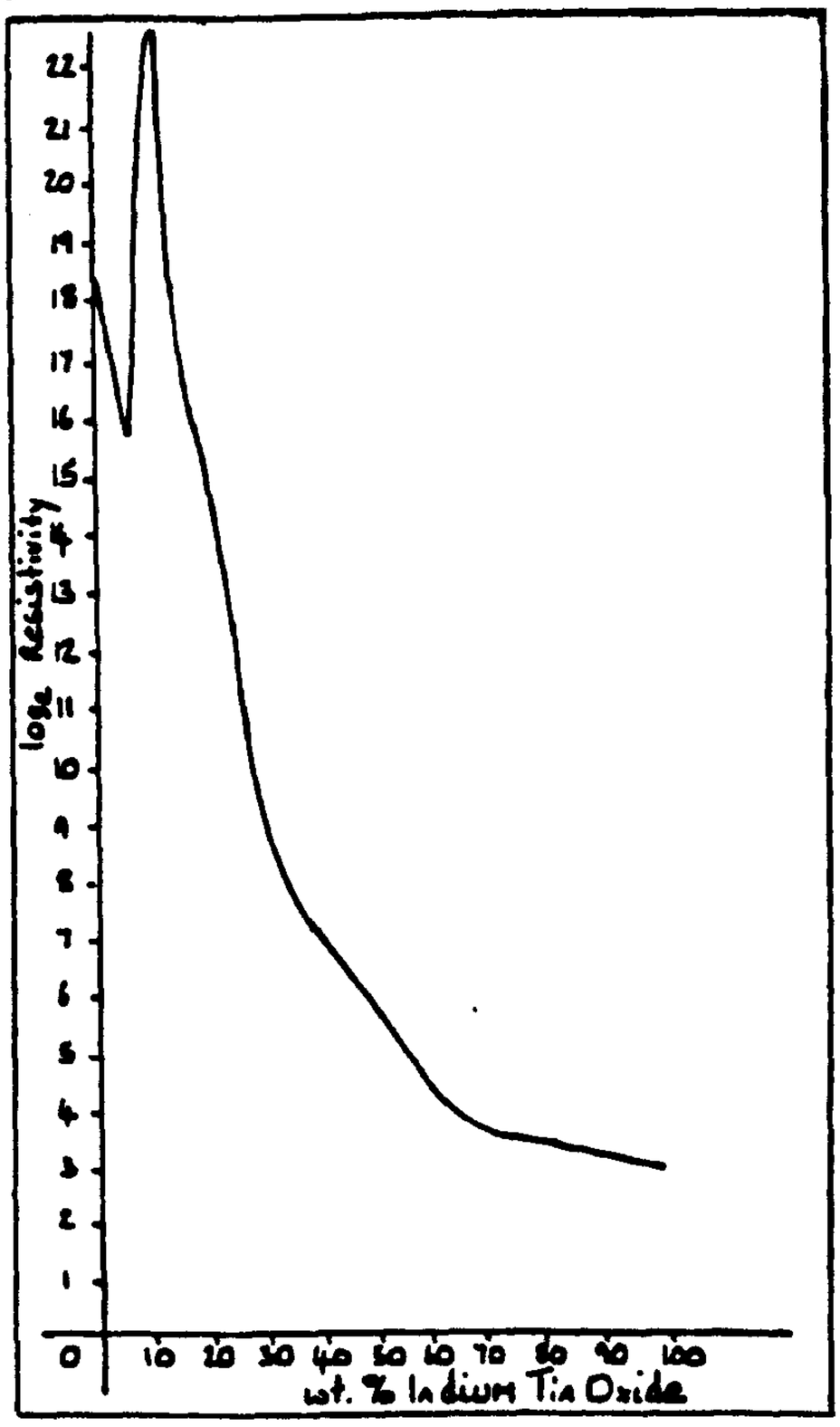

Figure Five - $\log_e$ Resistivity v. Composition of ZnO/In Sn Oxide Phases

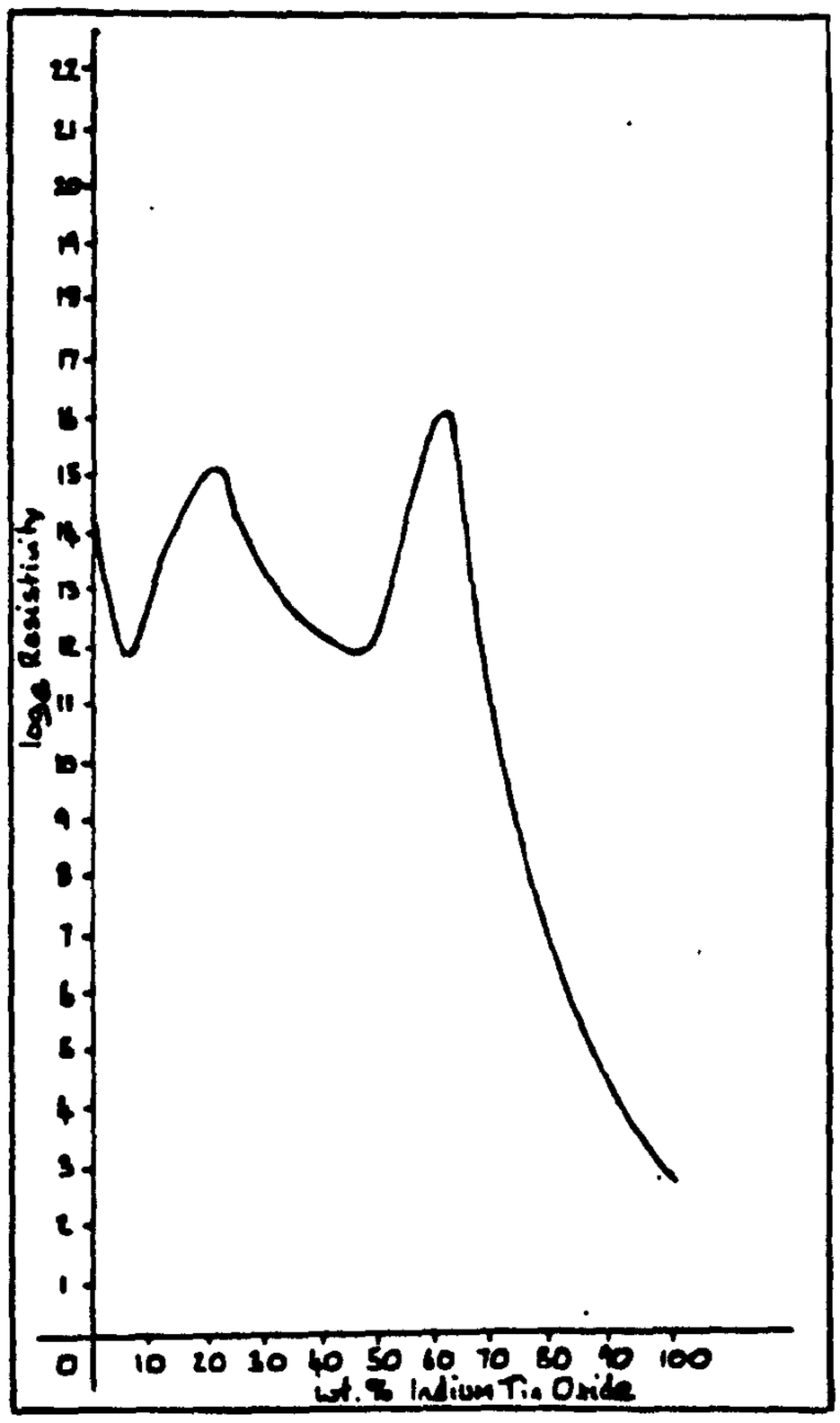


Figure Six - $\log_e$ Resistivity v. Composition of $SiO_2$/In Sn Oxide Phases

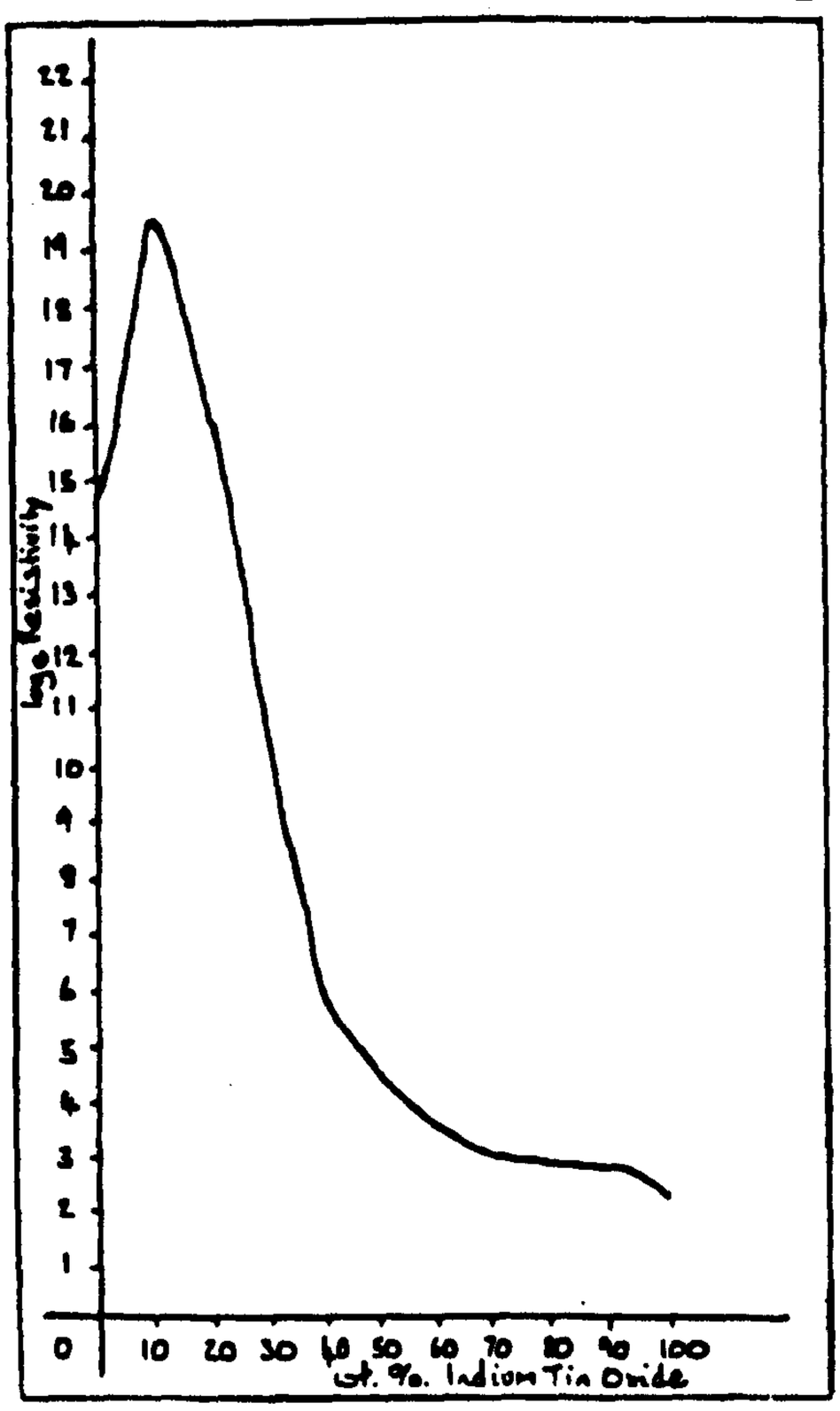

Figure Seven - $\log_e$ Resistivity v. Composition of Rasorite/In Sn Oxide Phases

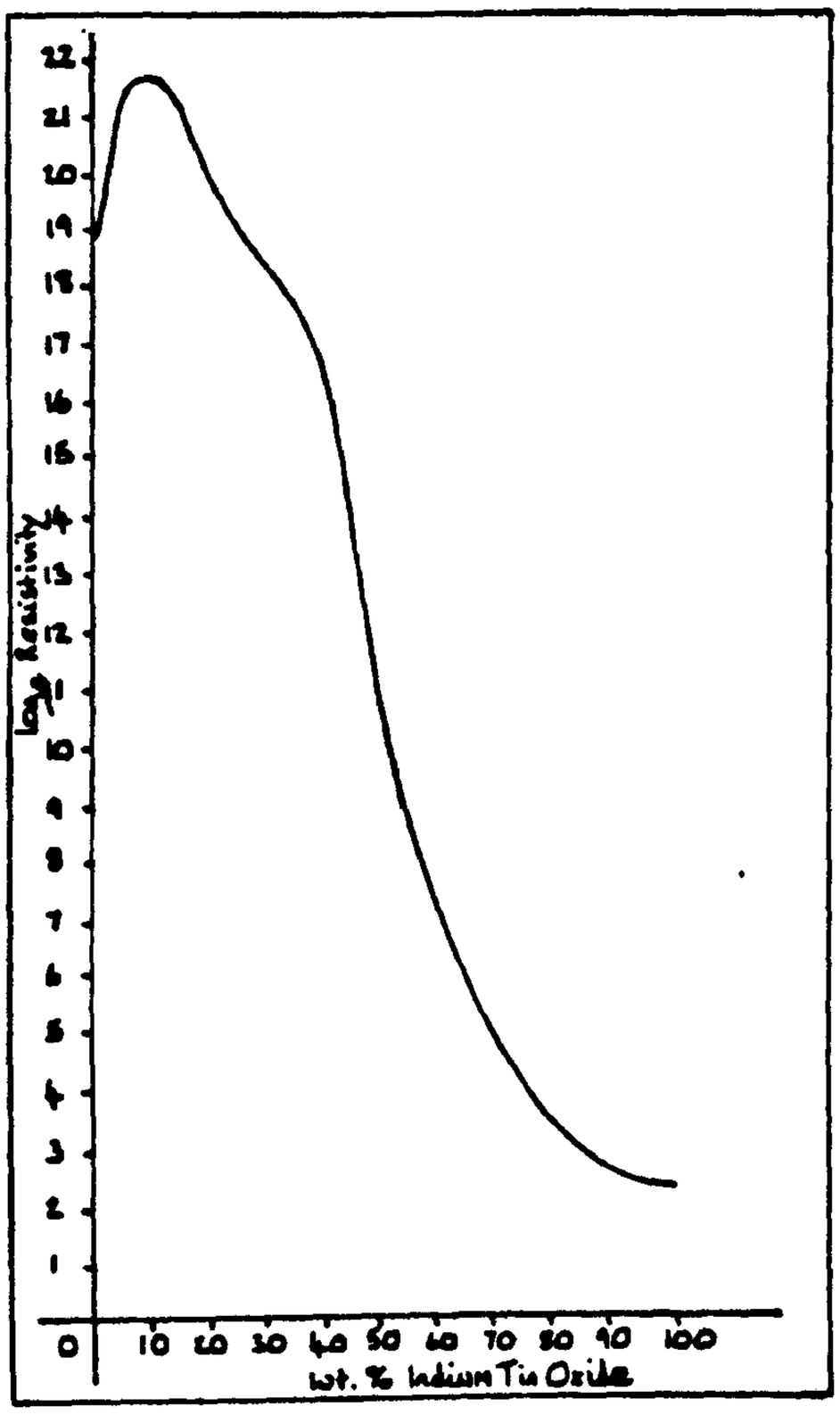


Figure Eight - $\log_e$ Resistivity v. Composition of Cryolite/In Sn Oxide Phases

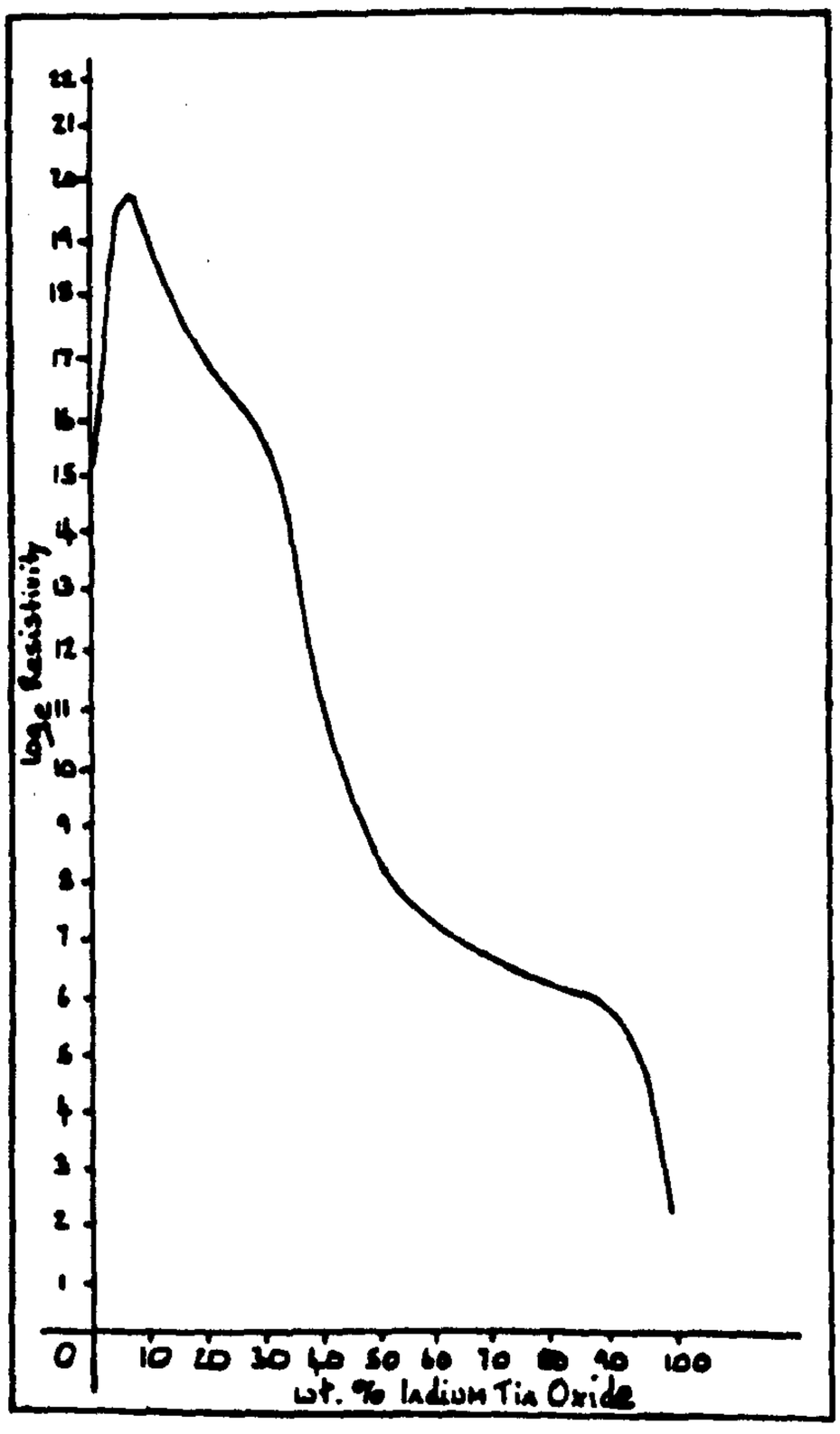

Figure Nine - $\log_e$ Resistivity v. Composition of $WO_3$/In Sn Oxide Phases

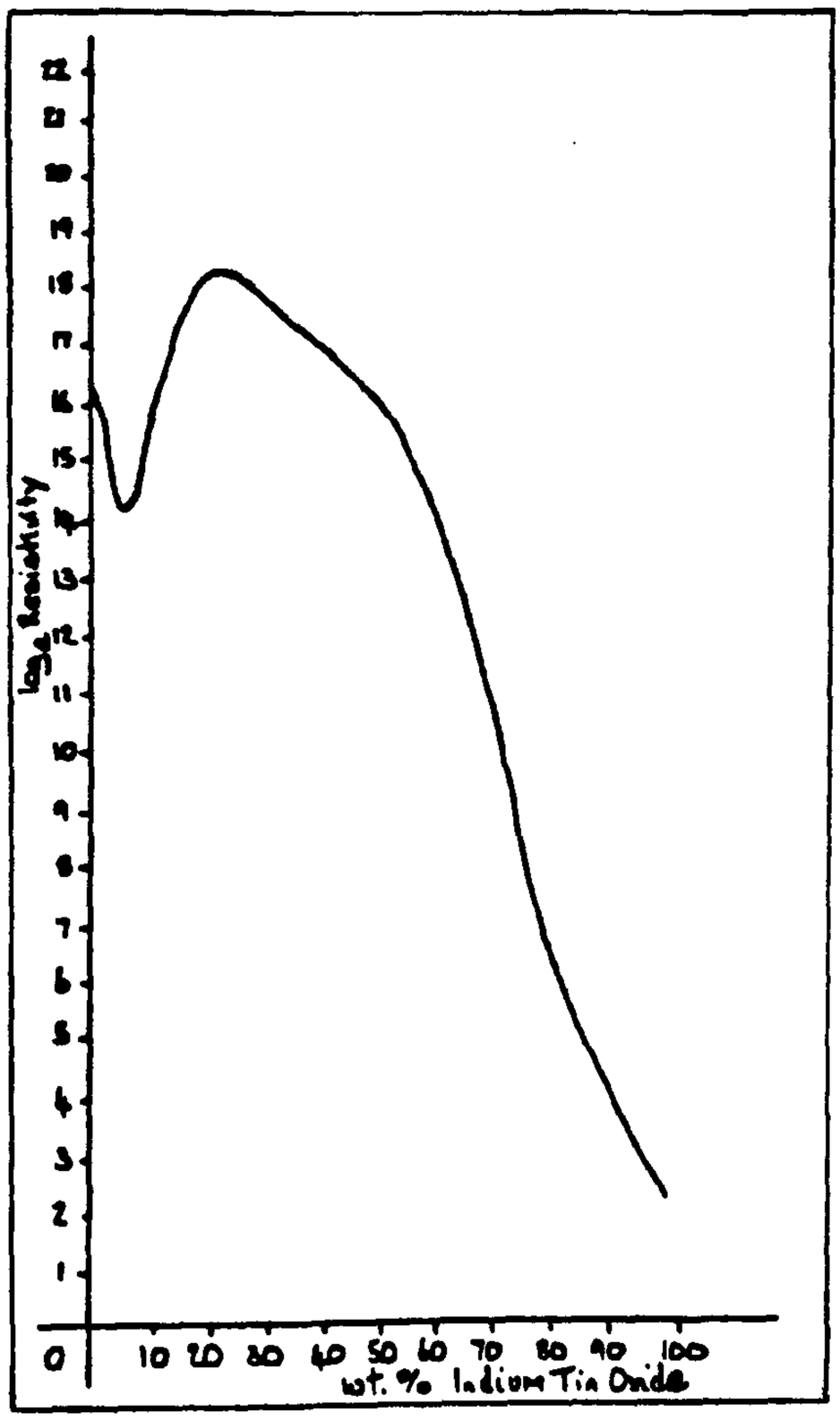


Figure Ten - $\log_e$ Resistivity v. Composition of $MoO_3$/In Sn Oxide Phases

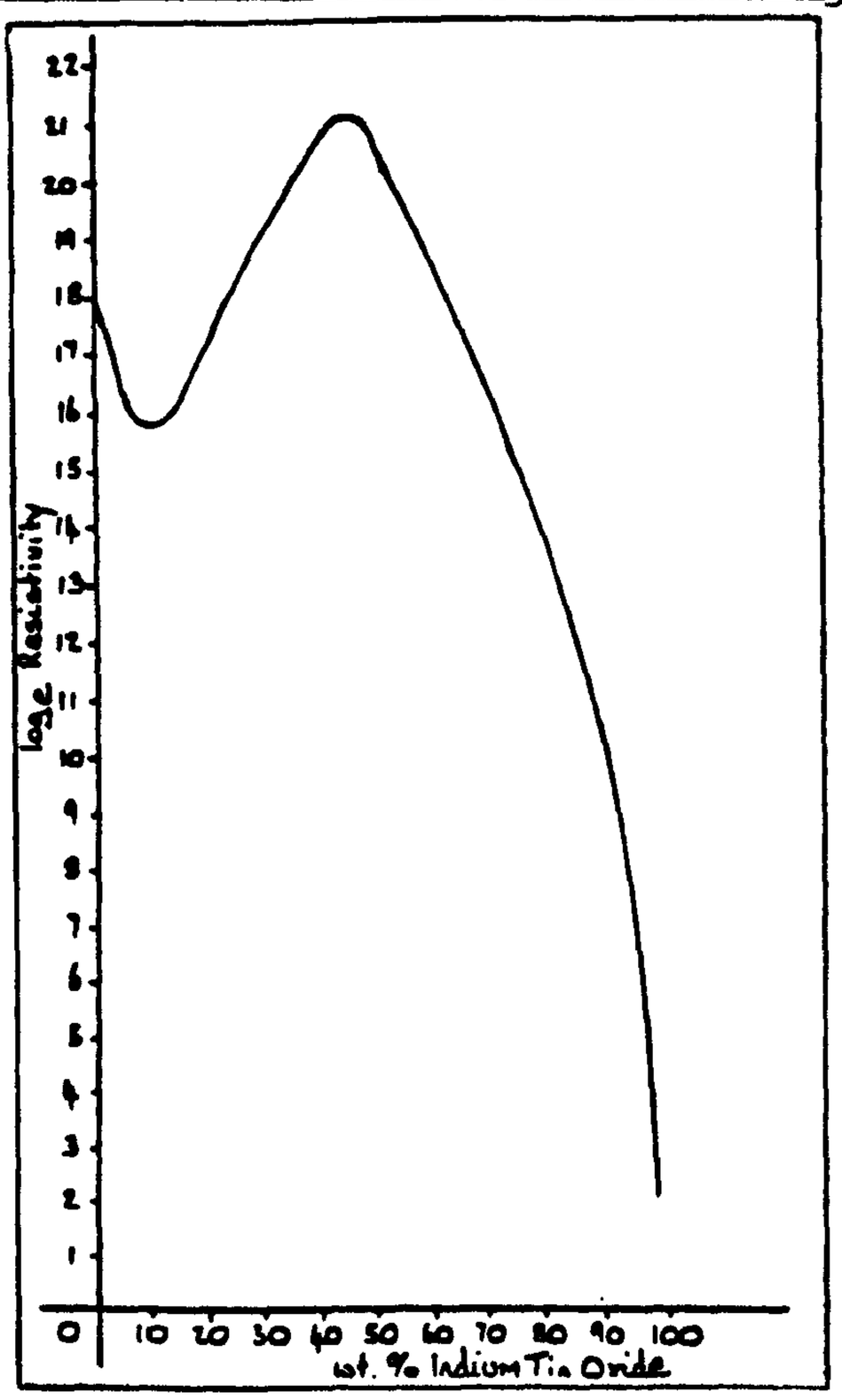

Figure Eleven - $\log_e$ Resistivity v. Composition of Talc/In Sn Oxide Phases

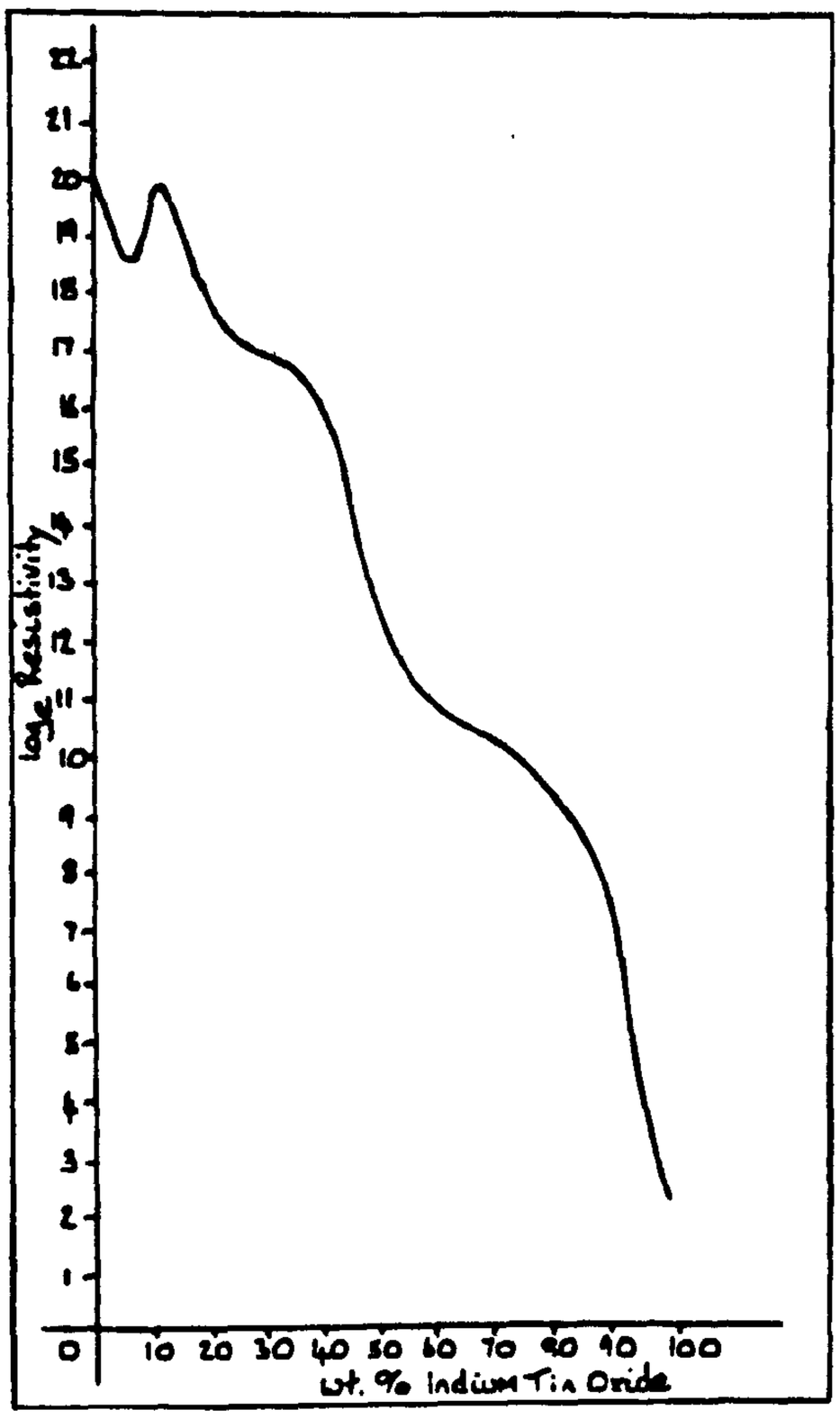


Figure Twelve - $\log_e$ Resistivity v. Composition of Zr Sand/In Sn Oxide Phases

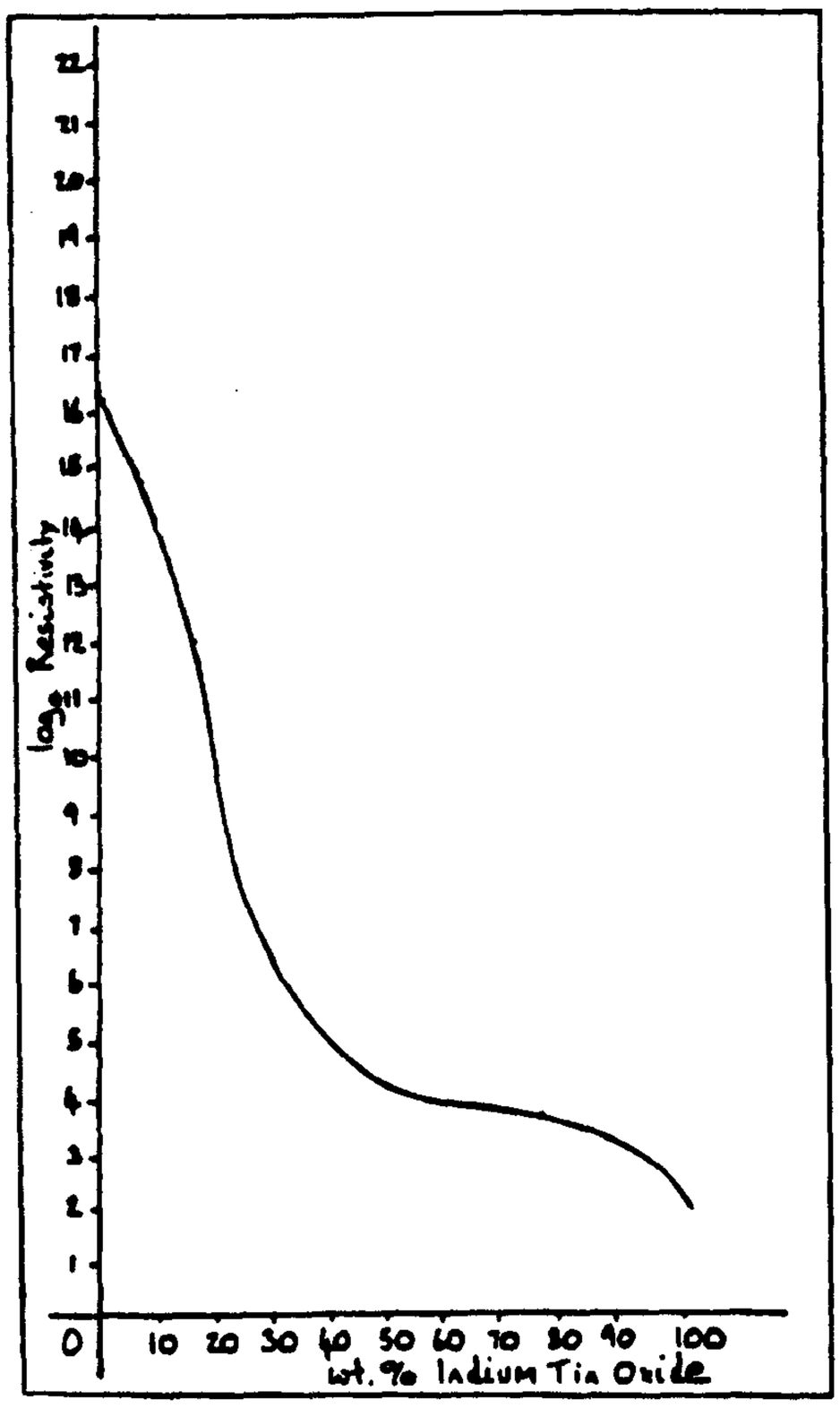

Table Thirteen - Calcination Temperatures and Resistivities of Diluted Indium Tin Oxide Phases

| Diluant | Calcination Temp. /$^{o}$C | % Weight Added Before $\rho$>20$\Omega$cm |
|---|---|---|
| Titanium Dioxide | 1050 | 8 |
| Zirconium Dioxide | 1050 | 20 |
| Aluminium Trioxide | 1050 | 10 |
| Zinc Oxide | 1050 | 2 |
| Silicon Dioxide | 1050 | 30 |
| Rasorite ($Na_2B_4O_7.4H_2O$) | 650 | 22 |
| Cryolite ($Na_3AlF_6$) | 725 | 1 |
| Tungsten Trioxide | 950 | 4 |
| Molybdenum Trioxide | 780 | 1 |
| Talc ($Mg_3(Si_4O_{10})(OH)_2$) | 800 | 3 |
| Zircon Sand ($Zr(SiO_4)$) | 1050 | 4 |

From table thirteen it can be seen that zirconium (IV) oxide, silicon (IV) oxide and rasorite were the most effective of the diluants for indium tin oxide. Attempts to analyse the results obtained for the eleven dopants for possible correlations between resistivity and fac--tors such as crystal structure, ionic radii, electronegativity, melt--ing points, availability of other valence states proved unsuccessful and it is most likely that the product resistivity is best expressed by a complex function containing several of the above parameters.

Three further experiments were carried out to investigate the effects on resistivity of milling zirconium (IV) oxide, silicon (IV) oxide and rasorite with low resistivity indium tin oxide.

Resistivity analysis of samples which had been prepared using the method described earlier in this chapter gave the results shown in table fourteen.

Table Fourteen - Resistivities of Doped Indium Tin Oxide Phases

| Dopant | Weight Added (%) to In Sn Oxide | Resistivity/$\Omega$ cm |
|---|---|---|
| None | 0 | 0·3 |
| $SiO_2$ | 10 | 4·4 |
| $ZrO_2$ | 10 | 2·6 |
| $Na_2B_4O_7$ | 10 | 10·3 |

The advantages of the addition of a filler such as zirconia to indium tin oxide in reducing the unit cost of the material were offset by the disadvantages of an increased product resistivity. The use of 10% of fillers could only be considered where resistivities of up to 10 $\Omega$cm in the product would be acceptable.

Following on from this work three experiments were conducted in order to investigate the effects of diluting indium (III) oxide with rasorite, silicon (IV) oxide and zirconium (IV) oxide. The preparative details employed were those outlined for diluted indium tin oxide phases earlier on in this chapter and the results of the resistivity analyses are given below.

| Species | Resistivity/$\Omega$ cm |
|---|---|
| 10%$Na_2B_4O_7$/90%$In_2O_3$ | 2·7 x $10^5$ |
| 10% $ZrO_2$ /90%$In_2O_3$ | 37·7 |
| 10% $SiO_2$ /90%$In_2O_3$ | 9·8 x $10^4$ |

Whilst none of the three mixed metal oxide phases represents a low resistivity system it is interesting to note how the absence of just a few weight percent of tin is able to drastically raise the resist-ivity of these species. These results show that the presence of tin is essential when attempting to prepare low resistivity doped indium oxide phases.

## 5.3. Mixed Metal Oxides

Four mixed metal oxide systems were investigated in this part of the research project in an attempt to find a new semiconducting material to replace indium tin oxide and tin antimony oxide phases. Preparative details for the four systems studied, europium tin oxide, antimony tin zirconium oxide, zirconium antimony oxide and zinc alum-inium oxide, together with the results of resistivity analyses are given in sections (a) to (d) of this part of the chapter respectively.

### (a) Europium Tin Oxide

Tin (IV) oxide (19·8g) and europium (III) oxide (0·2g) were ball milled in ethanolic media for 15 minutes and then oven dried at 110°C in an oven. The material was calcined (2 hours, 1050°C) in a silica cru-cible to encourage incorporation of the europium oxide into the tin (IV) oxide host rutile structure. After calcining,the mixed oxide was allowed to cool and was then ball milled for a second time for 15 minutes in ethanol and oven dried to prepare a homogenous sample of material for resistivity analysis.

$$SnO_2 + 4{\cdot}35\times10^{-3}Eu_2O_3 \xrightarrow{\Delta H} SnEu_{0{\cdot}0087}O_{2{\cdot}013-x}$$

Product Resistivity = $2 \times 10^6 \Omega$ cm

(b) Antimony Tin Zirconium Oxide

Antimony tin oxide (93·5/6·5, (10 - X)g) was ball milled in ethanol for 15 minutes with zirconium (IV) oxide($X_g$)& was then oven dried at 100°C. After drying the prepared material was calcined (1050°C, 2 hours) in a silica crucible to encourage the formation of any new phases within the material. After calcination the mixed oxide was allowed to cool and was then ball milled in ethanol for a second time and oven dried to prepare a homogenous sample for resistivity analysis. The results obtained from the resistivity analysis of 13 oxides of different compositions are given in table fifteen and are plotted in figure thirteen.

(c) Zirconium Antimony Oxide

Zirconium (IV) oxide (10 - Xg) and antimony (III) oxide (Xg) were ball milled in ethanolic media and then oven dried at 100°C. After drying the prepared material was calcined (1000°C, 1 hour) in a silica crucible to encourage the formation of any new phases within the material. After calcination the mixed oxide was allowed to cool and was then ball milled for a second time, for fifteen minutes in ethanol and oven dried to prepare a homogenous sample for resistivity analysis. The results of resistivity analysis carried out on seven samples of zirconium antimony oxide prepared in this manner are given in table sixteen.
All weight compositions of greater than 60% antimony (III) oxide, calcination at temperatures of 1050°C or higher resulted in the sublimation of antimony (III) oxide from the mixture, yielding products of uncertain stoichiometry.

Figure Thirteen - $\log_e$ Resistivity v. Composition of Antimony Tin Zirconium Oxide

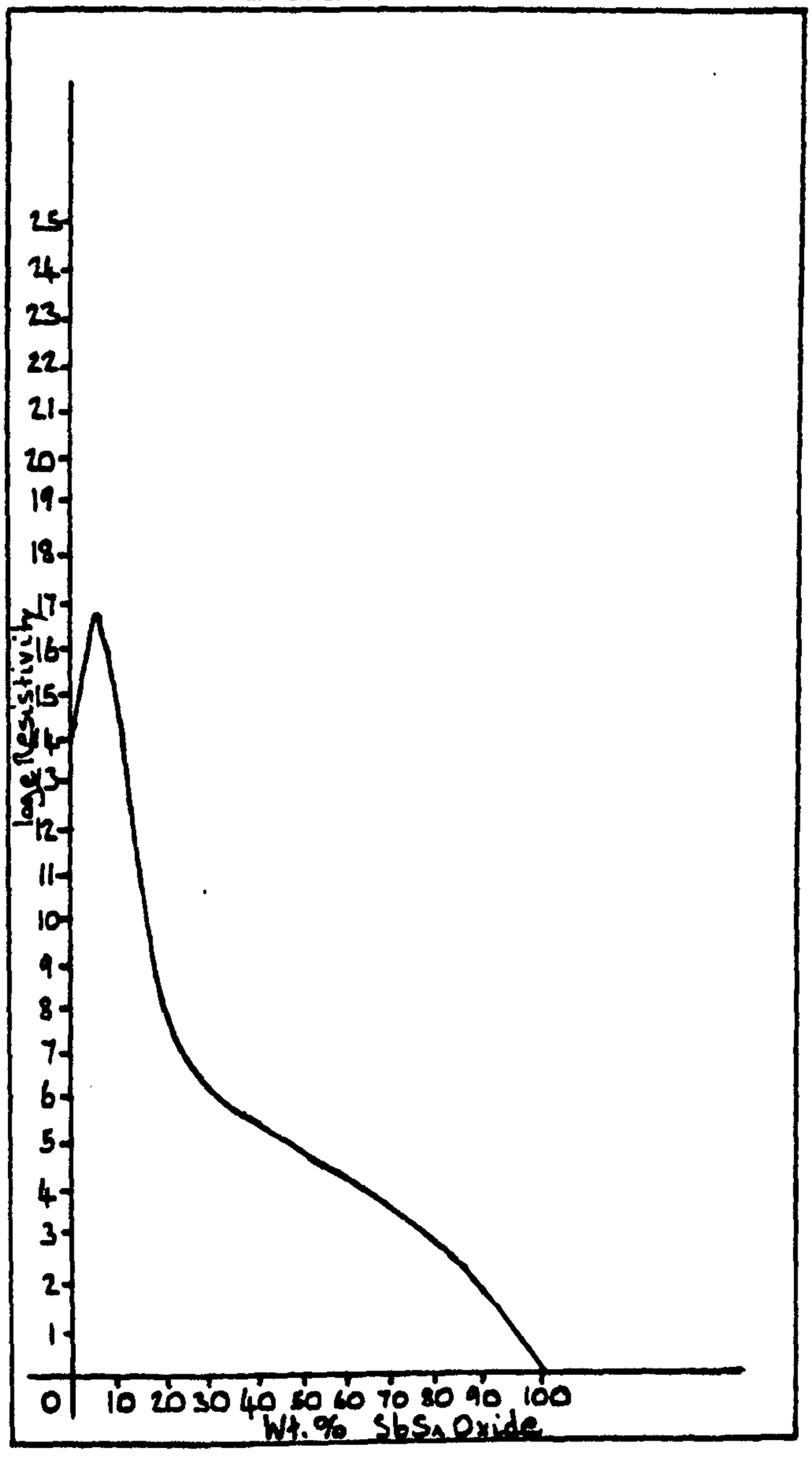

Table Fifteen - Resistivities of Antimony Tin Zirconium Oxides

| Wt. % $ZrO_2$ | Wt. % Sn Sb Oxide | Resistivity/Ω cm |
|---|---|---|
| 100 | 0 | $1{\cdot}2x10^6$ |
| 95 | 5 | $7{\cdot}9x10^6$ |
| 90 | 10 | $9{\cdot}9x10^6$ |
| 80 | 20 | $2{\cdot}3x10^5$ |
| 70 | 30 | 585·0 |
| 60 | 40 | 217·0 |
| 50 | 50 | 139·0 |
| 40 | 60 | 45·0 |
| 30 | 70 | 31·0 |
| 20 | 80 | 19·0 |
| 10 | 90 | 5·0 |
| 5 | 95 | 3·0 |
| 0 | 100 | 1·0 |

Table Sixteen - Resistivities of Zirconium Antimony Oxide Phases

| Wt. % $Sb_2O_3$ | Wt. % $ZrO_2$ | Resistivity/Ω cm |
|---|---|---|
| 0 | 100 | $3{\cdot}5x10^{11}$ |
| 10 | 90 | $1{\cdot}8x10^{10}$ |
| 20 | 80 | $9{\cdot}5x10^{10}$ |
| 30 | 70 | $1{\cdot}8x10^{10}$ |
| 40 | 60 | $4{\cdot}7x10^{10}$ |
| 50 | 50 | $8{\cdot}4x10^9$ |
| 60 | 40 | $2{\cdot}9x10^9$ |

(d) Zinc Aluminium Oxide

Zinc oxide (20 - Xg) and aluminium oxide (Xg) were ball milled in eth--anolic media for 15 minutes and then oven dried at 100°C. After drying the prepared material was divided into two equal portions, one half was then calcined at 700°C for 2 hours and the other half at 1100°C for 2 hours. After calcination the two batches of material were kept separate and were both ball milled for a second time in ethanol and oven dried to prepare homogenised samples for resistivity analysis. Results obtained from the resistivity analysis of eight samples of zinc aluminium oxide prepared by this route are given in table seventeen.

Table Seventeen - Resistivities of Zinc Aluminium Oxide Phases

| Wt.% $Al_2O_3$ | Wt.% ZnO | Resistivity/Ω cm | |
|---|---|---|---|
| | | Calcination Temp. 700°C | Calcination Temp. 1100°C |
| 0·05 | 99·95 | $3·4 \times 10^6$ | $1·2 \times 10^6$ |
| 0·10 | 99·90 | $1·0 \times 10^7$ | $2·2 \times 10^6$ |
| 0·50 | 99·50 | $4·0 \times 10^5$ | $8·0 \times 10^5$ |
| 1·00 | 99·00 | $1·3 \times 10^6$ | $4·6 \times 10^5$ |

Results of resistivity analyses carried out on the mixed metal oxides prepared in this section showed all of the materials to be unsuitable for high conductivity semiconductor applications.

The results from experimental series 5.3(b) and 5.3(c) show that alth--ough zirconium (IV) oxide and tin (IV) oxide exhibit many similar chemical and physical properties they are non-interchangeable insofar as their usage in antimony oxide doped semiconductors is concerned. Resistivity measurements show zirconium (IV) oxide to be unsuitable for use as a filler in tin antimony oxide and not important enough to warrant further investigation in this work.

Attempts at preparing zirconium antimony oxide semiconducting phases analogous to tin antimony oxide were also unsuccessful with the res--istivity of 93·5/6·5 zirconium antimony oxide being some 3 x $10^{11}$X greater than the corresponding tin antimony oxide species.

The use of zinc aluminium oxide as a conductive filler in nylon fibres has been reported in the literature[1,2,3,4,5] and at the start of this investigation it was hoped that this mixed metal oxide system might prove suitable for development. Unfortunately work carried out in this investigation failed to produce a low resistivity product. Takemura etal[1] found a relationship between colouration and conduct--ivity in zinc aluminium oxide systems and reported that the more strongly coloured phases exhibited the highest conductivities. Takemura etal[1] described the preparation of a sample of 'black' zinc aluminium oxide by calcination of the two mixed oxides at 1000°C in a reducing atmosphere. From Takemura etal's results, zinc aluminium oxide would thus appear to be an unlikely system to yield a white, low resistivity, semiconducting material.

The preparation of europium doped tin oxide phases has been described in the literature[6,7,8] and hence the present studies to determine whether the conductivity of a europium tin oxide phase was similar to tin antimony oxide. Unfortunately work carried out on 1 weight % europium doped tin (IV) oxide prepared in this investigation showed the material to be a poor conductor of electricity. Berry[6] concluded from the results of mössbauer spectroscopy that the doping mechanisms in antimony and europium doped tin (IV) oxide must be different, thus it would appear that the processes which give rise to electrical cond--uction in tin antimony oxides do not occur in tin europium oxides.

Poor electrical conductivity in tin europium oxide phases has also been reported by Crabtree[7,8], however Crabtree also reported that cer-tain tin europium oxides exhibited excellent properties as phosphors[8]. This may represent an area for future research and development.

References

1. T. Takemura, M. Kobayashi, Y. Takada, K. Sato, Adv. Ceram., 1983, 7, 50.

2. H. Okuma, N. Amiji, M. Suzuki, Y. Tanno, Adv. Ceram., 1983, 7, 41.

3. Jpn. Kokai Tokkyo Koho, J.P. 82,53903.

4. Jpn. Kokai Tokkyo Koho, J.P. 82,53904.

5. Jpn. Kokai Tokkyo Koho, J.P. 57,165252.

6. F. Berry, Inorg. Chim. Acta., 1982, 62(2), 123.

7. D.F. Crabtree, J. Phys. D: Appl. Phys., 1974, 7, L17.

8. D.F. Crabtree, J. Phys. D: Appl. Phys., 1975, 8, 107.

Chapter Six - Tin (IV) Oxide: Novel Synthetic Routes for the Preparation of Fine Particles.

Section 6.1 - From Basic Tin (II) Nitrate

Section 6.2 - From Basic Tin (II) Sulphate

Section 6.3 - From Spray Dried Ammonium Hydroxystannate

Section 6.4 - Conclusion

## Chapter Six - Tin (IV) Oxide: Novel Synthetic Routes for the Prepar-ation of Fine Particles

Tin (IV) oxide has been traditionally manufactured by the high temp-erature, direct oxidation of tin metal by air. Tin (IV) oxide produced by this route consists of a finely divided white powder with a mean particle diameter of ~0·6 microns. The development of new tin oxide based semiconductors by Keeling and Walker Ltd. has lead to a requirement for tin (IV) oxide of ultrafine particle size (below 0·1 micron) which it proved impossible to manufacture by existing processes. Therefore in order to try to prepare tin (IV) oxide of ultrafine part-icle size it was decided to look into novel synthetic routes. Three of which were investigated at City University during the course of this work.

### 6.1. The Preparation of Tin (IV) Oxide From the Explosive Decomposition of Basic Tin (II) Nitrate.

Several attempted preparations of basic tin (II) nitrate have been des-cribed in the chemical literature. An explosive tin (II) nitrate was prepared by Weber[1] by the addition of sodium carbonate to a freshly prepared solution of tin (II) oxide in nitric acid. Weber gave the tin nitrate he prepared the formula $Sn_2O(NO_3)_2$. Bury and Partington[2] were unable to prepare a truly explosive tin nitrate. A report of the government chemist[3] mentions the formation of basic tin nitrate as being the cause of an explosion in a flour mill. Donaldson and Moser[4] were however successful in preparing a truly explosive basic tin nitrate which they analysed as $Sn_3(OH)_4(NO_3)_2$. Donaldson and Moser[4] also studied the explosive thermal decomposition of basic tin nitrate which was found to occur at 125°C and gave tin (IV) oxide, water and nitrogen oxides as products.

Because of the violent nature of the decomposition of basic tin nit--rate, tin (IV) oxide is produced in the form of very fine particles. In this investigation a sample was prepared for particle size analysis to find out whether or not the decomposition of basic tin nitrate represents a viable route to tin (IV) oxide of a fine particle size. The experimental procedure followed for the preparation of the basic tin nitrate was that of Donaldson and Moser[4] which is given below.

Experimental

Metallic tin (50g) was added to a solution of copper (II) sulphate in water (500cc) and sulphuric acid (20cc) which was then boiled for 1½ hours until the solution became colourless. The resulting sol--ution of tin (II) sulphate was then filtered off and treated with ammonia solution to precipitate out white, hydrous tin (II) oxide. The precipitate was washed by decantation until it became free from ammonia and was then filtered off by suction to give a hydrous oxide paste.

Nitric acid (26ml, d = 1·42) and water (39ml) were cooled to approx--imately -20°C in ice/salt. The hydrous oxide paste was then added gradually to this cold solution in small quantities with continuous stirring until the acid solution became saturated. The temperature was then allowed to rise and addition of the hydrous oxide continued until a boiling saturated solution was obtained. The solution was then filtered and crystals of basic tin (II) nitrate precipitated out upon cooling which were filtered off, washed in acetone and left to dry in a vacuum dessicator.

The prepared nitrate was decomposed by heating a small sample (c0·5g) in an evacuated round bottomed flask over a bunsen flame.

Attempts at analysing the product particle size by coulter counter were unsuccessful due to a large proportion of particles being below the threshold detection limit of the machine(0·8 microns). Particle size analysis was eventually carried out by optical microscopy which showed the average particle size to be 0·25 microns.

$$CuSO_4 + Sn \longrightarrow SnSO_4 + Cu$$

$$SnSO_4 \longrightarrow SnO.nH_2O$$

$$SnO.nH_2O + HNO_3 \longrightarrow Sn_3(OH)_4(NO_3)_2$$

## 6.2. The Preparation of Tin (IV) Oxide From the Explosive Decomposition of Basic Tin (II) Sulphate.

Many attempted preparations of basic tin (II) sulphate have been des--cribed in the chemical literature and it is obvious that some confusion existed as to the exact composition of the material. Preparations have been descibed by Berthelot[5], Lungi[6] and later by Ditte[7] who reported the existance of three basic sulphates $5SnO.SnSO_4.H_2O$, $2SnO.SnSO_4.3H_2O$ and $4SnO.2SnSO_4.3H_2O$. Carson[8] reported the existance of two distinct phases $SnOSnSO_4$ and $Sn_2OSO_4$, in addition Wernfurs also reported $Sn_2OSO_4$[9]. Donaldson and Moser[10] finally succeeded in preparing crystalline samp--les of basic tin sulphate which they analysed as $Sn_3O(OH)_2SO_4$. Donaldson and Moser[10] also managed to explain the confusion in the literature in terms of the pH dependance of the composition of the basic salt precipitated. When the pH of the solution is between 1·5 to 2·7 the material $Sn_3O(OH)_2SO_4$ is always precipitated, however when the pH is raised to above 3·3 the product composition varies as $SO_4^{2-}$ in the lattice is replaced by $OH^-$.

Basic tin sulphate undergoes a two stage thermal decomposition to give tin (IV)oxide.

At 236°C basic tin sulphate loses water to give tri-tin (II) oxysulphate and it is this material which decomposes explosively to give tin (IV) oxide and sulphur oxides.

$$Sn_3O(OH)_2SO_4 \xrightarrow{236^{\circ}C} Sn_3O_2SO_4 + H_2O$$

$$Sn_3O_2SO_4 \xrightarrow{405^{\circ}C} SnO_2 + \text{Sulphur Oxides}$$

Experimental

Tin metal (50g) was added to a solution of copper (II) sulphate (50g) in water (500cc) and sulphuric acid (20ml) which was then boiled for about 1½ hours until the solution became colourless. The resulting solution was filtered and adjusted to a pH of 2·0 with sodium hydroxide solution. The solution was then reduced to about one third of its original volume using a rotary evaporator and crystals of basic tin (II) sulphate precipitated out upon cooling. The crystalline product was filtered off under vacuum and dried over silica gel in a vacuum desiccator.

The basic tin sulphate was decomposed by heating it in a crucible under a bunsen flame in air. The material exploded with little violence and the tin (IV) oxide produced was collected, washed with water and oven dried at 110°C. Analysis of the product by Coulter Counter and optical microscopy showed the average particle size to be around three microns.

## 6.3 The Preparation of Tin (IV) Oxide from Ammonium Hydroxystannate Sprayed Gel.

Early kilogramme trials on metastannic acid production carried out at City University had produced about four kilogrammes of material of rather coarse particle size.

As part of this investigation it was decided to study whether or not this material could be processed to yield finer particles of tin (IV) oxide or metastannic acid. Grinding and milling operations though effective in reducing particle size introduced contamination into the material which was undesirable, therefore the possibility of chemical processing was investigated. Hydroxystannate gels can easily be prep-ared from metastannic acid and it was hoped that the spray drying of these gels would provide the necessary control step for production of fine particles which could then be thermally decomposed to give tin (IV) oxide.

A detailed study of the thermal decomposition of bivalent metal hydroxy-stannates has been carried out by Ramamurthy and Secco[11] who suggested the following two stage decomposition pathway.

$$M[Sn(OH)_6] \longrightarrow MSnO_3 + 3H_2O$$

$$\left[\begin{array}{l} 2MSnO_3 \longrightarrow M_2SnO_4 + SnO_2 \\ MSnO_3 \longrightarrow MO + SnO_2 \end{array}\right]$$

The thermal decomposition of potassium hydroxystannate has been studied by M. Tournoux[12] who reported the following decomposition pathway.

$$\left.\begin{array}{l} K_2Sn(OH)_6 \longrightarrow K_2SnO_3.H_2O + 2H_2O \\ 3K_2SnO_3.3H_2O \longrightarrow 3K_2SnO_3.2H_2O + H_2O \\ 3K_2SnO_3.2H_2O \longrightarrow 3K_2SnO_3 + 2H_2O \end{array}\right\} \text{Loss of Water}$$

$$\left.\begin{array}{l} 3K_2SnO_3 \longrightarrow K_2Sn_3O_7 + 2K_2O \\ K_2Sn_3O_7 \longrightarrow 3SnO_2 + K_2O \end{array}\right\} \text{Loss of } K_2O$$

However for the purposes of the present investigation one problem associated with using metal hydroxystannates is that on decomposition they leave behind a metal residue as well as tin (IV) oxide.

One consequence of this would be that a further processing stage would be needed to yield a pure product. Ammonium ions would not leave a stable oxide species like the alkali and alkaline earth metals and so a different decomposition pathway would be expected. The thermal analysis traces of ammonium hydroxystannate are shown in figure one. The percentage weight loss is consistent with that expected for a res-idue of pure tin (IV) oxide and so the following pathway is most likely.

$$[Sn(OH)_6]^{2-}\ (NH_4)_2^{+} \xrightarrow{\Delta H} SnO_2 + \text{Water} + \text{Ammonia} + \text{Ammonium Hydroxide}$$

The relatively straightforward decomposition of the ammonium hydroxy-stannate and the purity of the final tin (IV) oxide product provided the best gel for spray drying.

In the spray drying process, the feed material which is in liquid or mobile form, is sprayed into a large chamber into which hot air (or another gas) is introduced. The liquid in the spray is rapidly evap-orated leaving particles of solid which must then be separated from the air. The motion of the air and the material is more or less co-current. The product is always a powder, but the form of the part-icles depends upon the substance being sprayed. When the feed is in solution or emulsion form the dried particles (cenospheres) are usually spherical or nearly so and are frequently hollow, the dried cenospheres being much larger than the particles in the spray medium.

## Experimental

Metastannic acid (150g, from B5) was blended with hydrochloric acid (170ml, 1·18sg) and Water (800ml) for two hours on an end-runner mill using a zirconia pot and media.

Figure One - Thermal Analysis of Ammonium Hydroxystannate

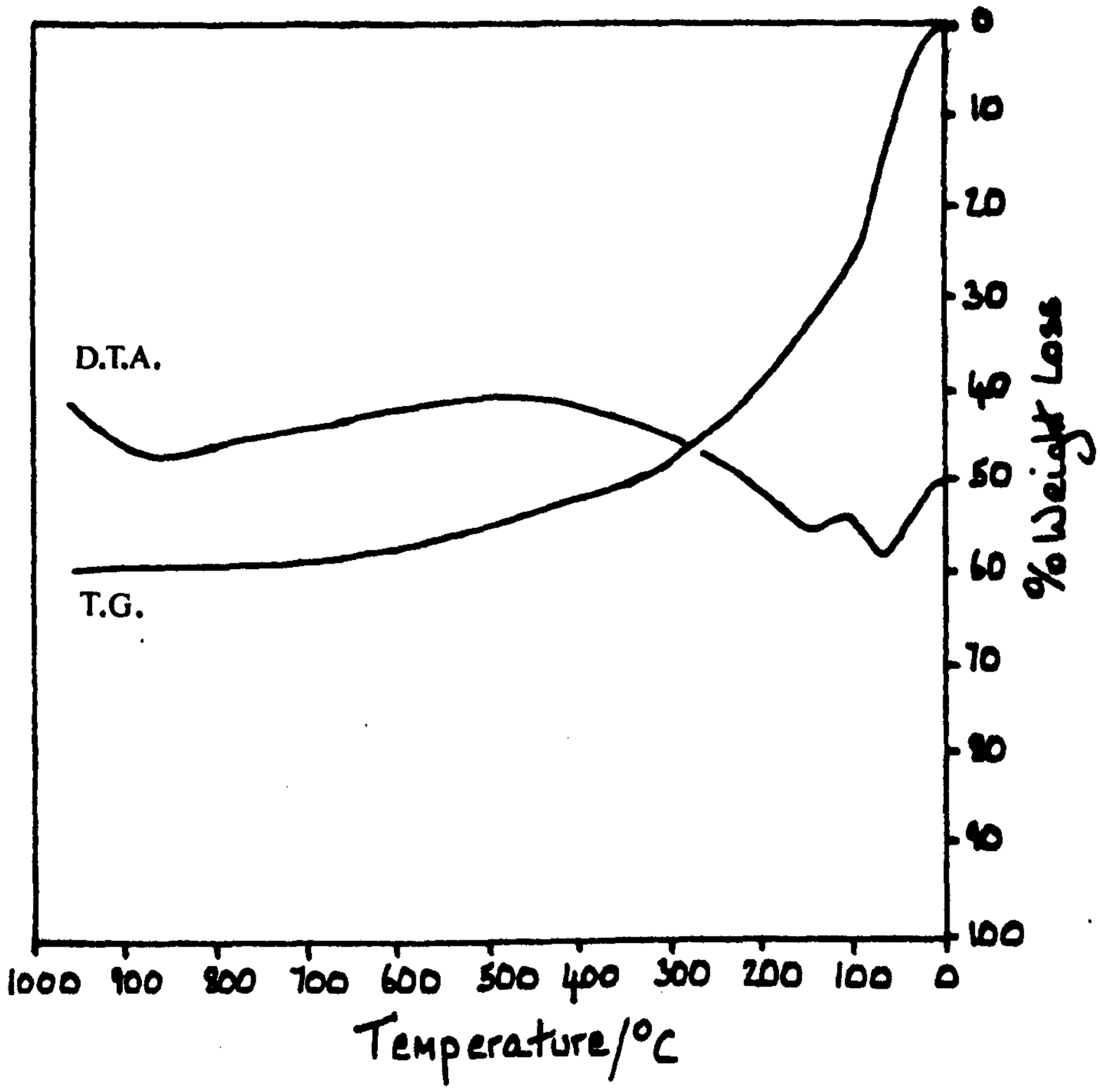

The resulting solution of $\beta$stannyl chloride was diluted with water to make up four litres and then made alkaline (to pH 8·5) by addition of ammonia solution. At pH 3·5 the ammonium hydroxystannate fell out of solution as a white gelatinous precipitate which was then washed by decantation with 50 volumes of water to remove excess ions. The prepared gel was then spray dried using a Lab Plant Spray Drier Model CAE-1 fitted with a specially prepared spray nozzle of diameter 0·17mm. The collected dried gel was then treated over a bunsen flame for 1½ hours to convert the material to tin (IV) oxide and then cal--cined in a furnace for 1 hour at 1000°C to remove any adsorbed water or ammonia.

$$SnO_2.nH_2O + HCl \longrightarrow SnOCl_2 + H_2O$$

$$SnOCl_2 + NH_3/H_2O \longrightarrow [Sn(OH)_6](NH_4)_2 + NH_4Cl$$

$$[Sn(OH)_6]\ (NH_4)_2 \xrightarrow{\Delta H} SnO_2$$

Particle size analysis of the product, together with a sample of the starting material was carried out by Sedigraph by B.C.R.A. at Stoke--on-Trent. The Sedigraph analyses of both materials are given in figures two and three, the starting material was found to have a mean particle diameter, $\bar{x}$ = 7·7 microns and a standard deviation, $\sigma$ = 5·9 microns whilst the processed stannic oxide gave figures of $\bar{x}$ = 2·9 microns and $\sigma$ = 2·5 microns respectively.

## 6.4 Conclusion

In conclusion to this section of the project it can be stated that all three of the attempted syntheses proved to be disappointing. Decomposition of the basic salts although explosive did not produce products with particle size less than that obtained by jet milling metastannic acid.

Figure Two - Sedigraph Analysis of Metastannic Acid

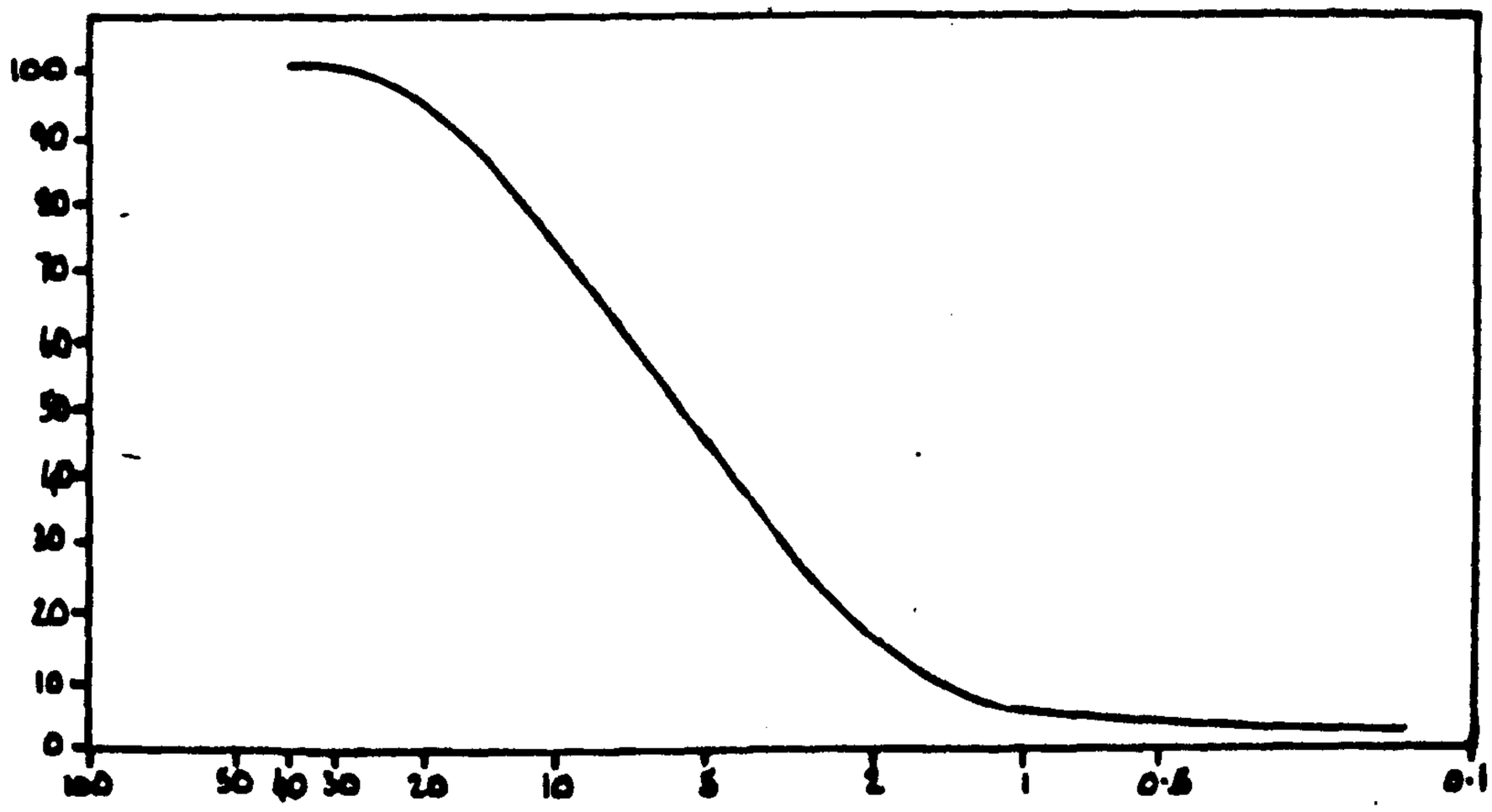


Figure Three - Sedigraph Analysis of Spray Processed Tin (IV) Oxide

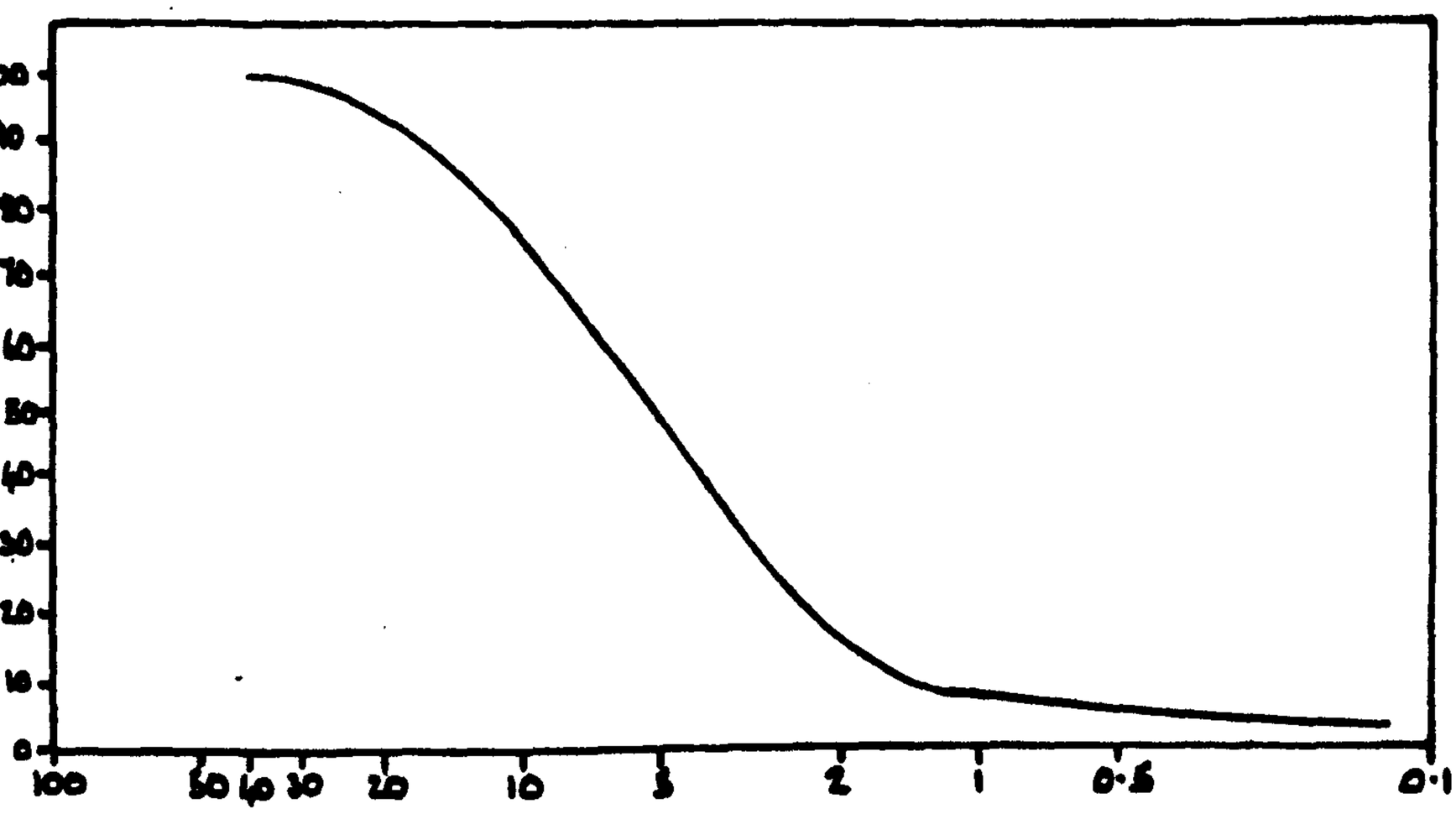

The spray processing of ammonium hydroxystannate did not prove to be a very satisfactory route to ultrafine tin (IV) oxide particles. Though the process did achieve a 62% reduction in the mean particle size and a 57% reduction in standard deviation, the process would be very costly to operate on an industrial scale both in terms of chemicals and man-power. Therefore it would appear that none of the chemical methods investigated provides a satifactory synthetic route to tin (IV) oxide of the ultrafine particle size required by Keeling and Walker Ltd.

References

1. Weber, J.Prakt. Chem., 1882, 26, 121.

2. Bury, Partington, J. Chem. Soc., 1922, 121, 1998.

3. Report of the Government Chemist, 1922-23.

4. J.D. Donaldson, W. Moser, J. Chem. Soc., 1961, 1996.

5. A.B. Berthelot, Mem. d'Arcueill, 1807, 161, 1.

6. A. Longi, L'Orosi, 1885, 235.

7. A. Ditte, Ann. Chim. Phys., 1882, 27, 159.

8. C.M. Carson, J. Amer. Chem. Soc., 1926, 48, 906.

9. G. Werfurs, Acta. Chem. Scand., 1961, 15, 1007.

10. J.D. Donaldson, W. Moser, J. Chem. Soc., 1960, 4000.

11. P. Ramamurthy, E.A. Secco, Can. J. Chem., 1971, 49, 2813.

12. M. Tournoux, Ann. Chim., 1964, 9, 579.